U.PORTO

FEUP FACULDADE DE ENGENHARIA
UNIVERSIDADE DO PORTO

STRUCTURAL IDENTIFICATION OF OLD STEEL BRIDGES: MONITORING AND REHABILITATION ASSESSMENT

A thesis submitted for the degree of Doctor of Philosophy in Civil Engineering

at the Faculty of Engineering of the University of Porto

Bruno José Afonso Costa

Supervisor

Prof. Joaquim de Azevedo Figueiras

November 2012

To my great friend João Crespo,
my grandparents Miguel Costa and Maria Amélia,
and my dear Professor Andrzej J. Pietrzak.
Naturally, we will be reunited in the future!

Abstract

Old steel bridges, in particular the ones that are centenary, exhibit a diversity of typical problems that require the use of specific procedures and methodologies in structural identification for their objective condition assessment, in order to assist either the decision-making process in their management and maintenance or the appraisal of engineering works performed on them.

In this context, non-destructive field testing and numerical modeling emerge as key tools of a successful structural identification framework within its experimental and analytical arts, respectively. Additionally, the adoption of the latest monitoring technologies and techniques, as well as an effective utilization of the computational resources currently available based on engineering expertise, can play a central role in understanding the actual behavior of old steel bridges and in the reliable assessment of their structural safety, simultaneously contributing to the widespread use of structural identification among the technical community.

Based on these principles, in a first stage, this work presents a field experimental evaluation of two different measuring techniques, one conventional, electric based, and the other exhibiting innovative features provided by the fiber optic technology. To this end, a combined monitoring system was implemented in a steel railway bridge (Trezói Bridge), which was also designed to enable a first insight on the characteristic structural behavior of truss bridges and to permit the integration of a basic weight-in-motion system.

The next stage of this work has addressed the conception and development of new sensors, both electric and fiber optic, for the monitoring of old steel bridges. Methodologies and procedures for their field installation were established with the goal to attain the necessary requirements of durability and metrological stability for long-term measurements, which included novel protection systems devised for shielding the sensors.

The performance of the sensors and their protections were tested at the laboratory in terms of accuracy and reliability of the collected data.

Afterwards, the developed sensing solutions were implemented in two permanent monitoring systems: one installed on a double-deck steel truss arch bridge and constituted only by fiber Bragg grating sensors (Luiz I Bridge), and the other applied to a through truss parabolic bridge relying only on electric sensors (Pinhão Bridge). As both monitored structures underwent rehabilitation and strengthening processes, the monitoring systems were used in the static field tests performed for assessing the bridges behavior. Complementary, ambient vibration tests were also carried out to estimate their modal parameters. Both testing programs, static and dynamic, were planned and executed so that a direct experimental assessment of the changes produced in the structural performance between the pre- and post-conditions could be enabled.

The complete structural identification of both case studies was accomplished with the development of numerical models suitable for an accurate simulation of the local and global behaviors based on the collected field data. For that, specific modeling strategies were established, which can constitute a guideline for future studies of similar bridges. In turn, the numerical analyses provided the results for the appraisal of the rehabilitation and strengthening plans, and enabled the validation of the implemented instrumentation procedures and options made in the design and installation of the permanent monitoring systems. Additionally, the numerical models were used to estimate the forces and stresses in critical members of both bridges, produced by the actions specified in the codes and standards adopted at the design stage, with the purpose of appraising the actual level of structural safety.

Resumo

As pontes em aço antigas, em particular as que são centenárias, apresentam um conjunto diversificado de problemas típicos que requerem a utilização dos mais recentes procedimentos e metodologias na identificação estrutural para uma avaliação objectiva do seu estado, com o último propósito de auxiliar o processo decisório na sua conservação e gestão ou a avaliação dos trabalhos de engenharia nelas realizados.

Neste contexto, os ensaios não-destrutivos de campo e a modelação numérica surgem como ferramentas essenciais numa identificação estrutural bem sucedida no quadro das suas componentes experimental e analítica, respectivamente. Adicionalmente, a adopção das mais recentes tecnologias e técnicas de monitorização, bem como uma utilização eficaz dos recursos computacionais actualmente disponíveis fundada nos melhores conhecimentos de engenharia, pode desempenhar um papel central na compreensão do comportamento real das pontes em aço antigas e na correcta avaliação da sua segurança estrutural, e contribuir simultaneamente para o uso generalizado da identificação estrutural entre a comunidade técnica.

Fundado nestes princípios, o trabalho começa por apresentar uma avaliação experimental de campo de duas tecnologias de medição distintas, uma convencional, de base eléctrica, e outra inovadora, suportada em fibras ópticas. Com este propósito, foi implementado um sistema de monitorização misto numa ponte metálica ferroviária (ponte de Trezói), cuja concepção tornou também possível uma primeira percepção do comportamento estrutural característico de pontes treliçadas e a integração de um sistema básico de caracterização de tráfego.

A fase seguinte deste trabalho abordou a concepção e desenvolvimento de cabeças sensoras, eléctricas e em fibra óptica, para a monitorização de pontes em aço antigas. Metodologias e procedimentos para a sua instalação foram estabelecidos com o objectivo de atingir os requisitos necessários de durabilidade e estabilidade metrológica para o seu

uso em observações de longo prazo, com particular ênfase no desenvolvimento de sistemas de protecção dos sensores. O desempenho dos sensores e suas protecções foi testado em laboratório em termos da exactidão e fiabilidade dos resultados obtidos.

Posteriormente, as soluções desenvolvidas para instrumentação foram implementadas em dois sistemas de monitorização permanentes: um instalado numa ponte treliçada em arco com dois tabuleiros a cotas distintas, constituído apenas por sensores de rede de Bragg (Ponte Luiz I), e o outro aplicado a uma ponte em viga treliçada parabólica suportado em sensores eléctricos (Ponte do Pinhão). Uma vez que ambas as estruturas monitorizadas sofreram processos de reabilitação e reforço, os sistemas de monitorização foram empregues nos ensaios estáticos realizados com vista à avaliação do comportamento das pontes. Complementarmente, foram também efectuados ensaios de vibração ambiental para estimar os seus parâmetros modais. Ambos os programas de ensaio, estático e dinâmico, foram planeados e executados de modo a permitir uma avaliação experimental directa das alterações produzidas no desempenho estrutural entre os estados pré e pós intervenção.

A completa identificação estrutural dos dois casos de estudo foi conseguida com a implementação de modelos numéricos adequados à simulação dos comportamentos local e global suportados nos dados experimentais adquiridos. Para tal, foram estabelecidas estratégias específicas de modelação, que podem constituir directrizes em estudos futuros de pontes semelhantes. Por sua vez, as análises numéricas proporcionaram resultados para a avaliação dos projectos de reabilitação e reforço, e permitiram a validação dos procedimentos de instrumentação implementados e das opções adoptadas na concepção e instalação dos sistemas de monitorização permanentes. Adicionalmente, os modelos numéricos foram utilizados para estimar as forças e tensões nos elementos críticos das duas pontes, gerados pelas acções regulamentares consideradas na fase de projecto, com o objectivo de avaliar o efectivo nível de segurança estrutural.

Acknowledgments

First of all, I am grateful to my supervisor, Professor Joaquim Figueiras, for the support given during the research work, for the confidence in me to lead tasks and make decisions within projects of great responsibility, as well as for the fruitful discussions and for the provided working conditions at the research unit headed by him and, most important, for the motivation always evidenced.

I am deeply indebted to Professor Álvaro Cunha for the experimental data provided that decisively contributed to the enrichment of this work, as well as for his continuous advices and support throughout this journey.

I wish to express greatest thanks to the Portuguese Foundation for Science and Technology for the funds provided through the PhD grant referenced as SFRH/BD/13138/2003.

I would like to thank the construction companies Soares da Costa, SGPS, S.A. and OPCA – Obras Públicas e Cimento Armado, S.A., in charge of the rehabilitation projects implemented on the Luiz I Bridge and Pinhão Bridge, respectively, for the opportunity and assistance provided in the installation of the structural health monitoring systems. All cooperation made available by the bridge owners Metro do Porto, S.A. (Luiz I Bridge), EP – Estradas de Portugal, S.A. (Pinhão Bridge) and REFER - Rede Ferroviária Nacional, E.P.E. (Trezói Bridge), and by the design offices GRID – Consultas, Estudos e Projectos de Engenharia, Lda (Luiz I Bridge) and GEG – Gabinete de Estruturas e Geotecnia, Lda (Pinhão Bridge) is also gratefully acknowledged. The technical assistance gave by FiberSensing S.A., particularly by Nuno Costa, during the installation of the monitoring system in the Luiz I Bridge is also very much appreciated.

I would like to express special thanks to my colleagues and friends Américo Dimande, Hélder Sousa and Filipe Cavadas for their assistance in the execution of some works,

fellowship, sharing of personal experiences and stimulating conversations along the years, which have always concurred for the improvement of this thesis.

The dedication, commitment and work experience of the technician Amândio Pinto were fundamental for the successful installation of the monitoring systems, and consequently they are greatly appreciated. I also would like to thank the Engineer Rémy Faria for his interest and for his helpful support in the load test carried out on the Pinhão Bridge after its rehabilitation.

I also wish to express my sincere gratitude to Filipe Magalhães for his solidarity and friendship, but also for his availability and support in the discussion of the results concerning the dynamic analyses of joint publications. I could not forget, and fail to mention, special thanks to my colleague and friend Diogo Ribeiro, who have shared with me a similar academic career in the last years, for the long hours of good disposition and critical discussion, which owing to his peculiar personality helped me to sail in the most troubled times.

I would like to thank all of my colleagues at LABEST/FEUP that contributed for the good work environment, wise opinions and cheerful conversations, especially to Hélder Silva, José António, Miguel Azenha and Helena Figueiras, and also, to Leonel Ramos of VIBEST/FEUP and to my colleague Clemente Pinto at UBI. Additionally, I would like to acknowledge the precious collaboration of the technical staff of LABEST/FEUP (Alberto Monteiro, Cláudio Ferraz, Cláudia Correia, Marta Poínhas Costa and Maria Vitória Freitas), and in addition I would like to particularly thank to Paula Silva for her patience and help.

Last but not least, a special word of appreciation and affection for the unlimited and unconditioned love, sacrifice and support throughout my entire life from my parents and my twin brother, and more recently from my sister-in-law. I also would like to thank the encouragement, confidence and patience of my close friends during all these years, and I express a special gratitude to my godson Vítor Saraiva and his wife Ana Conde, and to my good friend Ana Sílvia Rocha.

Table of Contents

List of Figures

List of Tables

List of Symbols and Abbreviations

Roman letters

A	Model A (before the rehabilitation); passage A; loading of all spans; cross-sectional area; arch
AASHTO	American Association of State Highway and Transportation
A/D	Analog-to-digital
AD	Arch diagonal
AAGR	Annual average growth rate
Ai	Variant *i* of Model A
ALC	Arch lower chord
ANPSD	Average normalized power spectral density function
ANPSDs	Average normalized power spectral density functions
AREMA	American Railway Engineering and Maintenance Association
ASi	Acquisition system *i*
AUC	Arch upper chord
AV	Arch vertical
B	Model B (after the rehabilitation); passage B
B*	Model B with nonlinear supports
BFD	Basic Frequency Domain method
Bi	Variant *i* of Model B
BOTDR	Brillouin optical time domain reflectometry
B-WIM	Bride weight-in-motion
cm	Centimeter(s)
C	Model C; loading path aligned with the bridge centerline; loading of the centre span; member in compression
c	Distance perpendicular to the bending axis from the most stressed fiber to the center of gravity of the cross-section

CES	Conventional electric strain gage
CFRP	Carbon fiber reinforced polymer
Ci	Sub-model *i*
COS	Central Observation Station
CPU	Central Processing Unit
D	Model D; dynamic loading scenario; loading path in the downstream side; downstream side; cumulative damage
DAFs	Dynamic amplification factors for recorded strain
DASS	Data Acquisition Sub-System
d.c.	Direct current
DH-EG	Transducer measuring the horizontal displacement at the south abutment
DH-EP	Transducer measuring the horizontal displacement at the north abutment
DH-P4	Transducer measuring the horizontal displacement at Pier P4
DH-i	Transducer *i* for measuring the horizontal displacement
DOF	Degree-of-freedom
DOFs	Degrees-of-freedom
DSPSS	Data Storage/Processing Sub-System
DV-Ti	Transducer *i* for measuring the vertical displacement at the deck
DV-TiJ	Transducer for measuring the vertical deflection of the deck span *i* in the downstream side
DV-TiM	Transducer for measuring the vertical deflection of the deck span *i* in the upstream side
E	Young's modulus (modulus of elasticity)
EA-Di	Strain gage *i* placed in a diagonal of the arch
EA-Ii	Strain gage *i* placed in a lower chord of the arch
EA-Si	Strain gage *i* placed in an upper chord of the arch
EA-Mi	Strain gage *i* placed in a vertical of the arch
ECCS	European Convention for Constructional Steelwork
E_{CFRP}	Young's modulus of the CFRP
E_{ea}	Young's modulus of the epoxy adhesive
EFPI	Extrinsic Fabry-Perot interferometer
Ei	Abutment *i*
EM	Electromagnetic
EM-Di	Strain gage *i* located in a diagonal of a suspension tie
EM-Ti	Strain gage *i* located in a cross bar of a suspension tie
EM-Pi	Strain gage *i* located in a leg of a suspension tie

EN1990	Eurocode 0
EN1991-2	Eurocode 1 – Part 2
EN1993-1-1	Eurocode 3 – Part 1-1
EN1993-1-9	Eurocode 3 – Part 1-9
E_n	Young's modulus of the neoprene
E_{nc}	Young's modulus of the new concrete
E_{ns}	Young's modulus of the new-added steel
E_{oc}	Young's modulus of the original concrete
E_{os}	Young's modulus of the original steel
EP	Estradas de Portugal (Portuguese Institute of the Road Network)
EP-Di	Strain gage *i* located in a diagonal of a steel pier
EP-Pi	Strain gage *i* located in a leg of a steel pier
EP-Pi	Strain gage *i* located in a cross bar of a steel pier
E_{rs}	Young's modulus of the reinforcing steel
ES	Electric strain gage
E_s	Young's modulus of the steel
ESGi	Electric strain gage *i*
ESi-j	Electric strain sensor j at section *i*
ET-Ci	Strain gage *i* located in a crossbeam of the deck
ET-Di	Strain gage *i* located in a diagonal of the deck
ET-Ii	Strain gage *i* located in a lower chord of the deck
ET-Si	Strain gage *i* located in an upper chord of the deck
f	Frequency
f_c	Cut-off frequency
FBG	Fiber Bragg grating
FBGs	Fiber Bragg gratings
FE	Finite element
FEM	Finite element model
FEs	Finite elements
FEUP	Faculty of Engineering of the University of Porto
FFT	Fast Fourier Transform
F_{max}	Maximum loading force
FOS	Fiber optic sensor
FOSs	Fiber optic sensors
FOSE	Fiber optic splice enclosure
FOSi	Fiber optic sensor *i*

FOSs	Fiber optic sensors
FP	Fabry-Perot
FPGA	Field Programmable Gate Array
FPI	Fabry-Perot interferometer
FRP	Fiber reinforced polymer
f_y	Yield strength of the steel
g	Gravity acceleration
G_{dl}	Characteristic force or moment generated by the permanent loads
Gi	Strain gage *i*
G_p	Gain factor for pressure
GPa	Gigapascal(s)
GPS	Global positioning system
h	Hour(s)
Hz	Hertz
I	Cross-sectional inertia
IBN	Belgium Institute for the Standardization
IP	Ingress protection
km	Kilometer(s)
km/h	Kilometer(s) per hour
kN	Kilonewton(s)
kN/m	Kilonewton(s) per meter
kN/m^2	Kilonewton(s) per square meter
L	Lower deck
L*	Longitudinal direction
LABEST	Laboratory for the Concrete Technology and Structural Behavior
LC	Load case
LCD	Liquid crystal display
LED	Light-emitting diode
LOS	Local Observation Station
LVDT	Linear variable differential transformer
LVDTs	Linear variable differential transformers
m	Meter(s)
m^2	Square meter(s)
MAC	Modal Assurance Criterion
MAC(0)	MAC indicator correlating the identified and calculated mode shapes before the bridge rehabilitation (numerical estimates from the viability study)

MAC(1)	MAC indicator correlating the identified and calculated mode shapes before the bridge rehabilitation
MAC(2)	MAC indicator correlating the identified and calculated mode shapes after the bridge rehabilitation
MAC(3)	MAC indicator correlating the calculated mode shapes before and after the bridge rehabilitation
MAC(4)	MAC indicator correlating the identified mode shapes before and after the bridge rehabilitation
Mi	Bending moment *i*; Suspension tie *i*
mm	Millimeter(s)
M_{max}	Bending moment at mid-span
MPa	Megapascal(s)
m/s	Meter(s) per second
m/s^2	Meter(s) per square second
$M_{y,Ed}$	Design value of the bending moment about the strong axis
$M_{y,Rd}$	Design resistance for bending moments about the strong axis
$M_{z,Ed}$	Design value of the bending moment about the weak axis
$M_{z,Rd}$	Design resistance for bending moments about the weak axis
n	Number of points for calculating the MAC indicator
N	Loading of the north span
N_{Ed}	Design value of the axial force
n_{eff}	Mean effective refractive index
n_i	Number of cycles associated with the stress range $\gamma_{Ff} \cdot \Delta\sigma_i$ for band *i*
N_i	Number of cycles obtained from the factored fatigue strength curve ($\Delta\sigma_C/\gamma_{Mf}$)
nm	Nanometer(s)
NPSD	Normalized power spectral density function
NPSDs	Normalized power spectral density functions
N_{Rd}	Design resistance for axial force
OS	Fiber optic sensor; Observation Station
OSi-j	Fiber optic strain sensor *j* at section *i*
OTDR	Optical time domain reflectometry
P	Piers; design axial force
PAC	Programmable Automation Controller
PC	Personal Computer
P_E	Euler critical load

P_{ε}	Strain-optic coefficient
Pi	Pier *i*
PL	Pier leg
pm	Picometer(s)
P_{max}	Load capacity of a column
PP	Peak-Picking method
Pt	Platinum
Q	Quasi-static loading scenario
Q_{ll}	Characteristic force or moment due to the remaining variable actions
Q_{SV}	Characteristic force or moment due to the design train in the upper deck
Q_{w}	Characteristic force or moment due to the wind
R	Ratio between maximum stress ranges from the validated and design models; reference section
R&D	Research and Development
REFER	Rede Ferroviária Nacional (Portuguese Railway Administration)
R. F.	Rating factor
R. F.(1)	Rating factor computed using only the mandatory internal axial force or bending moment
R. F.(2)	Rating factor computed taking into account the axial force and the bending moments
RSAEEP	Portuguese regulation for the safety and actions of buildings and bridges
RTD	Resistance Temperature Detector
RTDs	Resistance Temperature Detectors
s	Second(s)
S	Static loading scenario; loading of the south span
SDM	Spatial-Division Multiplexing
S. F.	Safety factor
S. F.(1)	Safety factor computed using only the mandatory internal axial force or bending moment
S. F.(2)	Safety factor computed taking into account the axial force and the bending moments
SGi	Strain gage *i*
SHM	Structural health monitoring
Si	Section *i*
SLED	Superluminescent light-emitting diode
SOFO	Surveillance d'Ouvrages par Fiber Optiques

SSI-COV	Covariance-driven stochastic subspace identification method
ST	Suspension ties
St-Id	Structural Identification
t	Ton(nes)
T	Member in tension; transverse mode
T*	Transverse direction
TDM	Time-division multiplexing
TO	Torsional mode
TS	Temperature sensor
TSi	Temperature sensor at section *i*
TT-Ii	Temperature sensor *i* located in a lower chord of the deck
TT-Si	Temperature sensor *i* located in an upper chord of the deck
U	Loading path in the upstream side; upstream side; upper deck
UD	Upper deck
UDC	Upper deck crossbeams
UDD	Upper deck diagonals
UDLC	Upper deck lower chords
UDUC	Upper deck upper chords
UIC	Union Internationale des Chemins de Fer (International Union of Railways)
UNESC	United Nations Economic and Social Council
USA	United States of America
UV	Ultraviolet
V	Vertical mode
V*	Vertical direction
VIBEST	Laboratory of Vibrations and Structural Monitoring
WIM	Weight-in-motion
WDM	Wavelength-division multiplexing
ºC	Celsius grade(s)
1+φ	Dynamic amplification factor
2D	Two-dimensional
3D	Three-dimensional

Greek letters

α_F	Coefficient of thermal expansion of the optical fiber
α_M	Coefficient of thermal expansion of the material
γ_{Ff}	Partial safety factor for the equivalent constant amplitude stress range
γ_{Mf}	Partial safety factor for the fatigue strength
γ_g	Partial safety factor for permanent actions
γ_q	Partial safety factor for variable actions
$\gamma_{q,1}$	Partial safety factor for variable actions other than train actions
$\gamma_{q,2}$	Partial safety factor for train actions
γ_w	Partial safety factor for wind actions
δ	Displacement; camber of the bar
Δ	Relative percent difference or percentage change
δ_c	Displacements under centered loading per 1000 kN of applied load
δ_{nc}	Displacements under non-centered loading per 1000 kN of applied load
$\Delta\varepsilon$	Strain variation
Δf	Natural frequencies ratio
δ_{FEM}	Displacements calculated by the FE model
δ_i	Displacements measured in test *i* (per 100 kN/1000 kN of applied load)
$\Delta\lambda_B$	Shift of the grating central wavelength
$\Delta\lambda_\varepsilon$	Wavelength variation due to the maximum expected strain
$\Delta\lambda_{is}$	Minimum wavelength interval between two consecutive peaks required by the interrogation system for their accurate identification
$\Delta\lambda_{min}$	Minimum wavelength interval between two neighboring gratings
$\Delta\lambda_T$	Maximum wavelength difference between any two sensors placed in the same fiber lead due to the temperature
ΔK	Modal stiffness ratio
ΔM	Modal mass ratio
Δp	Pressure variation
$\Delta\sigma_{vm}$	Maximum stress range from the validated model
$\Delta\sigma_{dm}$	Maximum stress range from the design model
$\Delta\sigma_i$	Stress range in the model *i*;
$\Delta\sigma_D$	Fatigue limit for constant amplitude stress ranges
$\Delta\sigma_L$	Cut-off limit
$\Delta\sigma_R$	Fatigue strength
ΔT	Temperature variation

ε	Strain
ε_{FEM}	Strain calculated by the FE model
ε_c	Strains under centered loading per 1000 kN of applied load
ε_{nc}	Strains under non-centered loading per 1000 kN of applied load
ε_i	Strain measured in test *i* (per 100 kN/1000 kN of applied load)
ζ	Thermo-optic coefficient
Λ	Grating period (pitch length)
λ_B	Bragg wavelength
$\mu\varepsilon$	Microstrain(s)
μm	Micrometer(s)
ν	Poisson's ratio
ν_{CFRP}	Poisson's ratio of CFRP
ν_{ea}	Poisson's ratio of the epoxy adhesive
ν_n	Poisson's ratio of the neoprene
ν_{nc}	Poisson's ratio of the new concrete
ν_{ns}	Poisson's ratio of the new-added steel
ν_{oc}	Poisson's ratio of the original concrete
ν_{os}	Poisson's ratio of the original steel
ν_{rs}	Poisson's ratio of the reinforcing steel
ν_s	Poisson's ratio of the steel
σ_{dl}	Normal stress due to the permanent load
σ_{dli}	Normal stress due to the dead load in the *i*-th model
σ_{Ed}	Design value of the normal stress
σ_{ll}	Normal stress due to the remaining variable actions
σ_{rd}	Design strength of the steel
σ_{SV}	Normal stress due to the standard vehicle or train
σ_w	Normal stress due to the wind
ϕ_{ik}	Modal coordinates for the *i*-th mode shape
ϕ_{jk}	Modal coordinates for the *j*-th mode shape
ψ_0	Combination factors
Ω	Ohm(s)

Chapter 1

Introduction

1.1. Scope and general considerations

Condition assessment of old steel bridges

Since early ages, case studies of failures have constituted invaluable sources of insight and understanding for the design and construction of structures, particularly the ones with an innovative component (Petroski, 1995). However, during the second half of the 19th century the explicit discussion of the root causes of failures was not pursued, an attitude that is thought to be related with the embarrassment caused at the time by a great number of tragic collapses of railroad iron bridges. Only when a combination of a climate of overconfidence in the state of the art, lack of knowledge, and sum of a series of human errors led to the sudden collapse of the Quebec Bridge in 1907 during its construction, the technical community turn back to properly value once again the failure of real structures as lessons to learn in bridge engineering (Pearson and Delatte, 2006). Indeed, the structural behavior knowledge and the relatively today's high safety are the result of a continuous learning from the successive bridge collapses in history (Biezma and Schanack, 2007). Yet, in the present days advances in knowledge concerning the actual behavior of structures and their safety, in particular for metallic bridges, must not be pushed forward only after the occurrence of dramatic failures or in response to a sequence of smaller errors and/or defects. Collapses such as the one occurred in 2007 with the 40 years old I-35W steel deck truss bridge (see Figure 1.1) over the Mississippi River in Minneapolis are no more acceptable (Astaneh-Asl, 2008).

(a) (b)

Figure 1.1 - I-35W Bridge: (a) Before the collapse; (b) After the collapse.

Although the current infrastructure maintenance and management systems, such as those related to bridges, continue to use the periodic visual inspections as the main source of information, among the technical and scientific communities the view that this approach cannot effectively meet the growing demands of modern societies is consensual. In fact if, on the one hand, the full operational potential of the structures cannot be explored by conservative decision-making processes based on scarce and non measurable information, on the other hand, the financial resources available for repair, rehabilitation, strengthening, upgrade or replacement are increasingly limited (DeWolf *et al.*, 2002). Furthermore, often problems not perceived by visual inspection can only be disclosed through procedures that include the measurement of key quantities. Consequently, the use of non-destructive testing tools is emerging as a valuable solution to assist the assessment of the existing condition of structures, both in terms of the load-carrying capacity and serviceability. Moreover, data obtained through these means are essential for the quantification of parameters and identification of mechanisms that are to be integrated in the numerical studies that support reliable and objective structural evaluation (Farhey, 2005).

The inadequacies usually found in old iron and steel bridges can be generally grouped into the following categories (Ghosh and Ghoshal, 2002):

i. Widespread or localized corrosion due to lack of maintenance, poor detail of the structural elements or inadequate connection between components;
ii. Individual members may suffer from natural deterioration or be damaged due to man-made causes;
iii. Inbuilt structural deficiency, new loading and traffic conditions or novel design standards may require retrofit, strengthening or upgrading works;

iv. Even though the bridge is structurally safe, its geometry is unfit to satisfy the functional requirements of changed traffic demand, as is the case of wider and taller vehicles.

Any rehabilitation plan to overcome these problems must address a set of important issues. Firstly, appropriate details must be adopted in order to prevent corrosion problems at key locations. Secondly, the rehabilitation scheme must be well planed and conceived so that restrictions to the bridge's operation are minimized. Thirdly, whenever possible the total load applied to the structure should be reduced. Fourthly, if the bridge constitutes a historic landmark aesthetics must always guide the rehabilitation solutions to be adopted, and ultimately be imperceptible to the untrained eye. Fifthly, steel should be the eligible material for the engineering work.

In what concerns the structural assessment of old steel bridges typical features and/or problems emerge (Geissler, 2002). The deck system, accomplished either by a concrete deck plate or through a metallic grid floor system, increases considerably the bridge stiffness and contributes as well to its load-bearing capacity, which in turn significantly alters the forces distribution among the primary structural elements. On the other hand, former design practices usually led to a variation of the sectional area of the main girder chords along the bridge according to the dead load bending moment, which may lead in the so-called zero-moment sections to high live load stress ranges and fatigue prone points. In addition, for the large majority of these bridges built at the turn of the 19th to the 20th century fatigue limit state was not an issue addressed in the design and buckling was a phenomenon incipiently known and studied (Helmerich *et al.*, 2007).

In the light of the above, several evaluation studies have allowed to draw a number of conclusions:

i. Because the original design was conservative many old steel bridges are capable of carrying present loads;
ii. If the numerical model of the bridge reflects realistically its behavior the forces acting in the primary elements of the girders tend to be more favorable;
iii. Even though their design did not took into account the fatigue phenomenon, a major topic concerning railway bridges, the use of new methods for its assessment has demonstrated for a large number of structures that safety is assured under today's in-service conditions and has helped to estimate the remaining fatigue life;

iv. Members under compressive forces are generally in need of strengthening, mainly for an adequate reduction of their slenderness.

In this context, it is imperative that the state-of-the-art techniques of inspection, diagnosis, characterization and observation are used with the purpose of identifying, preventing and solving problems affecting existing structures. On the other hand, and perhaps first and foremost, the collection of data as accurately as possible of a structure's condition, or concerning the state of a set of structures representative of an infrastructure cluster, allow for their rational maintenance and management, which translates in reduction of costs and saving of public funding in the medium and long term.

The structural safety assessment of steel bridges is a subject that, although has attracted an increasing attention from the technical and research community in the last decade, has been addressed in a rational and systematic form since the middle of the past century. The American Railway Engineering Association had established at the time a set of rules for rating existing iron and steel bridges lying on the following guidelines (Borges *et al.*, 1955):

i. Strength evaluation would be derived from the analytical calculation of the stresses based on the design;
ii. The information supplied by inspection and testing of the material would be taken into account;
iii. Experimental determination of the stresses in the structure would be performed if necessary.

Since then, a similar procedure was also adopted by the Portuguese National Laboratory of Civil Engineering (LNEC), in which the loading test of a bridge would only be prescribed when the estimation of the structure's safety was not clear and after a strengthening process to check its efficiency. Nevertheless, forty years later the widespread methodology for condition assessment of bridges had not experienced any relevant development, being generally conducted visually and described by subjective indices (Aktan *et al.*, 1996). Bridges rating continued to be supported on the same idealized models and procedures adopted in the design, which did not incorporated the bridges' existing state and actual behavior.

Examination strategies of existing bridges

A new integrated numerical and experimental approach was proposed by Aktan *et al.* (1996) in the beginning of the 1990's, founded on the following:

i. Non-destructive and destructive field testing and structural identification to enable the formulation of a methodology for the bridge condition assessment and reliability evaluation at the serviceability, fatigue and ultimate limit states;
ii. Field-calibrated numerical models, developed for structural identification, in order to understand the real behavior and performance of actual bridges and to quantify relative contributions of different stiffness and resistance mechanisms.

Indeed, several load tests performed on bridges have shown that the actual load-carrying capacity is higher than the one predicted by numerical models, and this safety reserve is often useful in demonstrating the suitability of the structure to meet the requirements (Saraf and Nowak, 1998). Consequently, field testing stands as a useful tool to determine whether restrictions to traffic conditions are imperative, to evaluate the need for repair, retrofit or strengthening, to assist their planning and design, and ultimately to appraise the bridge behavior in its new condition (Sartor *et al.*, 1999).

Shortly after, further efforts sought to conceptualize a damage and deterioration assessment methodology for aged steel bridges (Farhey *et al.*, 1997). A rational approach was developed for accurately identifying and incorporating the effects of material aging and deterioration on the bridge safety evaluation, establishing a connection between the material performance at the microscopic level and the mechanical behavior of a structural element, and ultimately of the bridge as a whole. The proposed methodology comprised the steps that are listed:

i. Structural analysis of the bridge to reveal the critical members;
ii. Extraction of samples from the corresponding regions using a sampling technique that does not compromise the structural safety;
iii. Microstructural analysis;
iv. Mechanical characterization;
v. Microscopic modeling and analysis of the critical regions to disclose the stress concentration and gradient effects.

In recent years, an advance in bridge management has been proposed by Farhey (2005). Given that instrumentation and monitoring of a large bridge population is virtually impossible, the integration of diagnostic for structural-identification-based evaluation through field-calibration still constitutes an optional alternative in bridge management, commonly termed as diagnostic bridge management. However, if a management strategy for a certain type of structures, similar in age, structural system, material characteristics and operating conditions is intended, then a prognostic approach is recommended by

evaluating a representative bridge or a short group of bridges in order to establish a set of baselines. Through failure analysis using a periodically updated field-calibrated model, this strategy provides the analytical capability for predicting structural performance, studying the global and local load-carrying capacity, identifying resistance mechanisms and forecasting likely failure modes.

Although the behavior, diagnostic and proof load tests stand as effective investigative tools for condition assessment, in certain cases they are too expensive and time-consuming to be considered. Moreover, as it is common for steel bridges, if the study is fatigue related or aims at determining realistic dynamic amplification factors and damping ratios, data for an accurate assessment can only be provided by a continuous monitoring of the structure response under in-service conditions over an adequate period (Howell and Shenton III, 2006). On the other hand, monitoring systems installed on bridges for performing load tests can and should be employed in their continuous or periodic observation under normal operation conditions, since the beneficial of the collected information largely surpasses the additional direct costs, which in general are low. Yet, the traffic characterization may constitute an indispensable tool for a good interpretation of the measurements taken from the structural behavior, and therefore some kind of weigh-in-motion system may as well be necessary.

Structural identification

A well conceived numerical model is the keystone of any successful analytical study. Even if the procedures adopted in creating it are thorough and the available calculation tools very powerful, there are always assumptions and simplifications made (DeWolf *et al.*, 2002). Therefore, the usefulness of the model can only be validated by data provided through non-destructive evaluation concerning the actual performance and condition of the structure. This process of quantifying the parameters of a numerical model given experimental information is usually known as Structural Identification (St-Id), and has been defined in a wider sense by Aktan *et al.* (1997) as *"the art of analytically conceptualizing, modeling, designing experiments for measuring, and quantifying structural behavior as well as the phenomena affecting it, in order to make engineering decisions"*. A standard methodology for St-Id is depicted in Figure 1.2. However, at the modeling level, it presents limitations that arise primarily from the materials properties, geometric complexity, uncertainty of boundary and continuity conditions, loading environment and the imperfect knowledge and errors in modeling structures (Catbas *et al.*, 2007). Stiffness and inertia distribution and connectivity within the structure are also major aspects to

attend in order to achieve physical completeness of the model (Aktan *et al.*, 1998). The closer are the predicted and measured data the more representative of the reality becomes the model, and in consequence more reliable are the analyses based on it. Force mechanisms, generically known as load path, constitute one of the most demanding modeling issues as they control the simulation of the structure response, and consequently the accurate estimation of the effects to be checked at the serviceability, ultimate and fatigue limit states.

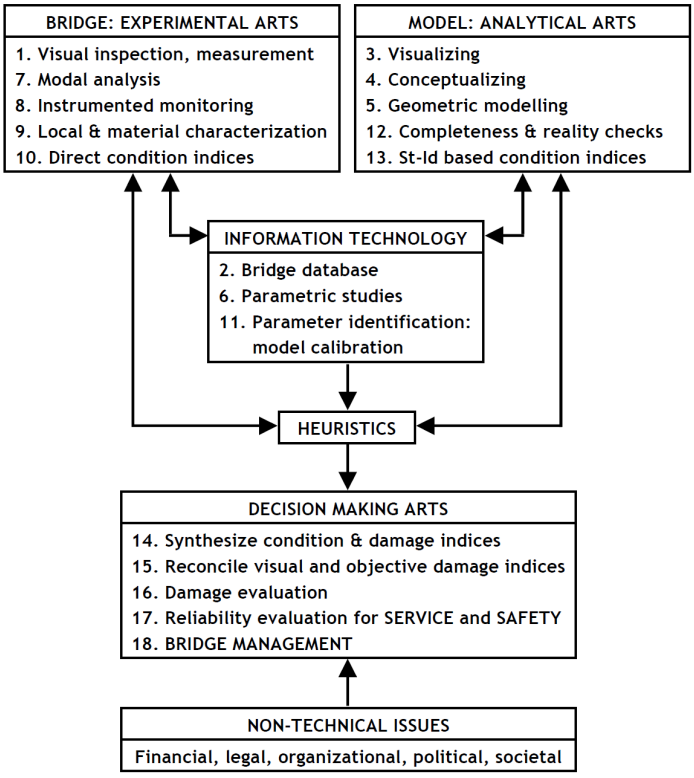

Figure 1.2 - Standard St-Id methodology (Aktan *et al.*, 1997).

Some studies on this subject have been conducted comprising field data collected from critical quantities during load scenarios accomplished by standard, in-service vehicles and finite element model updating anchored in the physical behavior of the relevant properties (Enevoldsen *et al.*, 2002). On the whole, they were orientated towards the evaluation of the:

i. Global distribution of forces in the primary structure;
ii. Interaction between the primary truss-structure and the upper super-structure;
iii. Distribution of sectional forces between the primary and secondary members;
iv. Effects from global and local deformation.

From the results it was possible to conclude that the interaction between global and local effects are substantial and that although the simplifications and assumptions adopted in

the design of such old structures are generally safe in what concerns the primary forces acting on the main load-carrying members, they also lead to the complete disregard of secondary forces responsible for the deformation-induced fatigue cracking (Al-Emrani *et al.*, 2004). On the other hand, for old iron and steel bridges of greater structural complexity as those that integrate cables in their load-carrying systems, the field-measurement of the stress state of some elements is inevitable if a reliable numerical model is intended (Spyrakos *et al.*, 1999).

Another major aspect to consider in modeling a bridge is the detail level to adopt. For physic-based models it may be executed at the macroscopic level (smeared), element level, microscopic level, or a mixture of these approaches, where the predicted quantities may be related to local stresses, strains, and deformations in the actual structure (Catbas *et al.*, 2007). According to Aktan *et al.* (1998) a recommended modeling approach is to represent the critical elements and regions in microscopic detail by taking advantage of the finite elements made available by the software, while representing the reminder of a structure-foundation-soil system in a combination of element-to-element and macroscopic idealizations. Moreover, the discretization level in modeling must depend on the field data used for validation or analysis. If the bridge monitoring is accomplished only by recording global parameters, such as vibrations, deflections or rotations, the model can be simplified using truss, beam or frame elements. However, when strains are measured the adoption of plate, shell or even volumetric elements may be necessary, which calls for greater computing resources. This improvement in the precision of the model is all the more important as the stress concentrations or the forces gradient in the instrumented region tend to rise (Kiss and Dunai, 1998).

Field testing and bridge monitoring

With regard to the monitoring in the context of the experimental component of St-Id applied to bridges, two main fields are well established, usually known as static testing and dynamic testing (Mufti, 2001). The major difference between these two testing strategies is related with the nature of the loading applied to the structure from which the response is to be measured. For the former, the loading is accomplished under controlled conditions and, generally, vehicles placed on the bridge at a crawling speed are used. Regarding the latter, the loads excite the dynamic behavior of the structure and are provided by artificial or natural sources. Some relevant features can be pointed out to each of these testing approaches. While static field testing requires a momentary service interruption, that is not a necessary condition for several dynamic tests, and for some the

bridge normal operation is even useful. The instrumentation setup adopted in dynamic testing is usually less laborious whereas the installation of the monitoring system for static testing is more time-consuming. However, a major advantage of the static field tests is the possibility of investigating the performance of the bridge for loading levels much closer to its load-carrying capacity. Moreover, the data post-processing is easier and it does not involves the utilization of complex software based on powerful mathematical tools.

Static field testing comprises three types of tests: behavior, diagnostic and proof load tests (Chajes *et al.*, 1997). The first type, the most common, is usually performed to appraise the load distribution among various elements of the bridge or to validate some analytical method to adopt, in which the loading level is lower than the maximum for service conditions (Boothby and Craig, 1997; DelGrego *et al.*, 2008). The diagnostic test distinguishes from the first type in what concerns the objective, as it is carried out to identify the effects of component interaction or the causes for a change in the load acting on a component (Chajes *et al.*, 1997; Farhey *et al.*, 2000). A proof load test aims at determining the safe load-carrying capacity of the bridge by gradually increasing the loads, and hence the maximum operating loading scenario applied to the structure frequently surpasses the permitted service loads (Saraf and Nowak, 1998).

Dynamic field testing comprehends two main categories of tests. The first kind is carried out with moving loads, either under service or controlled conditions, to experimentally determine the dynamic amplification factors for different crossing speeds or to collect strain time series to be translated into strain ranges histograms for fatigue analysis (Alampalli and Lund, 2006; Zhou, 2006). The second set of dynamic tests targets the extraction of modal parameters (i. e. mode shapes, natural frequencies and damping ratios) from the vibrations recorded through accelerometers or seismographs. Depending on the excitation source and nature of the bridge's response these tests are classified as ambient, forced or free vibration tests. Ambient vibration testing takes advantage of natural vibration sources (e. g. wind, waves and seismic activity) and of the passing traffic (Catbas *et al.*, 2007; Hsieh *et al.*, 2006). Forced vibration testing is characterized by permitting the control of the input vibration using vibrators, shakers, impulse hammers or dropping masses, but in turn they generally impose restrictions to the normal operation of the structure (Cunha *et al.*, 2001; Ren *et al.*, 2004b). Free vibration testing consists in applying a static pre-deformed shape to the structure followed by the sudden release of the accumulated potential energy, constituting the ultimate experiment for estimating

damping ratios with partial restrictions to the traffic (Aktan *et al.*, 1997; Salawu and Williams, 1995).

Independently of either the loadings acting on the bridge or the component of its behavior to be measured, monitoring can be carried out according to two different strategies based on the frequency with which readings are collected from the structural response.

Typically, periodic monitoring is performed on a regular basis with a predefined periodicity, using field testing, either static or dynamic, or tracking in time the evolution of the bridge's behavior due to the environmental loading and/or rheological properties of the constituent materials. Customarily, this type of monitoring is well suited for detecting changes in the bridge's response caused by normal deterioration, to appraise alterations in it produced by rehabilitation, repair, strengthening or retrofit works, to check their effectiveness and/or efficiency or to verify the performance of an innovative material or technique (Fu *et al.*, 2007).

On the other hand, continuous monitoring is commonly associated to real-time evaluation of the structure's integrity or health, this being understood as the procedure integrated into the monitoring framework that aims at detecting extreme events or sudden damages by taking a short time gap between the data acquisition and the diagnostics (Ko and Ni, 2005). Given the expensive cost associated to this monitoring approach its implementation is only justified when the bridge in question is extremely important, it will likely experience severe actions, it was constructed using a novel technique or undertook a rehabilitation process of which there is limited knowledge, or substantiated concerns exist regarding the structural integrity.

Structural parameters and sensors in bridge monitoring

Monitoring may include the quantification of a variety of parameters, which demand the utilization of a wide range of sensors and transducers. In general, the mechanical response of the bridge is monitored by measuring displacements, rotations, velocities and accelerations, quantities that target the global behavior, or by gauging strains, deformations or crack widths for giving an insight of the local or member's performance. Some parameters are characteristic of static monitoring, as is the case of the deflections in spans, while others are attributed to dynamic monitoring, naturally accelerations. The environmental loading is also a component commonly monitored, which usually comprises the acquisition of data from the temperature, humidity, wind velocity and direction. A new monitoring component that has experienced a great development in

recent years is related to durability issues affecting structures, particularly in reinforced concrete bridges, in which the measurement of the corrosion in the steel reinforcement, moisture content in the concrete or chloride penetration is frequent (Sousa *et al.*, 2011). The selection of the quantities to gauge intrinsically depends on the objectives to accomplish with the monitoring, but also on the time span that it will require (e. g. long-term monitoring calls for temperature measurement). Another key aspect for this decision is the indices to be extracted from the field data, since most of them involve the observation of different quantities using distinct procedures (e. g. influence lines and modal parameters) (Catbas and Aktan, 2002).

In the experimental evaluation of a steel bridge strain measurement is a fundamental component, if not the most important, of any monitoring plan to implement. However, it faces unique difficulties that must be properly addressed in order to obtain meaningful and reliable data. In the first place, unlike concrete structures, strain sensors cannot be embedded in the host material, and therefore unless a specific protection is applied they are directly exposed to the environmental agents. This is particularly true when dealing with old steel bridges since they are usually truss structures that cannot even ensure a primary protection to the gages. In the second place, the structural members exhibit in general strain fields with high spatial gradients, namely near joints and connections, requiring a careful positioning of the sensors. Additionally, truss structures are made of a great number of elements and components that are likely to be instrumented, which calls for a thorough selection of the monitored sections based on an adequate structural analysis.

Nowadays, two main technologies are available for structural monitoring, one relying on conventional electric sensors and the other based on fiber optic solutions. Up to now there is no consensus regarding the best option for steel bridges. However given the unique features of the fiber optic sensors (FOSs) they have become increasingly popular in the last years. Owing to the chemical nature of the optical fiber FOSs are resistant to corrosion, constituting a major advantage for field applications, and present a stable behavior, which is crucial for long-term monitoring (Zhan-feng *et al.*, 2007). Most of the fiber optic systems for monitoring have the ability of acquiring the signals of multiple sensors placed along the same fiber lead (multiplexing property) (Liang *et al.*, 2005). Due to their dielectric nature FOSs are also immune to electromagnetic and radio frequency interferences, which is an attribute particularly important for the monitoring of steel bridges. In addition, FOSs generally exhibit high signal to noise ratio and are very sensitive, with good resolution and accuracy (Deng and Cai, 2007). Nevertheless, electric sensors have also some decisive

points in their favor. For these sensors a great variety of commercial solutions exist on the market, which is usually translated into lower costs. On the other hand, and perhaps more important, given their use for some time there is a history of numerous applications that enable an accurate evaluation of their long-term performance, making possible to choose the best solution available. Also, the data loggers for collecting and storing the signals from electric sensors are much cheaper than the interrogators for FOSs. However, fiber optic systems become economically more competitive when medium-to-large scale bridges are at stake and the number of sensors is high, since the lower cost of the optical fiber and the multiplexing capability play a decisive role in those conditions.

1.2. Motivation and objectives

Bridges constitute key elements in transportation networks as they often control their operationality, efficiency, cost-effectiveness and longevity. Many structures were built in the turn of the 19th to the 20th century due to the fast expansion of the railway lines boosted by both the industrial revolution and the perception that the steel was a relatively cheap material endowed with a strength well suited for the engineering challenges at the time. However, and despite their old age, many of these bridges are still in operation, which poses several problems to the authorities in charge of managing the infrastructures.

In fact, today's traffic conditions on old steel bridges are much more severe than those adopted in their design, either in terms of travelling speed or applied loads (total or by axle). On the other hand, the increasing traffic flow, particularly in what concerns the transport of goods, makes the fatigue resistance a topic of major concern, which is even further aggravated by the fact that designers and constructors of centenary steel bridges were not aware of this failure phenomenon. Furthermore, the evaluation of the load-carrying capacity of compressive members was not accurate, and even safe, since the knowledge of the buckling resistance was incipient at the time. Additionally, the lack of proper maintenance on many old steel bridges over the years has led to serious deterioration problems. In this context, the reliable condition assessment of these bridges stand out as imperative if the following goals are to be achieved (Olofsson and Elfgren, 2008):

i. Increase of the transport capacity;
ii. Extension of the residual service life;
iii. Enhancement of the management, strengthening and repair systems.

To this end, St-Id emerge as a crucial strategy by comprehensively integrating both experimental and analytical tools.

With regard to the rehabilitation and/or strengthening of old steel bridges, and in spite of their intrinsic specificities, the common practice of design and planning often adopts idealized models and assumptions which, although might be admissible in building new structures, can lead to costly solutions, and ultimately conduct to misleading decisions. Moreover, the serviceability and structural safety may not be enhanced as it would be expected by using standard schemes, and in extreme cases may even be downgraded. Therefore, the development of a data base holding a consolidated and objective knowledge regarding the effectiveness and/or efficiency of different rehabilitation and strengthening approaches, as well as the quantification of the changes produced by those in the structural behavior, arises as an emergent need.

Taking into account the context previously described, this thesis sought to accomplish the following main objectives:

- Design, implementation and validation of monitoring systems for old steel bridges, either electric or fiber optic based, in order to obtain accurate estimates of the structural response from data collected during field tests or under normal operation;
- Planning and execution of field tests with the purpose of acquiring experimental data aiming at an objective and clear analysis of the changes produced in the behavior of old steel bridges as a result of rehabilitation and strengthening processes;
- Development of modeling strategies perfectly suited for the type of bridges within the scope of this research work, targeting an accurate simulation of their behavior, both global and local, either static or dynamic, on the basis of numerical tools available in commercial software;
- Assessment of the effectiveness and efficiency of strengthening and rehabilitation schemes that have been adopted in this type of engineering works, and analysis of the validity and correctness of assumptions and methodologies taken on the practice of their design.

Other objectives to attain with this PhD research project are as follows:

i. to conceive and develop new sensors, as well as methodologies for their application, suited to the specific requirements of the monitoring projects implemented on old steel bridges, namely in terms of robustness, reliability, easiness and fastness of installation, with special attention to the attachment technique. For that, numerical tools and laboratory experimentation were employed;
ii. to develop and laboratory test protection systems for shielding the strain sensors attached to the steel surface of the monitored bridge, with the goal of ensuring a control and/or mitigation of the environmental loading on the sensors response, as well as for achieving the durability and metrological stability required in long-term monitoring;
iii. to evaluate the complementarity or redundancy of different field testing techniques for collecting the relevant information aiming at the structural identification of old steel bridges, particularly truss structures, that are in need of rehabilitation and strengthening, before and after the construction works;
iv. to contribute for an improved understanding of the mechanisms governing the forces distribution among the several structural elements, which control the interaction between the different constituent structures of the bridge in terms of load transmission and deformation;
v. to establish which condition parameters should be used to evaluate the performance of old steel bridges according to the proposed objectives, and consequently to identify the most appropriate techniques for acquiring field data from which the indices are to be extracted.

1.3. Outline of the thesis

This thesis comprises an introductory chapter, followed by seven chapters dedicated to the state of art and the research work, either experimental or numerical, ending with a chapter where the conclusions are drawn and future perspectives are pointed out.

The structure of the thesis was conceived so that each of the main seven chapters might be addressed almost independently from the remaining. Thus, each chapter holds introductory and closing sections, which has led to at least one journal paper for each of the main chapters, either published or submitted. However, and occasionally, some issues are treated in different chapters and therefore some repetition arises.

A summarized description of the contents of each chapter is given in the following paragraphs.

Chapter 2 describes and discusses two parallel monitoring systems installed in an old steel bridge comprising two types of sensors: electric and fiber optic. Field data collected by both systems are compared and analyzed with the purpose of drawing conclusions regarding the capabilities and limitations of both sensing technologies for the bridge condition and fatigue assessment. Additionally, some insight on the structural performance is given and an approach to the development of a weigh-in-motion system for a railway bridge is addressed.

Chapter 3 presents the electric based monitoring system implemented in a centenary steel road bridge (Pinhão Bridge), during and after its rehabilitation and strengthening. The guidelines considered in the design of the system and the procedures adopted in its installation are presented. Special attention is dedicated to the laboratory testing of the new strain sensor holders and of their shielding, emphasizing the procedures and methodologies developed for the project.

Chapter 4 is dedicated to the experimental and numerical study of the Pinhão Bridge, performed for the static analysis of the structure before and after the intervention. The procedures for the field testing and the methodology employed to develop and validate the numerical models are highlighted. The effectiveness and efficiency of the adopted strengthening schemes are appraised. In addition, the safety assessment of the bridge for its new condition is made and compared with design estimates.

Chapter 5 is focused on the modal analysis of the Pinhão Bridge carried out for the evaluation of the changes produced in its dynamic properties as a result of the undertaken construction works. The experimental program is described and field data were correlated with the results provided by the numerical models in order to conclude about the impact of the rehabilitation and strengthening on the bridge performance. Furthermore, the viability of using modal information for this task and the suitability of the adopted modeling strategy are duly discussed.

Chapter 6 addresses the design and installation of a fiber Bragg grating (FBG) based monitoring system applied to a centenary steel arch bridge (Luiz I Bridge) during its strengthening and rehabilitation. A brief overview on the application of fiber FBG sensors to steel bridges is made. The principles and requirements that governed the development of the monitoring project are presented. The experimental evaluation of the sensors and

protection systems is focused and the results analyzed. The numerical analyses carried out to support the development of the novel strain sensors are reported. The chapter ends with the presentation of some monitoring results of the bridge response collected during the initial period of the new operation stage.

Chapter 7 deals with the experimental and numerical assessment of a centenary steel arch bridge (Luiz I Bridge), which underwent an extensive rehabilitation and strengthening process in order to integrate its upper deck in the infrastructure of the Porto Metro Light Rail Network. The field tests conducted before and after the construction works are described, focusing on the adopted loading procedures and installed instrumentation. The numerical models developed to simulate the bridge response, and the modeling strategy proposed to improve the replication of the strain fields in the members, are detailed. Important conclusions concerning the changes produced in the structural behavior and the suitability of the implemented strengthening schemes are highlighted. In addition, the safety level of the bridge is evaluated for the new service conditions, based on the validated numerical models and according to the present regulations.

Chapter 8 reports the modal analysis of the Luiz I Bridge. The ambient vibration test conducted after the completion of the rehabilitation and strengthening works is presented, and the differences in relation to the test carried out during the viability study are properly outlined. Field data were used to evaluate the structural changes experienced by the bridge regarding its dynamic behavior, as well as to update the numerical models previously developed. Additionally, these models served to analyze the impact of several structural variables on the modal parameters.

Chapter 9 synthesizes the conclusions of the thesis and lists some topics for future developments.

Some tasks described in some chapters had no direct involvement of the doctoral student, but their description and/or presentation of the corresponding results proved to be essential to achieve the objectives proposed in this PhD research project. From this fact the reader should not conclude that the student was not able to perform these works and is not competent to discuss them. On the contrary, either the tasks were performed before the beginning of the PhD program or were conducted by a R&D unit to which the student is not formally associated. In this respect, and for the sake of clarity of the work herein reported, a list of all the tasks whose participation and responsibility should not be ascribed to the student is presented, as well as their rightful authors.

In **Chapter 7**, the field test conducted before the rehabilitation of the Luiz I Bridge, in the year 2002, was conceived by Prof. Carlos Félix under the supervision of Prof. Joaquim Figueiras. Yet, the results concerning this test that are presented in this work were processed from the raw data by the doctoral candidate.

In **Chapter 5**, both ambient vibration tests were carried out by the R&D unit VIBEST under the direction of Prof. Álvaro Cunha, as well as the field data processing and the extraction of the corresponding modal parameters, whose execution is attributed to Prof. Filipe Magalhães.

In **Chapter 8**, the first ambient vibration test took place in 1999, and was conducted by Prof. Rui Calçada under the guidance of Prof. Álvaro Cunha. As regards the second testing program, carried out just after the bridge rehabilitation, the VIBEST was responsible for its planning and preparation, with the doctoral student also engaged in its execution. Yet, the data processing and subsequent estimation of the modal parameters was accomplished by Prof. Filipe Magalhães.

Chapter 2

Appraisal of electric and fiber optic strain sensors

2.1. Synopsis

Old steel bridges that integrate the existing railway lines are structures built with materials that are no longer used and whose knowledge has being lost over the years, often presenting severe problems of deterioration and subjected to loading environments very different from those for which they were designed. In this context, adequate strain monitoring is a crucial tool in supporting the behavior characterization and safety assessment of these structures.

This chapter presents and discusses the monitoring systems installed in the Trezói Bridge, within a research project aimed at developing and applying procedures for evaluation of the structural integrity of steel railway bridges. The field observations of the structural behavior were accomplished by using two different types of sensors: electric and fiber optic strain sensors. The electric monitoring system was designed and installed on the bridge to supply the experimental data for the research project, while the fiber optic monitoring system was firstly applied to evaluate the reliability of the former and to check its efficiency, and secondly to provide some redundancy of the measurements at critical locations. The obtained results are analyzed to characterize the bridge behavior and the capabilities and limitations of both types of sensors to acquire the relevant data for the bridge service condition and fatigue assessment are discussed, namely in what concerns the ability to accurately capture the static and dynamic components of the structural response and the frequency content of interest.

2.2. Introduction

2.2.1. Economic context

Bridges are fundamental elements for building transportation networks but also play a decisive role in their operationality, efficiency, cost-effectiveness and longevity. These aspects are even more significant when it comes to rail networks. The electrified network comes up as the best natural option to transport goods and passengers since it is less dependent on non-renewable energy sources which became a mandatory issue to account for in developed countries. On the other hand, the recent guidelines for environmental protection related with human consumption and waste production, are based on three concepts: reduction, reuse and recycling. In this perspective, bridges can and should be seen as products used by modern societies, and therefore maintenance, rehabilitation, strengthening and upgrading of existing structures should be preferred to their decommissioning and replacement.

2.2.2. Key problems concerning in-service old railway bridges

At the present time, old railway bridges are being subjected to live loads very different from the ones established in their original design. Not only the traffic flow has increased but also the characteristics of the crossing vehicles are diverse and their operating speed and axle loads are higher (Alampalli and Lund, 2006; Olofsson and Elfgren, 2008). Thus, the need for reliable and updated data related with current traffic patterns is crucial for any evaluation to be made, in particular the fatigue related one (Tobias *et al.*, 1996).

As it is well known, fatigue in steel structures depends on the stress distribution among their constituent elements under transient loads, mainly those caused by passing vehicles, as well as on its fluctuation in time. These forces induce strain/stress cycles in the material that can lead to fatigue cracks and their propagation at the points where amplitudes reach higher values, typically in connection details. Furthermore, these areas are frequently more prone to material degradation, and consequent cross-section loss, which reduce the load-carrying capacity (Farhey *et al.*, 2000).

Accurate evaluation of the structural condition of an element or connection, in special their fatigue resistance, is of great importance for the bridge assessment. Guidelines as part of an integrated fatigue assessment for old structures are already available, of which the most relevant are AREMA (2011), AASHTO (1992) and ECCS (2008). These documents

draw attention to strain field measurement as a mean of collecting reliable data concerning the structure behavior. One of the most important aspects that distinguishes these structures is the material they are made of, since many of them are more than one hundred years old. The knowledge of its properties is sometimes deficient among most technical actors, especially the youngest (Helmerich *et al.*, 2007).

2.2.3. Monitoring for assessing and management

Until recently, bridge management had been relying mainly on periodic visual inspection, idealized modeling and simple analysis. Evaluation based on structural identification provided by field observation was only an optional action even if the bridge was suspected of being structurally deficient (Farhey, 2005). This conventional procedure often led to incorrect decisions, both in safety and costs. Thus, in the last decade health monitoring has become an integrated tool within several management systems (Costa *et al.*, 2006; Wong, 2007). Monitoring data made available by a well designed and implemented observation system can be used for reliability assessment and to update prediction models (Frangopol *et al.*, 2008; Spyrakos *et al.*, 2004), as well as to detect symptoms of any risk to the structure and its users (Aktan *et al.*, 2000). Moreover, loads acting on the structure may also be measured in order to accurately characterize the loading environment (Tobias *et al.*, 1996).

The electric based monitoring systems installed in steel railway bridges are prone to present unwanted noise in the signals caused by electromagnetic interferences, due both to the material nature and to the fact that railway lines are electrified (Mufti, 2001). For this reason, the fiber optic based instrumentation for railway steel bridges has being preferred, since immunity of such sensors to this phenomenon is well known (Shehata and Rizkalla, 1999). One example of a successful field application is the strain monitoring sub-system based on Fabry-Perot optic sensors deployed on Wuhu Yangtze River Railway Bridge, in China (Zhan-feng *et al.*, 2007). Costa *et al.* (2006) have also applied an extensive and comprehensive monitoring system to a centenary steel arch bridge, comprising fiber Bragg grating (FBG) sensors, to assist the evaluation of the rehabilitation operations performed on the structure and to appraise its behavior under the new exploitation. A fiber optic monitoring system has been installed on the Tsing Ma Bridge, the world longest road and railway suspension bridge, in order to assess the possibility of using the FBG sensors developed by Chan *et al.* (2006) for structural health monitoring, and Tsamasphyros *et al.* (2006) have implemented a study to investigate the applicability of

FBG sensors on a late 19th century steel railway bridge located at Nea Peramos near Athens in Greece.

2.2.4. Objectives and scope

As mentioned before, the problems concerning the in-service railway steel bridges are in need of urgent attention. European project Sustainable Bridges (Olofsson and Elfgren, 2008) is one recent example that aimed at bringing additional knowledge on this matter. Its ultimate goals were to:

i. Increase the transport capacity of existing bridges;
ii. Extend the residual service life of structures;
iii. Enhance management, strengthening, and repair systems.

At national level, officials are now beginning to be aware of the necessity to develop more extensive programs to deal with specific problems of aged railway infrastructure. Even though some efforts have been addressed to modernize the Portuguese network, several of its structures do not benefit from major interventions for decades, and as a result may not meet the current requirements for railway transportation. In this context, a research project has been performed aimed at developing and applying procedures for assessing the structural integrity of railway steel bridges within the national railway network, taking into consideration fatigue resistance and remaining fatigue life under past, present and expected loading environments.

For this study a bridge was selected as test bed. The structure was opened to the public in the middle of the last century, and is located on the international Beira Alta route, nowadays the principal rail connection of the country to Europe. In a first stage, records of train induced vibrations and data collected by an ambient vibration test were used to validate and update a 3D finite element model of the bridge, thus making possible the simulation of the bridge dynamic behavior and fatigue analysis (Marques *et al.*, 2009). The second stage and respective preliminary results are to be presented in this chapter. For this stage a monitoring plan was designed and implemented in order to continuously collect steel strain records induced by railway traffic. The established objectives are as follows:

i. To characterize the structural behavior, both local and global, and thus to enable the improvement of the numerical model previously developed;
ii. To check strain/stress paths and patterns in critical elements and connections;
iii. To obtain experimental strain/stress histograms suitable for fatigue analysis;

iv. To gather data concerning the crossing vehicles in terms of speed, moving direction, number of axles and distances between them.

To accomplish the outlined goals two parallel monitoring systems were deployed, the first based on electric strain gages (primary) and the second constituted by fiber optic strains sensors (secondary). The sensors were applied to cross-sections of bars which experience the higher tensile stress ranges, near the joints and at a quarter and half-length. In addition, rails sections in the vicinity of both abutments, but outside the bridge, were instrumented with strain gages.

The results obtained with both installed systems, electric and fiber optic based systems, are presented and, through their confrontation, some conclusions related to the advantages and disadvantages of each system are drawn, mainly regarding the feasibility of using the primary monitoring system to meet the experimental goals established within the research project. In this chapter the monitoring plan and procedures are analyzed and discussed, which includes options related to the installation techniques, sensors, sampling frequency of the signals and observed sections. The quality of the strain readings to support fatigue analysis through the concept of damage accumulation, making use of counting algorithms for strain/stress ranges, is discussed. Finally, the most significant features of the observed structural behavior are pointed out, and the reliability of the traffic data extracted from the adopted instrumentation is evaluated.

2.3. Test bridge

The bridge is located near the village of Trezói in the center of Portugal, and is in continuous operation since August 20th of 1956. Its construction was accomplished with funds from the Marshall Plan, and took place during the decommissioning and substitution of all bridges in the same route, built by Eiffel House. The new larger structures, including Trezói Bridge, were designed, manufactured and assembled by the German House Fried Krupp (Marques *et al.*, 2009).

Figure 2.1 - General view of Trezói Bridge.

Two inverted Warren truss girders, 5.68 m high and 4.40 m apart between axes, constitute the steel deck of the bridge. Its total length is 126 m, comprising two extreme spans 39 m long and one central span 48 m long. The girders panels are 6.50 m wide in the central span and 6.00 m in the end spans. Two trapezoidal shape trusses acting as piers and two granite masonry abutments transmit the loads carried by the structure to the foundation (see Figure 2.1). All connections between the elements are riveted.

The superstructure's bearing supports are made of steel, allowing free rotations in the structure plane (see Figure 2.2(a)). At the east abutment the longitudinal displacements are constrained whereas at the west abutment they are permitted to embrace the deformations caused by thermal action. The connections between the deck and the piers tops are hinged, as well as their connections to the granite masonry bases, therefore behaving as pendula.

(a) (b)

Figure 2.2 - Details of the bridge structure: (a) bearing placed at the west abutment; (b) lower joint of the truss girder instrumented with strain sensors in its vicinity.

The chords and diagonals of the truss girders are formed by double "C-shape" sections, whereas the crossbeams that connect the top of the girders as well as the stringers resting on them are "I" profiles. The verticals are "H-shape" sections and the horizontal bracing of the chords is accomplished with angle bars. Figure 2.2(b) shows a typical joint of the truss girders at the bottom chord. The two stringers that carry the live loads are aligned with the rails of the single track.

2.4. Monitoring system

2.4.1. Framework

In an initial stage of the research project the analysis of the bridge dynamic behavior was performed with results obtained through an ambient vibration test. The collected data allowed the calibration of the finite element model, having as reference the natural frequencies and the corresponding mode shapes. The accomplished numerical analyses took into consideration the dynamic interaction between the passing vehicles and the structure, and the results were used to evaluate the remaining fatigue life of the most critical connections (Marques *et al.*, 2009).

The railway actions considered in the first stage of the project were based on information made available by REFER (Portuguese Railway Administration) and on traffic scenarios and load models established by the European design codes. With the purpose of conducting a fatigue assessment more adjusted to the actual operational conditions of the bridge, it became imperative to characterize the actual passing traffic. To this end, the monitoring system was designed to allow the collection of data on vehicle characteristics, including number of axles and their spacing, the velocity spectra, the moving directions and traffic density.

Traditionally, a strain monitoring system conceived for collecting railway traffic data consists in instrumenting the rails through an experimental setup usually referred to as strain gauge shear bridge configuration. This technique was used by Tobias *et al.* (1996) to measure the loading spectra to which railway bridges in North America are subjected to. Though capable of extracting the wheel loads it also requires a large number of sensors, and therefore of reading channels, which strongly determines the development of a comprehensive monitoring system, designed not only for weigh-in-motion purposes. Moreover, the measured forces automatically hold a dynamic component, enhanced by

possible wheel defects, making difficult to obtain the vehicles weight loads (Barke and Chiu, 2005), which were the values targeted in this project. In this context, the adopted strategy consisted in assessing the rail foot bending strains at half-span sections between sleepers, separated by an adequate distance. The system has been used successfully by Tam *et al.* (2007) to provide information on the loading and traffic status of the passenger cars crossing the Kowloon-Cantoon railway network at Hong Kong. Although this system is also able to gauge the axle loads, provided that proper and periodic calibrations are performed, the reliability of the results is questionable since the sleepers supports may experience non-linear behavior. Therefore, in this project the estimation of vehicle loads is to be accomplished through back-analysis of the measured response of the structure, supported on the finite element model duly validated, having as input the data collected during the crossing of each train.

The stresses computed in the numerical analyses to assess the fatigue damage can be considerably different from the values experienced by the structure's material. This fact is even more relevant when the models are validated with parameters only characterizing the global behavior, as it was performed in the first stage of the project, disregarding the forces distribution in the structure's elements (load path). To overcome this shortcoming, the monitoring system installed in the bridge was devised with the purpose of collecting satisfactory results of the structural behavior, both local and global, aiming at an accurate characterization of the static and dynamic response, in order to evaluate the fatigue in the connections where damage has a higher probability to emerge.

The initial design of the monitoring system for this project comprehended electric sensors only. However, taking into consideration the aforementioned aspects, a redundant fiber optic based observation system for some points to be assessed became a rational option, serving as a reference in order to disclose any related problems. Furthermore, this sub-system was envisaged to provide complementary readings on structural performance.

The installation accomplished for both observation systems was not planned to support a long-term monitoring, although protective solutions for the sensors were adopted. Continuous observations of 2-week periods during 1 year are expected to allow a complete characterization of the passing traffic over the bridge, as well as of the structure response to it.

2.4.2. Monitored sections

For assessing the bridge behavior and to characterize the moving vehicles running on it, 18 cross-sections were instrumented with strain sensors. In the rails, the gages were applied in 8 sections (sections S1 to S4 and S14 to S17), 4 near the west and 4 near the east abutment (see Figure 2.3), 2 per rail and 1.20 m apart. In the bridge, 10 bar sections of the northern truss girder were gauged, 5 in the upper chord at the support region (sections S10 to S13) and at mid-span (S6'), and the remaining in the lower chord at the middle region of the central span (sections S5 to S9). In all observed sections the applied gages were electric resistance sensors, except in section S6 for which fiber optic sensors were also attached. Section S6' in the upper chord, in correspondence with S6, is instrumented with fiber optic sensors only. Figure 2.3 illustrates the layout of the bridge instrumentation.

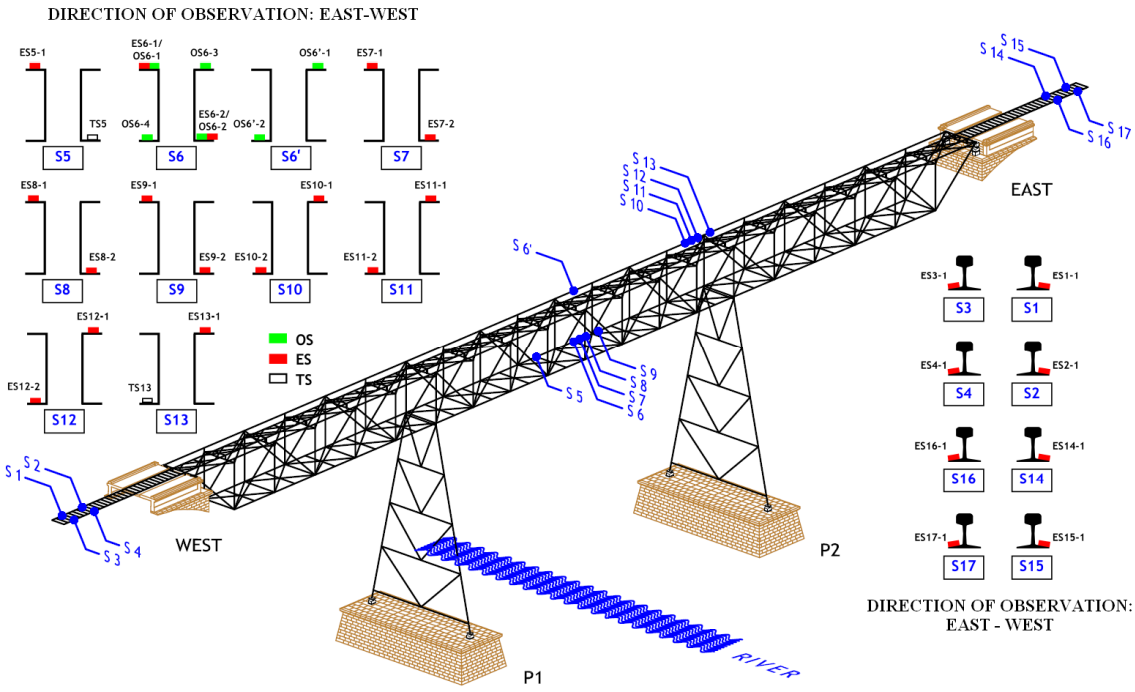

Figure 2.3 - Location of the 18 instrumented sections and corresponding distribution of the sensors.

The monitoring plan also comprised the measuring of the temperature. Two sensors were applied on the steel surface in sections S5 and S13, labeled as TS5 and TS13, and other two were used to appraise the air temperature in the vicinity of these sections (see Figure 2.3).

2.4.3. Strain and temperature sensors

The installed electric strain sensors, herein referred to as ES, consist of traditional 12.7 mm long foil strain gages pre-glued to rectangular epoxy bases acting as sensor

holders, and placed in their gluing face, as illustrated in Figure 2.4(a). These surface mountable sensors have already embedded the electric wires that connect to the sensing network for acquiring the signal, not requiring any soldering operations at the field. These features allow a more quick and flexible installation of the gages, assuring a more robust and safe application, and making possible their attachment in harsh environmental conditions. The foil strain gages used in the sensors fabrication were selected so that accuracy and stability required for dynamic measurement might be assured during the time span of the project.

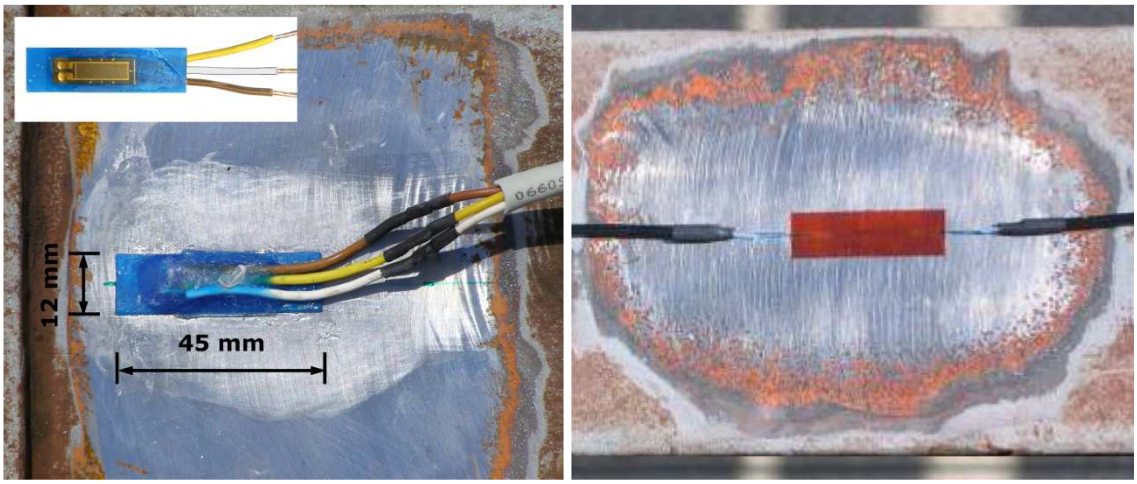

(a) (b)

Figure 2.4 - Sensors applied in the structure: (a) electric strain sensor (ES); (b) fiber optic strain sensor (OS).

The fiber optic strain sensors chosen for this project have the fiber optic grating protected and back supported on a polyimide base. The bare fiber with the 10 mm long grating written on it is not fixed to the polyimide base, thus allowing its direct and free gluing onto the surface to be assessed. These fiber optic strain sensors present similar characteristics to the common foil strain gages (FiberSensing, 2009). Henceforth the fiber optic sensors will be referred to as OS. In Figure 2.4(b) a fiber optic sensor applied to a bridge section is shown.

The four adopted temperature sensors (TS) for this application were platinum resistance temperature detectors Pt-100.

2.4.4. Installation procedure

The installation of both electric and fiber optic strain sensors, was performed in agreement with the following procedures:

i. Preparation of the surface to be instrumented – removal of the steel coating and traces of corrosion, followed by cleaning with water based solutions to eliminate dust and grease;
ii. Attachment of the sensors with an acrylate based adhesive by applying mechanical pressure to assure a suitable bonding contact;
iii. Protection of the sensors to prevent moisture ingress and direct sun radiation, accomplished with pliable butyl rubber sealant over a thin layer of epoxy resin, coated by aluminum tape;
iv. Protection of the steel in the surrounding area of the sensor through epoxy painting.

The performed application is depicted in Figure 2.5(a) and (b).

(a) (b)

Figure 2.5 - Sensors installation: (a) strain sensors ES6-1 and OS6-1 in section S6 during the gluing process; (b) final aspect for sensor ES9-1 in section S9.

2.4.5. Data acquisition

For acquiring the signals from all electric sensors a SCXI® measuring unit of National Instruments™ was used. This logger has the ability to perform a continuous recording of the readings with sampling rates suitable for dynamic observations. The control application of the acquisition system is accomplished by the graphical programming language LabVIEW®, well fitted for user developing.

The interrogation system selected for the fiber optic sensors was the sm130-500 model developed by Micron Optics, Inc. This equipment integrates a broad band light source, an optical spectrum analyzer and a CPU unit to record the reflection spectrum. The fibers

containing 6 sensors, with different Bragg grating wavelengths for each sensor, were connected in series to a single patch cord by using mechanical connectors, thus resulting in one single optical branch to be scanned. The simultaneous interrogation of the sensors was achieved via wavelength-division multiplexing, between 1520 and 1570 nm.

In the present field application, the time series were collected for all sensors, both electric and fiber optic, with a scan rate of 100 Hz, except for temperature sensors whose signals were measured every 5 minutes.

2.5. Analysis of results

2.5.1. Introduction

The structural response of the bridge due to the railway traffic was monitored in two different observation campaigns. The first one was carried out just after the sensors have been installed. During this period the vehicles speed was restrained to 30 km/h for safety reasons (Dimande *et al.*, 2008b). In a second stage, and without any constraints for the traffic speed, data was acquired to enable the characterization of the bridge behavior under normal operation conditions (Dimande *et al.*, 2008a). The monitoring aimed to observe the effects caused by different sets of railway vehicles in the instrumented points and sections, representative of passenger and freight trains using the route in both directions.

Two different train passages characteristic of the actual traffic are object of analysis, one for each of the two aforementioned observation stages. The first corresponds to a freight train crossing, moving in the west-east direction with an average speed close to 29 km/h, referred to as passage A. One locomotive, 6 open-topped wagons and 5 tankers comprise the 38 moving axles. The second is a passenger train crossing, composed by one locomotive and 4 coaches, each one presenting 4 axles, moving in the east-west direction at a speed of 90 km/h, designated as passage B.

This section only deals with field data collected during the aforementioned monitoring campaigns. The comparison of experimental results with FEM estimates can be found elsewhere (Marques *et al.*, 2011).

2.5.2. Rail strains and traffic data

Train speeds, number of axles, and correspondent distances between these were determined from the data collected by the strain sensors installed on the rails.

In Figure 2.6, the rail strains measured in sections S3 and S4 during the passage B are presented. It is possible to observe that the two time series are out-of-phase, and that section S4 is the first to experience the effect of the train crossing. Given the relative position of the rail sections one can infer that the train was heading west (see Figure 2.3). Figure 2.6(a) also reveals that the number of peaks is in correspondence with the number of axles of the train, in this case 20. The maximum strain level per axle is higher than 90 με and the signal-to-noise ratio is very high. Figure 2.6(b) presents the measured points collected after passing the first 4 axles, which are the heaviest of the train and belong to the locomotive. It is clear that the measured points describe adequately the rapid variation of the strains during the train crossing. The identification of peak values, as well as the corresponding time-instants, is achieved with minimum error in both records.

A point to note is the presence or absence of permanent deformations after the passage of trains, which is generally acknowledge as an indicator for possible settlements of the sleepers and non-elastic behavior of the ballast. In this case a total recovery of deformation was achieved. However, for some sensors in some passages it was possible to record residual values with some significance. That points for the difficulty in using the adopted instrumentation scheme for a reliable measurement of the axle loads.

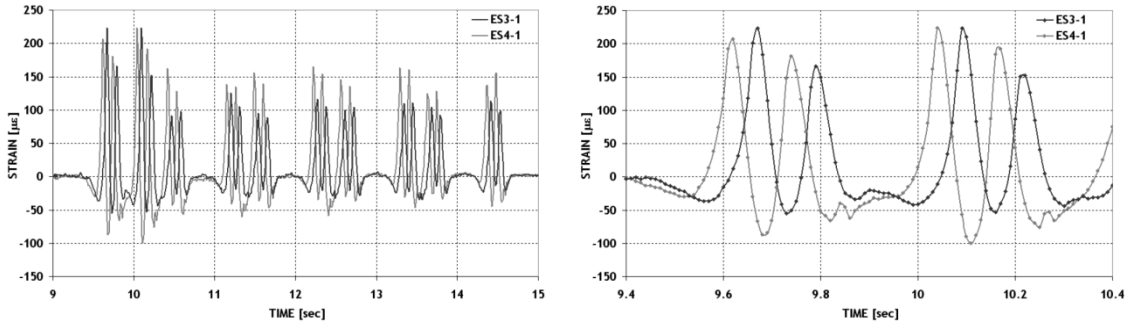

(a) (b)

Figure 2.6 - Rail strains measured in sections S3 and S4 during the passage B: (a) complete time series; (b) zoom window (first four axles).

Vehicles speed can be obtained by adopting the following assumptions:

i. The maximum effect generated by an axle in the strain measured by a sensor occurs when the axle is located directly over the sensor;

ii. At the instant in which the strain reaches its maximum value only one axle contributes to the sensor response, i.e. there is no overlapping of effects caused by different axles;

iii. The time-lag between peak strains captured by two sensors installed in the same rail, induced by a single axle, is the time required by this to move between the two instrumented sections:

iv. For each axle an estimate of the speed can be obtained, which enables to determine possible variations of this parameter throughout the crossing.

Figure 2.7(a) shows a projection of the speeds for the 20 axles of the train in passage B, obtained in each of the abutments, and taking the average of the estimates provided by the two instrumented rails. Values are very similar, with differences of less than 5 %, which indicates that the train did not experience any significant slowdown or acceleration while was crossing the deck. Furthermore, the data plotted in the graph also demonstrates that the posted limit for the speed of 90 km/h, set by the officials that operate the route, was not exceeded by the moving train. For all the monitored train crossings identical results were obtained, and therefore the proper functioning of the equipment that controls the train speed over the bridge could be confirmed.

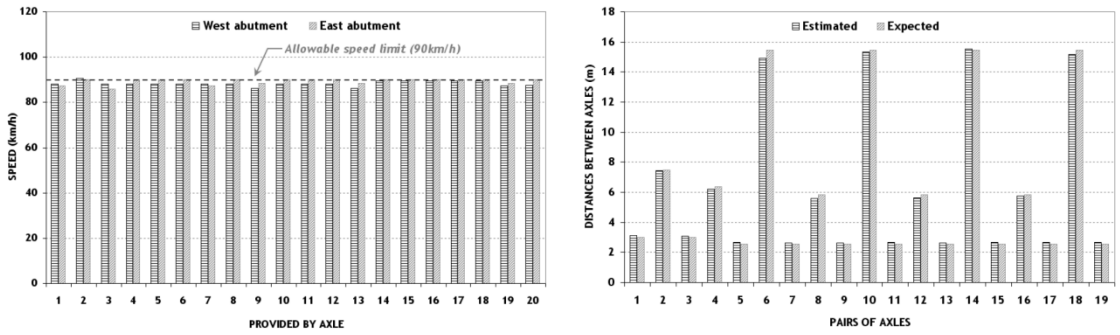

(a) (b)

Figure 2.7 - Traffic experimental data for passage B: (a) estimates of the average speed provided by each axle at each abutment; (b) average distances between consecutive axles: estimated and expected values.

Knowing the speed profile of the vehicle axles it is possible to determine the distances between them. For each one of the 8 sensors placed in the rails, estimates of the loads geometry can be obtained. For this purpose, an average of the estimated speeds for each pair of consecutive axles in each abutment is considered. The graph in Figure 2.7(b) compares the values estimated from the experimental data against the ones corresponding to the standard geometry of the train, constituted by 1 BS5600 locomotive and 4 carriages Corail type. The difference in percentage between the estimated and

expected values is less than 5 %, and therefore the results can be considered of good quality. It is also worth mentioning that, in general, the shorter distances (spacing of the bogies axles) are overestimated whereas the larger ones (between bogies) are undervalued.

The signals scan rate adopted in the acquisition of the data used to characterize the traffic proved to be well suited, given that it made possible the collection of the relevant values to their estimate, peak values and corresponding time-instants, without generating a massive amount of data. However, if there was a need to increase the resolution and/or accuracy of the speeds and distances estimates, then it would be advisable to acquire the signals with a higher sampling rate. Moreover, increasing the distance between instrumented sections of the rails minimizes the error in estimates of axle average speeds for lower acquisition frequencies.

2.5.3. Strains at the middle of the central span

The plots in Figure 2.8 present the strains collected by fiber optic sensors, installed in the upper and lower chords of the northern truss girder at the middle of the central span (see Figure 2.3), for the two passages under analysis.

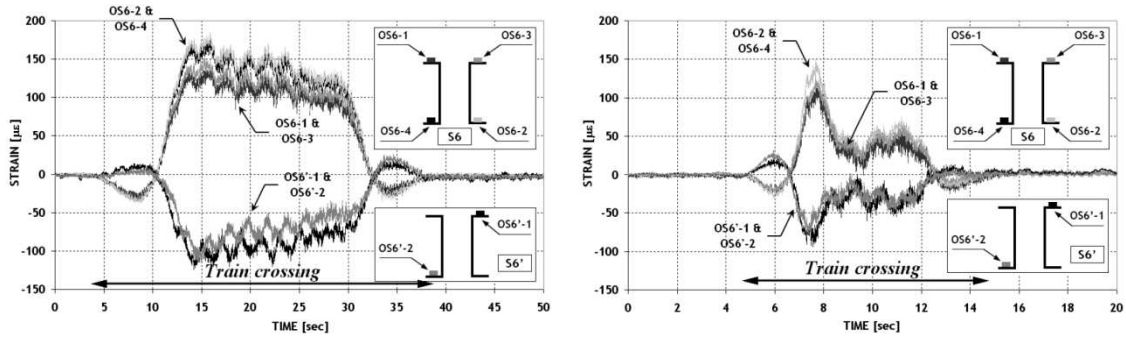

(a) (b)

Figure 2.8 - Strains collected by fiber optic sensors in section S6 and S6': (a) freight train moving in west-east direction with an average speed of 29 km/h (Passage A); (b) passenger train moving in east-west direction with a speed close to 90 km/h (Passage B).

In both graphs it is clear that during most of the vehicle crossing upper chord strains are negative, whereas for the lower chord the values are positive, revealing that for this deck section the upper bars act as a compressive flange and the lower ones constitute the tensile flange. However, even though cross-sections are equal and located on the same vertical alignment, the level of strain experienced by the chords is substantially different, 35 % less for the upper chord with respect to the lower one. This shows that elements

which are considered to be secondary, as they are responsible for guiding the loads to the main structure, in fact play a relevant role in the cross-section equilibrium of the deck under service conditions.

By focusing only on strains measured in section S6 it comes clear that readings of sensors placed at the same level agree fairly well, which proves the absence of relevant out-of-plane bending. For both sections the strains are higher for the outer flanges, pointing for the existence of positive in-plane bending in both chords.

Also, it is worth mentioning another significant difference in behavior between the two observed sections. While strain cycles, perfectly distinguishable in passage A, are in phase for all readings collected in section S6, the opposite occurs in section S6'. This suggests the existence of two bending components, one steady and the other transient, the former appearing in both sections and the latter only in the upper chord. This behavior seems to indicate that rotations at the nodes of the lower chord present a quasi-uniform value during the train crossing, whereas at the upper chord they vary considerably.

2.5.4. Strains in chords submitted to tensile forces

The static strains measured by electric sensors attached to chord sections at maximum bending regions of the truss girder are plotted in Figure 2.9. These values were obtained by running a 2nd order low-pass Butterworth filter with a cutting frequency of 1.0 Hz on the raw signals.

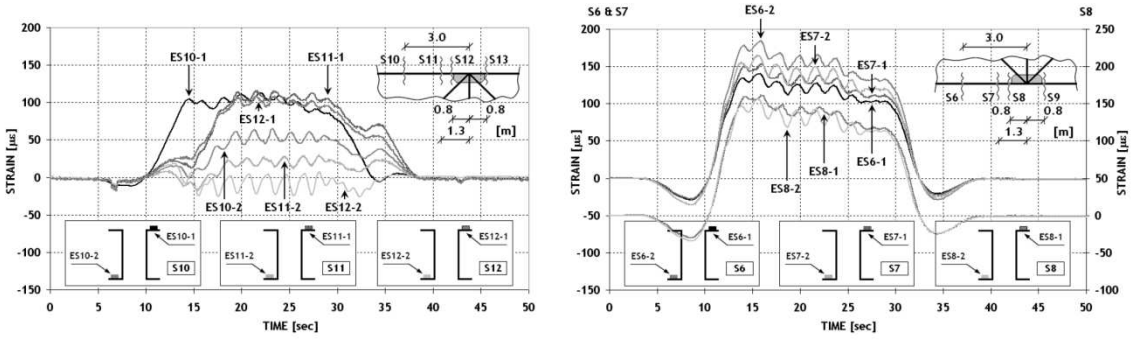

(a) (b)

Figure 2.9 - Static component of the strains recorded by electric sensors in tensile bars during passage A: (a) upper chord in the support region of the truss girder; (b) lower chord in the mid-span region of the truss girder.

For the upper chord sections, strains collected in the upper and lower flanges are very different. First, the maximum strain level experienced by the upper flange along the chord

remains almost constant, whereas the lower flange presents a progressive decreasing towards the joint, reaching even negative values. Second, for all sections upper and lower flange strain cycles have local extremes at the same time-instants. This points for in-plane bending of the bar caused by the continuous crossing of axle sets. Third, strain history recorded by sensor ES10-1 seems to be displaced in time by 5 s in relation to the other readings. Such reveals a high chord bending as the train enters the center span.

In what concerns lower chord sections, all sensors measured maximum strain values of the same magnitude. As the section is located closer to the joint the difference between the lower and upper flange strains diminishes. At the joint the relative magnitude of the flange strains is inverted, i.e. the upper flange becomes more strained than the lower one. At last, flange strain cycles are in phase at section S6 but have a time-lag for the remaining.

2.5.5. Comparison of strains measured by electric and fiber optic sensors

In this section some results obtained with fiber optic and electric sensors installed in section S6 are presented, the differences between them are discussed and likely causes for their existence are indicated.

Figure 2.10 shows the time series collected for the two different train passages, representative of each monitoring campaign. By observing both graphs it is possible to perceive that in the time history segments collected by the sensors applied in the same point, average readings present similar values, i.e. gages placed side by side experience in average the same input deformation, not depending on its electric or fiber optic nature. On the other hand, the fiber optic sensor data apparently have in both records a more perturbed signal when compared with the corresponding signals from electric gages, strongly suggesting the existence of noise, and therefore questioning one of the major advantages consensually endorsed to fiber optic measuring techniques. In what concerns to the mechanical behavior of the instrumented section, the results reveal that bar deformations present a relevant bending moment component, since sensors at different cross-section levels present unequal readings, which should be inexistent in a pure truss system. This issue has been already addressed in previous sections.

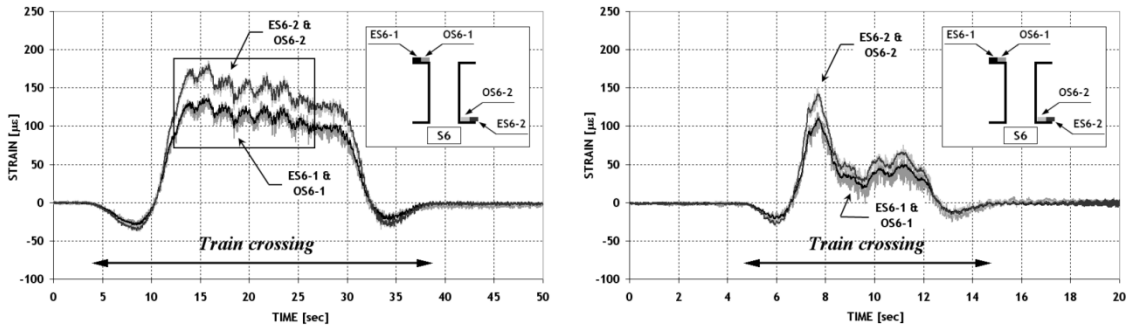

(a) (b)

Figure 2.10. Time series obtained by sensors installed in section S6: (a) freight train moving in west-east direction with an average speed of 29 km/h (Passage A); (b) passenger train moving in east-west direction with a speed close to 90 km/h (Passage B).

For a better understanding of the differences between the signals acquired by sensors of both systems, a spectral analysis in the frequency domain is necessary to perform on the time series. For this effect, and taking into consideration the data collected in the monitoring campaigns (Dimande *et al.*, 2008a; b), the readings acquired during passage A are considered representative of the effects induced by the traffic, and therefore can be chosen for this analysis. The plots of Figure 2.11 are the average power spectra of the time history data collected by the electric sensors (in the left) and by the fiber optic sensors (in the right), placed at section S6. To minimize the contribution carried by frequencies less than 0.4 Hz, associated to the static component of the structure response, the time series were pre-treated with a 2nd order high-pass Butterworth filter with a cutting frequency of 0.4 Hz.

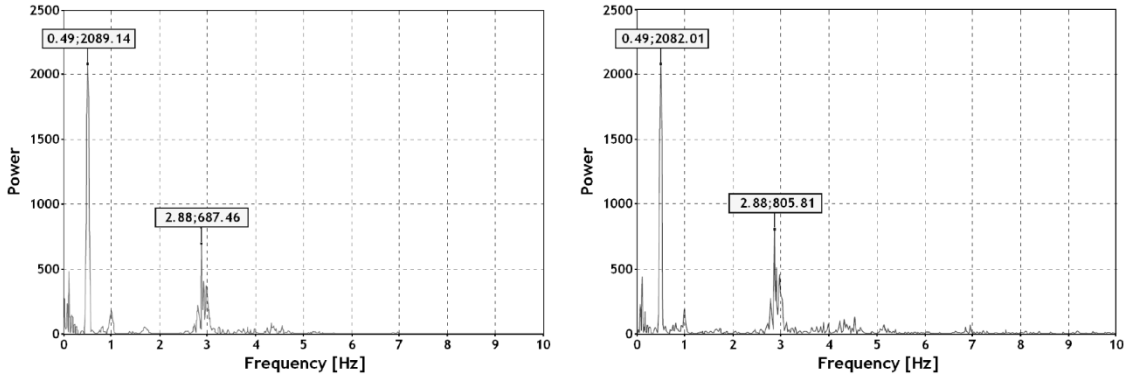

(a) (b)

Figure 2.11 - Average power spectra for the readings collected during passage A: (a) electric strain sensors ES6-1 and ES6-2; (b) fiber optic strain sensors OS6-1 and OS6-2.

The graphs in Figure 2.11 are very similar and reveal two clear peaks at frequencies 0.49 Hz and 2.88 Hz. The first peak corresponds to the primary frequency of the action

applied to the structure. In fact, taking into consideration the average distance between the bogies of the train, which was found to be 1.60 m, and that average speed is 29 km/h, the estimated frequency for the action is close to 0.50 Hz. This agrees with the 2 s period of the 7 strain cycles highlighted in the box of Figure 2.10(a). Concerning the second peak, its value is very close to the first natural frequency of the structure, which is 2.95 Hz, associated to a lateral mode and obtained through an ambient vibration test carried out in the first stage of the research project (Marques *et al.*, 2009).

The spectra also reveal that electric sensors signals have an insignificant content for frequencies higher than 5 Hz, in opposition to what can be perceived in the fiber optic gages data, in spite of its small amount. For assessing the importance of the content related with these frequencies in the time history data collected by the fiber optic sensors, a 2nd order low-pass Butterworth filter with a cut-off frequency of 5 Hz is applied to them and the results are plotted in Figure 2.12.

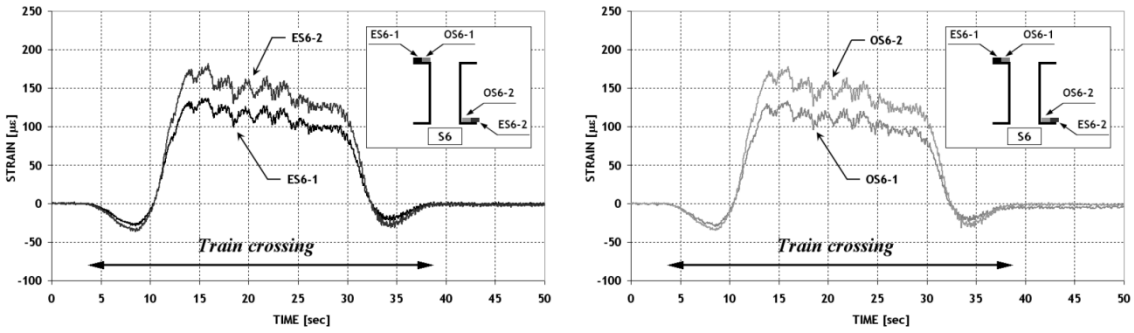

(a) (b)

Figure 2.12 - Time series for passage A: (a) collected by sensors ES6-1 and ES6-2; (b) recorded by sensors OS6-1 and OS6-2 and treated with a 2nd order low-pass Butterworth filter (f_c = 5 Hz).

By comparing the plots in Figure 2.12, an excellent agreement between the collected raw data of the electric sensors and the filtered time series of the corresponding fiber optic gages is clear. Having as reference the raw data depicted in Figure 2.10(a), those plots point out the real weight of the higher frequencies content in the fiber optic signals composition during the train crossing. Figure 2.13(a) shows the filtered dynamic component above 5 Hz of the signals for both fiber optic sensors in section S6, where it is obvious the effect of the vehicle crossing, since it can be clearly distinguished from the noise at the beginning and at the end of the records, thus granting reliability to the fiber optic results. These plots were obtained by subtracting the filtered time series to the raw data collected by the fiber optic sensors.

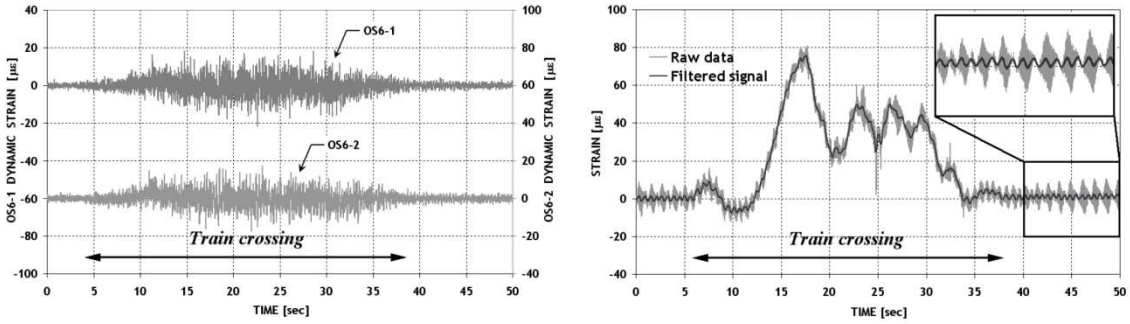

(a) (b)

Figure 2.13 - Dynamic component and noise content: (a) filtered dynamic component of the signals of sensors OS6-1 and OS6-2 (Passage A); (b) time series of sensor ES10-1 with clear presence of noise.

This different ability of the two types of adopted sensors, fiber optic and electric, for an accurate monitoring of the dynamic behavior of the instrumented bars, may point for some limitations in the use of electric strain gages, if similar procedures to the ones adopted in this installation are implemented. Considering the methodology adopted for the strain sensors, it is possible to infer from the field results that the gluing of Bragg gratings may be less intrusive than the application of the electric sensors. In fact, the epoxy base to which the foil strain gages are pre-glued, may present some stiffness, which makes the set mechanically more demanding, and therefore can act as a natural filter for deformations in the higher frequency range. Aiming to disclose the causes for this unlike behavior between these two systems, comparative laboratory tests with different types of sensors, including foil resistance strain gages directly applied to the steel surface using standard procedures, have been accomplished. In the following section the devised experiment is presented, the results obtained through it are analyzed, and important conclusions are drawn.

The joint observation of the deformations experienced by a bar through different technological based systems enabled to assess the quality of the results collected with the main electric system, revealing the pertinence of the option taken. Contrary to what would be expected taking into account the structure's material and the existence of an electrified route carried by the structure, there were no significant interferences in the signals of the electric sensors. However, the readings of the sensors applied to the upper chords sections, close to the rail level, had in general a noise level slightly higher than the results from the gages placed at lower chords. Figure 2.13(b) shows a strain record captured by gage ES10-1 during a specific crossing in which the noise is depicted. Such a high level of noise was observed only occasionally.

2.6. Laboratory experiment

2.6.1. Objectives and setup

With the aim of identifying the causes ruling the differences between the records collected by electric and fiber optic sensors, a laboratory experiment has been devised. The conducted tests have permitted the comparison of strain time histories obtained by various sensors, in response to controlled dynamic actions, varying the parameters of interest.

The laboratory experiment is based on the instrumentation of a steel bar, fixed at the top and suspending a mass on a plate at the base, thus acting as a pendulum. When the bar is deviated from its equilibrium position by imposing a horizontal displacement to the vibrating mass, the response of the structure in free vibration, to be measured by sensors attached to it, is governed by the dynamic characteristics of the bar, particularly its natural frequency (or vibration period).

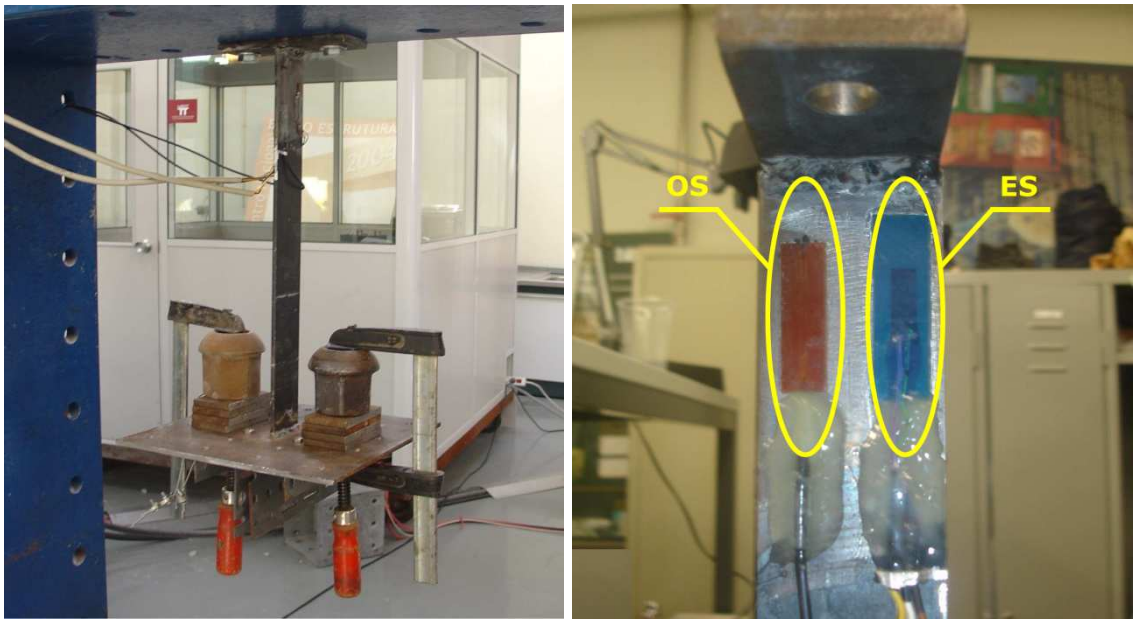

(a) (b)

Figure 2.14 - Setup for the laboratory experiment: (a) general view; (b) sensors after installation (Side 2).

The bar 500 mm long, 50 mm wide and 5 mm thick, has been instrumented with 4 strain sensors applied 40 mm below the fixed support, 2 fiber optic and the remaining electric, one of each type in each side of the bar cross-section. One of the electric sensors is a conventional foil strain gage directly glued onto the steel surface, termed as CES, whereas

the other is of the same type as the ones installed in the bridge, referred to as ES. The two fiber optic sensors are equal to the ones used in the field observation, serving as reference to compare. The distance of the glued face of all sensors to the plate surface is similar and less than 0.1 mm, considering the type of glue employed. The signal acquisition was accomplished with the same two interrogation units adopted for the bridge monitoring. Figure 2.14 illustrates the experimental setup.

A progressive change of the mass on the plate allowed for the variation of the natural frequency of the oscillator, ranging between 2 and 17 Hz. The pre-set initial displacement was established so that starting strain in the sensors was locked in 400 με, tensile at side 1 and compressive at side 2.

2.6.2. Analysis of results

Figures 2.15 and 2.16 present the strain time series measured by the sensors for vibration frequencies of 2 and 12 Hz, respectively, using in the acquisition a low-pass filter with a cut-off frequency set in 1000 Hz. By comparing the plots it is possible to state the following:

i. In both tests readings obtained with the conventional electric strain gage (CES) and with the electric strain sensor head (ES) are entirely identical, except for the sign since they are applied on opposite sides of the bar;
ii. In all tests and for both sides of the bar fiber optic strain sensors reveal a very similar behavior;
iii. In the free vibration test with a natural frequency of 2 Hz there is a perfect correspondence between the signals of electric and fiber optic sensors on both sides, which was not reproduced when the frequency increased to 12 Hz;
iv. In the test with the highest frequency, and for the electric sensors, it is noted that for the first vibration cycle the amplitude is not the double of the initial strain, i.e. in practical terms it seems to occur a sudden drop of the initial pre-set strain;
v. In each test, the logarithmic decrement varies less than 5 % between different time series, and therefore damping captured by sensors can be considered as equal.

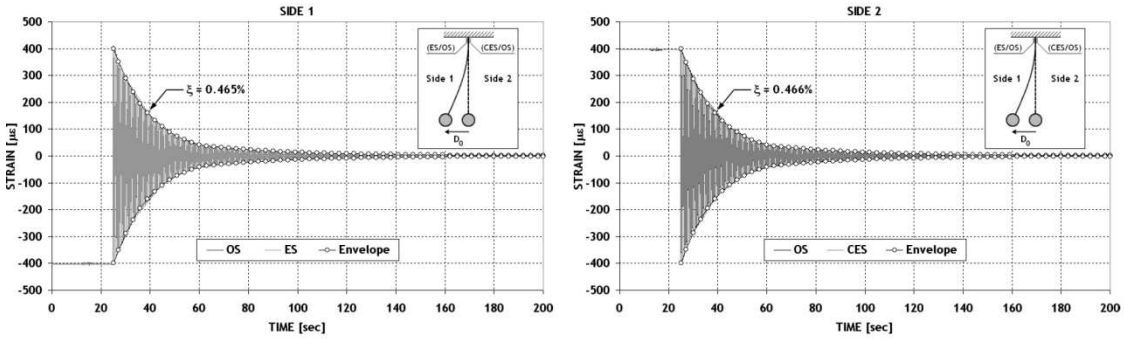

(a) (b)

Figure 2.15 - Strain time histories in free vibration (f = 2 Hz): (a) sensors applied to side 1; (b) sensors applied to side 2.

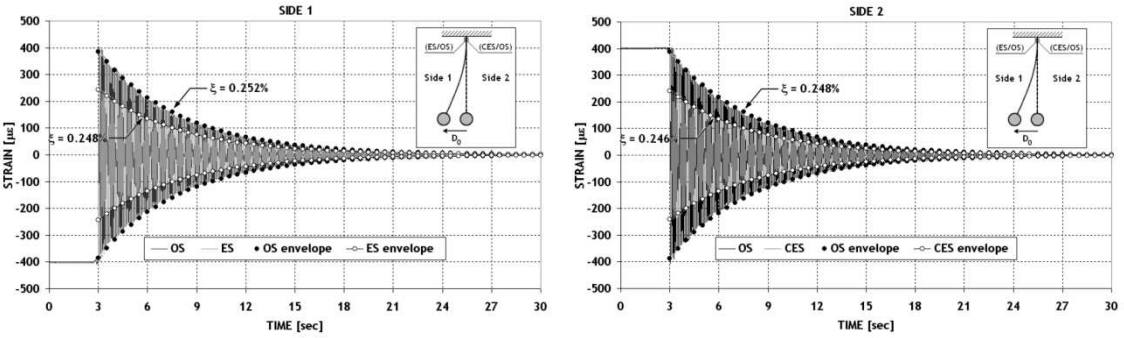

(a) (b)

Figure 2.16 - Strain time histories in free vibration (f = 12 Hz): (a) sensors applied to side 1; (b) sensors applied to side 2.

From these tests one can conclude that the procedure adopted for the electric sensors installation in the field, i.e. prior placement of the foil strain gages in resin sensor heads, brings no lower capacity for dynamic strain measurement. Free vibration tests were conducted for several frequencies within the range of 2 to 17 Hz, so that deviation introduced in the readings of electric sensors along the frequency could be appraised. Figure 2.17 shows the obtained results in terms of a ratio of the integrals in time of the signals absolute values between electric and fiber optic sensors placed in each side of the bar, as well as the estimated polynomial trend line, its equation and corresponding error. This parameter was used because it gives an indication of the energy captured by the sensors. For frequencies up to 5 Hz the ratio is higher than 0.95, which can be considered as good since it implies only a 5 % deviation between signals. Yet, from this point forth the ratio rapidly decreases hitting a minimum value less than 0.45 at the frequency of 17 Hz. The coherence between these results and deviations encountered during field measurements is fairly good.

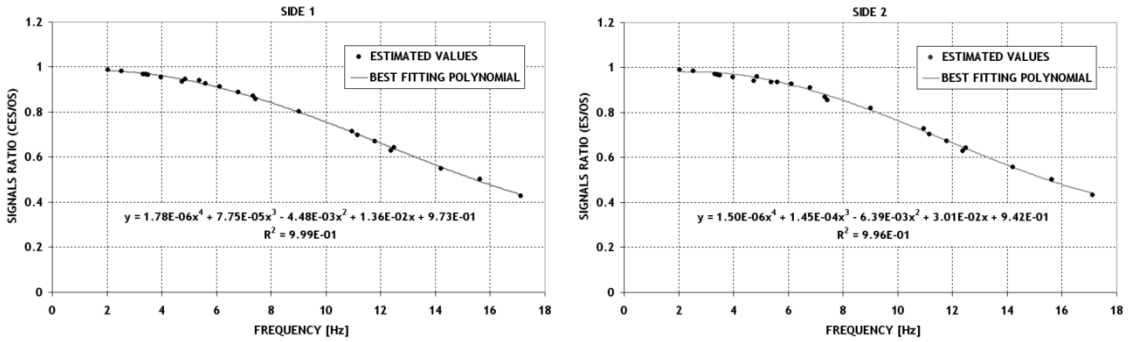

(a) (b)

Figure 2.17 - Ratio of the integrals in time of the signals absolute values: (a) sensors applied to side 1; (b) sensors applied to side 2.

As the differences in dynamic strain monitoring between fiber optic and electric sensors were not due to the implementation procedure adopted for the latter, the hypothesis of an anomaly in the acquisition equipment came to be considered for evaluation. Aiming at checking this hypothesis two new tests were performed for a frequency of 12.5 Hz, in which electric signals were scanned by a different reading unit in each test. The first, termed as AS1, was the acquisition system used in the observation campaigns of the bridge, a SCXI® unit, while the second, referred to as AS2, was a CompactRIO® unit. Both systems are marketed by National Instruments™.

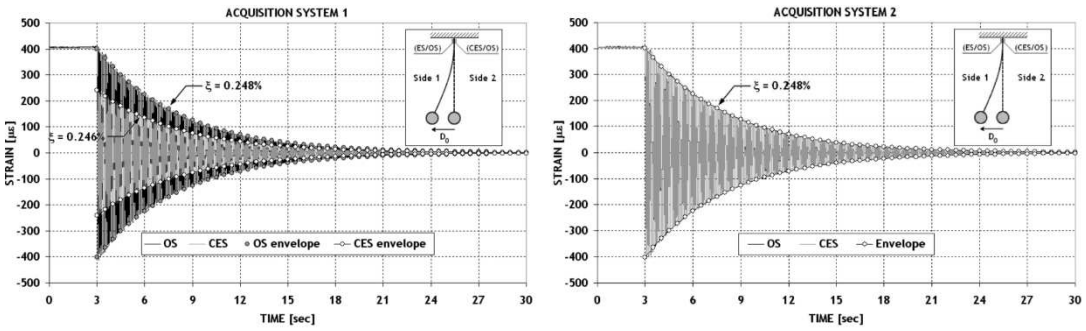

(a) (b)

Figure 2.18 - Strain time histories in free vibration (f = 12.5 Hz): (a) acquisition system AS1; (b) acquisition system AS2.

In Figure 2.18 the results gathered with these tests are depicted. Plots allow the conclusion beyond doubt that the differences found are due to factors associated with the unit AS1. Later, it was possible to detect an anomaly in the acquisition board of the equipment responsible for poor performance in the dynamic interrogation.

2.7. Reliability of electric sensors data for fatigue analysis

In what concerns the estimation of fatigue life for bridge components using measured strains, the main objective to pursuit with the monitoring, the author consider that results obtained by electric sensors present minimum quality for its accomplishment. In fact, although the strains in the higher frequency content were not captured by the installed electric sensors with the adopted reading unit, their cycles are of low amplitude and correspond to strains variations whose values do not reach 40 με, which corresponds to an 8 MPa stress range for a steel with a Young modulus of 200 GPa. This stress range does not introduce fatigue in the material, though in some details of the joints the stress level may increase 50 %. On the other hand, additional data for the research project can be accurately acquired by the electric monitoring system deployed on the bridge as long as a proper measuring unit is used.

It is noteworthy to mention that sampling frequencies adopted to collect the data revealed to be suitable for an adequate definition of the strain time series. Thus, strain/stress histograms could be obtained by using cycle counting, such as the rainflow method (Lu and Mäkeläinen, 2003), and therefore essential data for assessing the fatigue problem through the concept of damage accumulation could be provided. Figure 2.19 illustrates typical strain histograms computed from the readings of electric and fiber optic sensors placed at section S6, by using a rainflow algorithm integrated in dedicated software (Sousa *et al.*, 2010).

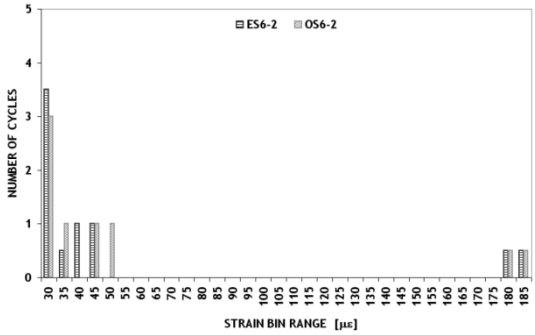

Figure 2.19 - Strain histograms with a threshold of 30 με (Passage A).

2.8. Summary and conclusions

The chapter presents the development and the application of procedures for the evaluation of the structural integrity of existing steel railway bridges, based on dynamic

strain monitoring. Trezói Bridge has been selected as test bed to accomplish field observations, since it was considered representative of the structures comprehended by the national railway network, in terms of age and use.

With this purpose, two parallel short-term observation systems were installed, each one relying on a different technology. The primary comprised 24 electric strain sensors, constituted by common foil strain gages pre-glued to epoxy resin bases, of which 16 were applied to chord sections of the northern truss girder and 8 to rail foots at strategic locations. Four Pt 100 sensors also gauged the temperature at the steel surface and in the air. The secondary system had only 6 FBG strain sensors, 4 attached to a single lower chord section, also instrumented with electric sensors, and the remaining 2 installed in the corresponding upper chord section at middle of the central span. The first system intended to: assess the global structure behavior; appraise the strain/stress distribution throughout the most tensile strained bars and at their connections; obtain strain/stress time-series in points previously identified as the more prone to develop fatigue problems; collect data concerning the traffic flow crossing the bridge. The second system has allowed for the collection of data to serve as reference for readings acquired by the first system, so that any possible anomalies in the electrical signals could be perceived, namely EM interferences caused by the power line running over the bridge. Therefore, in this particular case, fiber optic sensors were used to check electric sensors performance rather than the contrary as it is common in the laboratory research. Similar procedures for gluing and protection of the sensors were adopted in both systems.

Two strain monitoring campaigns were accomplished. In each one, the effects of different categories of trains in the structure response were captured. The first observation period took place under speed restrictions for the traffic, while the second occurred with normal operation conditions.

As regards the traffic monitoring and the bridge behavior the collected results led to the following conclusions:

i. Traffic characterization in terms of vehicles' speed, crossing directions, number of axles, and their spacing, was successfully accomplished by using a simple, effective and easy to apply experimental scheme;
ii. Chords exhibited a relevant in-plane bending component, and therefore the instrumented girder is not a pure truss system;
iii. Contrary to what one would expect the truss girder top chord near the support experienced a level of deformation considerably lower than the one recorded in

the mid-span bottom chord, so this and their connections are the critical points to assess fatigue resistance.

Regarding the evaluation of the strain monitoring systems the main conclusions drawn were:

i. The two monitoring campaigns described in this work and their results aimed mainly at checking the suitability of the installed electric monitoring system to initiate the continuous measurement of the bridge response under normal service conditions, and if needed, to undertake the corrective measures required to fully accomplish the proposed objectives;
ii. Static components of the signals acquired by both systems, fiber optic and electric based, during the field measurements were in excellent agreement;
iii. However, the electric signals were not able to capture the dynamic component with a frequency content higher than 5 Hz, which was later ascribed to be caused by a malfunction of the acquisition system used in the field tests;
iv. The suitability of the procedure adopted for the installation of the electric strain gages was confirmed by experimental data obtained through laboratory tests, and the anomaly of the acquisition system for scanning the signals of the electric sensors at the site was clearly identified;
v. The results also led to the conclusion that the sensors of both monitoring systems have alike capability for dynamic observation, provided that interrogation units are duly selected and in perfect operating conditions;
vi. Even if the faulty electric interrogation unit would have been used for the research project the measurements would have sufficient quality to conduct a suitable fatigue analysis in the studied bridge, since the portion of the dynamic component of the strains incorrectly measured is associated to stress cycles of low amplitude that do not contribute for material fatigue as they are below the cut off limit.

Chapter 3

Design and installation of the Pinhão Bridge monitoring system

3.1. Synopsis

This chapter presents the architecture of the electric based monitoring system installed in a centenary metallic road bridge, recently subjected to strengthening and rehabilitation works. The observed parameters and the sensors that allow its monitoring are described and the guidelines for the selection criteria of points and sections to be instrumented are presented. The location of the observation stations and the array of sensors connected to each one are discussed. The cares and methodologies adopted during the system installation aiming at achieving its maximum durability and reliability are analyzed. The laboratory tests conducted to validate the behavior of the novel strain sensor holders and to appraise the performance of the protection system developed for the project are detailed. At last, the factors conditioning the selection of the acquisition and communication systems are pointed out.

3.2. Introduction

In the last decade the monitoring systems have been useful tools in assisting the assessment of bridges condition and structural safety (Farhey, 2005; Olund and DeWolf, 2007). These systems allow the collection of data concerning the structures response, during the construction, rehabilitation or/and strengthening, and under operational conditions. Subsequently, the appraisal of the bridges behavior by confronting the field

measurements with the results predicted through analytical methods, either deterministic (Costa *et al.*, 2008b) or probabilistic (Catbas *et al.*, 2008), is made possible. In the context of Structural Health Monitoring, these systems should be able to provide reliable information pertaining to the safety and integrity of the bridges, ultimately leading to the detection of damage or deterioration, and to the determination of the health or condition of the bridges (Bergmeister, 2001; Brownjohn, 2007; Farrar, 2007).

In addition, the monitoring systems applied to bridges allow a better knowledge of the loads acting on these structures as they can be used to acquire data concerning the live loads (Karoumi *et al.*, 2005), temperature, wind and seismic loads (Kashima *et al.*, 2001), which constitutes valuable information for reducing the uncertainties in the reliability analyses (Frangopol *et al.*, 2008). Moreover, they can provide useful data for improving the characterization of loads established by the design codes. With respect to the long-term monitoring systems, several components can be comprehensively integrated, such as static, dynamic, environmental, and durability (Sousa *et al.*, 2011), and their selection depends mainly on the characteristics of the host bridge and on the monitoring objectives.

The bridge, hosting the monitoring system presented in this chapter, was recently subjected to strengthening and rehabilitation works aiming at extending its service life, and consequently, making possible the continuation of its relevant role in the regional road network. The gentleness of some of these operations, the appraisal of the strengthening solutions performance and the historic, cultural, and economic significance of this bridge made the structural monitoring of its behavior mandatory.

The monitoring system consists of an electric sensors network deployed on the bridge to provide long-term observation of its structural response and safety. The system was designed to be installed during the strengthening and rehabilitation works so that it could be possible to take advantage of the access means to the structural members, such as the general scaffolding system and articulated boom lifts.

The system comprises the measurement of steel strains in the primary bridge members, longitudinal displacements at the sliding supports of the bridge, rotations in some relevant sections of the deck, and temperature of the ambient and at the steel surface of several cross-sections instrumented with strain gages.

The monitoring system deployed in the bridge integrates novel electric strain sensor holders developed for this project. New application procedures, suited to the structure's material and to the aggressive environment, were adopted. Aiming at assuring a long life

for the monitoring system and a minimum visual impact of the whole installation, special protection measures for the surface mountable sensors and electric cables were considered. In addition, the selection of the interrogation and communication systems took a special care, since the ability to provide satisfactory information, either quantitatively or qualitatively, in a useful period of time, depends on them, mainly when dynamic observations are carried out.

3.3. Pinhão road bridge

The bridge allows the crossing over the Douro river, linking the districts of Viseu and Vila Real near the village of Pinhão in the north of Portugal, and was opened to the traffic in 1906 (see Figure 3.1). After a thorough inspection to the structure in 2004, the Portuguese Institute of the Road Network (EP – Estradas de Portugal, E.P.E.) decided to post the bridge with speed and weight restrictions for the crossing vehicles. Then, a viability study for the bridge rehabilitation was conducted, which included an in-depth campaign for the complete characterization of its structural behavior. It led to the rehabilitation and strengthening of the bridge in 2006, making it suitable for the present traffic conditions established in the current design codes. In its new operation stage the bridge only comprises a single lane, hence not allowing the crossing of vehicles travelling in opposite directions.

Figure 3.1 - Pinhão road bridge over the Douro river.

The steel superstructure comprises three main through-truss spans, 68.60 m long between supports, and a highly skewed curved deck plate girder span, 10 m long, in the south entrance, resting on three piers and two abutments made of granite masonry. In its rehabilitated scheme, the floor system of the main spans presents a typical slab-on-girder concrete-steel cross-section, approximately 6.50 m wide and 1.00 m high, constituted by an orthotropic steel grid of crossbeams (17) and stringers (5), upon which the reinforced concrete slab (0.17 m thick) and the asphalt layer (0.07 m thick) lie on (see Figure 3.2(b)). The slab was made by pouring a 0.10 m thick layer of concrete over 0.07 m thick precast

concrete slabs placed over the stringers. Between the two sidewalks, 0.62 m wide each, the single traffic lane, 4.60 m wide, has its place.

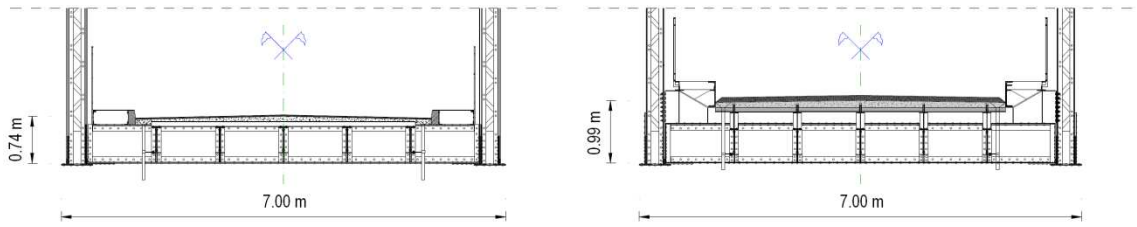

(a) (b)

Figure 3.2 - Bridge cross-section: (a) before the rehabilitation; (b) after the rehabilitation (Pinto, 2005).

The main spans were originally supported by pin bearings in the north side and roller bearings in the south side (see Figure 3.3(a)), which were replaced by pot and disk bearings during the rehabilitation, respectively. Therefore, for both conditions (pre and post) the longitudinal displacements were blocked in one support line and allowed in the other (simply supported spans).

(a) (b)

Figure 3.3 - Pinhão Bridge before the rehabilitation: (a) roller (left) and pin (right) bearings; (b) intersection node of a diagonal with a vertical.

In each main span the two truss girders are constituted by two chords, the upper one presenting a parabolic geometry and the lower one absolutely straight, connected by verticals and diagonals with different cross-sections. The girders height varies from 2.67 m at the supports to 8.86 m at the center of the span. For preventing out-of-plane instability phenomena, the truss girders are braced by horizontal diagonals at the lower level in all 16 panels and by cross bars and diagonals at the upper level in the 10 central panels. The bracing elements are accomplished by angles connecting the chords flanges through gusset plates. Additionally, transverse upper truss girders combined with the verticals and

crossbeams constitute the sway frames at the 11 central points. Figure 3.4 depicts some views of the bridge.

The elements pertaining to the original metallic structure are built-up members fabricated by assembling various plates and angles through riveted connections, a typical steel construction technique at the beginning of the twentieth century. The chords are U-type sections, while the crossbeams and stringers are I-sections. Pairs of double angles connected by lacings and pair of plates with no shear connection constituted the original verticals and diagonals, respectively (see Figure 3.3(b)).

(a) (b)

Figure 3.4 - Pinhão Bridge before the rehabilitation: (a) side and bottom views; (b) view from the road (inner view).

The strengthening of the floor system was performed by adding a new grid of commercial steel I-profiles over the old one. Angles were used as reinforcements of the chords. The diagonals were strengthened with either angles or C-profiles. The connections between the original structure and the new steel elements, although initially planned to be riveted, were executed with round head preloaded bolts, except for crossbeams and stringers in which hexagonal bolts were used.

3.4. Instrumentation system

3.4.1. Introduction

The instrumentation system installed in the structure for monitoring its behavior comprises the observation of the following parameters:

i. Steel strains in sections of the truss girders members, namely chords, diagonals and verticals, as well as of deck crossbeams and stringers;

ii. Longitudinal displacements in the sliding supports of all three main spans;
iii. Crossbeams rotations;
iv. Ambient temperature and at the steel surface of chords.

The measuring system is composed by two data acquisition units located near the structure in different points. Figure 3.5 presents the layout of the instrumentation designed for monitoring the bridge.

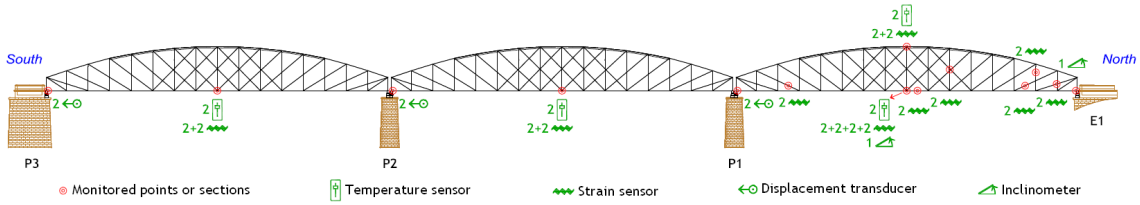

Figure 3.5 - Layout of the bridge instrumentation.

3.4.2. Steel deformations

The monitoring of strains in the elements that rule the bridge behavior, and therefore its safety, is accomplished by 16 pairs of strain sensors applied in as much cross-sections to be monitored.

For both truss girders of the three main spans the lower chords were instrumented at mid-span, and the upper chords strains of the north span are also monitored at the same span cross-section. Yet for this span, the steel strains of three diagonals cross-sections and of two verticals in the upstream truss girder are also measured. The mid-span crossbeam has two cross-sections instrumented, one at its mid-span and the other near to the downstream support. The only monitored cross-section of a stringer is located in the central beam of the set, close to the mid-span. Figure 3.6 depicts the general location of the strain sensors applied to some cross-sections of bridge members.

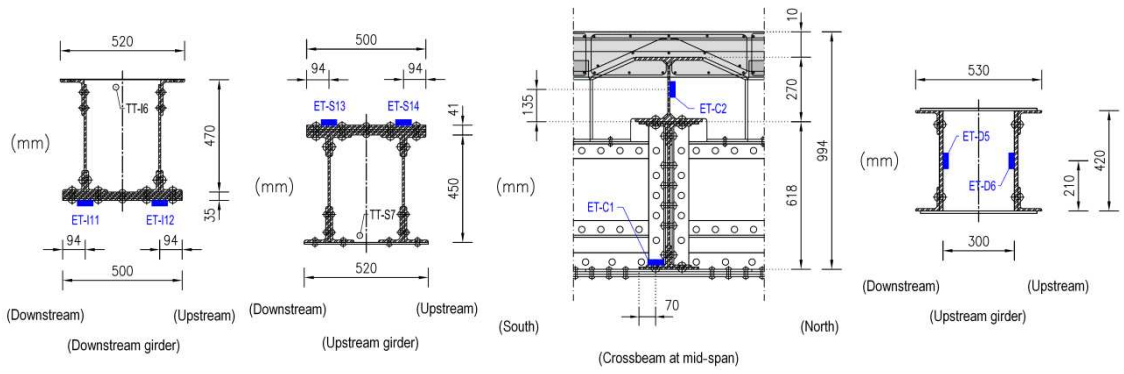

(a) (b) (c) (d)

Figure 3.6 - Examples of cross-sections instrumented in the north span: (a) lower chord; (b) upper chord; (c) crossbeam; (d) diagonal.

In selecting the cross-sections to be monitored several criteria had to be considered. The first, and foremost, was the assessment of the members performance whose response is representative of the spans global behavior by using a few pairs of sensors. To this end, all lower chords of the truss girders at mid-span are provided with strain gages. The strain monitoring of these members will allow the appraisal of the spans bending forces at their critical cross-sections. The second principle to attend was the strain measurement of the maximum number of cross-sections that had been monitored during the field tests carried out to support the viability study (Costa *et al.*, 2008a). By comparing the results collected in the load tests conducted before and after the rehabilitation works it would be possible to experimentally assess the changes in the bridge behavior and to evaluate the effectiveness of the adopted strengthening solutions. The last criterion was related to the implementation of a B-WIM system in order to enable the characterization of the traffic that crosses the bridge. Therefore, a judicious positioning of key sensors would allow the collection of data concerning the loads, geometry, average speed and moving direction of the vehicles.

3.4.3. Displacements in sliding supports

Displacements transducers were installed at the bearings of the bridge where the longitudinal movements are allowed (see Figure 3.5). LVDTs were used in this project, one for each sliding bearing. Therefore, the movements of the expansion joints are indirectly assessed and correlated with the daily and seasonal temperature cycles. These displacements are measured taking as fixed reference the top of the masonry piers where the bearings rest, and as moving target the crossbeams at the spans ends.

3.4.4. Rotations in crossbeams

Near the upstream lower chord of the north span two inclinometers were fixed to the crossbeams for assessing the rotations in the corresponding structure joints. The sensor located at the north support enables the monitoring of longitudinal span rotations, while the other located at mid-span allows the measurement of the transverse rotation of the deck at the crossbeam level. The first rotation measures the span flexibility and the second allows the coupled assessment of torsion and bending stiffnesses due to the lower chord and to the mid-span transverse frame, respectively.

3.4.5. Ambient temperature and at the steel surface

For an accurate interpretation of the long-term evolution of the steel strains, displacements in sliding supports and cross-sections rotations, a suitable characterization of the thermal action applied to the structure is essential. To this end, temperature sensors were distributed throughout the structure at key points in order to obtain a representative measurement of this parameter under different conditions of sun exposure. The sensors were installed at the mid-span of all truss girders, at the lower (three spans) and upper levels (north span) (see Figure 3.5).

The data collected by these sensors enable a proper description of the variations in time of the average temperature experienced by the surrounding environment and the steel surface. Daily and seasonal temperature cycles can be captured, as well as the temperature distribution in the bridge. The system was also designed to allow the assessment of discrepancies between both temperatures, either in terms of time lag or extreme values, caused by the thermal inertia of the structural elements, thermal properties of the material and atmospheric conditions (e. g. cloudiness). The distribution of the sensors was made in such a way that two sensors of the same type are not in the same vertical or horizontal alignment of the span cross-section.

3.4.6. System architecture

The monitoring system comprises a sensing network, data acquisition units, data storage units and a communication system. These equipments are concentrated at two points of observation designated as Observation Station (OS) and Central Observation Station (COS), which are located beneath the deck. OS is located over the pier P2 and COS is located nearby the north abutment.

The sensing network spreads from the two observation stations throughout the bridge using a tree structure, with a central set of 20-wire cables serially branching into 12, 8, 6, and 4-wire cables up to the sensors, grouped by parameter to be measured and by points or sections to be instrumented. Figure 3.7 depicts the spatial positioning of the system network branches.

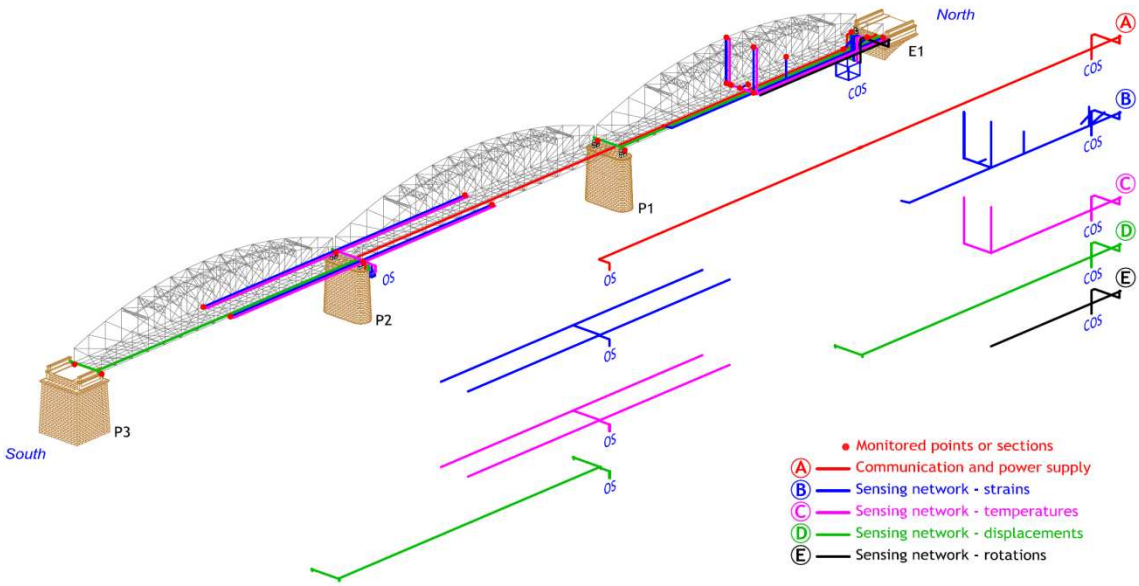

Figure 3.7 - Network architecture of the monitoring system.

The electrical signals from all sensors of the monitoring system are measured by two acquisition units, each one housed in a different observation station. Their location and the number of reading channels had to attend the sensors positioning on the structure and their distance to the observation stations, in order to minimize the cables length and to optimize the number of reading modules to be integrated in each data logger. Therefore, the signals of sensors placed in the south and central spans are acquired by the unit located at the OS whereas the remaining are measured by the logger installed at the COS. The data storage in the field is a two-stage process. First the data are saved in the internal memories of the acquisition equipments and then the information is gathered in a host PC located at the COS.

The communication between the host PC and the data logger inside the COS is supported by Ethernet through the use of a Switch/Hub. The communication between the COS and the OS is accomplished through the electric cable that provides the power supply to the electric devices inside it. For this effect, a kit of powerline Ethernet adapters that enables the communication between electronic equipments connected to the same electrical network is used, by plugging the devices into power sockets at both stations. In this case, the communication is established between the Switch/Hub at the COS and the Router placed at the OS. For accessing the data stored in the host PC the Connect Box and Router are used, thus providing a wireless communication with the exterior. The architecture of the communication network implemented in the monitoring system of this bridge is presented in Figure 3.8.

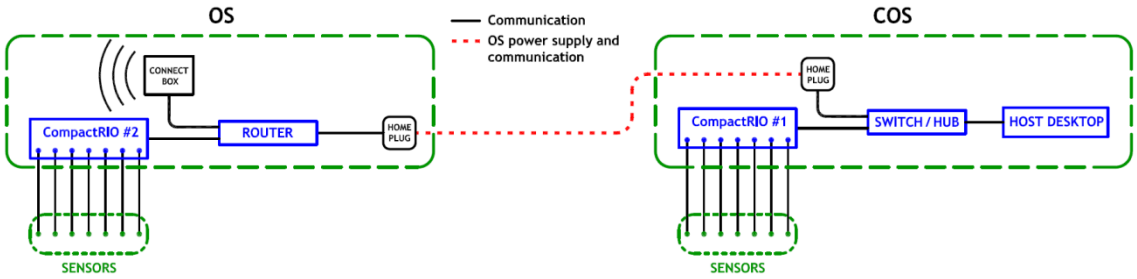

Figure 3.8 - Communication network.

3.5. Sensors and protection systems

3.5.1. Strain sensors

The strains in the steel are measured with electric resistance strain gages pre-glued to the bottom face of a thin resin plate. When compared with the classic gluing process of strain gages to metallic surfaces this kind of application presents considerable advantages, one of which is the suppression of soldering operations at the site. Therefore, a faster installation by excluding time consuming tasks is allowed, as well as the execution of works under less proper atmospheric conditions, such as cold, windy and humid. On the other hand, the materials used in this installation can assure higher durability levels than those granted by common adhesives due to their improved resistance to environmental factors.

The strain gages within the strain sensors are self-temperature compensated at 24 ºC, presenting a thermal output less than 10 με for a temperature range between 17 ºC and 60 ºC when directly applied to a non-restricted steel bar. These apparent deformations are caused by the direct effect of temperature on the strain gage when the steel has no restrictions to deform, and must be subtracted to the readings collected by the acquisition units in order to obtain the stress induced strains in the steel. For this matter self-temperature compensation curves provided by the gages manufacturer must be used.

3.5.1.1. Sensors attachment

The first operation to perform in applying the sensors is the surface preparation. This stage begins with the removal of the weathering layer by using mechanical means. The epoxy coating is removed with an electric hand-held angle grinder equipped with a sanding disc. The smoothed steel surface is then cleaned using soaked gauzes and water based surface cleaners.

After the surface preparation a thin coat of epoxy adhesive is applied to the contact side of the sensor. The strain sensor is then correctly aligned and pressure is carefully applied with the help of a cramp or other mechanical device. The epoxy used in the bond process has a short gel time, of about 5 minutes. The adopted setup allows a uniform transmission of the pressure all over the sensor holder and enables the elimination of the excess adhesive applied in the interface resin/steel so that a thin layer of adhesive is achieved.

3.5.1.2. Sensors protection

In order to shield the sensors from hits, shocks, insolation and agents in the surrounding environment, an adequate protection has been devised.

The primary protection applied for these sensors is accomplished by FRP material, with a low stiff fiber tissue embedded in an epoxy matrix, over a layer of thermal insulating material (cork as instance), covered by the coating applied to the metallic surface. Consequently, the overall appearance of the installation is very discreet. Figure 3.9 presents the protection system previously described.

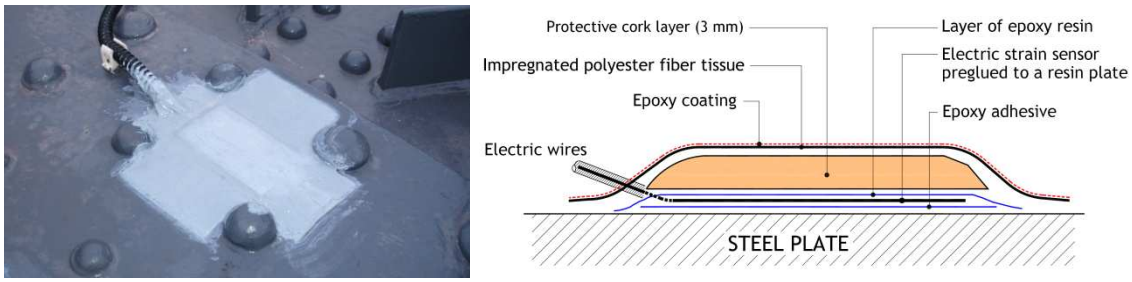

(a) (b)

Figure 3.9 - Strain sensors protection: (a) application to a sensor; (b) schematic representation.

3.5.2. Temperature sensors

For measuring the temperature, either of the environment or of the steel surface, Resistance Temperature Detectors (RTDs) were used. The sensors adopted for this monitoring system are made of platinum and present a nominal resistance of 100 Ω at 0 ºC, and thus are also named Pt-100 sensors, where Pt stands for the constitutive material (Platinum) and 100 for the resistance.

All temperature detectors were encapsulated in small steel tubes sealed with epoxy resin. In order to prevent direct insulation over the sensors installed to measure the temperature at the steel surface a protection with thermal insulating material, similar to

the one described for the strain sensors, was applied. Therefore, the readings collected by those sensors correspond to the actual temperature in the steel.

3.5.3. Displacement transducers and inclinometers

The inclinometers selected to integrate the monitoring system are pendulum type, while the displacement transducers are Linear Variable Differential Transformers, usually named as LVDTs. All these transducers are placed inside plastic enclosures with a minimum Ingress Protection of IP 65, thus securing protection against environmental factors such as moisture, extreme temperatures and/or sun rays exposure, but also preventing from direct impacts, birds' excrements and other biological attacks (see Figure 3.10).

To assure that LVDTs are only subjected to imposed displacements along their axis, i. e. no shear and bending forces are applied to the transducers that may cause damage to them or perturbations in the measurement, rod-end bearings were installed.

(a) (b)

Figure 3.10 - Protection systems applied to sensors: (a) inclinometers; (b) displacement transducers.

3.5.4. Protection of the system components

All electric cables linking the sensors to the acquisition units are guided and protected by galvanized steel tubes or reinforced flexible thermoplastic conduits, acting both as jackets, thus assuring minimum protection against environmental exposure, preventing rain, moisture, sun exposure and other hazards. As much as possible, cables were conducted along the bridge inside the technical galleries under the sidewalks. Connections between

electric wires were performed with precision mechanical adapters to minimize the signals noise, and moisture ingress was prevented by sealing them with epoxy resin.

In any electrical network the connections are fragile links of the system and therefore their inspection must be possible when potential anomalies occur. Therefore, all connections were placed inside plastic enclosures with IP 65. Plastic glands used to connect the tubes and conduits to the enclosures were also sealed. The electronic devices that integrate both observation stations are placed inside protection cabinets, assuring a controlled temperature and humidity environment as it can be seen in Figure 3.11.

(a) (b)

Figure 3.11 - Observation stations of the monitoring system: (a) Observation Station (OS); (b) Central Observation Station (COS).

3.6. Laboratory tests

3.6.1. Static behavior

In order to assess the sensors performance when subjected to static deformation, a laboratory experiment was conducted with a simply supported I-plate steel beam. A pair of concentrated forces separated by 0.50 m, and centered with the span, was applied to load the beam at a constant rate up to the maximum value of $F_{max} = 60$ kN. After keeping the maximum load applied during three minutes, the beam was completely unloaded in two steps, first at a low constant rate up to $F_{max} = 9$ kN, and then rapidly following a steady period of about six minutes.

The beam was instrumented in the central region with two foil strain gages at the bottom and top flanges, referred to as CES1 and CES2, respectively, classically applied to the surface. Two other sensors similar to those installed in the bridge were also attached to

the beam by adopting the same procedures described in section 3.5.1. Their location imitates that of the conventional electric strain gages, with the sensors labeled as ES1 and ES2, respectively at the bottom and at the top of the cross-section. All sensors were transversely placed at the middle of the flanges. Figure 3.12(a) shows the instrumented beam used in the test and Figure 3.12(b) displays the results acquired during the experiment.

The plots reveal an excellent correspondence between the sensors placed at the same flange. In addition, all sensors experience the same level of maximum deformation, tensile in the bottom and compressive in the top, very close to the yielding point. Therefore, this test proved the ability of the sensors to capture the static deformation at the surface of steel members.

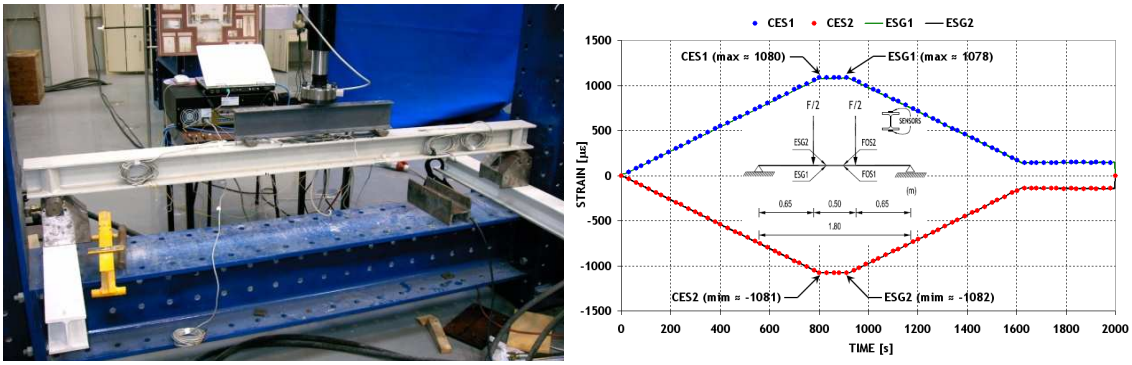

(a) (b)

Figure 3.12 - Static load test: (a) instrumented beam; (b) experimental results.

3.6.2. Fatigue testing

The performance of the sensors under cyclic loading was assessed through a tension-to-tension fatigue test carried out on the beam presented in the previous section. The mean load applied to the beam was 12.75 kN and the load range 20.45 kN, thus generating load cycles with a maximum to minimum load ratio of 9 at a loading frequency of 10 cycles per minute. The test was devised so that the maximum strain applied to the beam was kept below 40 % of the yielding point of the steel, a value much higher than the maximum strain amplitude predicted for the most critical member of the bridge under service conditions. Figure 3.13 depicts the evolution of the mean strain and of the strain range experienced by sensor ESG1. In spite of some irregularity in the readings no clear trend can be identified, and therefore no degradation of the sensors ability to gauge the steel deformation has occurred.

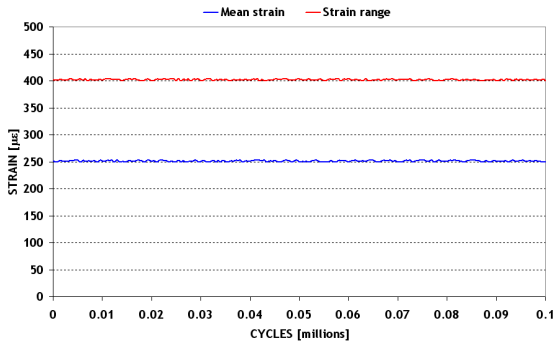

Figure 3.13 - Evolution of the mean strain and of the strain range during the cyclic load test.

3.6.3. Creep evaluation

The assessment of the combined behavior of the epoxy adhesive and of the sensor resin plate under permanent high state of strain was accomplished by applying a high load to the beam previously presented for a period of 100 days. By replicating an identical loading setup under controlled ambient conditions, the load was applied up to 64 kN, producing a maximum strain in the steel very close to the yield strain of the material. The results collected by sensors ESG1 and CES1 are plotted in Figure 3.14 with a logarithmic time axis. The sensors readings experienced no significant variation between the end of the loading and the end of the test, with an increase smaller than 0.5 %. Therefore, it was concluded that no abnormal behavior was expected as a consequence of creep in the adhesive or resin.

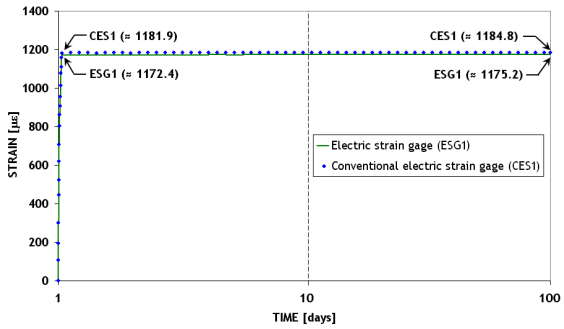

Figure 3.14 - Evolution of the strain readings under constant load during 100 days.

3.6.4. Assessment of temperature effects

The response of the sensors under thermal variations was investigated by conducting an experiment on a specimen sampled from the bridge. The bar was instrumented with a novel sensor, herein identified as ESG3, duly protected with the shielding described in section 3.5.1.2 (see Figure 3.15(a)). A temperature sensor was placed close to the strain

sensor so that temperature at the steel surface beneath the shielding could be measured. Eleven cycles of temperature were applied at a rate of 1.05 cycles per day, in which the temperature varied from 0 ºC to 55 ºC. Figure 3.15(b) shows the readings collected by the sensor and the temperature acquired at the strain sensor. In addition, it is also depicted the signal expected for the foil strain gage that integrates the sensor holder, referred to as theoretical strain, computed on the basis of the steel temperature and of the thermal output curve made available by the strain gages manufacturer. If the foil strain gage was self-temperature compensated no readings different from zero would be detected, which is clearly not the case.

The plots point to a fair correspondence of the strain readings with the predicted signal for the foil strain gage directly applied to the steel surface. Therefore, three main conclusions can be drawn: i) the strain sensor exhibited a repetitive behavior under extreme temperature amplitudes; ii) if the steel temperature is measured in the vicinity of the strain sensor the compensation of the readings is perfectly possible, and consequently stress induced strains can be captured; and iii) thermal shielding was effective in that the strains, measured and predicted, are coincident. Finally, it is also worth mentioning that peaks at the regions of maximum strain are caused by the non-linear thermal output of the foil strain gages as the curve is a quartic polynomial.

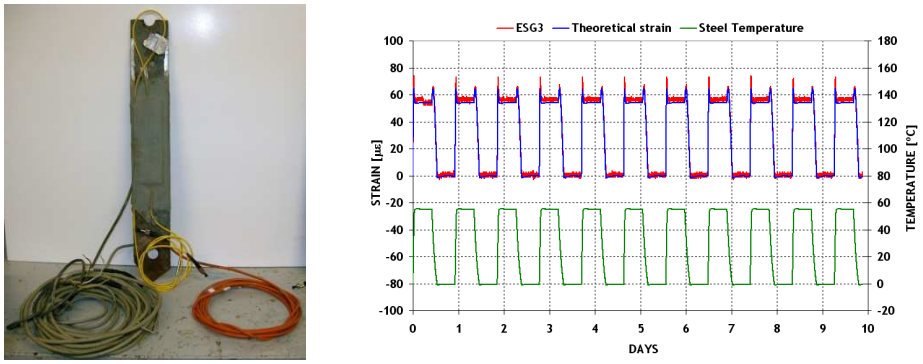

(a) (b)

Figure 3.15 - Cyclic temperature test: (a) instrumented specimen; (b) evolution of the strain readings.

3.6.5. Evaluation of humidity effects

An experiment was carried out on the same sample tested in the thermal test to appraise the effect of the humidity on the sensors, and therefore in the readings supplied by them. Five humidity cycles were applied by varying the relative humidity between 35 % and 85 % at constant temperature. Figure 3.16(b) depicts the variation of the relative humidity

inside the climatic chamber throughout the test, as well as the results acquired by the strain sensor ESG3 and by an additional foil strain gage applied to the bar (CES3), duly protected. For both sensors the impact of the humidity variation is very small and no tendency in the response can be identified. Therefore, the shielding applied to the sensors is capable of preventing any negative effects of the humidity on the field measurements.

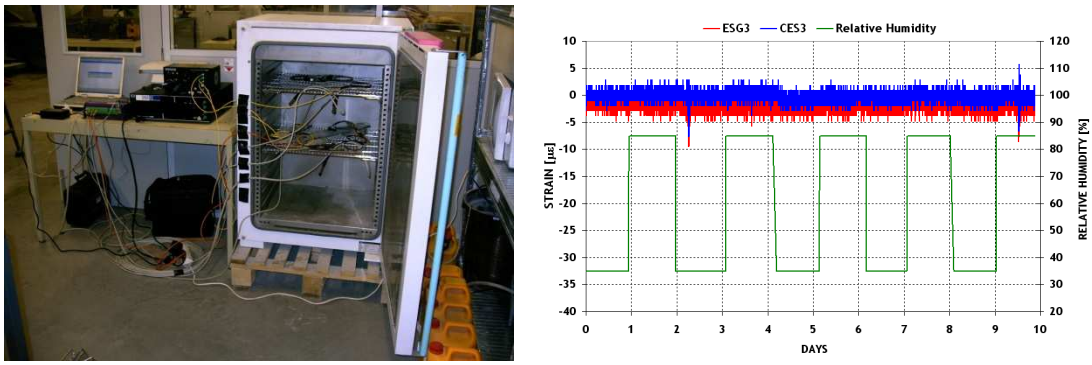

(a) (b)

Figure 3.16 - Cyclic humidity test: (a) climatic chamber; (b) evolution of the strain readings.

3.7. Data collection system

3.7.1. Data Acquisition Sub-System (DASS)

The DASS includes a host Desktop located at COS and two acquisition units, one in each observation station. Both units are CompactRIO models from National Instruments™, known to be a small, rugged industrial control and acquisition system, presenting features of a Programmable Automation Controller (PAC) capable of real time operations, and endowed with internal memory, a chassis and several I/O reconfigurable modules. The chassis includes FPGA technology (acronym for Field Programmable Gate Array) making possible the interface with the swappable I/O modules, which include signal conditioning for direct connection to sensors and actuators. Figure 3.17 illustrates a CompactRIO unit. The applications accomplished with this equipment make use of LabVIEW® software.

CompactRIO is an embedded system, which means that typically it is a component within a larger system, operating in a headless fashion, meaning there is no user interface, such as a keyboard, monitor and mouse (NI, 2007). The major fields of application for this platform are machine and industrial systems control, as well as the monitoring of their behavior. CompactRIO is mainly employed in embedded systems for applications such as in-vehicle

data acquisition, mobile noise, vibration, harshness testing, and embedded machine control systems.

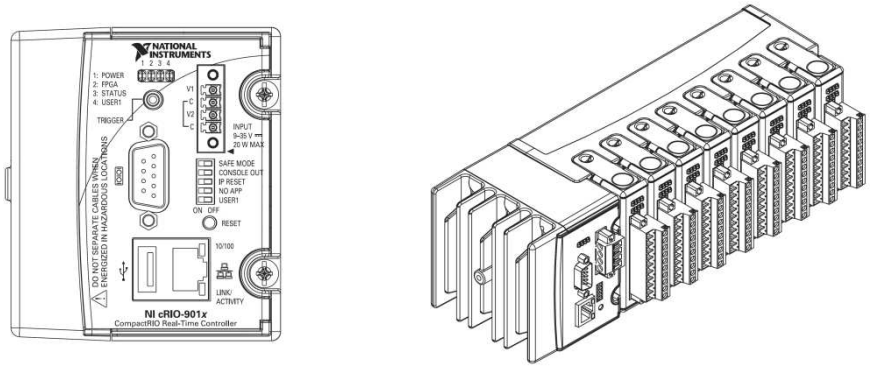

(a) (b)

Figure 3.17 - CompactRIO acquisition system (NI, 2007): (a) top view; (b) 3D view.

The host desktop at the COS receives the control software of these acquisition units, specifically developed for the monitoring system presented in this chapter. The LabVIEW® program allows to select the sensors whose signals are to be acquired, the associated control parameters, the sampling rate and data file size. The maximum acquisition frequency for a simultaneous reading of all sensors is 100 Hz, which is not only suitable for an accurate assessment of the structure dynamic behavior, but also makes possible the data collection for applying B-WIM techniques to characterize the crossing traffic. Nevertheless the default settings of the control software establish a 5 minute period between successive readings, most suitable for long-term monitoring.

3.7.2. Data Storage/Processing Sub-System (DSPSS)

A server, located at LABEST/FEUP, is responsible for the storage, management and processing of field observation data. The raw data, in the form of electrical quantities, are continuously collected by the DASS, stored in weekly files, and then transferred to the DSPSS server by the Connect Box inside the OS at the bridge. The DSPSS converts the raw data files in strain, displacement, rotation and temperature records. The collected readings are processed to remove the direct effects of the temperature on the sensors, making possible a proper assessment of the structure response due to the thermal actions on the bridge, but also enabling the appraisal of potential drifts in the structural behavior that may indicate structural damage, either local or global.

A website portal for the monitoring system has been developed to allow, with a high level of interactivity, the access to results by the bridge owner. The selection of the sensors and

time periods for graphic visualization of retrieved data is permitted, and surveillance and alert thresholds are defined for all sensors and can be updated by an authorized user. Other options available by the application are the emission of periodic reports with the monitoring results and the sending of alerts by electronic mail whenever the thresholds values are exceeded.

3.8. Summary and conclusions

The Pinhão road bridge is a centenary infrastructure that plays a relevant social and economic role in the vineyard region of Douro. In 2004 the structure was thoroughly inspected and in consequence some restrictions were made to vehicles passing over it. Following these measures a viability study for the bridge rehabilitation was performed aiming to fit the structure to the new and more demanding traffic conditions. The intervention works proposed in the study were accomplished in 2006. To appraise the effectiveness of the strengthening solutions adopted and the changes in the structural behavior induced by them, the installation of an electric based monitoring system became mandatory, so that a continuous assessment of the structural response and safety is achieved.

The system was deployed during the strengthening and rehabilitation works, and enables the observation of four different parameters: steel strains, longitudinal displacements, rotations and temperatures of the ambient and at the steel surface. The sensing network comprises 48 sensors. Sixteen cross-sections were instrumented with pairs of strain sensors, located in chords, diagonals, verticals, crossbeams and stringers, and all six sliding supports have their displacements monitored. Two inclinometers measure rotations in the north span and eight temperature sensors are positioned in chords at mid-span cross-sections, four to capture the ambient temperature and the remaining to monitor the steel temperature.

In order to assure a suitable durability and reliability to the monitoring system, proper methodologies and materials were used to accomplish the installation and protection of its several components, namely in the accommodation of the electric cables and wires and in the sensors application. Special care was also taken in selecting the electric network components. Laboratory tests were conducted to validate the sensors performance and to appraise the effectiveness of the protection systems installed in the bridge.

The sensors signals are acquired by data loggers that allow simultaneous readings with a sampling rate up to 100 Hz, suitable both for the use of B-WIM techniques to disclose traffic characteristics and for collecting data related with the dynamic component of the bridge behavior. The long-term monitoring of the structural response is accomplished by a pre-set program that establishes for all sensors 12 readings per hour. After a proper treatment of the raw data collected at the field, the strains, displacements, rotations and temperatures measured by the monitoring system are provided to the bridge owner through a website.

Chapter 4

Static and safety analyses of the Pinhão Bridge

4.1. Synopsis

The rehabilitation of old steel bridges is a field of growing relevance in terms of economic impact. However, at the level of engineering practice it still presents significant shortcomings with respect to the existing techniques and the experimental strategies of assessing their effectiveness and efficiency.

The state-of-the-art and state-of-the-practice in non-destructive testing and evaluation emerge as crucial issues for an accurate condition assessment of bridges, which is a powerful mean to assist the decision making process, to improve the rehabilitation projects in the design stage, as well as to identify the actual impact of the modifications introduced in the structural performance.

In this chapter the experimental and numerical study of a centenary steel bridge, the Pinhão Bridge, which underwent an extensive rehabilitation and strengthening process, is reported. The objectives to be achieved by the implementation of the structural monitoring project, as well as its scope, are outlined. The field tests and procedures adopted for their execution are described. The analysis of the measurement results collected before and after the construction works is performed and the validation of the three-dimensional numerical models developed to simulate the bridge's behavior for the different phases is presented. Finally, the safety assessment of the new bridge condition under the loading environment is carried out.

4.2. Introduction

Although many old iron and steel bridges constitute inseparable symbols of the landscape and milestones of the industrial heritage, for some of them, particularly the ones from the early days, the restoration or rehabilitation may be unfeasible. Technical reasons related to the poor condition, non-compliance with the contemporary structural safety codes or inability to meet the present traffic demands, besides obvious economic issues, may dictate the decommissioning, scrapping or replacement of these structures. Nevertheless, the number of rehabilitation and strengthening projects performed in steel and iron bridges has rapidly increased in the last decades, mainly driven by changes in the social, economic and technical environments.

Some of the various examples that can be found in the literature are described herein. Ghosh and Ghoshal (2002) have reported the repair schemes implemented in three structures located in Asia. The first bridge consisted of riveted through steel truss spans, one of which had suffered serious damage after a missile attack (see Figure 4.1(a)). The second bridge, a balanced cantilever steel truss suspension superstructure, underwent the repair or replacement of several elements and devices after a thorough survey have revealed extensive damages. In the third case new heavier and fastest locomotives compelled the strengthening of a through Pratt railway truss bridge (see Figure 4.1(b)).

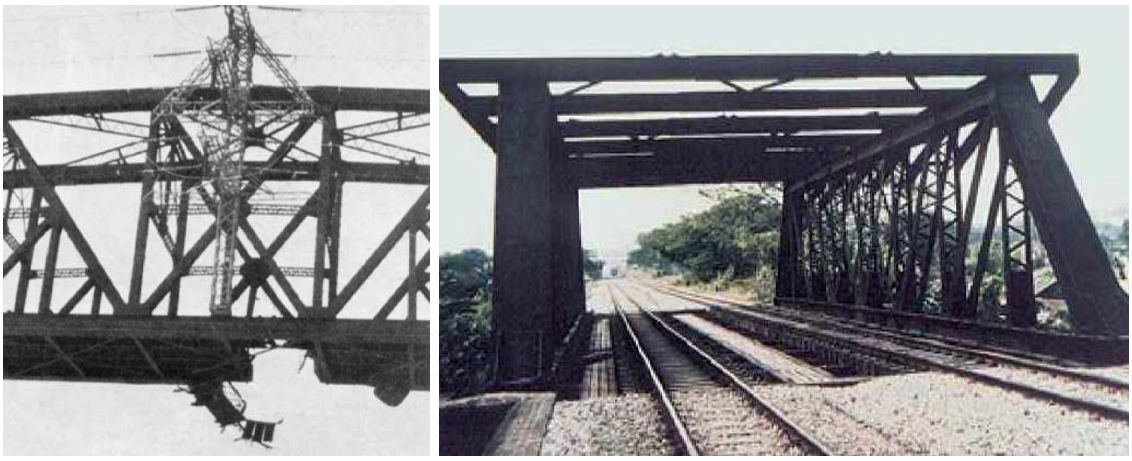

(a) (b)

Figure 4.1 - Rehabilitation projects of steel bridges in Asia: (a) damaged structure due to a missile attack; (b) railway truss bridge unfit to sustain new vehicles (Ghosh and Ghoshal, 2002).

Kääriäinen and Pulkkinen (2002) have presented the strengthening and rehabilitation of a riveted steel truss structure located in Northern Finland, whose main problem was the corrosion of the steel aggravated by the de-icing salts used on the road surface (see Figure 4.2(a)). The Kamp Bridge, in Lower Austria, is an example of a well successful

rehabilitation process performed on a wrought iron structure, whose design took into account the requirements of today's railway standards without producing visual changes in the structure, as depicted in Figure 4.2(b) (Holzinger *et al.*, 2002). Extensive construction works have been executed to upgrade a centenary double-deck steel arch bridge located in Northern Portugal, with the goal of providing the required capacity to safely withstand the new load conditions due to the integration of the upper deck in a light rail network (Lopes *et al.*, 2008).

(a) (b)

Figure 4.2 - Rehabilitation projects of steel bridges in Europe: (a) Tornionjoki steel Bridge (Kääriäinen and Pulkkinen, 2002); (b) side view of the old Kamp Bridge (Holzinger *et al.*, 2002).

State-of-the-art methodologies for structural condition assessment have been applied to assist the decision-making process in the management of old iron and steel bridges. In all of them, the adoption of suitable experimental and numerical tools is crucial. Within a standard framework, non-destructive testing techniques supply valuable data for the calibration of models, ultimately leading to a complete structural identification. Only through a combined and rational approach of these arts is possible to detect, characterize and quantify useful reserves in the load-carrying capacity or to identify the weakest links in the structural resistance.

Several projects can be pointed as references in the condition assessment of old iron and steel bridges. Chajes *et al.* (1997) have performed the load rating of a posted 3-span steel-girder-and-slab bridge through a diagnostic loading test. The experimental results allowed to obtain the mechanical properties of the composite girders to be adopted in the finite element analyses, which in turn were later used to validate the measured response of the structure and to assess its load-carrying capacity by accounting for different scenarios. Chakraborty and DeWolf (2006) have carried out load tests on a 3-span slab-on-steel-girder bridge to validate a FE model used to assist the determination of live load distribution factors for comparison with the values stipulated by the AASHTO

Specifications. Bancila and Cristescu (1998) have reported the successful assessment of a combined railway and highway truss girder bridge. In this study the material was identified, in situ tests were conducted to validate and/or calibrate the models, and structural analyses were performed in accordance with modern codes and traffic volume forecasts. O'Connell and Dexter (2001) have measured the strain responses of several members of two different steel truss bridges under controlled truck loads. The readings were compared to predicted quantities provided not only by simplified structural analyses but also through 2D and 3D FE models. Allen and Rens (2004) have presented the results of a strain gage study performed on a slab-on-girder bridge that underwent significant structural changes during its rehabilitation. Shortly afterwards the completion of the works, structural distress in most of the ending piers prompted a detailed evaluation to assess their condition and to determine the urgency and extent of necessary corrective measures. Fu *et al.* (2007) planned an extensive performance evaluation of a truss bridge, in which the replacement of the concrete deck by a fiber-reinforced polymer (FRP) composite one constituted the major upgrade task (see Figure 4.3(a)). Strain measurements were taken from several bridge members while loading the structure. The collected data permitted to investigate the structural role played by the FRP deck, the live load distribution factors and the bridge load rating. Short-term strain monitoring campaigns were carried out by Rodrigues *et al.* (2012) on a double-deck steel truss bridge (see Figure 4.3(b)) using fiber Bragg grating strain sensors, in order to appraise key issues concerning the behavior and safety of the structure at the beginning, during and after the strengthening works.

(a) (b)

Figure 4.3 - (a) Placement of a new FRP composite deck on a truss bridge (Fu *et al.*, 2007); (b) double-deck steel truss bridge monitored by means of fiber Bragg grating sensors.

In this chapter the experimental and numerical study of a centenary steel bridge, the Pinhão Bridge, which underwent an extensive rehabilitation and strengthening process, is

reported. The main objectives to achieve through the implementation of the structural assessment program were:

i. To supply field data for the validation of the numerical models developed to simulate the behavior of the bridge during different phases;
ii. To assist the design in order to select and/or optimize the upgrade strategies and solutions to be adopted;
iii. To allow an easy interpretation of the changes produced in the bridge performance as a result of the construction works carried out;
iv. To evaluate the effectiveness of the implemented strengthening schemes.

With the purpose of meeting these requirements specific procedures were devised for the field tests related both to the loading process and to the instrumentation. Finally, the safety assessment of the bridge for the new loading conditions is carried out.

4.3. Background

4.3.1. Geographic, economic and historical context

The Pinhão Bridge establishes a key roadway link over the Douro River between the districts of Viseu and Vila Real, near the village with the same name in the north of Portugal. According to the available historical elements, the structure was built between 1903 and 1906, and was opened to the traffic in 1907 after a field test had been performed. Nowadays, the bridge stands as a significant heritage of the industrial history and still plays a major role in the roadway infrastructure of the Alto Douro vineyard region, being the only river crossing available in a 25 km radius.

The tragic failure in March of 2001 of the Hintze Ribeiro Bridge located downstream in the same river, worldwide reported by the media at the time, brought to light weaknesses in the maintenance and management systems of the country's infrastructures. This unfortunately event caused a great concern in the responsible authorities and alarm among the general population. In response, the National Roadway Institute (E.P. - Estradas de Portugal) engaged a national campaign of inspections to assess the condition of several bridges and viaducts, particularly the structures crossing the same river spanned by the collapsed bridge. One of such surveys was conducted on the Pinhão Bridge by means of a step-by step procedure, between 2003 and 2004, and led to traffic restrictions in terms of the vehicles gross weight and speed (Pinto, 2005). Then, the condition assessment of the

bridge was carried out, which included an in-depth experimental campaign for the complete characterization of the structural behavior. The results enabled to conclude that it was viable to repair and strengthen the bridge to withstand the current operation conditions, in accordance with the Portuguese national code (RSAEEP, 1983). Figure 4.4 shows the main geometric features of the Pinhão Bridge.

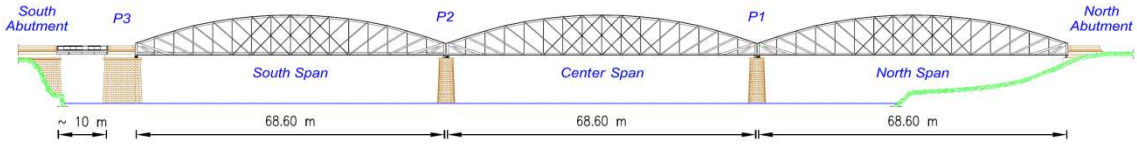

Figure 4.4 - Elevation of the Pinhão Bridge.

4.3.2. Anomalies and rehabilitation project

During the in-depth survey carried out to support the viability study several problems were identified, being the poor condition of the steel protective coating and the large transverse vibration amplitudes of the very slender diagonal plates the most critical. Other inadequacies were:

i. Cross-section loss in some elements caused by severe corrosion, particularly at the expansion joints;
ii. Extensive corrosion of the bridge under the floor system, namely in the chords, bracing, crossbeams and gusset plates;
iii. Delamination and defoliation at the sections edges as consequence of the corrosion;
iv. Localized deformation of the sections plates at the riveted connections of the composite members caused by rust between steel layers;
v. Partial locking of the bearings due to deterioration and/or lack of maintenance;
vi. Clogging of the draining system in the lower chords and at the roadway pavement;
vii. Housing of infrastructure cables and deposition of organic material and dust inside the lower chords;
viii. Severely degraded thin asphalt layer.

Figure 4.5 illustrates some of the existing problems before the bridge rehabilitation.

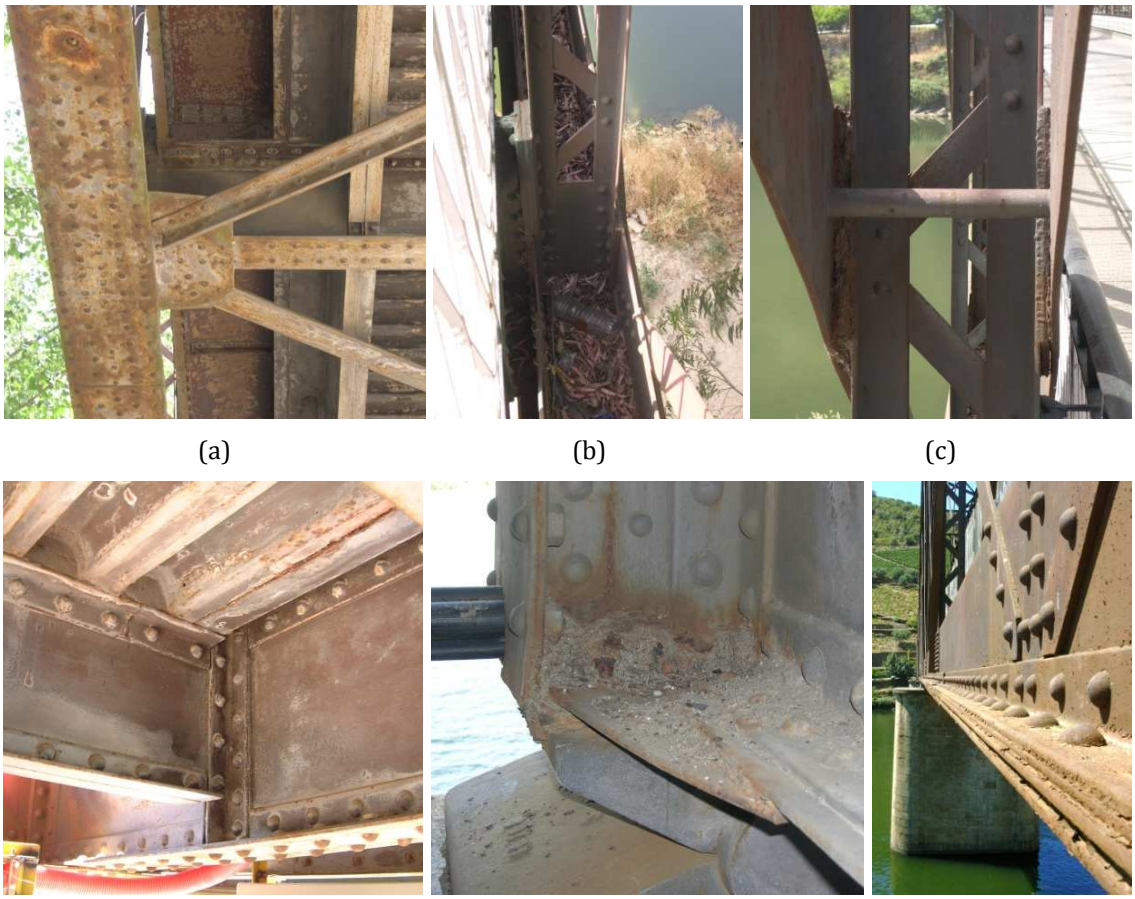

(a) (b) (c)

(d) (e) (f)

Figure 4.5 – Anomalies of the Pinhão Bridge before the rehabilitation: (a) deteriorated coating and widespread signs of rust; (b) leaves and garbage inside the lower chord; (c) cracks in the connection between a diagonal and a vertical due to inappropriate welding; (d) corrosion of the steel sheet under the deck slab; (e) pocket of severe corrosion near a girder support; (f) corrosion between the layers of riveted plates in the lower chords.

The rehabilitation plan of the structure sought:

i. To repair all deficiencies due to lack of maintenance;
ii. To correct the poor design and construction of some details that led to durability issues;
iii. To strengthen all elements that had revealed unsuitable behavior in the bridge condition assessment;
iv. To extend the life of the bridge for 30 years endowing it with the load-carrying capacity to withstand heavy vehicles weighing no more than 30 tons travelling at a speed below 50 km/h.

The rehabilitation works included the:

i. Repair of damaged elements;

ii. Cleaning of whole steel surface through hydroblasting and application of a new 3-layer epoxy painting;
iii. Strengthening of the deck floor system by attaching a new steel grid on its top (see Figure 4.6(a) and (b));
iv. Replacement of the old concrete-steel composite slab by a reinforced concrete one, fabricated by pouring a 0.10 m thick layer of concrete over 0.07 m thick precast concrete slabs shear connected to the supporting grid (see Figure 3.2);
v. Addition of reinforcement angles to the chords and some diagonals (see Figure 4.6(c));
vi. Replacement of the diagonals plates by pairs of C-sections endowed with proper shear connection (see Figure 4.6(d));
vii. Thickening of the verticals flanges with flat plates (Figure 4.6(e));
viii. Replacement of the original roller and pin bearings by modern pot and disk bearings, respectively, as well as of the expansion joints (Figure 4.6(f)).

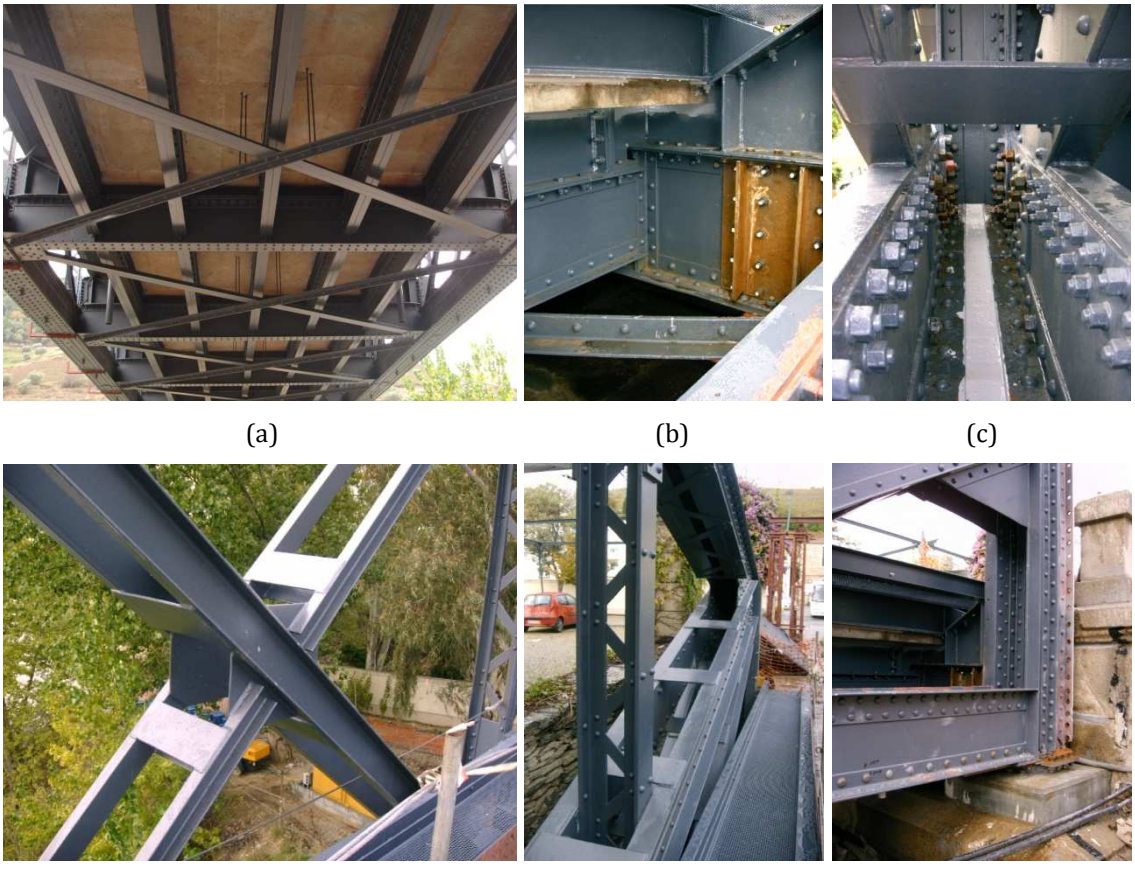

(a) (b) (c)

(d) (e) (f)

Figure 4.6 - Pinhão Bridge after the construction works: (a) strengthened floor system with the new concrete slab; (b) detail of the strengthening applied to a crossbeam at its end; (c) strengthened lower chord (new-added angles at the webs tops); (d) new diagonals; (e) strengthening of a vertical; (f) new disk bearing at the north abutment.

4.4. Bridge testing

4.4.1. Objectives

The controlled field tests were planned in order to accomplish several purposes according to the stage in which they were conducted, described as follows:

i. The test carried out before the bridge rehabilitation, henceforward named as Test 1, served as a diagnostic test in that it enabled an improved understanding of the load paths, deformation mechanisms and behavior of the joint connections between different structural elements. Therefore, the stiffness of the joints, secondary effects of the deformation and composite action of the floor system, between the deck slab and the steel grid, were analyzed;
ii. These experimental results were also used to validate and/or update the FE model that would be adopted to support the analyses for studying different strengthening schemes at the design stage;
iii. The test performed after the completion of the rehabilitation works, from now on termed as Test 2, aimed at assessing the effectiveness of the strengthening solutions;
iv. Field data from this test would be necessary to validate the FE model so that it could accurately simulate the structure response under the new operating conditions and thus support the periodic characterization of the passing traffic;
v. Testing after the rehabilitation would provide a baseline condition to serve as a reference for the data collected by the structural monitoring system, which was installed on the bridge to detect any deviation of the structure behavior over the time (Costa *et al.*, 2009);
vi. The loading and instrumentation in both tests should allow the direct comparison of the structure performance, before and after the rehabilitation, and consequently favor the drawing of conclusions.

4.4.2. Loading procedures

With the bridge temporarily closed to traffic, three types of loading scenarios were implemented in the field tests, static, quasi-static and dynamic. For any of them it was expected that the bridge response would remain within the linear-elastic range. Moreover, all the tests were conducted early in the morning to reduce the temperature variation effects on the structure response. Three-axle single-unit trucks were used in each test to

accomplish the load configurations, having an average gross weight of 120 kN in Test 1 and 126 kN in Test 2. For all trucks the tandem axles were 1.40 m apart while the distance between the front axle and the first tandem axle ranged between 3.10 m and 4.75 m.

In the static load cases sets of test trucks, in a longitudinal line formation, were positioned at pre-defined locations over the bridge. Quasi-static testing was carried out by single trucks crossing the bridge in one direction at a crawling speed of approximately 3 km/h. The dynamic tests consisted in single trucks passing over 2 cm high bumps placed at the mid-span with approaching and traversing speeds around 40 km/h and 10 km/h, respectively. In order to appraise the lateral load distribution the test trucks travelled along three different paths, one coincident with the bridge centerline, and the others close to either the upstream girder or the downstream girder.

For Test 1 a set of three trucks was sequentially positioned along the bridge to accomplish six static load cases, distributing the load over a length of 22.90 m. In the first three cases the set of trucks was centered in each main span, while the remaining three load cases were carried out only in the north span by positioning the front axle of the center vehicle over the axis of the 7th, 4th and 3rd crossbeams, respectively. After that, three slow crossings in the north-south direction took place one for each test path.

As regards to Test 2 it also comprised six static load cases, two in each main span. The first three were performed with a set of seven trucks immobilized in their center and the other three carried out with only three trucks. The loading line for the highest load cases was 57.30 m long while for the remaining was shortened to 23.80 m. Additionally, one slow crossing and two dynamic tests were conducted in the south-north direction.

Table 4.1 – Identification codes for loading events.

Code entry	*Description*	*Configuration*																			
1	Test	1									2										
2	Load case	1[a]	2[a]	3[a]	4[b]	5[c]	6[d]	7	8	9	1[a]	2[a]	3[a]	4[a]	5[a]	6[a]	7	8	9		
3	Loading scenario	S						Q			S						Q	D			
4	Path	C						D	U	C	C										
5	Loaded spans	S	C	N				A			S	C	N	S	C	N	A				

Code entry 3 - Static (S), Quasi-static (Q), Dynamic (D);

Code entry 4 - Center (C), Downstream (D), Upstream (U);

Code entry 5 - South span (S), Center span (C), North span (N), All spans (A);

[a] Centered in each main span; [b] Front axle of the center vehicle is lined up with the axis of the 7th crossbeam; [c] Front axle of the center vehicle is lined up with the axis of the 4th crossbeam;. [d] Front axle of the center vehicle is lined up with the axis of the 3rd crossbeam.

For the interpretation and analysis of the results presented in the following sections a 5-key identification code is given for each loading event so that the test, load case, loading scenario, path and loaded span are easily recognized. Table 4.1 summarizes the information for the labeling of the loading events.

The first two numbers specify the test and load case numbers, respectively. The third entry, either S (static), Q (quasi-static) or D (dynamic), identifies the loading scenario, whereas the fourth denotes the load path as C (center), U (upstream) or D (downstream). The fifth entry in the code points to which of the main spans is loaded, with the north, center and south spans identified by letters N, C and S, respectively, while the loading of all spans is represented by letter A. As an example, 18QUA is the code for the eighth load case in the Test 1, conducted as a quasi-static crossing in the upstream path along the entire bridge.

4.4.3. Instrumentation and data collection

For the Test 1, conducted before the rehabilitation, five parameters were measured:

i. Strains in the steel structure;
ii. Vertical displacements in the middle of the three main spans and at the third crossbeam of the north span;
iii. Deck longitudinal displacements at the roller bearings;
iv. Rotations of the girders supports;
v. Ambient temperature.

In Test 2, carried out just after completion of the rehabilitation works, the permanent structural health monitoring system was used (Costa *et al.*, 2009), supplemented by additional sensors set in place for measuring the deflection of the girders in all spans. Table 4.2 presents the type and number of sensors used to measure the quantities in both tests, as well as their location on the bridge.

Figure 4.7 shows de location of the instrumented points and cross-sections in the north span, for which the suffix '-' or '+' in their designation means that the cross-section strains were monitored before or after the rehabilitation, respectively. The position of the strain gages in the cross-sections, as well as their labels, is depicted in Figure 4.8.

Table 4.2 – Instrumentation in the field tests.

Test	Quantity	Location	Sensors (No.)
1	Strains	Chords, diagonals, verticals, stringers and crossbeams of the north span	Foil strain gages (34)
	Vertical displacements	Middle of the main spans (lower chords)	Liquid leveling system (4)
		Third crossbeam of the north span	Displacement transducers (3)
	Longitudinal displacements	Roller bearings of the north span	LVDTs (2)
	Longitudinal rotations	Supports of the downstream girder of the north span	Biaxial inclinometers (2)
	Ambient temperature	Middle of the center and north spans (lower chords)	RTDs (4)
2	Strains	Chords in all main spans and diagonals, verticals, stringers and crossbeams of the north span	Foil strain gages (32)
	Vertical displacements	Middle of the main spans (lower chords)	Liquid leveling system (6)
		Middle of the north span (lower chords)	Displacement transducers (2)
	Longitudinal displacements	Sliding supports of all main spans	LVDTs (6)
	Longitudinal rotations	Upstream end of the 1st crossbeam in the north span	Uniaxial inclinometer (1)
	Transverse rotations	Upstream end of the 9th crossbeam in the north span	Uniaxial inclinometer (1)
	Steel & Ambient Temperature	Middle of all spans (lower and upper chords)	RTDs (8)

The interrogation and recording of the signals from all sensors was performed by four data loggers *dataTaker® DT800* in Test 1 and two acquisition systems *CompactRIO* from *National Instruments™* in Test 2. In the first test the data were sampled at 1 Hz while in the second test the readings were collected with a rate of 100 Hz.

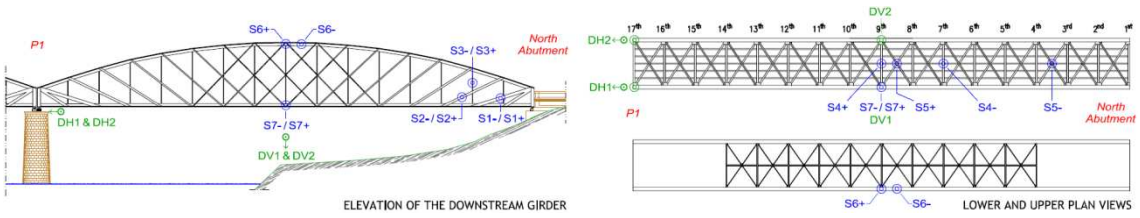

Figure 4.7 - Sections and points of the north span monitored during the field tests.

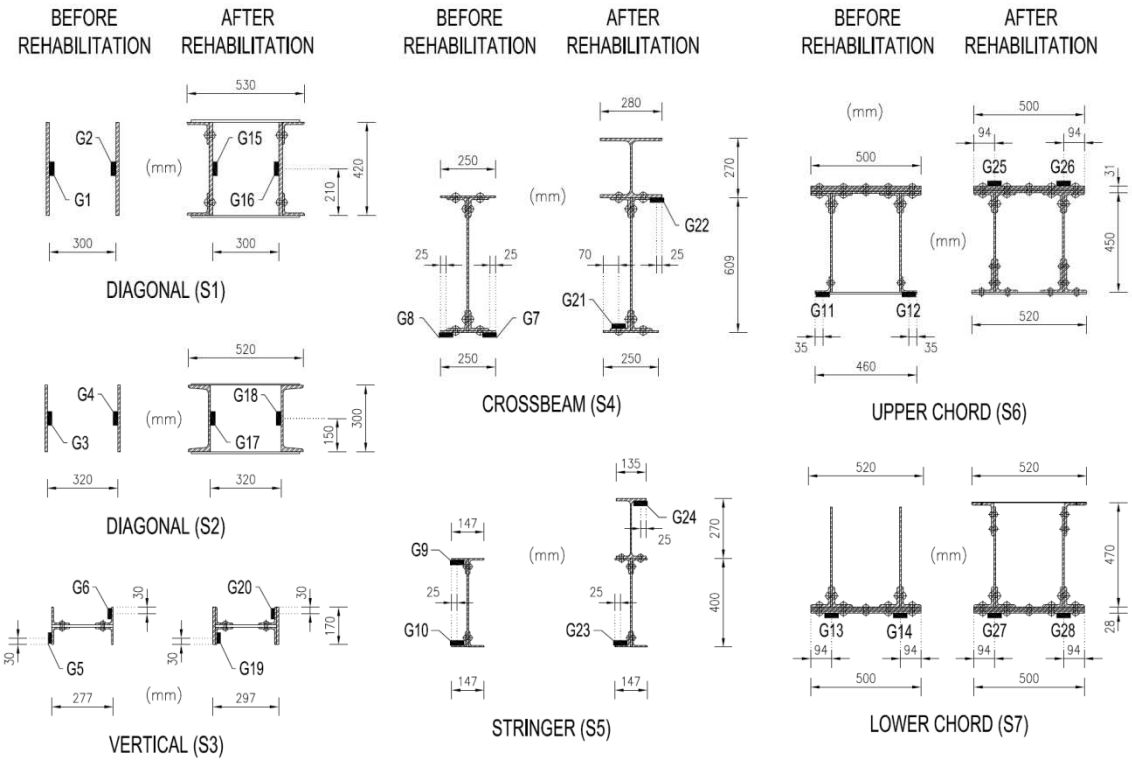

Figure 4.8 - Strain gages location at the cross-sections of the structural elements.

4.5. Finite element modeling of the bridge

4.5.1. Introductory remarks

In spite of the large number of reported works concerning the modeling of truss bridges, the conceptualization of a model capable of integrating the several structural subsystems still poses a great challenge (Catbas *et al.*, 2007). A strong structural engineering expertise and an accurate definition of the structure geometry in the as-is state are a good starting point for constructing any numerical model. However, its physical completeness requires a thorough and complete simulation of the: material behavior; boundary and continuity conditions; stiffness distribution and structural connectivity; key mechanisms of external and intrinsic loading transfer; and displacement kinematics (Zhou, 2006).

On the other hand, the designed model must take into account several factors, such as the objectives to be accomplished, the quality, quantity and characteristics of field data available for validation and/or calibration, adopted analysis software and relative weight of the model resolution versus computational effort (Aktan *et al.*, 1998). Ultimately, for the vast majority of tested bridges a deterministic physics-based 3D model can provide a

reliable estimate of the structure response by assuming linear and elastic behavior under stationary loads (Catbas *et al.*, 2007).

4.5.2. General features

The model developed for the analysis of the Pinhão Bridge replicates a single main span. It utilizes a 3D mixed meso-micro level modeling approach by means of frame and shell finite elements, having all nodes six degrees-of-freedom (DOF). For the sake of clarity, a frame element represents a bar with six internal forces, which are the axial force, torsion, two shear forces and two bending moments about two perpendicular axes. The shear deformations of the frame elements are taken into account. A shell element simulates simultaneously the slab and plate actions of a thin two-dimensional structural element. The numbers of the constructed model are as follows: 53460 DOFs, 4090 frame FEs and 6220 shell FEs. The general aspect of the model can be seen in Figure 4.9.

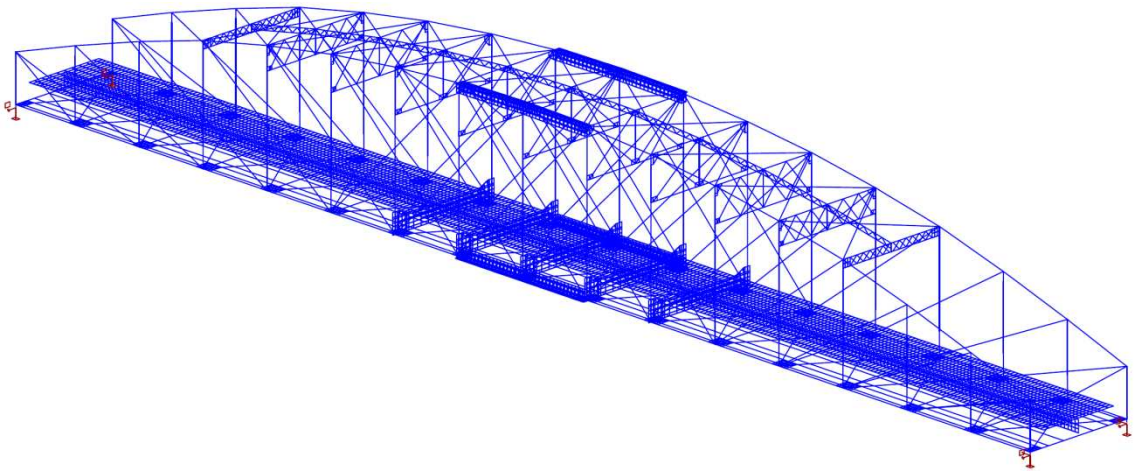

Figure 4.9 - Numerical model of a single span.

4.5.3. Modeling strategy

The in-plane and out-of-plane deformations of the deck slab are modeled through four node rectangular shell elements, positioned at its mid-height. Figure 4.10 illustrates the discretization of the floor system cross-section for both pre and post-rehabilitation conditions.

The diagonals and verticals in the main girders, as well as the bracing system and transverse sway trusses, are simulated by frame elements. For these structural elements the stress field is mainly ruled by the axial force. The flexural bending is only a result of the rigid connections at their end nodes.

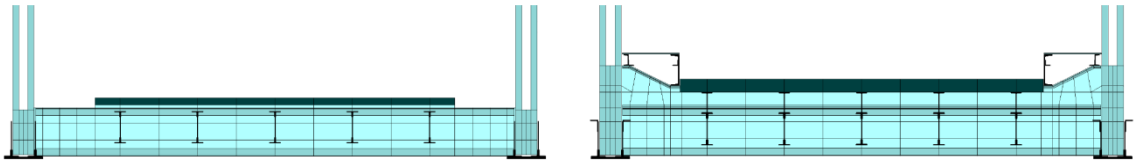

(a) (b)

Figure 4.10 - Modeling of the floor system cross-section: (a) before the rehabilitation; (b) after the rehabilitation.

In what concerns the crossbeams and stringers of the floor system, the modeling is carried out using two different approaches. The elements whose strains had been gauged in the field tests are simulated using four node rectangular shell elements in the webs (see Figure 4.10) and frame elements in the flanges (angles and plate), while the remaining elements of the steel grid are simulated by frame elements.

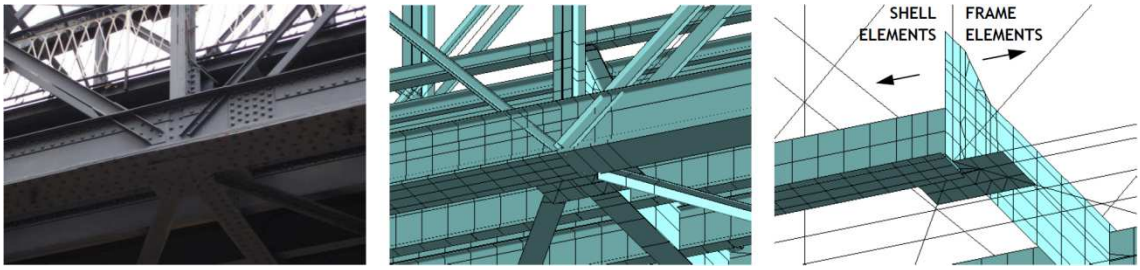

(a) (b) (c)

Figure 4.11 - Lower girder joint where the modeling of some components changes from frame to shell elements: (a) bottom view of the bridge; (b) bottom view of the model with the bars shown as extruded profiles and the shell elements represented with their thickness; (c) view of the model picturing the shell elements and the axes of the frame elements.

This same principle was adopted in modeling the girders U-chords. However, in this case all the flat plates of the composed section are represented by shell elements and only the angles are modeled by frame elements. Hence, in the two central panels the chords are simulated through a combination of frame and shell elements, whereas in the other panels only frame elements are adopted. The bottom view of the model near a lower girder joint, where the I-type and U-type members are shown, is depicted in Figure 4.11. Figure 4.12 shows the detail of a girder upper joint.

This modeling strategy for the floor system grid and chords served two main purposes. Firstly, a finer discretization of the elements under bending, or combined bending and axial force, would improve the correlation between calculated and measured strains. Secondly, the geometry and mechanics of the joints may induce significant secondary stresses on the connected elements which cannot be reproduced by a simpler frame based modeling.

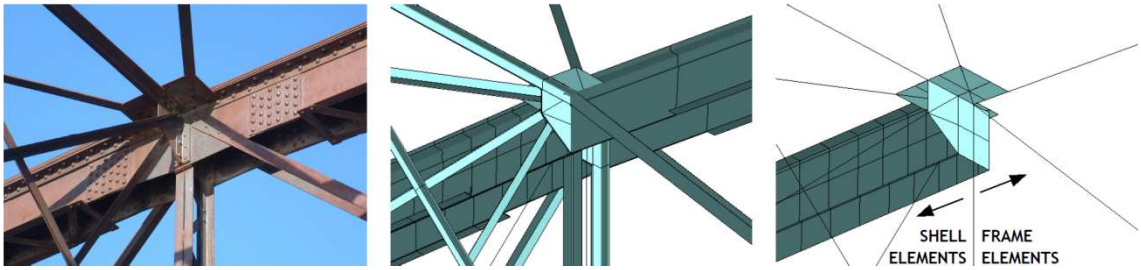

(a) (b) (c)

Figure 4.12 - Upper girder joint where the modeling of the chord changes from frame elements to shell elements: (a) side view of the bridge; (b) side view of the model with the bars shown as extruded profiles and the shell elements represented with their thickness; (c) side view of the model picturing the shell elements and the axes of the frame elements.

4.5.4. Connections, supports and materials

The crossbeams and stringers are attached to the deck shell elements through rigid links, by connecting either the top of the webs shell elements or the axes of the frame elements. The continuity in the chords between panels modeled differently is assured by body constraints at the corresponding joints. The connections between the bracing bars and chords are accomplished by shell elements simulating the gusset plates, so that the out-of-plane joints rigidity could be accurately incorporated (see Figures 4.11 and 4.12). The two bearings at one end of the span allow the longitudinal rotation (pin/pot bearings) whereas in the other end the longitudinal displacements are also permitted (roller/disk bearings).

The Young's modulus (E) and Poisson's ratio (ν) of the materials are as follows:

i. Original steel, $E_{os} = 202$ GPa and $\nu_{os} = 0.25$;
ii. New-added steel, $E_{ns} = 210$ GPa and $\nu_{ns} = 0.30$;
iii. Original concrete, $E_{oc} = 30$ GPa and $\nu_{oc} = 0.166$;
iv. New concrete, $E_{nc} = 34$ GPa and $\nu_{nc} = 0.166$.

4.5.5. Additional procedures in the modeling

Other major aspects were considered in the modeling process. Firstly, in order to accurately represent the structure geometry the centers of gravity of the frame elements are correctly positioned in space by offsetting them from the reference axes connecting the model nodes. Secondly, the cross-sectional properties of the truss members are defined based on design documents produced during the survey conducted before the rehabilitation. Thirdly, as the original and new-added steels do not present the same

elastic parameters, the cross-sectional properties of the frame elements representing the strengthened members had to be computed for an equivalent section made of a single material (weighed properties). Finally, given that the structure has two symmetry planes the model should keep the same feature, e.g. the stringers in a certain panel are simulated in the same manner in the symmetric panel.

4.6. Analysis of the results

In this section the field results collected during the static load cases of both tests are presented, and the capability of the developed models to supply accurate estimates of the structural response, both global and local, is evaluated. The analysis of the changes produced in the bridge behavior as a result of the rehabilitation process will only be addressed in the following section.

4.6.1. Displacements

Table 4.3 lists the horizontal displacements (DH) at the sliding bearings and the girders deflections (DV) measured in Tests 1 and 2, as well as the predicted values by the numerical analysis. The loading events selected are the ones that maximized the observed quantities.

Table 4.3 – Measured and calculated displacements for the static loading scenarios.

Before the rehabilitation					*After the rehabilitation*				
Test code	*Gage*	δ_1 *(mm)*	δ_{FEM} *(mm)*	Δ *(%)*	*Test code*	*Gage*	δ_2 *(mm)*	δ_{FEM} *(mm)*	Δ *(%)*
13SCN	DV1	7.65	7.63	-0.26	23SCN	DV1	10.95	11.27	2.89
	DV2	7.59	7.64	0.66		DV2	10.94	11.27	3.01
	DH1	1.36	1.63	19.85		DH1	2.34	2.38	1.87
	DH2	1.27	1.63	28.35		DH2	2.30	2.39	3.82

δ_1 – Displacements measured in Test 1; δ_2 – Displacements measured in Test 2; δ_{FEM} – Displacements calculated from the FE model; $\Delta = \delta_{FEM}/\delta_i - 1$; Total load applied in Test 1: 361 kN (22.9 m); Total load applied in Test 2: 885 kN (57.3 m).

The correlation between experimental and numerical results is very good, except for the horizontal displacements before the rehabilitation. This considerable deviation was caused by the poor condition of the roller bearings due to lack of proper maintenance. During the survey carried out for the viability study, dirt, bird droppings and corrosion were extensively detected in the supports regions, which combined with the insufficient

lubrication of their components led to some restrictions to the free movement of the structure. In spite of this discrepancy in the supports displacements, it is possible to conclude that the FE modeling accurately simulates the global behavior of the bridge.

4.6.2. Strains

The maximum strains collected during the field tests and the corresponding numerical estimates are presented in Table 4.4. Focusing on the readings, the results show a non-uniformity of the stress state in the elements that are not subjected to direct loading (vertical, diagonal and chords), being larger for the vertical and minimum for the diagonals. This indicates the existence of a significant bending component in these elements, which was not expected for a truss structure. Although it might not be completely clear from the static loading results the strains acquired in the slow crossings leave no doubts, as depicted in Figure 4.13. This fact is even more relevant for the lower chord in which the plots have no scale correspondence. In this case, a local disturbance of the strains at the peak region is noticed, which is due to the flexural and torsion deformations induced by the crossbeam that transfers the deck load at the joint.

Table 4.4 – Measured and calculated strains for the static loading scenarios.

	Before the rehabilitation					*After the rehabilitation*				
Element (Section)	*Test code*	*Gage*	ε_1 ($\mu\varepsilon$)	ε_{FEM} ($\mu\varepsilon$)	Δ (%)	*Test code*	*Gage*	ε_2 ($\mu\varepsilon$)	ε_{FEM} ($\mu\varepsilon$)	Δ (%)
Diagonal (S1)	15SCN	G1	38.65	38.36	-0.76	26SCN	G15	15.75	17.48	10.95
		G2	37.14	33.82	-8.94		G16	15.15	14.33	-5.41
Diagonal (S2)	14SCN	G3	45.71	46.43	1.57	26SCN	G17	23.56	23.03	-2.23
		G4	45.00	43.14	-4.14		G18	22.58	22.07	-2.27
Vertical (S3)	14SCN	G5	-37.14	-32.51	-12.46	26SCN	G19	-18.52	-16.85	-9.02
		G6	-15.71	-25.19	60.32		G20	-8.71	-14.74	69.28
Crossbeam (S4)	14SCN	G7	42.56	45.19	6.18	26SCN	G21	24.85	26.01	4.67
		G8	41.65	43.10	3.48		G22	0.37	1.19	222.5
Stringer (S5)	16SCN	G9	1.43	1.74	21.67	26SCN	G23	21.25	20.12	-5.30
		G10	33.05	30.31	-8.29		G24	---	3.87	---
Upper chord (S6)	13SCN	G11	-11.43	-15.58	36.27	26SCN	G25	-43.54	-48.02	10.28
		G12	-18.57	-17.27	-7.02		G26	-45.12	-48.25	6.93
Lower chord (S7)	13SCN	G13	32.86	34.15	3.92	26SCN	G27	28.09	28.38	1.04
		G14	34.33	36.19	5.41		G28	25.68	26.59	3.55

ε_1 – Strains measured in Test 1; ε_2 – Strains measured in Test 2; ε_{FEM} – Strains calculated from the FE model; $\Delta = \varepsilon_{FEM}/\varepsilon_i - 1$; Total load applied in Test 1: 361 kN (22.9 m); Total load applied in Test 2: 377 kN (23.8 m).

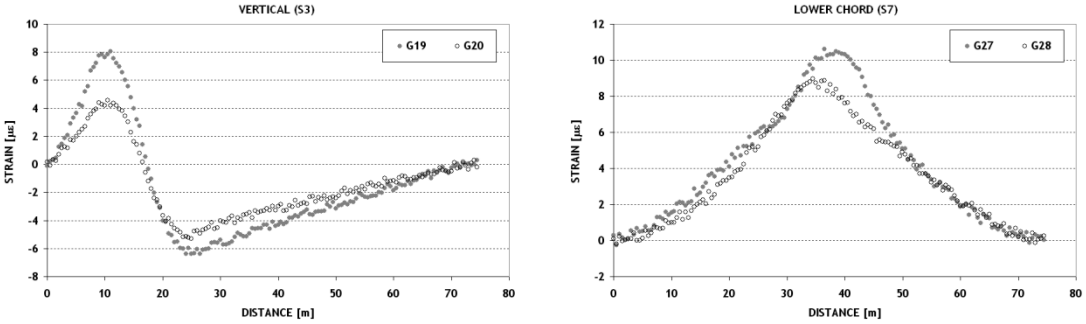

(a) (b)

Figure 4.13 - Strains collected during the quasi-static loading in Test 2 (27QCA) for an equivalent truck weighing 100 kN: (a) vertical (S3); (b) lower chord (S7).

Regarding the numerical results for the static loading, in general they compare well with the gauged strains. The correlation for the diagonals, lower chord, and lower flanges of the crossbeam and stringer, is very good, with an average difference lower than 5 %. However, experimental and numerical data from the vertical and upper chord are largely divergent.

In what concerns the vertical, the strain fields are highly influenced by the out-of-plane bending deformation compelled by the joint rotation at the lower end (see Figure 4.11). When the floor system is loaded in the panels adjacent to the vertical, the corresponding crossbeam is subjected to bending that causes the rotation of its ends. Consequently, this rotation is imposed to the vertical inducing its bending. In both models the verticals are modeled by means of a single bar, assuming the lacing system as a perfect shear connection between the flanges (pairs of angles). However, this behavior is not real, and for that reason the deformation of the inner flange (gages G5 and G19) is increased and that of the outer flange is decreased (gages G6 and G20) with respect to the numerical simulation.

For the differences observed in the upper chord two different reasons can be specified. For Test 1, in the analysis of the results it is necessary to bear in mind that strain gages were attached to the lower angles of the U-section (see Figure 4.8). These flanges are interrupted at an average distance of 1 m from the joint, thus leading to a considerable change in the load path, which in turn results in a reduction of the carried stresses/strains by the angles at the middle of the panel. Instead of contributing directly to the sectional properties these elements act only as edge stiffeners of the webs preventing their buckling. In Test 2, although the strains have been measured in the flange of the section at the joint, in this region the webs are reinforced with cover plates that locally increase the stiffness (see Figure 4.12), and therefore cause a reduction of the section deformation.

4.6.3. Quality of the numerical results

Although the ability in predicting the local behavior from the numerical analysis is not as good, in the overall assessment the correlation between the tests results and the values predicted by the FE models can be considered as satisfactory. Thus, it can be concluded that the adopted modeling approach was accurate for predicting the structure response, and in consequence the assumptions on which it relied on are sound. The bridge performance is better described by a frame structure, as assumed, than considering a truss system. Additionally, the composite action between the concrete deck and the supporting steel grid is clear when looking at the beams strains (crossbeams and stringers). At the bottom flanges large deformations were found whereas at the top the values are close to or fall within the measurement error (2 με).

4.7. Experimental assessment of the bridge rehabilitation

4.7.1. Displacements

Table 4.5 enables the direct comparison of the displacements collected before and after the bridge rehabilitation, so that conclusions can be drawn concerning the changes occurred in the global structural response. In order to make an accurate evaluation, similar load events have to be selected. As the static loading events in Test 1 were carried out with a 3-truck set, the field data chosen for characterizing the structure performance in its new condition are supplied by the equivalent load cases in Test 2. Moreover, as the trucks used in the tests were not the same, and hence nor their gross weights, the results are presented as a ratio per 100 kN of load applied to the bridge.

Table 4.5 – Displacements measured for comparable static loading scenarios.

	Before the rehabilitation		*After the rehabilitation*		
Sensor	*Test code*	δ_1 *(mm)*	*Test code*	δ_2 *(mm)*	Δ *(%)*
DV1	13SCN	2.08	26SCN	1.64	-21.28
DV2		2.06		1.65	-19.78
DH1		0.37		0.30	-18.13
DH2		0.34		0.30	-12.81

δ_1 – Displacements in Test 1 per 100 kN of applied load; δ_2 – Displacements in Test 2 per 100 kN of applied load; $\Delta = \delta_2/\delta_1 - 1$; Total load applied in Test 1: 361 kN (22.9 m); Total load applied in Test 2: 377 kN (23.8 m).

From the comparison of the pre and post-rehabilitation girders deflections an overall increment of 20.5 % for the vertical stiffness can be inferred. With respect to the horizontal displacements at the supports their assessment requires some caution. The results show that the structure response experienced an average 15 % reduction. However the readings of Test 1 were taken when restrictions affected the regular performance of the supports.

4.7.2. Static strains

As with the previous table, strains in Table 4.6 were computed to assist a direct analysis of the variation in the structure deformation as a result of the rehabilitation. For the sections whose elements have the deformation mainly controlled by the axial force the values listed are average strains, whereas for the crossbeam and stringer the table displays only the strain measured at the lower flange, either averaged or simple.

Table 4.6 – Strains measured for comparable static loading scenarios.

	Before the rehabilitation		*After the rehabilitation*		
Element (Section)	*Test code*	ε_1 ($\mu\varepsilon$)	*Test code*	ε_2 ($\mu\varepsilon$)	Δ (%)
Diagonal (S1)	13SCN	7.79	26SCN	4.02	-48.42
Diagonal (S2)	13SCN	10.34		6.00	-41.99
Vertical (S3)	13SCN	-5.30		-3.54	-33.24
Crossbeam (S4)	14SCN	11.44		6.46	-43.50
Stringer (S5)	16SCN	8.98		5.53	-38.45
Lower chord (S7)	13SCN	9.12		6.99	-23.34

ε_1 – Strains in Test 1 per 100 kN of applied load; ε_2 – Strains in Test 2 per 100 kN of applied load; $\Delta = \varepsilon_2/\varepsilon_1 - 1$; Total load applied in Test 1: 361 kN (22.9 m); Total load applied in Test 2: 377 kN (23.8 m).

Given that some monitored sections in Test 1 were changed for Test 2, the selection of comparable static loading events in Test 1 for each case had to take that into account. Firstly, as the location of the sections pertaining to both diagonals, vertical and lower chord was not changed, the load case similar to the 3-truck static loading conducted in Test 2 was chosen. Secondly, for the crossbeam the adopted load case was the one in which the front axle of the center truck was aligned with section S4-. Although in Test 2 the corresponding axle was not positioned over the section S4+, the numerical analysis proved that for the rehabilitated bridge the exact location of the vehicle is not that important for capturing the peak value, as it will be shown in section 4.7.3. Thirdly, the comparable load cases for the analysis of the stringers deformation are those in which the load centers of the rear truck axles positioned in the corresponding panels are close to the

instrumented sections. For both stringers and crossbeams the boundary conditions at the ends are very alike in terms of stiffness coefficients. Fourthly, regarding the collected strains in the upper chords the values cannot be correlated since the gages were attached to points with significantly divergent response.

The comparison of the results allows to conclude that a clear reduction of the steel strains has occurred, in average, higher than 45 % in the diagonals and surpassing 40 % in the floor system grid. However, for the vertical that had been heavily strengthened the readings decreased less than 35 %. On the other hand, and in spite of the light reinforcement applied, the lower chord experienced after the rehabilitation a level of deformation 23 % lower than that measured in the first test. This result confirms that both the stringers and the concrete deck, through its diaphragm action, positively contribute to control the flexural bending of the span, and consequently the changes in the floor system impact in the lower chords axial forces.

4.7.3. Quasi-static strains

Experimental and numerical influence lines for the strains collected and calculated before and after the bridge rehabilitation are shown in Figures 4.14 and 4.15. For the sake of comparability, the graphs are plotted for a truck with a reference gross weight of 100 kN.

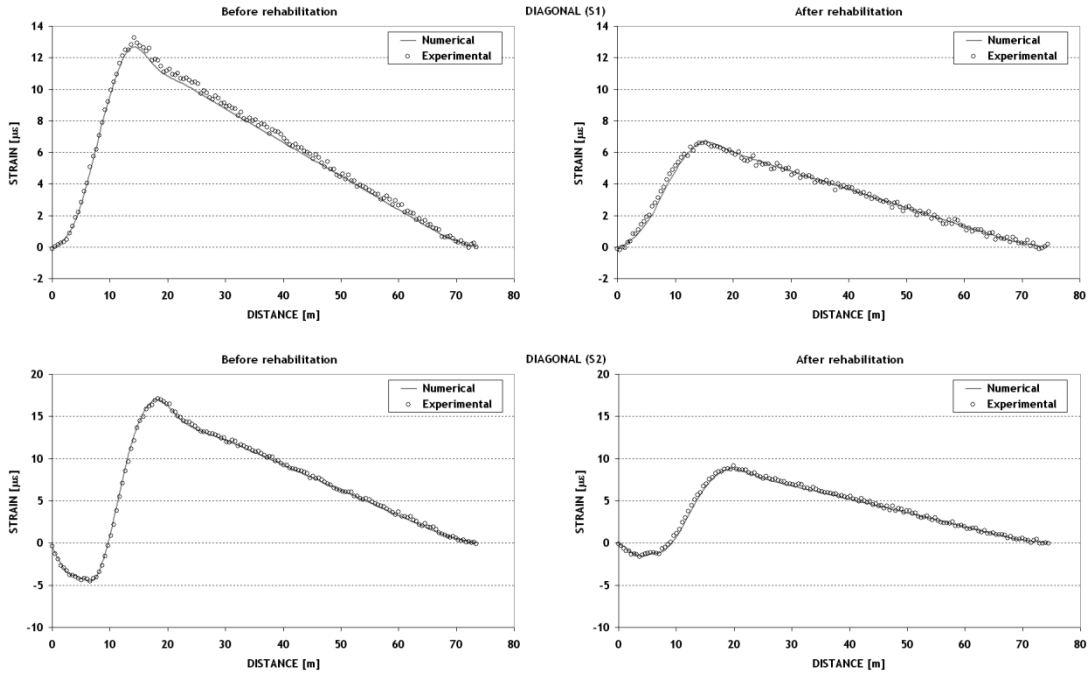

Figure 4.14 - Influence lines of strains before and after the rehabilitation (north span) (I).

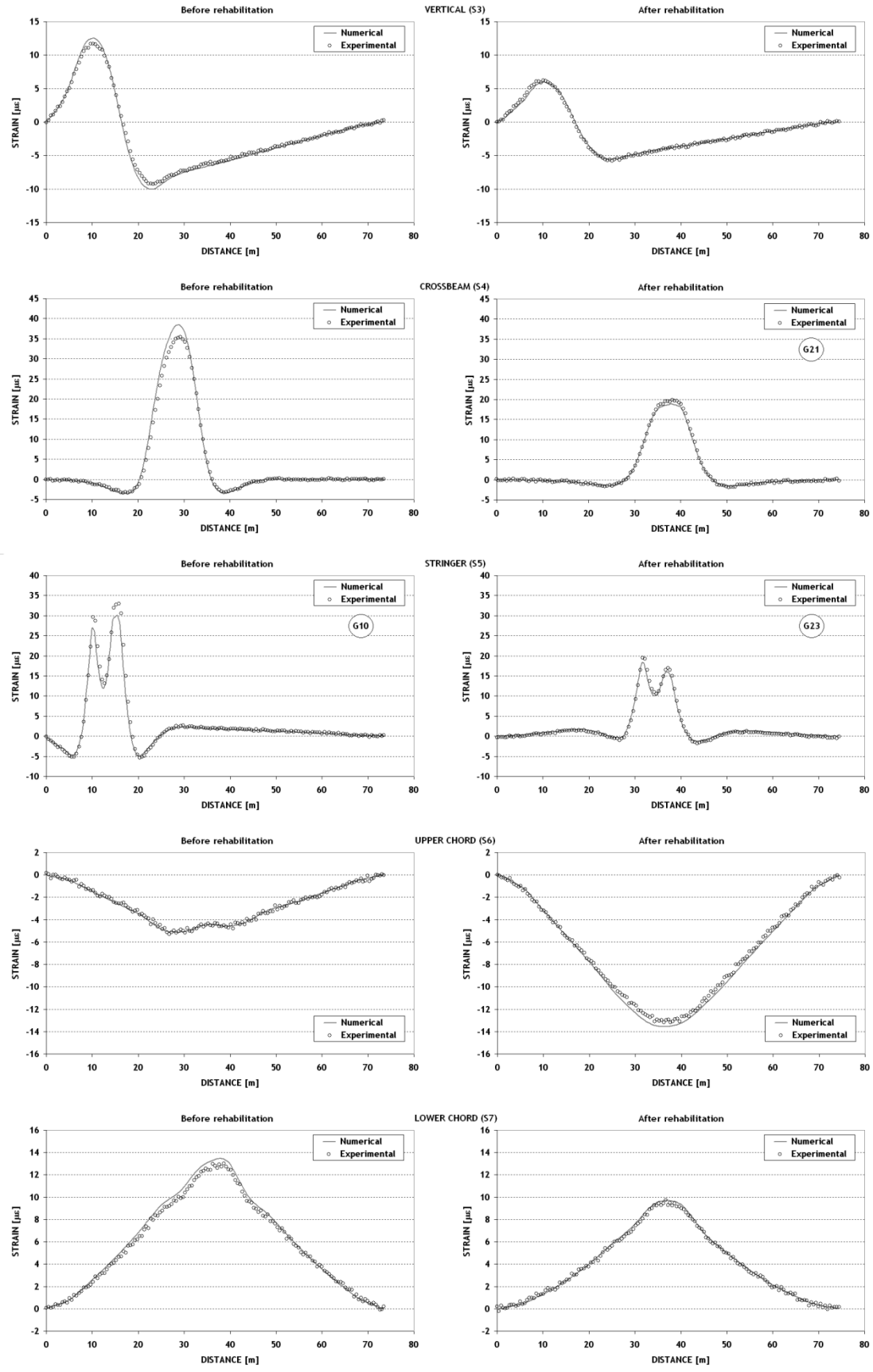

Figure 4.15 - Influence lines of strains before and after the rehabilitation (north span) (II).

The plots refer to average strains in the instrumented cross-sections, except for the ones pertaining to the crossbeam and stringer where the plots are provided by the single gage attached to the lower flange. The horizontal axis represents the distance of the vehicle from the north abutment. In Test 1 the truck crossed the bridge heading north while in Test 2 travelled in the opposite direction, taking in both cases the central path.

For almost all influence lines a very good agreement is exhibited between the field data and numerical estimates in terms of magnitude and shape. Except in the case of the upper chord, bridge strains were considerably reduced after the rehabilitation However, for the elements with a more localized response the peak strains have some considerable deviation. For the crossbeam the FE model overestimates the strains before the rehabilitation while the reverse occurs in the stringer for both pre and post-rehabilitation conditions. Furthermore, a flat region around the highest strains is clearly perceptible for the bottom flange of the crossbeam after the rehabilitation, which indicates an improved distribution of the load applied over the deck as a result of the floor system stiffening.

It is also worth underlining the significant differences shown by the chords plots. While before the rehabilitation a clear fluctuation took place around the region of maximum strain, that is not the case for the new bridge condition. Particularly for the lower chords this smoothing is related to the load transfer from the deck, which after the strengthening is accomplished through smaller secondary torsion and bending forces at the joints. With regard to the upper chord strains the influence lines cannot be compared as the sensors were placed at distinct positions in the tests (web edge angles in Test 1 and cross-section flange in Test 2), thus experiencing different strains.

Table 4.7 – Peak strains for the measured influence lines.

	Before the rehabilitation		*After the rehabilitation*		
Element (Section)	*Test code*	ε_1 ($\mu\varepsilon$)	*Test code*	ε_2 ($\mu\varepsilon$)	Δ (%)
Diagonal (S1)	19QCA	13.27	27QCA	6.64	-50.00
Diagonal (S2)		17.13		9.16	-46.52
Vertical (S3)		11.70		6.21	-46.97
Crossbeam (S4)		35.43		19.87	-43.93
Stringer (S5)		32.96		19.50	-40.84
Lower chord (S7)		13.00		9.73	-25.14

ε_1 – Strains in Test 1 per 100 kN of applied load; ε_2 – Strains in Test 2 per 100 kN of applied load; $\Delta = \varepsilon_2/\varepsilon_1 - 1$.

The positive peak strains measured during the slow crossing tests are listed in Table 4.7. The comparison of the readings points to a decrease of the structure deformation slightly

higher than that predicted by the static data. Still, with respect to the vertical these results indicate a much higher strain reduction, even exceeding 45 %, which is more in line with the performed strengthening.

4.7.4. Dynamic strains

The increment of the bridge response during the dynamic tests is appraised in terms of dynamic amplification factors (DAFs). DAF is herein taken as the ratio between the maximum measurement recorded when a test vehicle travelled on the bridge at normal speed, passing over the mid-span bump, and the maximum reading obtained from the crossing of a test vehicle at a crawling speed. Since the quasi-static and dynamic loading events of Test 2 were conducted with different trucks, the maximum values of interest for computing the DAFs are previously divided by the corresponding truck weights. The maximum values collected during Test 2 are listed in Table 4.8 for each type of member.

Table 4.8 – Dynamic amplification factors for recorded strains.

Element (Section)	*DAF*
Diagonals (S1, S2)	1.12
Vertical (S3)	1.15
Crossbeam (S4)	1.24
Stringer (S5)	1.45
Upper chord (S6)	1.11
Lower chord (S7)	1.14

The values for the elements not pertaining to the floor system remained at or below 1.15, which can be considered as small, whereas for the crossbeam and stringer DAFs were higher, reaching 1.45. Still, these results are merely indicative since they were obtained for a specific set of vehicles travelling at controlled speed, which may not be statistically representative of the real traffic conditions.

4.8. Safety assessment of the bridge

4.8.1. Introduction

It is well known that in civil engineering general practice several conservative assumptions are often adopted in the development of numerical models for design

purposes. However, this strategy should not be followed when characterizing the behavior of an existing bridge as it can lead to great differences between field and estimated parameters, and thus may result in a costly outcome or even in a premature decommissioning. In spite of the field data collected before the rehabilitation to assist the viability study, the strengthening schemes were designed taking into account the estimates provided by a model developed according to the classical approach, i.e. assuming the load-carrying structure constituted only by the two truss girders. Therefore, an assessment of the impact of such a decision becomes imperative.

4.8.2. Ultimate and serviceability limit states

The design value of steel tensile strength, σ_{rd}, was experimentally obtained with coupons extracted from the bridge. The design value of steel compressive strength took into account the buckling phenomenon on each structural element. Except for crossbeams and stringers, the bridge members are subjected to predominant axial forces and minor bending moments. Therefore, the compressive strength was estimated by multiplying the tensile strength by a reduction factor, which translates the ratio between the buckling resistance of the member and its tensile capacity, both calculated as established by the specifications in Eurocode 3 – Part 1-1 (EN1993-1-1, 2005).

The design value of the applied normal stress, σ_{Ed}, was computed through the following expression

$$\sigma_{Ed} = \gamma_g \cdot (\sigma_{dl1} + \sigma_{dl2} + \sigma_{dl3} + \sigma_{dl4}) + \gamma_q \cdot \sigma_{ll} \qquad 4.1$$

where γ_g (1.35) and γ_q (1.5) are the partial factors for permanent and variable actions, respectively, adopted according to Eurocode 0 (EN1990, 2003); $\sigma_{dl\mathrm{i}}$ is the normal stress generated by the dead load in the i-th construction stage estimated with a suitable numerical model; and σ_{ll} is the normal stress caused by the live load. For checking the ultimate limit state two base models representative of the bridge in its pre and post-rehabilitation conditions, denoted respectively as Model A and Model B, were considered, whose characteristics have been presented in section 4.5. In order to account for the progress of the rehabilitation works in the permanent stress fields, four additional models were idealized, which will be referred to as Model 1, 2, 3 and 4, described as follows:

Model 1 – Model A with the concrete deck removed and the self-weight of the steel structure as the only acting load;

Model 2 – Model 1 holding just the dead load of the floor system strengthening;

Model 3 – includes all the contributions of the strengthening and replaced bars to the stiffness upgrade and the applied load is the self-weight of the new concrete deck and steel sidewalks;

Model 4 – the stiffness of the concrete deck is added to Model 3 and the dead load of the asphalt layer and parapets is accounted for.

The estimate of the permanent stresses is obtained by adding the contributions of Models 1 to 4. Although this strategy is not the most accurate, it constitutes, however, a good approach since the construction method used to build the bridge is not completely known. The normal stresses caused by the live load are estimated by Model B.

Given that the rehabilitation project was developed assuming the actions for a class II bridge established by the Portuguese national code (RSAEEP, 1983), the analysis was carried out with two traffic load models:

i. A lane uniformly distributed load of 3 kN/m² combined with a single transverse linear load of 30 kN/m located at the most unfavorable position;
ii. A standard vehicle with 3 axles equally spaced (1.5 m) holding each one a 100 kN load.

Table 4.9 – Maximum normal stresses for the ultimate limit state.

Element	σ_{dl} *(MPa)*	σ_{ll} *(MPa)*	σ_{Ed} *(MPa)*	σ_{rd} *(MPa)*	*S. F. (1)*	*S. F. (2)*
Diagonals (C)	24.50	6.89	43.42	67.78	0.64	0.47
Diagonals (T)	81.31	22.55	143.60	172.5	0.83	0.98
Verticals (C)	60.57	15.42	104.90	137.67	0.76	0.91
Verticals (T)	35.34	17.13	73.41	172.5	0.43	0.75
Stringers	27.80	16.99	63.01	172.5	0.36	0.72
Crossbeams	19.07	15.45	48.92	172.5	0.28	0.78
Lower chords (T)	70.10	25.06	132.22	172.5	0.77	0.98
Upper chords (C)	101.89	42.40	201.15	167.82	1.20	1.01

(C) – Member in compression; (T) – Member in tension; (1) – Validated model; (2) – Design model;

$\sigma_{dl} = \sigma_{dl1} + \sigma_{dl2} + \sigma_{dl3} + \sigma_{dl4}$; $S.F. = \sigma_{Ed}/\sigma_{rd}$.

Table 4.9 holds the maximum normal stresses produced by the axial forces and bending moments acting in the most strained bridge elements of each type, as well as the tensile and compressive strength of steel considered in the calculation of the safety factors ($S.F.$). These factors were calculated as the ratio of the maximum stress in the critical section to the steel strength, either tensile or compressive. The estimated safety factors are listed in the two right hand columns of the table, the first concerning the values predicted with the

field validated model and the second holding the values obtained from the rehabilitation design. The results allow to draw important conclusions.

Firstly, and the most important, the critical elements are the upper chords, for which and above all the ultimate limit state is not verified by a large amount (about 20 %). The problem is further compounded by the fact that these elements are prone to buckling and/or control the overall stability of the structure. Secondly, except for the upper chords and the diagonals in compression, all the remaining elements have a decrease of the safety factors in relation to the estimates at the design stage, particularly the floor system grid for which the values decreased more than half. Note that these elements had been considered critical in the viability study. Thirdly, it is interesting to note the large discrepancy between the safety factors of the upper and lower chords computed with the validated model. At the design stage these values had been predicted close to one, which indicates an overestimation of the stresses for the lower chords coupled with an underestimation in the upper chords.

The results that support the last conclusion were caused by the use in the design stage of a simplified 2D model that only took into account the main girders, therefore neglecting the contributions from the floor system and concrete deck for the structure response. The increase of the upper chords stresses is due to the fact that the arm of the compression forces in relation to the deck's cross-section centroid is much longer in the 3D validated model than in the simplified model (close to half-height of the bridge deck), which largely surpasses the increment of the deck's bending stiffness. On the contrary, the shorter arm of the tension forces leads to smaller stresses in the lower chords.

With respect to the serviceability limit states the maximum bridge deflection was checked for the characteristic combination of actions. The maximum vertical displacement was calculated with the validated model as being 67.80 mm, corresponding to a span to displacement ratio of 1020, significantly larger than the standard limit of 800, and above the design value of 910 (Pinto, 2005).

4.8.3. Fatigue limit state

A fatigue assessment was also accomplished based on data provided by the field validated numerical model and laboratory fatigue tests. Test results on coupons sampled from the bridge revealed that the S-N curves corresponding to the detail category D of the AASHTO specifications (AASHTO, 1992) and to the detail category 71 of the Eurocode 3 – Part 1-9 (EN1993-1-9, 2005) could be conservatively adopted (Figueiredo *et al.*, 2004). As the

rehabilitation design aimed at extending the bridge service life for at least 30 years, traffic data made available by the bridge owner was used to estimate the number of heavy vehicles that would cross the bridge in that period, which was found to be approximately 1 million. Therefore, the fatigue resistance of 1 million cycles at a constant stress range could be taken as 89.67 MPa (Figueiredo *et al.*, 2004). However, to account for a likely traffic increase the fatigue resistance was considered to be 71.17 MPa for 2 million cycles.

The fatigue limit state was checked by comparing this limiting stress range with the maximum variation predicted for each critical element from the numerical analysis carried out with the traffic loads of the Portuguese national code (RSAEEP, 1983). The results, $\Delta\sigma_1$, are shown in Table 4.10, as well as the values reported in the design, $\Delta\sigma_2$. All the stress ranges are far below the safety threshold and consequently fatigue related problems are not expected. In addition, the design stress ranges were overestimated between 19 % for the upper chord and 236 % for the crossbeams.

Table 4.10 – Numerical maximum stress ranges.

Element	$\Delta\sigma_{vm}$ *(MPa)*	$\Delta\sigma_{dm}$ *(MPa)*	*R*
Diagonals	34.27	52.1	1.52
Verticals	33.70	64.7	1.92
Stringers	22.48	53	2.36
Crossbeams	20.92	66.6	3.18
Lower chords	25.57	51	1.99
Upper chords	44.14	52.6	1.19

$\Delta\sigma_{vm}$ – Data from the validated model; $\Delta\sigma_{dm}$ – Data from the design model; $R = \Delta\sigma_{dm}/\Delta\sigma_{vm}$.

4.8.4. Load rating

For the new operation stage the traffic over the bridge was restricted to vehicles weighing less than 30 ton, in direct correspondence with the standard vehicle stipulated by the Portuguese national code for bridges of class II (RSAEEP, 1983). Therefore, load rating appears as the right tool to assess the usefulness and validity of that decision. The rating factor ($R.F.$) of each element was computed based on the equation

$$R.F. = \frac{\sigma_{rd} - \gamma_g \cdot \sigma_{dl}}{\gamma_q \cdot \sigma_{SV}} \qquad 4.2$$

where γ_g (1.35) and γ_q (1.5) are the partial factors for permanent and variable actions, respectively, adopted according to Eurocode 0 (EN1990, 2003); σ_{dl} is the stress induced

by the dead load; σ_{SV} is the stress generated by the standard vehicle, accounted the dynamic effects; and σ_{rd} is either the tensile or compressive strength of steel. The rating factors are summarized in Table 4.11.

Table 4.11 – Computed rating factors.

Element	σ_{dl} *(MPa)*	σ_{SV} *(MPa)*	σ_{rd} *(MPa)*	*R. F.*
Diagonals (C)	17.43	10.55	67.78	2.79
Diagonals (T)	81.31	11.87	172.50	3.52
Verticals (C)	60.57	7.03	137.67	5.30
Verticals (T)	23.41	20.58	172.50	4.56
Stringers	27.80	20.79	172.50	4.33
Crossbeams	19.07	19.92	172.50	4.91
Lower chords (T)	70.10	12.54	172.50	4.14
Upper chords (C)	101.89	20.67	170.36	1.06

(C) – Member in compression; (T) – Member in tension.

These results indicate that the bridge's load-carrying capacity is conditioned by the upper chords, confirming once again these elements as critical. The rating is dangerously close to 1, thus making the posting limit compulsory. It is also worth noting that except for the upper chords the bridge could carry more than twice the prescribed load limit.

4.9. Summary and conclusions

This chapter presents a comprehensive study on a centenary trough-truss deck steel bridge subjected to an extensive rehabilitation process. It included the execution of field testing before and after the rehabilitation works were carried out. The bridge response was monitored under three different loading scenarios, namely static, quasi-static (vehicles slow crossings) and dynamic. The installed instrumentation allowed the measurement of global quantities such as deflections and horizontal displacements at the supports, as well as the local deformation of several critical elements. In a first stage, field data was used to assess the actual condition of the structure and to assist the rehabilitation project. After the completion of the site works field results enabled to detect the changes introduced in the structure performance and to determine the effectiveness of the applied strengthening. Numerical analyses, based on 3D FE models developed through a mixed element and detailed level modeling strategy, helped to understand the force and deformation mechanisms controlling the bridge behavior.

The results have permitted to conclude the following:

i. The structure response is well simulated as a 3D frame system;
ii. The floor system, both the steel grid and the concrete deck, undoubtedly contributes for the global performance and impacts on the forces induced in the main truss girders;
iii. The strengthening may be considered effective in that the rehabilitation led to an increase of the global vertical stiffness of the spans close to 20 %, and to an average decrease of the strains in the elements higher than 40 %, yet only reaching 25 % in the lower chords;
iv. The numerical estimates compared well with the experimental results indicating a good ability of the models for predicting global quantities with errors below 5 % and less than 15 % in what concerns local parameters.

A safety and serviceability assessment was performed for the new operation phase of the bridge. The findings brought some light regarding the balance and adequacy of the strengthening. Firstly, according to the design loads the ultimate limit state for normal stresses cannot be verified for the upper chords, consequently pointing these elements as the weak points of the structure. Still, all the remaining elements were found to have a large safety margin. Secondly, the simplifications made in the model of the bridge at the design stage led to an underestimation of the design stresses in the upper chords, together with an overestimation of the stresses in the lower chords by the same proportion, which translates in an unbalanced rehabilitation design. Thirdly, fatigue poses no problem in the 30 years of extended life span and the bridge deflection is well below the limit for contemporary loadings. Fourthly, the bridge's live load-carrying capacity is very close to the current posted level. However, if a judicious strengthening of the upper chords would be accomplished in the future the traffic loads could be significantly enlarged.

Chapter 5

Modal analysis of the Pinhão Bridge

5.1. Synopsis

Modal testing through ambient vibration holds unique advantages over other experimental techniques, including static load tests, for the measurement of global parameters that characterize the bridges' behavior, among which are the fastness of execution, low cost, non-compulsory restriction of the traffic during the test, and the ability of simultaneous evaluation of different directions. Moreover, quantities that decisively influence the structural safety, such as damping for the fatigue resistance in old steel bridges, can only be measured through appropriate dynamic testing.

On the other hand, the use of this non-destructive testing technique to assess the changes in rehabilitated structures and to enable the evaluation of the actual effectiveness of different rehabilitation strategies emerge as extremely important, since the current knowledge in this field is short and therefore demands an improvement in order to achieve more cost-effective designs without lowering the required safety levels.

This chapter presents the ambient vibration tests conducted on a centenary through-truss steel bridge before and after its rehabilitation, with the purpose of evaluating the changes in its dynamic properties as a result of the adopted strengthening strategy. The implemented testing program, experimental setup, data processing and modal identification technique are described. Field data validated numerical models for the analysis of the structural changes produced by the strengthening process are presented. Significant conclusions were drawn by comparing the experimental and numerical results between the pre and post-rehabilitation conditions, namely in what concerns the vibration

level experienced by the structure, its stiffness variation, suitability of the adopted modeling methodology, and some important unexpected alterations could even be detected and validated.

5.2. Introduction

The recent emergence of rehabilitation, repair and upgrading projects on old steel bridges has been driven by the profitability of the economic potential inherent to the existing infrastructures but also targeted a better management of available funds for their maintenance and operation. It brought a renewed need for non-destructive testing and evaluation techniques either in objective decision-making, validation of numerical models or assessment of the implemented solutions. In this context, the chapter reports a case study of a centenary steel bridge recently rehabilitated on which field dynamic testing was performed before and after the completion of the construction works.

Modal testing, besides the characterization of the vibration level, aims at determining the most relevant modal parameters of the structural system, i.e. natural frequencies, mode shapes and damping ratios (Farhey, 2005), or in other words, deals with the performance of an experimental modal analysis. Modal testing presents several advantages over other experimental techniques, particularly in relation to static load tests, one of which is the ability to provide global mechanical characteristics of a structure-foundation-soil system by direct measurement (Aktan *et al.*, 1997; Catbas *et al.*, 2007), as is the case of the flexibility coefficients of a structure associated to a coordinate system with a fine spatial resolution.

The experimental modal analysis can be accomplished with three major testing procedures: ambient vibration, forced vibration and free vibration. This classification is based on two criteria, which are the excitation source that induces the vibration of the structure and the type of response to be measured and/or analyzed. Further details about the three alternatives can be found elsewhere (Cunha and Caetano, 2006), being the work presented in this chapter focused in ambient vibration testing. For ambient vibration testing different sources may be used, such as wind, traffic, seismic activity, waves or tidal fluctuations (Catbas *et al.*, 2007; Hsieh *et al.*, 2006). Some advantages in its adoption are the little or no interference with the normal operation of the structure (Cunha *et al.*, 2001), its fastness, easiness and low cost (Ren *et al.*, 2004b), long-term nature of the excitation and frequency content suitable for long-span and flexible bridges (Hsieh *et al.*, 2006). On

the other hand some inherent drawbacks are the variable nature of the excitation in terms of amplitude, direction, duration, as well as the difficulty in measuring it (Hsieh *et al.*, 2006). In order to extract the modal properties from the recorded data output-only identification techniques are used (Magalhães and Cunha, 2011), both on the frequency and time domains, usually regarding the excitation as being stationary with a flat frequency spectrum around the bandwidth of interest (Ren *et al.*, 2004b; Salawu and Williams, 1995).

The main reasons for conducting full-scale dynamic tests have been listed by Salawu and Williams (1995). Firstly, the vibration field tests supply information to experimental databases from which analytical methods adopted in the design of new similar structures can be improved or evaluated. Secondly, dynamic measurements can assist in the evaluation of the structure integrity after the occurrence of an extreme event, being also useful in determining the effectiveness of retrofit works. Thirdly, data provided by these tests are invaluable for the validation and upgrading of theoretical models of structures, ultimately leading to more economical designs by preserving suitable feasible safety levels. Fourthly, field dynamic tests can accurately quantify some structural parameters that play a decisive role in the safety evaluation, as is the case of dynamic amplification factors when an increase of live loading is envisaged. Fifthly, structural damage detection can be enabled if the dynamic response of a structure is followed up on a regular basis, for instance through a structural health monitoring system. Sixthly, vibration testing can be used to prove that the structure's performance is within the expectations. The uncertainty in the fatigue evaluation associated with the structural damping dependency can also be mitigated by reliable modal damping estimates mined through proper identification methods. At last but not least, results obtained by the dynamic tests supplement data collected through controlled static and quasi-static diagnostic loadings and are very useful to validate some of their findings.

Dynamic testing on steel bridges with the purpose of collecting field data to address one or more of the aforementioned challenges has been reported in scientific and technical literature over the years, and some representative examples are herein presented. In 1969 Marécos *et al.* (1969) have described the dynamic measurements carried out on the Tagus River Suspension Bridge during its construction and after the completion of the structure. Aiming at developing a structural dynamics based integrity monitoring system for a long span bridge, Wang *et al.* (1997) have established a baseline model validated by experimental modal data. Fu and DeWolf (2001) have presented the results of a study performed to assess the behavior of a bridge with partial restrained movements at the

roller supports. Zhao and DeWolf (2002) made an effort to detect the alterations in the dynamic properties of the same bridge induced by temperature. A combined field ambient vibration experiment and a computational modeling study were accomplished by Shama *et al.* (2001) on a cantilever truss bridge. Another cantilever truss bridge has been subjected to an ambient vibration test by Catbas *et al.* (2007). Dynamic field tests were carried out by Conte *et al.* (2008) on the Alfred Zampa Memorial Bridge, known as the New Carquinez Bridge, located in the San Francisco Bay.

This chapter firstly presents the objectives to be accomplished by conducting the tests, as well as the adopted experimental procedures and data processing. Then, the 3D numerical models constructed for simulating the pre and post-rehabilitation behaviors of the structure are also described. Finally, the correlation of the experimental data and the validation of the models led to significant conclusions concerning the changes produced in the structure performance and the viability of using modal information in their detection.

5.3. Objectives and scope

The Pinhão Bridge was commissioned in 1907 and since then it has been in continuous operation, still representing a vital link in the road infrastructure that serves the Douro vineyard region where the Porto wine is produced (see Figure 5.1). An in-depth rehabilitation of the bridge was undertaken following a viability study pushed forward by the tragic collapse in 2001 of an older bridge that crossed the same river (Wikispaces, 2011).

Figure 5.1 - Pinhão Bridge.

During the conducted surveys the most relevant problems were the widespread corrosion of steel due to lack of proper maintenance and the excessive vibration of some elements. Additionally, the safety level of the structure to carry the current loads and the evaluation of the need of a strengthening scheme to meet the contemporary standards were issues of concern. In this context, a first dynamic test was mandatory to support the rehabilitation project by enabling the bridge condition assessment and by supplying in-situ data for the validation of the numerical model to be used in the evaluation of alternative strengthening strategies.

After the completion of the construction works, a second field test sought to determine the changes introduced in the structure's dynamic behavior. It was also targeted the appraisal of the effectiveness of the implemented strengthening in terms of stiffness variation, not only associated with vertical displacements but also with transverse and torsional movements of the deck. Furthermore, the update of the model would enable its use in the simulation of the structure response under dynamic loadings in the new service stage, and consequently would turn possible its integration into a health monitoring system to detect alterations in the bridge behavior over the time.

5.4. Ambient vibration testing

The ambient vibration testing performed before and after the bridge rehabilitation primarily aimed at identifying the most representative parameters of the structure dynamic behavior, namely the natural frequencies and mode shapes, on the basis of measuring its vibration response under natural excitation, such as the one provided by the wind and road traffic. For that purpose, both tests were conducted without significant restrictions to the traffic. Acceleration time series were collected at 7 sections of each main span, aligned with as many verticals, as depicted in Figure 5.2. In both tests, each main span was individually tested. However, for the second test, measurements were also performed simultaneously in all spans.

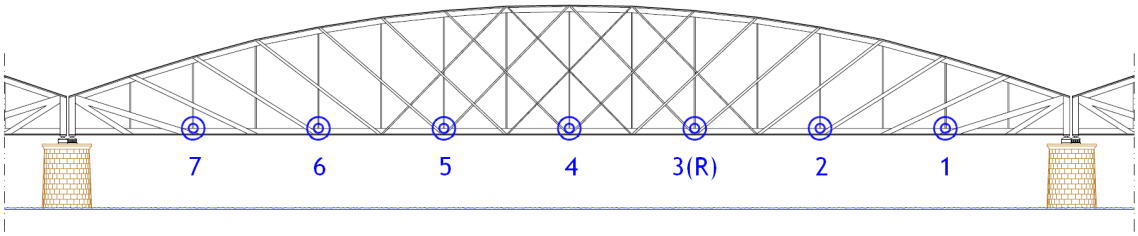

Figure 5.2 - Layout of the measurement sections.

For each measurement section the vibrations were recorded in the roadway at both upstream and downstream limits, thus allowing the accurate identification of vertical bending and torsional mode shapes (see Figure 5.3). Four tri-axial seismographs were used to acquire the accelerations in the longitudinal, transverse and vertical directions. Taking into account that the three simply supported spans were designed to have an independent structural behavior, for each span a different test was performed following the same procedure. Two devices were permanently stationed at section 3, which served as reference (Figure 5.2), and the remaining two were successively placed at the other six sections. The reference section was selected so that it would not be close to a node of a mode shape to identify. However, it is noteworthy that in the second ambient vibration test an additional setup was performed by simultaneously measuring the accelerations at the mid-span sections of all spans. As it will be presented in the section dedicated to the results analysis, this additional procedure helped to unveil a global mode shape of the whole bridge that initially was not expected.

(a) (b)

Figure 5.3 - Experimental setup: (a) seismograph; (b) position of the measuring apparatus on the deck.

Each measuring apparatus integrates one tri-axial force balance accelerometer, exhibiting linear behavior from d.c. to 100 Hz, 18-bit A/D converters, a battery that enables a 1-day test autonomy, a memory card for data storage, and an external GPS sensor in order to permit an independent and synchronized operation. The trigger parameters were previously programmed for each recorder using a laptop. As a result of this experimental setup the need for cables and hard labor in preparing the dynamic test was avoided. The time of acquisition for each setup was always 13 minutes so that a frequency resolution around 0.01 Hz for the average spectral estimates could be obtained. The adopted equipment forced the use of a sampling frequency of 100 Hz, which was more than enough for the present structure, with the most relevant modes below 20 Hz.

5.5. Modal identification

The experimental identification of the most relevant modal parameters was firstly performed using the Peak-Picking method (PP), also known as Basic Frequency Domain method (BFD), which was the first technique applied for data processing of the measured response of civil engineering structures under ambient excitation. The theoretical background of the method was developed by Bendat and Piersol (Bendat and Piersol, 1986) and its application procedure was re-organized, automated and extensively applied by Felber (1993) and Felber and Cantieni (1996). The method has been successfully applied for modal analysis of several structures, including the Portuguese cable-stayed bridges: Vasco da Gama Bridge (Cunha *et al.*, 2001) and International Guadiana Bridge (Magalhães *et al.*, 2007). Afterwards, the application of more sophisticated identification techniques (Hu *et al.*, 2009) has confirmed the estimates provided by the first analysis. Since for the purpose of the present work the quality of the estimates provided by the PP method is adequate, in order to avoid a discussion about the outputs of alternative identification techniques, the content of the current chapter is going to be limited to the characterization of the procedure and results of the PP method.

One premise that has to be assured when applying the PP method is an adequate separation of the natural frequencies in the bandwidth of interest (low modal interaction), which can constitute a major obstacle when dealing with experimental data from structures with closely spaced modes. However, a common procedure to improve the quality of the estimates consists in separating different types of modes by pre-combining the acquired signals. For bridge structures, the half-difference and half-sum of the vertical acceleration components measured at upstream and downstream sides of each section highlight the contribution of torsional and vertical bending signal components, respectively. Therefore, before the application of the method, for each instrumented bridge section, three combined signals were calculated: half-sum of vertical acceleration components, half-difference of vertical acceleration components and half-sum of transverse acceleration components.

The first step in the identification process lies in the determination of the normalized power spectral density functions (NPSD) for each instrumented section, as well as of the coherence functions in correspondence to simultaneous measurements at different locations. In this process, each 13 minutes record was subdivided into time segments of 8192 reading points (81.92 s) with an overlap of 50 %, which led to a frequency resolution of 0.0122 Hz. In order to evidence the resonance frequencies to be identified the NPSDs of

all signals of the same type were averaged. Figure 5.4 depicts the average normalized spectra (ANPSD) obtained for the north span in the range 0-18 Hz, before and after rehabilitation.

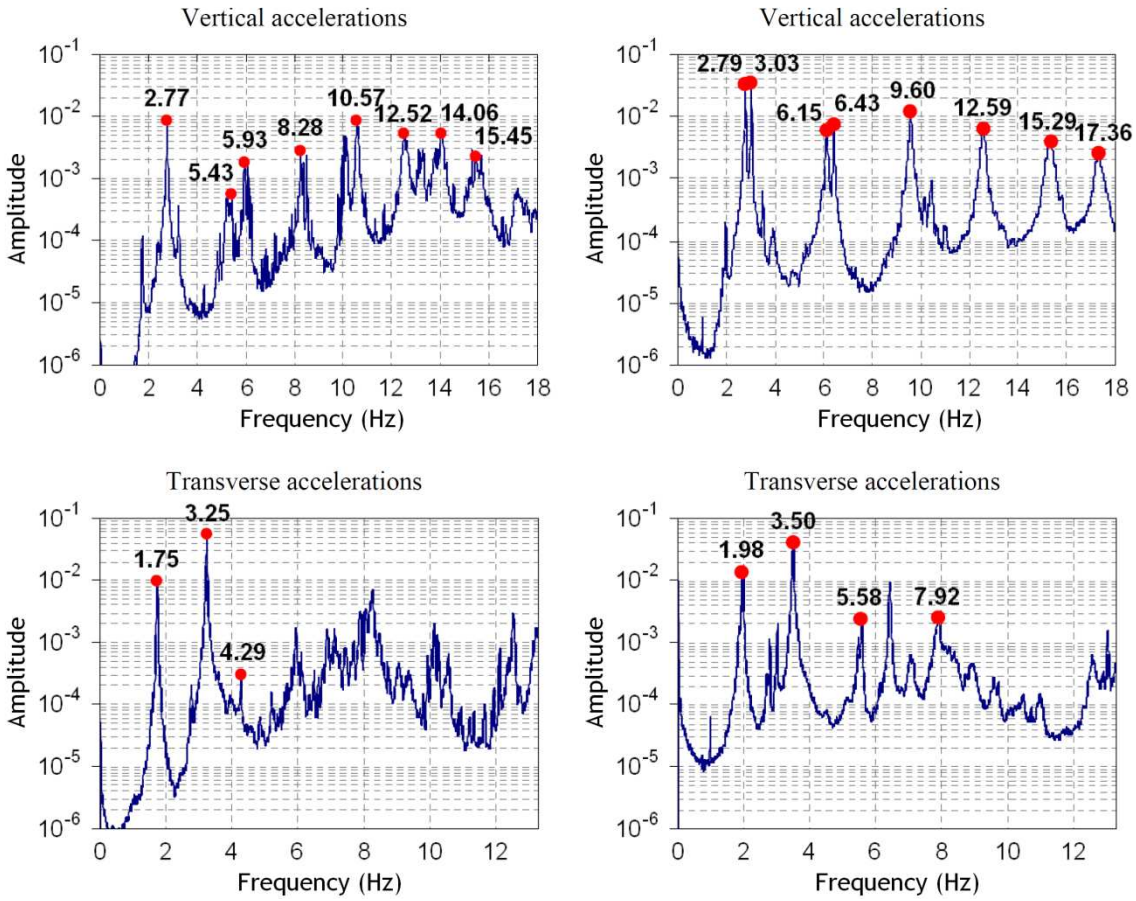

(a) (b)

Figure 5.4 - ANPSDs estimated for the north span during both ambient vibration tests: (a) before the rehabilitation; (b) after the rehabilitation.

These spectra exhibit clear peaks that are associated with the most relevant natural frequencies. The mode shapes were obtained by evaluating the transfer functions relating the ambient response measured at each section with the one collected at the reference section. For each identified natural frequency, the amplitude of each transfer function in a linear scale directly provided an estimate of the ratio between the modal coordinates in correspondence with the section under analysis and the reference section. The signal change in the coordinates of each mode shape was simultaneously detected by tracking the phase of the transfer functions at the resonant frequencies. The obtained experimental results are presented at section 5.7 together with the numerical counterparts.

5.6. Numerical modeling

The two base finite element (FE) models were developed for the analysis of a single main span, before and after the rehabilitation, which will henceforth be designated as Model A and Model B, respectively. The main features of the modeling, namely adopted strategy, connections, supports and materials, have been presented in Chapter 4. In this section only the specific aspects concerning the modal analysis are addressed.

The mass matrix was considered as lumped without rotations and the contributions of all non-structural elements such as guardrails, sidewalks, rivets, cover plates and asphalt layer were carefully taken into account.

For a sensitivity analysis aimed at identifying the factors that control the effective stiffness of the structure, and in turn the natural frequencies associated to the vibration modes, five sub-models were generated from model B by altering the elastic parameters of the materials of some structural elements, which are described as follows:

i. Model B1 targets the evaluation of the contribution from the slab by reducing the concrete Young's modulus of Model B to 1 GPa;
ii. Model B2 also further changes the Young's modulus of the stringers' steel to 1GPa, thus enabling to evaluate the impact of these members;
iii. Model B3 decreases 25 % the stiffness of the crossbeams of Model B1.
iv. Model B4 differentiates from Model B by presenting pinned joints at the extremities of the diagonals that integrate the upper transverse sway trusses;
v. Model B5 differs from Model B4 in that it includes semi-rigid connections between the transverse elements (sway trusses and crossbeams) and the verticals. The rotational stiffness coefficients for these connections were obtained from a calibration procedure, in which the bending moment for a given transverse rotation at the joint in the new model had to be made equal to the bending moment required by a detailed FE model of the joint under the same deformation. Figure 5.5 illustrates this operation for two typical joints.

It is worth mentioning that the changes in Model B2 in relation to the reference Model B were performed with the purpose of creating a 3D model endowed with stiffness characteristics in the longitudinal direction similar to those of the 2D model adopted at the design stage, since in this model only the stiffness contributions from the truss girders were considered, and consequently, only the vertical mode shapes and corresponding natural frequencies were numerically estimated (Pinto, 2005).

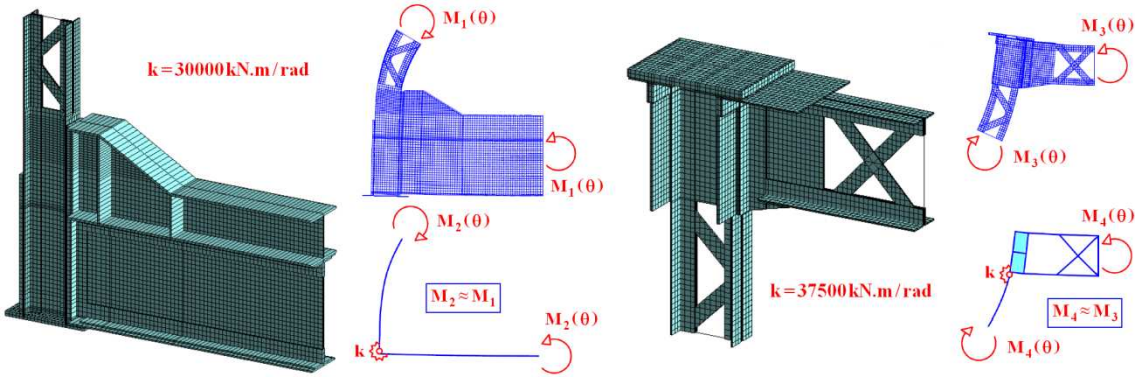

(a) (b)

Figure 5.5 - Calibration procedure of the rotational stiffness coefficients applied in Model B5: (a) lower joint; (b) upper joint.

Since in the second ambient vibration test a global mode shape of the whole bridge was identified (as will be detailed in section 5.7.4), the roles played by the new expansion joints and by the bolt-bars linking the bridge spans in this phenomenon were investigated. An eighth model, labeled as "C", was constructed by assembling three models of type B connected together via double hinged bars, linking the slabs in the alignment of each of the five stringers, as well as the end verticals at three different levels. As in both masonry abutments similar expansion joints were also applied, identical bars connect the bridge extremities to pinned supports. A detail of the developed model over an intermediate support is depicted in Figure 5.6, together with a picture of the linking region between two spans.

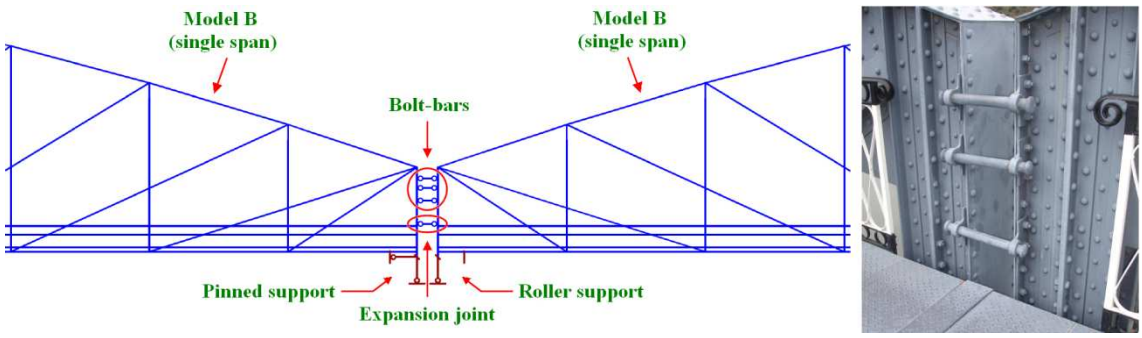

(a) (b)

Figure 5.6 - Connection between two spans: (a) Model C; (b) detail of the bolt-bars.

The total axial stiffness of the five bars that simulate the expansion joint was calculated through a planar linear elastic model of the reinforced elastomeric joint by means of shell elements, as shown in Figure 5.7. To this end, the geometric characteristics were retrieved from the technical sheet of the manufacturer and elastic properties were assumed with values common for the constituting materials:

i. Neoprene, $E_n = 2.25$ MPa and $\nu_n = 0.25$;

ii. Reinforcing steel, $E_{rs} = 210$ GPa and $\nu_{rs} = 0.30$.

The horizontal force applied to the expansion joint to achieve a unit relative displacement was taken as the total stiffness of the bars linking the slabs of two spans.

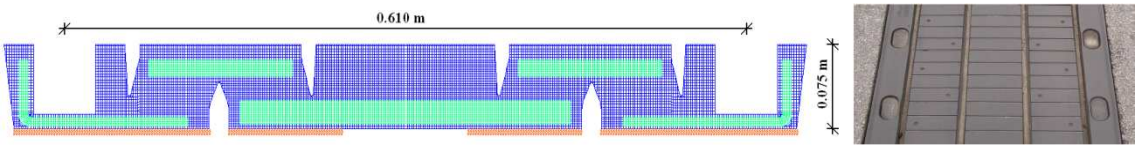

(a) (b)

Figure 5.7 - Expansion joint: (a) detail of the model; (b) top view.

5.7. Analysis of results

5.7.1. Vibration levels

As both ambient vibration tests were conducted without significant restrictions to the traffic on the bridge, it was possible to assess the level of vibration induced by the vehicles. In Figure 5.8, vertical acceleration time series containing the maximum values recorded before and after the rehabilitation at the reference section of the south span are displayed. On both graphs the traffic effect is easily identified and, assuming similar traffic characteristics during both testing periods, it is possible to infer that the level of vibration was reduced to less than one third, having the peak vertical acceleration decreased from approximately 1.5 m/s^2 to 0.5 m/s^2.

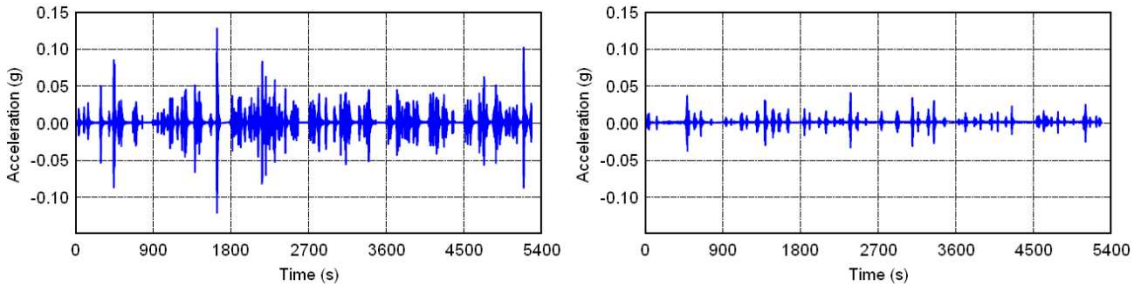

(a) (b)

Figure 5.8 - Vertical acceleration time series collected at the reference section of the south span during the time period for which this span was tested (1.5 h): (a) before the rehabilitation; (b) after the rehabilitation.

Figure 5.9 presents the acceleration time series recorded at sections where the peak values were found, before and after the rehabilitation. The plots reveal that the level of transverse vibration is considerable lower, not exceeding in general one sixth of the vertical accelerations. This difference in the vibration response of the structure has influenced the quality of the power spectral estimates provided by both tests, as shown in Figure 5.4. Furthermore, from these plots it is evident that spectra from the first test are noisier than the ones estimated after the rehabilitation since several small amplitude peaks are exhibited. Nevertheless, the natural frequencies estimates found for all three main spans in both tests presented a standard deviation less than 1.5 % from the average values, thus permitting to conclude on the accuracy of the measurements. Besides making the identification of the natural frequencies related to the global mode shapes of the bridge more difficult, these small peaks primarily exposed the influence of the local vibration modes associated with the slender flat plates that constituted the diagonals, whose excessive vibration had been well noticed during the viability study (see Figure 5.10).

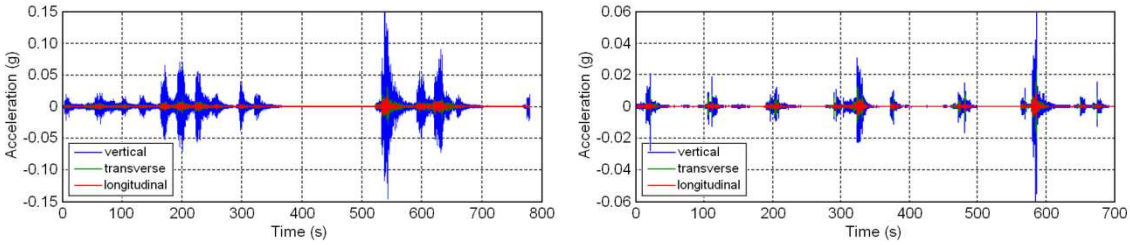

(a) (b)

Figure 5.9 - Acceleration time series recorded at section 5 of the center span (a) and at section 2 of the north span (b): (a) before the rehabilitation; (b) after the rehabilitation.

(a) (b)

Figure 5.10 - Diagonals of the truss girders: (a) before the rehabilitation; (b) after the rehabilitation.

5.7.2. Experimental *versus* numerical results

The subsequent analyses in this section are related only to vibration modes, and corresponding parameters, that were identified in both tests within the frequency bandwidth of 0-18 Hz. A combined inspection of the ANPSDs and Table 5.1 permits to perceive the existence of modes detected after the rehabilitation for which no correspondence could be found in the experimental data of the first test. Table 5.1 lists the natural frequencies identified before and after the bridge rehabilitation and compares those with the values calculated from Models A and B, respectively.

Table 5.1 – Summary of natural frequencies of the bridge.

		Before rehabilitation			*After rehabilitation*		
Mode number	*Mode type*	*Identified (Hz)*	*Numerical[1] (Hz)*	*Δ (%)*	*Identified (Hz)*	*Numerical[2] (Hz)*	*Δ (%)*
1st	T – TO	1.721	1.684	-2.15	1.912	1.972	3.14
2nd	V	2.779	2.752	-0.97	2.779	2.754	-0.90
3rd	T – TO	3.210	3.267	1.78	3.454	3.487	0.96
4th	T	4.273	4.359	2.01	5.510	5.417	-1.69
5th	V	5.460	5.341	-2.18	6.189	6.022	-2.70
6th	TO	5.937	6.670	12.35	6.368	7.078	11.15
7th	V	8.293	8.403	1.33	9.578	9.677	1.03
8th	V	10.604	10.814	1.98	12.573	12.618	0.36
9th	V	12.577	13.025	3.56	15.304	16.307	6.55

T – Transverse mode; V – Vertical mode; TO – Torsional mode; [1] – Model A; [2] – Model B; Δ = Numerical / Identified - 1.

In general, the correlation between the experimental and numerical frequencies is very good, except for the vibration mode 6, a pure torsion one, whose deformed configuration can be described in simple terms as corresponding to the antisymmetric vertical bending of the main girders with a small lateral deformation (see Figure 5.11). For a better understanding of this discrepancy and to evaluate the influence of several parameters in the structure stiffness, and consequently in the natural frequencies, a sensitivity study was carried out by performing modal analysis based on the models described in the previous section, whose results are summarized in Table 5.2. The conclusions can be drawn as follows:

i. The slab mainly affects the transverse modes and has a greater impact on the vertical bending modes as the order increases;

ii. The stringers influence both the transverse and vertical modes, even though their contribution to the latter is higher and more evident as the order of the mode rises;

iii. A decrease of 25% in the crossbeams stiffness has no significant effect on the vibration frequencies, even for the torsional mode where these elements are under in-plane bending;

iv. The flexural stiffness of the diagonals pertaining to the upper sway truss girders has no influence on the vertical bending modes, yet has some impact on the transverses modes and clearly influences the torsion mode;

v. The rotational rigidity of the connections at the joints of the sway frames, which are formed by the verticals, crossbeams and upper truss girders, controls the natural frequency of the torsional mode (see Figure 5.11) with a lower influence in the transverse modes.

Table 5.2 – Natural frequencies from the sensitivity analysis (Hz).

Mode number	*Mode type*	*Model B*	*Model B1*	*Δ (%)*	*Model B2*	*Δ (%)*	*Model B3*	*Δ (%)*	*Model B4*	*Δ (%)*	*Model B5*	*Δ (%)*
1st	T – TO	1.972	1.712	-13.18	1.547	-21.55	1.690	-14.30	1.932	-2.03	1.868	-5.27
2nd	V	2.754	2.703	-1.85	2.548	-7.48	2.674	-2.90	2.755	0.04	2.755	0.04
3rd	T – TO	3.487	3.281	-5.91	3.193	-8.43	3.268	-6.28	3.425	-1.78	3.360	-3.65
4th	T	5.417	4.863	-10.23	4.419	-18.42	4.855	-10.37	5.270	-2.71	5.101	-5.83
5th	V	6.022	5.875	-2.44	5.334	-11.43	5.851	-2.83	6.028	0.11	6.028	0.11
6th	TO	7.078	7.041	-0.52	6.879	-2.81	6.993	-1.20	6.760	-4.50	6.395	-9.65
7th	V	9.677	9.152	-5.43	8.334	-13.88	9.078	-6.19	9.612	-0.67	9.606	-0.74
8th	V	12.618	11.557	-8.41	10.336	-18.09	11.384	-9.78	12.721	0.82	12.716	0.78
9th	V	16.307	13.924	-14.61	10.590	-35.06	13.683	-16.09	16.402	0.59	16.387	0.49

T – Transverse mode; V – Vertical mode; TO – Torsional; $\Delta = [Bi] / [B] - 1$.

Therefore, the best-fitting model for the post-rehabilitation condition of the bridge, on the basis of the first nine vibration modes, would be Model B5. Similar conclusions would be found if the sensitivity analysis had been conducted by taking Model A as the base model and field data from the first test as reference.

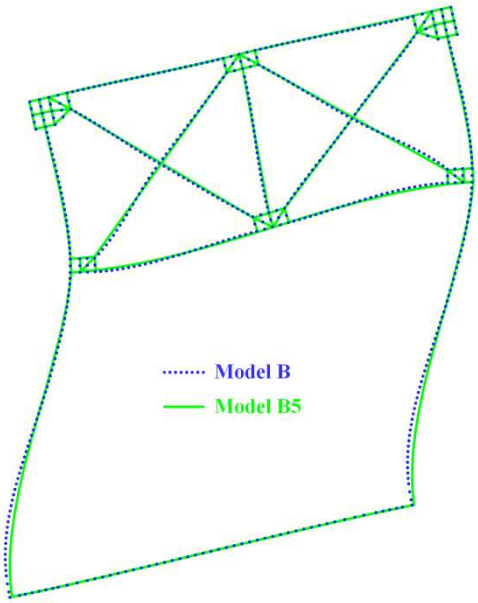

Figure 5.11 - Deformation of the mid span cross-section for mode 6.

The vibration modes supplied by Model A are illustrated in Figures 5.12 and 5.13, where the deformed configuration of the girders is represented in elevation (left-hand side) and that of the chords is depicted in plan view (right-hand side). The analysis of the correlation between the identified and computed parameters was performed either by a graphical comparison of the modal coordinates extracted from the test data with the numerical mode shapes or using the Modal Assurance Criterion (MAC) (Allemang, 2003). This criterion enables the evaluation of the likeness of 2 mode shapes through the following parameter

$$MAC = \left(\sum_{k=1}^{n} \phi_{ik} \cdot \phi_{jk}\right)^2 \Big/ \left(\sum_{k=1}^{n} {\phi_{ik}}^2 \cdot \sum_{k=1}^{n} {\phi_{jk}}^2\right) \qquad 5.1$$

where n is the number of points used for calculating the indicator, whereas ϕ_{ik} and ϕ_{jk} are the modal coordinates for the *i*th and *j*th mode shapes at point K, respectively.

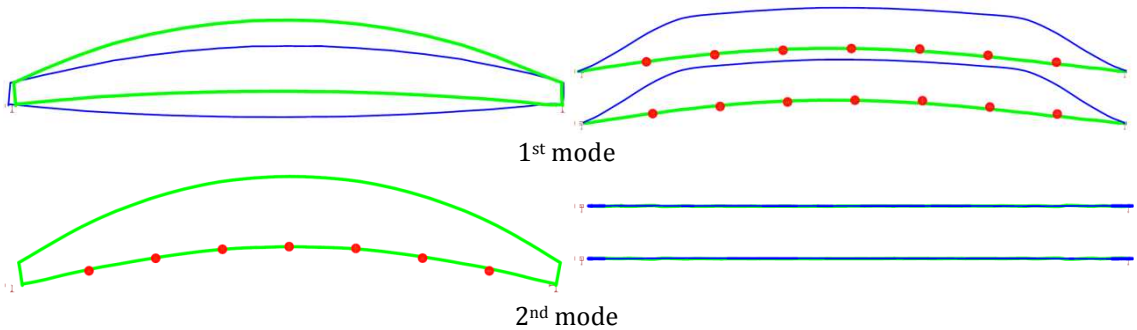

Figure 5.12 - Identified mode shapes of the main spans (I). Experimental coordinates:
Left: elevation, upstream girder, downstream girder.
Right: plan view, lower chords, upper chords.

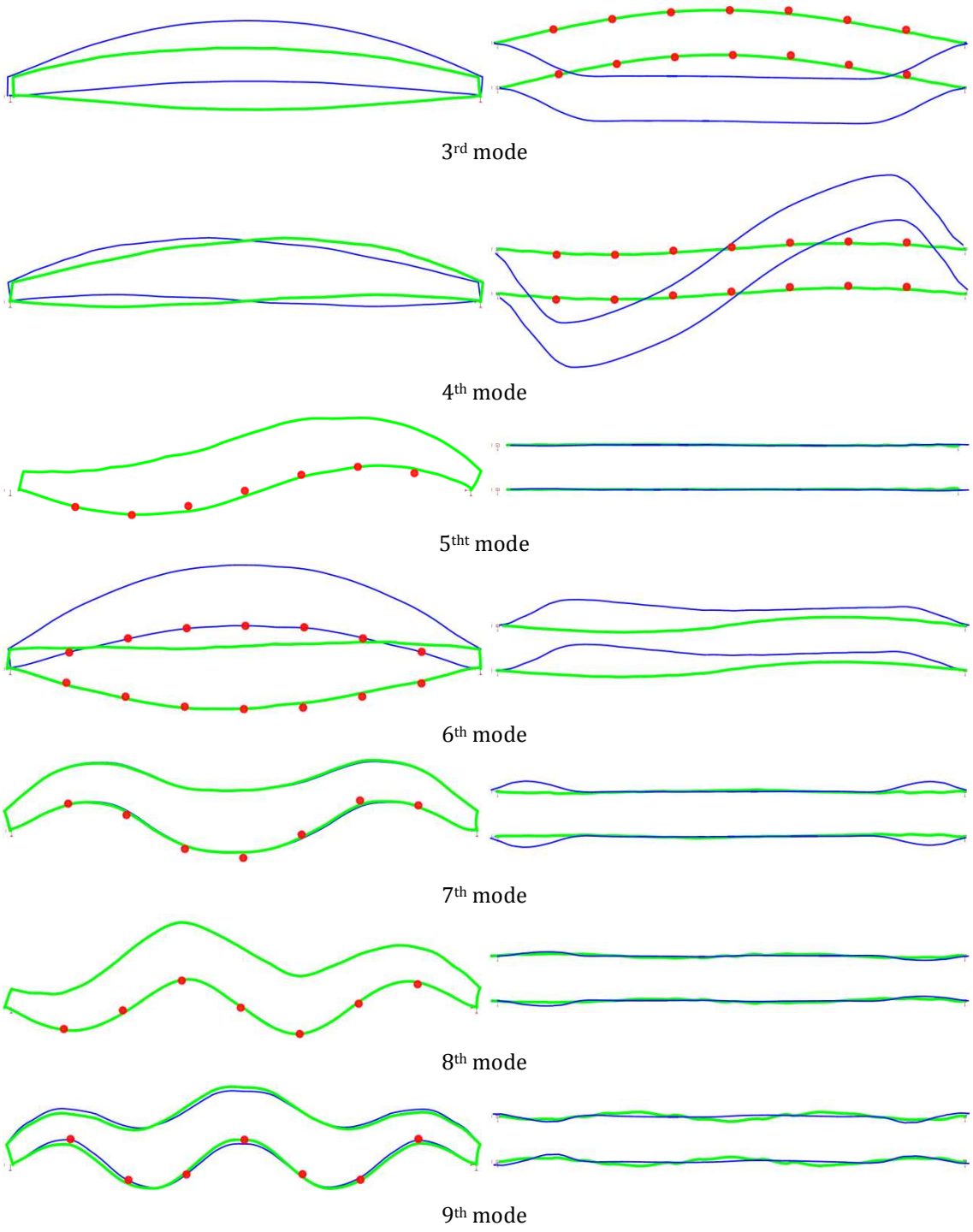

Figure 5.13 - Identified mode shapes of the main spans (II). Experimental coordinates: ●
Left: elevation, ——— upstream girder, ——— downstream girder.
Right: plan view, ——— lower chords, ——— upper chords.

It should be noted that the experimental components are plotted only for the lower level of the north span and that vertical coordinates are displayed for the vertical bending and torsional modes whereas for the transverse modes only the lateral displacements are represented.

Figure 5.14 shows the MAC values relating the identified and calculated mode shapes before and after the bridge rehabilitation, generically labeled as MAC(1) and MAC(2), respectively. As it can be seen, for any of the vibration modes the MAC indicators are always above 0.96, with an average value higher than 0.98, which reveals a very good correlation. Even though, it is important to clarify the causes for the lower quality of MAC(1) for vibration modes 4, 5 and 7. With regard to the first two the experimental data did not lead to a deformed configuration perfectly antisymmetric about the measurement section 4, which might indicate some deterioration in the condition of the north span. In what concerns vibration mode 7, the higher modal coordinates cannot be captured by the spatial resolution adopted in the test, and therefore it is prone to greater deviations.

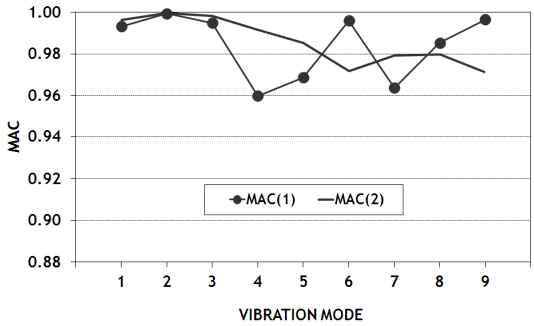

Figure 5.14 - MAC estimates (I): MAC(1) – identified and calculated mode shapes before the rehabilitation *versus* MAC(2) – identified and calculated mode shapes after the rehabilitation.

5.7.3. Evaluation of the changes produced by the rehabilitation

In any rehabilitation process of a bridge involving strengthening works both the structure's mass and stiffness will be altered to a greater or lesser degree depending on the strategy adopted. If for the former its quantification is easily accomplished through the amounts of material removed from or added to the bridge, with respect to the latter its variation can only be accurately assessed by conducting field tests.

In the case of modal testing the parameters that can be directly estimated are modal properties, such as the natural frequencies and mode shapes, both depending mainly on the relation between mass and stiffness. Therefore, knowing the variation of the structure mass and its spatial distribution, as well as the deformed shape of the vibration modes, it is possible to estimate the stiffness shifts produced for the main components, in the vertical and transverse directions.

For this effect, Table 5.3 lists the mass for several structural members and/or at different levels and the corresponding variations caused by the rehabilitation. It points for a total

increase by 22 %, mainly due to the changes operated at the deck level where the mass is concentrated. On the other hand, the intermediate members experienced the highest average proportional increment, as opposed to the upper level.

Table 5.3 – Distribution of the mass in the bridge.

Level	*Structural elements*	*Before rehabilitation[3] (t)*	*After rehabilitation[4] (t)*	*Δ (%)*
Lower	Chords	26.3	28.8	9.20
	Bracing	8.8	8.8	-0.01
	Floor system	187.1	232.1	24.09
	Sub-total	222.2	269.7	21.37
Middle	Verticals	15.5	18.0	15.85
	Diagonals	16.7	25.5	52.16
	Sub-total	32.2	43.4	34.70
Upper	Chords	33.5	36.6	9.24
	Bracing and sway	7.5	10.7	42.44
	Sub-total	41.0	47.3	15.33
	Total	295.4	360.4	21.99

Δ = [4] / [3] - 1.

Table 5.4 summarizes the average estimates of the natural frequencies identified for the bridge main spans, before and after the rehabilitation. For any vibration mode the corresponding value remained unchanged or increased, which combined with the widespread increment of the mass clearly indicates a stiffening of the structure. However, a more detailed analysis must be performed if specific findings are intended.

Table 5.4 – Experimental natural frequencies.

Mode number	*Mode type*	*Before rehabilitation[5] (Hz)*	*After rehabilitation[6] (Hz)*	*Δ (%)*
1st	T – TO	1.721	1.912	11.10
2nd	V	2.779	2.779	0.00
3rd	T – TO	3.210	3.454	7.60
4th	T	4.273	5.510	28.95
5th	V	5.460	6.189	13.35
6th	TO	5.937	6.368	7.26
7th	V	8.293	9.578	15.49
8th	V	10.604	12.573	18.57
9th	V	12.577	15.304	21.68

T – Transverse mode; V – Vertical mode; TO – Torsional mode; Δ = [6] / [5] - 1.

As the natural frequencies obtained from both tests for the second mode are exactly the same and most of the bridge mass is displaced in the vertical direction (see Figure 5.12) it is possible to conclude that the stiffness of the structure for symmetric vertical loadings increased in the same proportion of the mass, i.e. its increment was approximately 22 %. Furthermore, the variation of the modal mass in the vertical direction associated with the second mode shape, computed from Models A and B, is around 21.9 %, as indicated in Table 5.5, thus validating this finding. This conclusion is also confirmed by the results collected during the static tests, from which a general increase of 20.5 % for the vertical bending stiffness was inferred (Costa *et al.*, 2008a).

Table 5.5 – Modal mass variation estimated from the numerical analyses.

		Before rehabilitation[7]			*After rehabilitation[8]*			*Δ (%)*		
Mode number	*Mode type*	*L** *(t)*	*T** *(t)*	*V** *(t)*	*L** *(t)*	*T** *(t)*	*V** *(t)*	*L**	*T**	*V**
1st	T – TO	0.115	53.078	2.998	0.138	62.385	4.299	19.44	17.53	43.38
2nd	V	5.298	0.003	107.145	4.774	0.003	130.582	-9.88	12.80	21.87
3rd	T – TO	0.483	119.997	10.265	0.819	157.657	19.357	69.57	31.38	88.57
4th	T	0.183	22.377	0.429	0.383	26.472	0.406	108.71	18.30	-5.35
5th	V	25.190	0.028	45.919	20.936	0.014	52.710	-16.89	-50.49	14.79
6th	TO	0.028	1.022	3.588	0.123	0.635	2.074	336.69	-37.88	-42.19
7th	V	0.341	0.041	7.652	0.193	0.553	3.996	-43.19	1260.42	-47.78
8th	V	0.168	0.126	7.169	0.460	0.052	15.598	173.13	-58.67	117.56
9th	V	1.093	0.054	87.027	0.657	0.161	73.584	-39. 90	199.66	-15.45

T – Transverse mode; V – Vertical mode; TO – Torsional mode; L* – Longitudinal direction; T* – Transverse direction; V* – Vertical direction; $\Delta = [8] / [7] - 1$.

Although the first mode presents some torsional deformation it is predominantly transverse, both lower and upper level masses are mobilized, and the deformed shape is symmetric. The ratio increase of the bridge transverse modal stiffness, ΔK , can then be estimated by the following expression

$$\Delta K = (\Delta f)^2 \times \Delta M \qquad 5.2$$

where Δf and ΔM are correspondingly the proportional variations of the natural frequency and mass, computed as a post to pre-rehabilitation condition ratio. Adopting Δf = 1.11 from Table 5.4 and ΔM = 1.18 from Table 5.5 the modal stiffening is estimated near 45 %. It is worth noting that the modal transverse displacements of the upper level are, in average, three times higher than at the lower level, which substantially reduces the

modal mass variation. Static results from the numerical analysis aim at the same value, which proves the excellent correlation between experimental and numerical estimates.

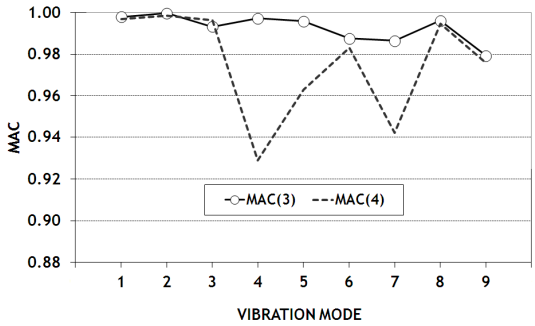

Figure 5.15 - MAC estimates (II): MAC(3) – numerical mode shapes before and after the rehabilitation *versus* MAC(4) – experimental mode shapes before and after the rehabilitation.

The assessment of the variation experienced by the mode shapes was performed by calculating the MAC indicator, either correlating the modal parameters provided by Models A and B, MAC(3), or comparing the experimental mode shapes obtained from both tests in the north span, MAC(4). The first indicator was computed with the modal coordinates at the panel points of both chords, whereas for the second only the points where the measurements were taken from have been accounted for. The values of these two variables for the nine vibration modes are plotted in Figure 5.15.

While indicator MAC(3) remains always above 0.98 with a declining trend as the modes order increases, MAC(4) exhibits three significant drops at vibration modes 4, 5 and 7. The first observation indicates that no significant change in the deformed configuration of the mode shapes would be expected due to the rehabilitation process. With respect to the second observation some causes have already been previously pointed out, which may be regarded as an indicator of some level of degradation of the north span prior to the rehabilitation. The deformed configurations for mode shapes 4 and 5 estimated from the first test are of poorer quality in the antisymmetry, contrary to the results provided by the second test, whereas maximum coordinates of mode 7 could not be captured with the adopted experimental setup.

5.7.4. Global vibration mode

Last but not least, a major feature highlights from the comparison of the results supplied by both tests, which is the identification of a global vertical bending vibration mode encompassing all the three main spans after the bridge rehabilitation, contrary to the

expected independent/decoupled behavior. In a first stage, the only alteration made to the structure that could explain this significant change was the installation of reinforced elastomeric expansion joints connecting the slabs of adjacent spans and the slabs of the end spans to the masonry abutments. In fact, before the bridge rehabilitation this connection did not exist as the joint was materialized with no physical link. Figure 5.16 depicts the expansion joint before and after the rehabilitation.

(a) (b)

Figure 5.16 - Expansion joint: (a) bottom view before the rehabilitation; (b) top view after the rehabilitation.

To test this hypothesis a modal analysis was carried out on the basis of Model C described in section 5.6. Given that the bolt-bars should be able to slide freely through their eye supports located in each of the end verticals (see Figure 5.6(b)), their axial stiffness was initially assumed to be almost zero. The first vertical mode shape calculated with this model is represented in Figure 5.17(a), as well as the mid-span modal coordinates extracted from the test data. It is clearly noticeable a large discrepancy between the two results. Furthermore, the corresponding numerical frequency was found to be 2.756 Hz, 9 % lower than the experimental value (3.027 Hz), and almost matching the natural frequency of the first vertical bending mode obtained through Model B.

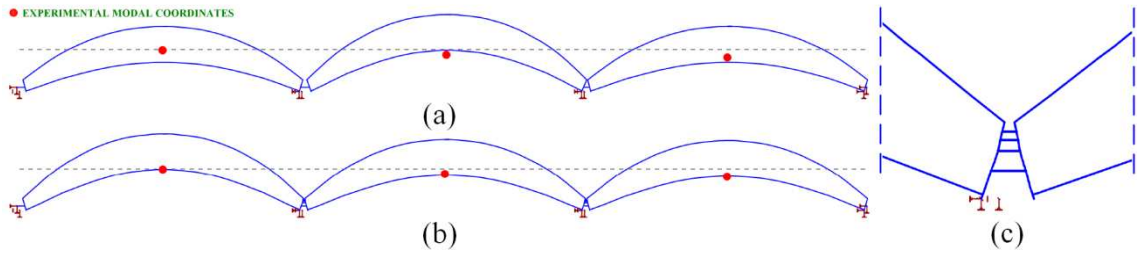

Figure 5.17 - Global mode shape computed from Model C: (a) connection between spans is accomplished only by the expansion joints; (b) blocked bolt-bars are also considered; (c) detail at one connection.

Consequently, in a second stage, the full axial stiffness of the bolt-bars was taken into account, which led to a new vertical mode shape depicted in Figure 5.17(b) with a natural frequency of 2.871 Hz. Although this value is more close to the frequency estimated by Model B than to the identified frequency for the global mode, experimental and numerical modal coordinates are very similar. In fact, after a thorough survey of the bridge just after performing the ambient vibration test, it was possible to confirm that almost all bolt-bars were blocked due both to the misalignment of the eye supports and to the small clearance as result of the new coating.

5.8. Summary and conclusions

This chapter presents a set of dynamic field tests conducted on a centenary through-truss steel bridge before and after its rehabilitation. These tests provided a unique opportunity to evaluate the changes in the dynamic properties of a structure as a consequence of the adopted strengthening strategy and construction works carried out. On the one hand, the experimental results were used to assist the viability study and to update the design numerical model, and subsequently data helped to confirm the adequacy of the rehabilitation plan. On the other hand, the dynamic tests were performed to complement and/or confirm the information obtained from the in-situ evaluation of the static response.

The procedures adopted during the ambient vibration tests, the bridge instrumentation, acquisition system and testing sequence were comprehensively described. Attention was also paid to data processing and system identification. Three-dimensional finite element models were developed to support the structural analysis, and in turn field data was employed to validate the numerical simulations. Two models of a simply supported span have replicated the pre and post-rehabilitation conditions of the bridge and other 5 models were utilized to conduct a sensitivity analysis for appraising the contribution of several factors to the dynamic properties. An eighth model encompassing all the main spans has helped to identify the existence of likely global vibration modes that could be observed from the tests. The results have allowed to draw the following conclusions:

i. Field data confirmed a large reduction of the vibrations at the deck level after the rehabilitation under similar traffic scenarios;
ii. The modal parameters identified from both tests, either the natural frequencies or mode shapes, fairly agreed with the numerical predictions;

iii. The natural frequencies of all identified vibration modes remained constant or greatly increased with the rehabilitation process, whereas the mode shapes did not indicate any significant variance between the pre and post-rehabilitation conditions;

iv. A detailed analysis to the changes produced in some natural frequencies has permitted to obtain excellent estimates of the changes in the structure's stiffness;

v. In general a 3D frame system is well suited to simulate the dynamic behavior of the bridge, even though hinged or semi-rigid connections for some joints might improve the accuracy of the modal estimates;

vi. While the stringers stiffness influences both the vertical and transverse modes, the slab mainly impacts on the latter and a significant variation of the crossbeams stiffness has little effect on the vibration frequencies;

vii. A global vertical bending mode was identified after the bridge rehabilitation, which was confirmed by the numerical analysis and ascribed to the blocking of the bolt-bars.

Chapter 6

Design and installation of the Luiz I Bridge monitoring system

6.1. Synopsis

In the last decade, fiber optic sensors (FOSs) have been increasingly preferred over electric ones to integrate structural health monitoring systems installed on new bridges. The added value of this sensing technology in appraising the behavior of centenary structures is also unquestionable. In this chapter the design of an advanced monitoring system based on fiber Bragg gratings (FBGs) and implemented in a XIX century steel arch bridge is reported. Three major requirements had to be attained with its installation. Firstly, welding solutions for attaching strain sensors to the steel surface were not permitted due to its chemical properties. Secondly, the monitoring system should provide reliable data concerning the structure's behavior at least for a decade. Thirdly, FOSs retrofitted to the bridge should have a minimum impact in its aesthetics. Techniques and materials adopted in the system installation and protection of sensors and optical components are pointed out. Data from numerical analyses aiming at the strain sensors optimum design and the estimation of their measurement accuracy are analyzed. Experimental tests carried out to comprehensively characterize the sensors response are described, and their results discussed. The guidelines considered in the development of the project, system architecture and objectives to accomplish are also presented. Additionally, some characteristic results of the bridge response during the initial monitoring period are shown.

6.2. Introduction

Fiber optic sensors have the ability to modulate some properties of the light that is launched by a source into the core of the fiber. This modulation can be caused by changes in strain, temperature and pressure experienced by the sensor through which the light travels. In consequence, an optical signal is generated and reflected towards a demodulation device to be translated into a measurement of the gauged quantity (Shehata and Rizkalla, 1999).

FOSs are well known for some of their advantages. These sensors are immune to electromagnetic and radio interferences due to their dielectric nature (Mehrani *et al.*, 2009; Tennyson *et al.*, 2001), which makes them suitable for monitoring metallic structures. Moreover, FOSs typically present high sensitivity, good resolution and accuracy (Lee *et al.*, 2002; Todd *et al.*, 2007), as well as high signal to noise ratio (Ansari, 2007), and can operate in a wide temperature range (Deng and Cai, 2007). Their light weight and small dimensions make them suitable for the embedment into the host structure, leading to the concept of smart structure (Betz *et al.*, 2003; Casas and Cruz, 2003). Chemical properties of the silica, the major component of the fiber, provide FOSs a natural resistance to corrosion in harsh environments (Zhan-feng *et al.*, 2007). Durability and stability characterize FOSs and are essential for long-term monitoring (Doyle *et al.*, 2007; Li and Wu, 2007; Maalej and Rizkalla, 2000). Contrary to conventional electric sensors, FOSs naturally enable distributed measurements which reduces the number of leads to be deployed along the structure (Liang *et al.*, 2005). Also, fiber optic systems have an excellent ability to transmit signal over long distances as the fibers themselves act both as sensing element and signal transmission medium (Majumder *et al.*, 2008). These two facts positively impact on the overall costs of a permanent observation system (Connolly, 2006), which are also expected to reduce as fiber optic technology rapidly evolves (Li *et al.*, 2004). It is worth mentioning that FOSs are flexible since they can be installed into complex surfaces (Zhan-feng *et al.*, 2007), and versatile as they can be produced in numerous configurations, with different dimensions and applied using diverse techniques (Mrad *et al.*, 2000).

Examples of FOSs for monitoring civil engineering structures are the Fabry-Perot (FP), SOFO (acronym for Surveillance d'Ouvrages par Fibre Optiques) and Brillouin sensors. The first sensor is an interferometer constituted by two semi-reflective mirrors positioned at a certain distance from each other, termed as the FP cavity. A major advantage of the FP sensor is that it can be easily produced to be temperature self-compensated taking into

account the coefficient of thermal expansion of the host material, and therefore strain readings are stress induced only (Shehata and Rizkalla, 1999). Additionally, it uses multi-mode fiber which is a simpler and cheaper technology. On the other hand, each optical fiber must connect to a single sensor, therefore naturally requiring parallel multiplexing. The second sensor is a long gage device which can be defined as a double Michelson fiber optic interferometer arrangement (Connolly, 2006). One of the fibers is prestrained and acts as a sensing arm being attached to the host structure, whereas the other is used as reference having a well known length. Since both fibers are side by side they experience the same temperature variation, thus making the sensor temperature insensitive. Contrary to Michelson interferometer, SOFO system uses as light source a broadband source, typically a LED or a SLED. The third sensor makes use of the Brillouin scattering which is produced by the nonlinear interaction of light and acoustic waves that induce a small dynamic change in the refractive index of the fiber core (Measures, 2001). The Doppler shift in the frequency of this scattered light depends on the refractive index which in turn is related to glass density. As the strain and temperature alter material density, Brillouin frequency can be used to measure those quantities along the fiber. Thus, by using optical time domain reflectometry (OTDR) distributed sensing is accomplished.

Despite FOSs have characteristics that are advantageous for their application to steel bridges as previously mentioned, they exhibit, however, an intrinsic fragility that requires extra care in their manufacture, handling and installation. On the other hand, contrary to concrete structures where the host material confers a robust protection to sensors and optical fibers by embedding them, in general, steel structures that incorporate fiber optic based monitoring systems have the components directly exposed to the environment if no additional measures are taken. If on steel box girder bridges some protection can be obtained by placing sensors and optical fibers inside the box, in what concerns truss structures such is not possible, and hence proper methodologies have to be adopted in their installation. Adding the fact that fiber optic technology is relatively recent, and therefore long-term behavior of the various existing systems is not yet well characterized, few fiber optic based monitoring systems are up to now deployed on steel bridges. Furthermore, examples of centenary structures are even more scarce. Table 6.1 identifies a number of steel bridges in which fiber optic based monitoring systems are installed as well as the type of technology adopted.

Table 6.1 – Steel bridges incorporating fiber optic based monitoring systems.

Bridge	*Type*	*Structure description*	*Sensors (No.)*
Winooski River Bridge in Waterbury-Duxbury Vermont (USA) (Fuhr *et al.*, 1999)	Truss	Steel girders & reinforced concrete deck	FBG [a] (8)
Bridge No. A6358 - U.S. Route 54 over Osage River (USA) (Matta *et al.*, 2008)	Slab-on-girder	Steel girders & reinforced concrete deck	BOTDR [b]
East 12th Street Bridge over I-235 Des Moines, Iowa (USA) (Hemphill, 2004)	Slab-on-girder	Steel girders & reinforced concrete deck	FBG [a] (40)
Île-d'Orléans Bridge (Canada) (Inaudi and Del Grosso, 2008)	Suspension	Steel deck & steel towers	SOFO [c] (6)
Götaälvbron (Sweden) (Glišić *et al.*, 2007)	Slab-on-girder	Steel girders & reinforced concrete deck	BOTDR [b]
Bridge in Port of Venice 'Marghera' (Italy) (Glišić and Inaudi, 2007)	Cable-stayed	Steel girders & reinforced concrete deck and towers	SOFO [c] (82)
Bridge over São Roque and Botirões channels, Aveiro (Portugal) (Barbosa *et al.*, 2008)	Cable-stayed	Steel deck & steel mast	FBG [a] (40)
Tsing Ma Bridge (Hong Kong) (Chan *et al.*, 2006)	Suspension	Steel deck & reinforced concrete towers	FBG [a] (40)
Stonecutters (Hong Kong) (Ko and Ni, 2005)	Cable-stayed	Steel deck & reinforced concrete towers	FBG [a]
Jiangyin Bridge (China) (Ko and Ni, 2005)	Suspension	Steel deck & reinforced concrete towers	BOTDR [b] & FBG [a] (116)
Wuhu Yangtze Bridge (China) (Zhan-feng *et al.*, 2007)	Cable-stayed	Steel truss deck & reinforced concrete towers	EFPI [d] (8)
Dafosi Bridge (China) (Ko and Ni, 2005)	Cable-stayed	Steel box girders & reinforced concrete towers	EFPI [d] (40)
Maocao Street Bridge (China) (Ou and Li, 2005)	Arch	Steel	FBG [a] (100)

[a] FBG – Fiber Bragg Gratings.

[b] BOTDR – Brillouin Optical Time Domain Reflectometry.

[c] SOFO® – Surveillance d'Ouvrages par Fibre Optiques.

[d] EPFI – Extrinsic Fabry-Perot Interferometer.

This chapter addresses the design and installation of a FBG based monitoring system applied to a centenary steel arch bridge during its strengthening and rehabilitation. A brief description of the sensing technology characteristics is made, in which its advantages when compared to other fiber optic systems are highlighted. The various factors and requirements that influenced the monitoring project are listed, as well as the goals to be achieved with its implementation. The gauged parameters are identified and the location of the sensors on the structure justified. The extensive experimental campaign undertaken to characterize the critical aspects of the project, such as the strain sensors behavior, their attachment to the steel and the in situ protection, is addressed and the results evaluated. Some results collected during the early operation and verification of the monitoring

system installed in the bridge are presented. Taking into account the key role played by the acquisition system in designing the fiber optic network architecture and in accomplishing the targeted goals, some insight on its selection is also given. At the end, a global assessment of the project is made regarding the survival rate of the sensors, easiness and suitability of the adopted installation procedures and ability of troubleshooting in the future.

6.3. FBG sensing technology

A FBG is a sensing element that has inscribed within it a permanent periodic perturbation of the core refractive index of a single-mode optical fiber (Chan *et al.*, 2006), usually around 10 mm (Li *et al.*, 2004), and therefore constitutes an intrinsic fiber optic sensor. This refractive index grating is written into the optical fiber due to its photosensitivity, and can be fabricated using several techniques (Othonos, 1997). When incident light from a broadband or a tunable laser source interacts with the grating a specific narrowband spectrum centered about a single wavelength, λ_B, known as Bragg wavelength, is back-reflected, therefore acting as a wavelength selective "mirror" (Shehata and Rizkalla, 1999). The remaining light wavelengths are simply transmitted through the sensor (Tennyson, 2001). The reflected light wavelength has to satisfy a diffraction law, so-called Bragg condition, expressed by

$$\lambda_B = 2 \cdot n_{eff} \cdot \Lambda \tag{6.1}$$

where Λ is the grating period (pitch length), and n_{eff} is the mean effective refractive index of the guided mode in the fiber.

As strain, temperature or pressure variations, $\Delta\varepsilon$, ΔT and Δp, respectively, influence both the effective refractive index and the grating pitch-width (Moyo *et al.*, 2005), the grating central wavelength in the reflected spectrum shifts by $\Delta\lambda_B$ in response to these three parameters through the following equation

$$\frac{\Delta\lambda_B}{\lambda_B} = P_\varepsilon \cdot \Delta\varepsilon + [P_\varepsilon \cdot (\alpha_M - \alpha_F) + \zeta] \cdot \Delta T + G_p \cdot \Delta p \tag{6.2}$$

where P_ε and ζ are correspondingly the strain and thermo-optic coefficients of the optical fiber, G_p is the gain factor for pressure, whereas α_M and α_F stand as the coefficients of thermal expansion of the host structural material and of the fiber itself, respectively. Table 6.2 lists values presented by several authors for these parameters, having as reference a

Bragg wavelength of 1550 nm. Knowing the exact values of the factors and coefficients it is possible to accurately determine the stress-induced strain variations.

Table 6.2 – Common values of the constants for determining the Bragg wavelength shift.

Coefficient / factor	*Values*
P_ε	$0.75 \times 10^{-6}\ \mu\varepsilon^{-1}$ - $0.82 \times 10^{-6}\ \mu\varepsilon^{-1}$ (Tennyson *et al.*, 2001)
G_p	$1.94 \times 10^{-6}\ \text{MPa}^{-1}$ - $2.70 \times 10^{-5}\ \text{MPa}^{-1}$ (Hill and Meltz, 1997; Moyo *et al.*, 2005)
ζ	$6.10 \times 10^{-6}\ ^{\circ}\text{C}^{-1}$ - $8.60 \times 10^{-6}\ ^{\circ}\text{C}^{-1}$ (Kister *et al.*, 2007; Othonos, 1997)
α_F	$0.50 \times 10^{-6}\ ^{\circ}\text{C}^{-1}$ - $0.55 \times 10^{-6}\ ^{\circ}\text{C}^{-1}$ (Kister *et al.*, 2007; Tennyson *et al.*, 2001)

One important feature of FBGs is their self-referencing capability, since the quantity to be measured is encoded into wavelengths, which is an absolute parameter and does not depend on the electric power supplied to the interrogator or on optical losses along the light path (Kersey *et al.*, 1997). Therefore no recalibration and/or re-initialization are needed for these sensors, a feature that is often termed as self-referencing (Tam *et al.*, 2007; Tennyson, 2001). Another key capability of FBGs is the possibility of being multiplexed, which consists on placing a large number of sensors along a single fiber provided that each grating is highly reflective and fabricated with a different resonant wavelength within the broadband source spectrum (Kersey *et al.*, 1997; Tennyson, 2001). Therefore, this capability shows potential for applications in the field of quasi-distributed sensing since the grating position is well identified (Wang *et al.*, 2001).

6.4. Description of the bridge

Luiz I Bridge constitutes a unique example of bridge engineering, worldwide known, which marked a time of the Portuguese industrial period (see Figure 6.1). Its distinctive feature is the existence of two decks at different levels supported by a single arch. This arch exhibits a parabolic geometry in elevation, spanning 172 m for a maximum rise of 45.1 m, with pinned supports at the lower chords end joints resting over the river banks. The 391.25 m long upper deck comprises 13 spans with lengths varying between 11.8 m and 50.7 m. Nine spans are formed by two 5 m high truss girders, spaced of 4.65 m between centerlines, other two have truss girders with variable height from 0.9 m to 5 m,

and in the remaining two, located over the arch crown, the trusses are substituted by 0.9 m high I-beams.

Figure 6.1 - Luiz I Bridge.

The upper deck rests on two masonry piers and five metallic piers, three of which shaped as truncated pyramids based on foundation plinths located in the banks and the other two materialized by plan panels directly supported on the arch. The lower deck is structurally identified as a pony truss bridge, with its five spans crossing a total length of 174 m. Its two lattice girders, 3.25 m high and 8.40 m apart, are suspended from the arch by four tie-trusses spaced at 36 m intervals, with heights equal to 25.5 m and 43.5 m at the sides and center, respectively.

Before the rehabilitation took place both decks presented a total width of about 8 m, which included 2 traffic lanes and 2 sidewalks, whereas for the new condition the upper deck is widened by 2 m. At the abutments of both decks and at the top of the piers located in the river banks the loads are transferred from the girders through roller bearings or disk bearings (only at the upper deck abutments for the new condition). In general, bars pertaining to the original structure have I, T or box shaped sections built by assembling several plates and angles through riveted connections, a typical technique of the steel construction of that time.

Despite some operations of rehabilitation and maintenance or minor changes suffered to accommodate the passage of new types of vehicles, the structure has been in continuous operation since its completion date in October 1886. However, lately a strengthening and rehabilitation process took place on this bridge, in order to allow the integration of its upper deck in the infrastructure of the Porto Metro Light Rail Network. One of the major operations fulfilled during this process was the replacement of the upper deck bridge floor

system by a suitable metallic profile grid, able to properly transmit the new railway traffic loads to the truss girders (see Figure 6.2). The structural elements strengthened with addition of steel profiles were the upper deck girders, the suspension ties, arch diagonals and bracing elements all over the bridge. All the pieces and structural components with severe corrosion problems were replaced. The old steel coating was removed and a new 3-layer weathering protection was applied to the surface.

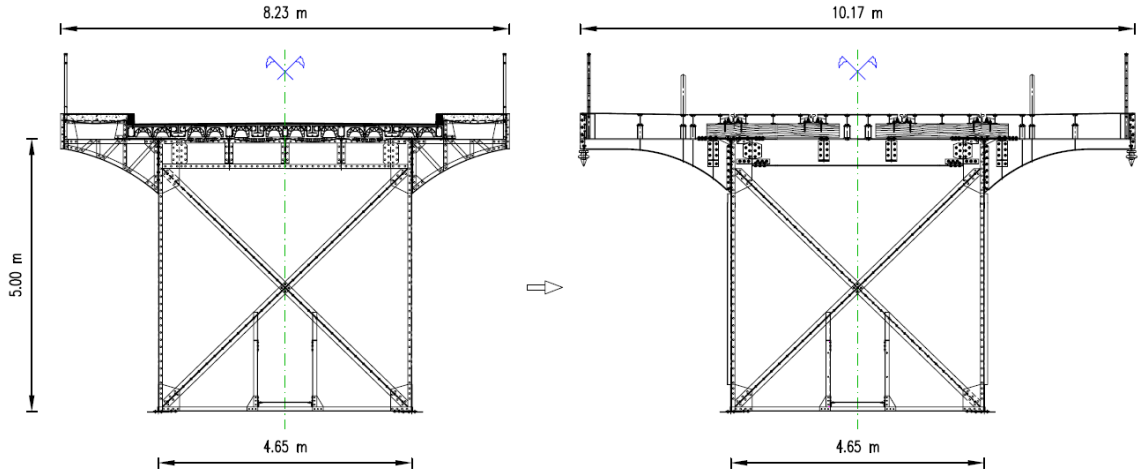

(a) (b)

Figure 6.2 - Upper deck cross-section: (a) before the rehabilitation; (b) after the rehabilitation (GRIDc), 2003).

6.5. Monitoring system

6.5.1. Objectives

The monitoring system designed for the bridge was implemented with the purpose of appraising the strengthening solutions performance and assessing the bridge in-service behavior. The location of some sensors took into account the sections observed during the load test carried out before the rehabilitation and strengthening works, in order to support the upgrade design (Figueiras *et al.*, 2005). Therefore, by applying the same load cases to the structure, a comparison between results of both load tests could be accomplished, which in turn could enable the assessment of changes in the structural behavior (GRID, 2005). On the other hand, the gentleness of some of the strengthening operations and the significance of this historical bridge made the monitoring of its in-service behavior imperative for structural surveillance and safety. The monitoring system

was designed to be installed during the construction process, taking advantage of the general scaffolding mounted for the bridge rehabilitation.

The monitoring system of Luiz I Bridge allows the measurement of (Costa *et al.*, 2004a; GRIDa), 2003):

i. Strains in selected truss elements of the arch, upper deck girders, metallic piers and suspension ties;
ii. Relative horizontal displacements of the expansion joints at the abutments, and between the bridge upper deck and the masonry piers;
iii. Temperature of the steel and environment, both in arch and in upper deck elements.

6.5.2. Instrumentation plan

6.5.2.1. Strain sensors

In order to appraise the strain state of the structure, a total of 118 fiber optic sensor holders were attached to the steel surface, distributed by pairs in the selected 59 key cross-sections of the elements to be observed. Figure 6.3 illustrates the general location of the strain sensors applied to the bridge. Details of sensors installed on the structure are shown in Figure 6.4.

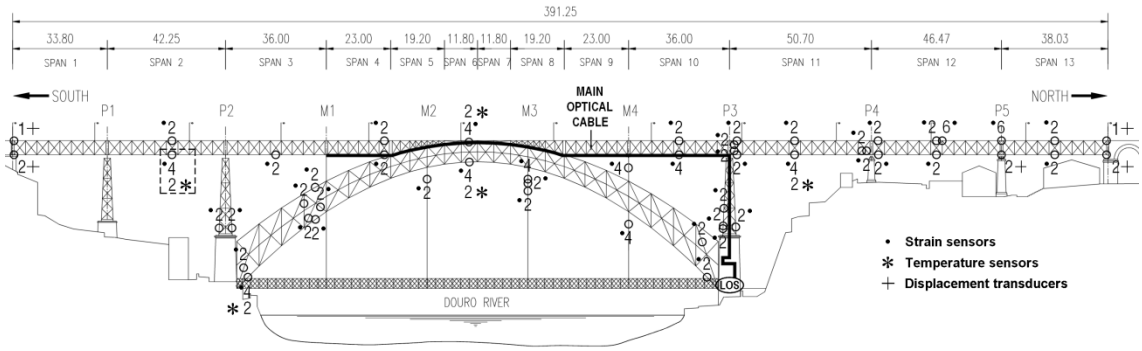

Figure 6.3 - Layout of the instrumentation installed in the bridge.

The adopted strain sensors are single FBGs written into pigtails embedded in carbon fiber reinforced polymer (CFRP) patches. They were developed and tested by the author in cooperation with the supplier company, FiberSensing S.A. The sensors have a sensitivity of 1.2 pm/με and a full scale range of ±4000 με (FiberSensing, 2009). Laboratory tests carried out to characterize their performance as well as to validate the adopted installation procedures and protection systems are reported in section 6.8.

(a) (b) (c)

Figure 6.4 - Details of strain sensors applied to arch chords: (a) schematic location; (b) strain sensors EA-S13 and EA-S14; (c) strain sensors EA-I15 and EA-I16.

6.5.2.2. Temperature sensors

Given that the FBG strain sensors used in this project are cross-sensitive to temperature, its measurement for thermal compensation of the strain readings became mandatory. On the other hand, temperature is one of the most relevant environmental load acting on the structure during its service time. From the observations performed in the structure, before and during the ongoing construction works, it was possible to appraise the temperature distribution. In fact, it was found that the temperature of the air is uniformly distributed throughout the upper deck, experiencing differences not greater than 0.4 ºC (Costa *et al.*, 2005). Nevertheless, substantial discrepancies between the steel temperature in some truss elements and the ambient temperature were observed. In light of the above considerations, the monitoring system has 10 temperature sensors, 6 located in the arch and 4 in the upper deck, as shown in Figure 6.3. Transversally, the sensors act like a couple collecting data from both sides, upstream and downstream, monitoring simultaneously the temperature in the environment and that experienced by the steel, i.e. for each sensor measuring the air temperature in one side there is another measuring the temperature in the steel on the other side.

The temperature sensors are FBGs written into a pigtail left loose inside an aluminum tube, manufactured and supplied by FiberSensing S.A. Their sensitivity is of 10 pm/ºC and operate correctly between -20 ºC and 80 ºC (FiberSensing, 2010).

6.5.2.3. Displacement transducers

The monitoring of the upper deck supports performance became crucial, since before the rehabilitation works, due to support bearings damage, its rigidity center related to horizontal movements was found apart from the arch crown by more than 30 m towards

the north abutment (Costa *et al.*, 2004b). Eight fiber optic transducers installed in the bridge enable the monitoring of relative displacements between the upper deck and the abutments and pier P5. Moreover, they are located in such a way that rotations of the upper deck can also be captured (see Figure 6.3).

The displacement transducers were specially designed and produced by LABEST for this monitoring system, and are capable of measuring relative displacements within ± 100 mm, which is suitable to access the bridge's bearings performance due to daily and seasonal temperature variations.

6.5.3. Fiber optic network

6.5.3.1. Introduction

The fiber optic network was designed taking into account technical and economical aspects, as well as the particularities of the bridge. It has a tree configuration with a main optical cable branching into each of the 14 optical fiber leads containing up-to 10 sensors serially connected.

6.5.3.2. Network architecture

A fiber optic cable installed in an existing sealed metallic gallery performs the monitoring system spinal column function. This gallery is located nearby the bridge technical walkway between the upper deck girders, facing the downstream side. The main fiber optic cable, 210 m long, is routed from the upper deck (M1-P3) to the Local Observation Station (LOS) located in a room next to the lower deck, at the masonry base of pier P3 (see Figure 6.3).

The main optical cable branches into 14 optical fibers, each one an optical channel, through 3 fiber optic splice enclosures, installed on the bridge technical walkway, close to the metallic gallery housing the cable. The fifteenth optical branch of the fiber optic network was not connected to the main optical cable. It holds the eight sensors attached to pier P3, and links directly to the interrogation system, located at the LOS. The fiber optic splice enclosures are located over piers M1 and P3 and at the arch crown. Figure 6.5(b) depicts the fiber optic splice enclosure placed over pier P3. The south enclosure connects 4 optical fibers, the central 3 and the north 7. The number of branches allocated to each of the enclosures is related to the relative positioning between the completed branches and the fiber optic splice enclosures. The maximum number of sensors that could be multiplexed on a single optical fiber, the sensors relative position on the structure and their distance to the nearest enclosure, have determined the sensors distribution among

the optical branches, as well as their quantity on each one. Figure 6.6 shows the fiber optic network deployed on the bridge.

(a) (b) (c)

Figure 6.5 - Fiber optic network: (a) main optical cable leaving an old metallic pipe at the masonry base of pier P3; (b) fiber optic splice enclosure; (c) junction box located at the base of pier M1.

In the bridge technical walkway several junction boxes were installed to house the connectors splicing the patch cords and sensors for each optical branch. For each pair of sensors monitoring a truss element in the upper deck, there are two patch cords connecting them to one of those boxes. Sensors applied in the remaining structure are also linked by patch cords which are connected at junction boxes fixed to the bridge in specific points (see Figure 6.5(c)). All the optical branches containing sensors attached to the arch, metallic piers and suspension ties are linked to enclosures placed in the bridge technical walkway, in which they are connected to upper deck sensors or guided towards the fiber optic splice enclosures.

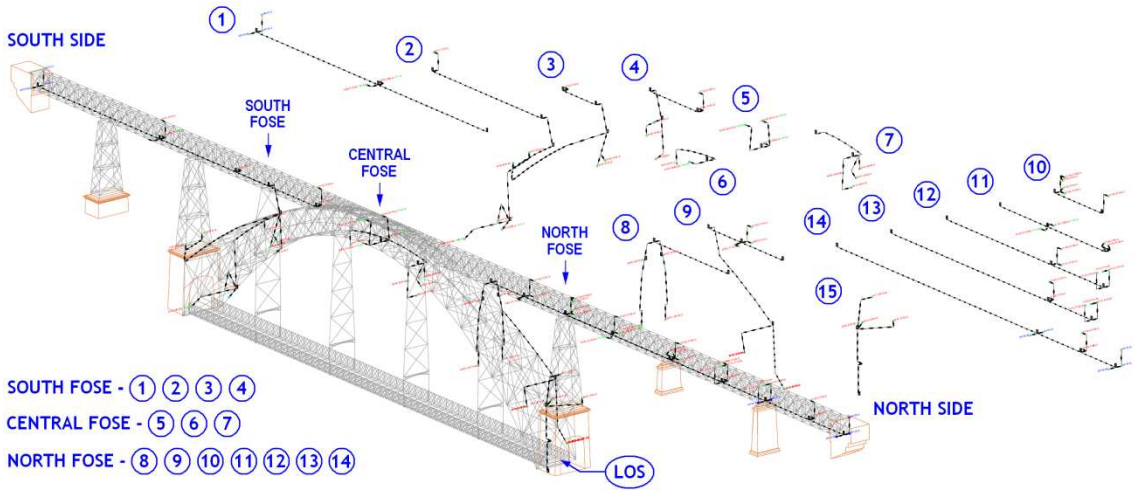

Figure 6.6 - Overview of the fiber optic network (FOSE – Fiber Optic Splice Enclosure).

Special attention was paid to the interchangeability of the gratings relative position in the light path of the optical branches. The designed arrangement for the fiber optic network allows to maximize the number of gratings able to be interrogated if breakage occurs in one or more points along the light path.

6.5.3.3. Multiplexing

Multiplexing has been defined by Tennyson (2001) as the ability to interrogate a large number of sensors using a single demodulation system, that is, to distinguish signals from different sensors in a sensor network. A hybrid scheme has been developed to acquire the optical signals from the sensors. Sets of serially multiplexed sensors, holding perfectly distinguishable Bragg wavelengths, are multiplexed in parallel into the 15 fiber optic strands that constitute the network.

Wavelength Division Multiplexing (WDM) was the main technique adopted in this monitoring system, which takes advantage of the fact that to each grating is coupled a Bragg wavelength that constitutes its signature. Since to different gratings match distinct Bragg wavelengths at several locations along the same fiber, all sensors can be identified in the reflected spectrum given that to each one is assigned a different peak. However, this multiplexing technique requires highly reflective gratings and a suitable wavelength separation between peaks in the spectrum so that no overlapping might occur due to measurand induced shifts (Chan *et al.*, 2006). Additionally, given that the sensors are positioned in different fiber leads, the Spatial Division Multiplexing (SDM) technique was also implemented through an optical switch that integrates the acquisition system (Hong He and Lin, 2009), located at the LOS.

The upper limit of the number of gratings that can be addressed in one single lead is a function of the light source optical bandwidth, operational wavelength range of each FBG sensor (Kersey *et al.*, 1997), and tuning range of the tunable filter (Chan *et al.*, 2006). Considering that the response of the sensor should only vary within the scanning bandwidth (Ansari, 2007), in the case of strain sensors applied to a real structure with no self-compensation for temperature, the operational wavelength range to consider must include both strain and temperature effects. Therefore, the wavelength interval between two neighboring gratings in the spectrum ($\Delta\lambda_{min}$) for one single optical fiber should be greater than the following value

$$\Delta\lambda_{min} = 2 \cdot |\Delta\lambda_{\varepsilon}| + |\Delta\lambda_{T}| + |\Delta\lambda_{is}| \qquad 6.3$$

where $|\Delta\lambda_\varepsilon|$ is the absolute wavelength variation caused by the maximum expected strain, tensile or compressive, $|\Delta\lambda_T|$ stands for the wavelength interval that corresponds to the maximum temperature difference between any two sensors placed over the same fiber lead, at the same time instant, and $|\Delta\lambda_{is}|$ is the minimum wavelength interval for which the interrogation system is capable to identify two peaks. For this project it was found that the minimum wavelength between two gratings of strain sensors would have to be 2 nm. Taking into account the wavelength range of the optical sensing interrogator, no more than 25 strain sensors could be placed in one single fiber strand. However, given that each optical fiber of each branch is accomplished by several patch cords linked by mechanical connectors, which have significant optical loss, it was set that no more than 10 sensors were to be multiplexed in one single optical fiber.

6.6. System installation

6.6.1. Sensors application and protection

6.6.1.1. Introduction

As it was previously stated the chemical composition of the steel did not allow the adoption of weldable fiber Bragg grating strain sensors, and therefore the gluing solution became the only one possible. In what concerns the fiber gratings protection, although they are shielded by the CFRP patches embedding them, the ingress and egress of the optical fibers emerge as fragile points due to the large discrepancy in stiffness between the fibers jacket and the composite material. On the other hand, in order to guarantee that strain sensors accurately sense the host material deformation is necessary to implement proper procedures in their application. In addition, their durability can only be achieved by endowing them with a suitable protection. On the contrary, the other sensors adopted on this monitoring project are sufficiently rugged and their installation does not jeopardize their health or longevity.

6.6.1.2. Surface preparation

The first operation to perform in attaching the strain sensors to the steel is the surface preparation. This stage begins with the weathering layer removal by using mechanical means. The epoxy coating is eliminated with an electric hand-held grinder equipped with a

sanding disk. The smoothed steel surface is then cleaned using soaked gauzes and water based surface cleaners to wipe out any dust or grease residues.

6.6.1.3. Adhering process

After the steel surface is prepared, a thin coat of epoxy resin is put on the contact side of the sensor composite patch. The strain sensor is then aligned correctly and pressure is carefully applied with the help of a clamp or other mechanical device, as it can be seen in Figure 6.7(a). The epoxy adhesive used in the bonding process has a short setting time, of about 5 minutes. The used setup enables a uniform transmission of the pressure all over the sensor and removes any epoxy excess applied on the interface CFRP/steel, therefore guarantying a thin layer of adhesive.

6.6.1.4. Sensors protection

To ensure an adequate longevity of a monitoring system special care has to be taken in installing the sensors, mainly if they are directly exposed to the environmental conditions, as is the case of surface mounted strain sensors attached to metallic bridges. Furthermore, as requested by the bridge owner, the sensors should ensure reliable measurements at least during a decade. A protective cork layer covered by a polyester sheet impregnated with epoxy resin was adopted. After the resin hardening, epoxy paint used on the weathering coat of the steel is applied to the installation surface. Figure 6.7(b) depicts a schematic of the implemented protection whose final aspect can be seen in Figure 6.4.

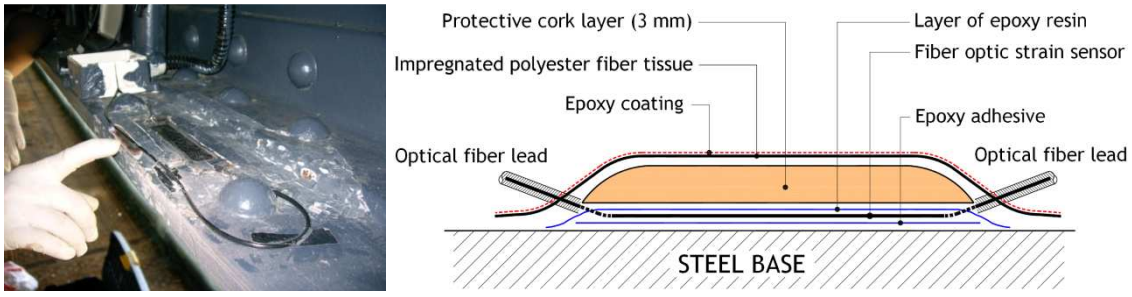

(a) (b)

Figure 6.7 - Strain sensors installation: (a) field application; (b) environmental and mechanical protection.

This type of cover applied to the sensors provides mechanical protection through the cork layer, but also prevents direct sun radiation over the sensor surrounding area. The protection resin and the paint enable the resistance against a variety of environmental factors, such as UV radiations, rain and moisture. Thus, the durability is ensured and the

intrusion level introduced on the readings is minimal. Moreover, the installation overall appearance is very discreet, fitting the aesthetic requirement.

6.6.2. Cable and fibers protection

All patch cords used to materialize the optical branches are guided and protected by flexible thermoplastic conduits, with reinforced spiral and smoothed inside wall, acting as jackets. The conduits at the bridge technical walkway were placed inside the metallic gallery, also used to house the main optical cable. This cable is a loose-tube one, and although this kind of cables have been adopted for outside-plant installation, it was double protected by two conduits with different diameters in the arch, where there is no gallery and therefore it is exposed directly to the environment.

The conduits were held in place by plastic zip ties or braces, fixed to the structure, and their ends connected to boxes and enclosures through plastic glands, sealed with epoxy resin, so that a suitable Ingress Protection (IP) could be achieved, no less than 65.

6.7. Numerical analyses for the development of the strain sensor holder

6.7.1. Introduction

In any monitoring system it is fundamental that sensors record the parameter to be gauged, but is also crucial that the measurement be as close as possible to the real value. Therefore, several numerical simulations were carried out for developing the strain sensor holder aiming at:

i. Determining the minimum length of the CFRP patches that would ensure a measurement of the steel strain with an error within acceptable values;
ii. The evaluation of the readings deviation from the actual strain acting on the host material influenced by the dimensions of the instrumented element.

To this end, it was assumed that the sensing optical fiber behaves similarly to the reinforcement fibers of the CFRP, having a perfect bond with the composite material (matrix + fibers). Therefore, the strain experienced by the sensing fiber is considered equal to that of the CFRP plate.

6.7.2. Finite element model

A three-dimensional finite element model was developed to simulate the behavior of a rectangular steel bar, instrumented with a fiber optic strain sensor, under a uniform uniaxial load longitudinally applied to the edges. The reference steel plate was 50 cm long, 15 cm wide and 1 cm thick whereas the sensor holder was modeled with a reference length, width and thickness of 10 cm, 2 cm and 0.1 cm, respectively. Figure 6.8 depicts the main geometric data of the problem. The applied load was such that induced a 100 MPa axial stress in the material. Given that the strain sensor is placed at the center of the steel plate and that both had two symmetry axis, one longitudinal and the other transverse, only one quarter of the plate and sensor was modeled using symmetry conditions. As a result, the finite element mesh could be refined to improve the results without putting at stake the calculation speed.

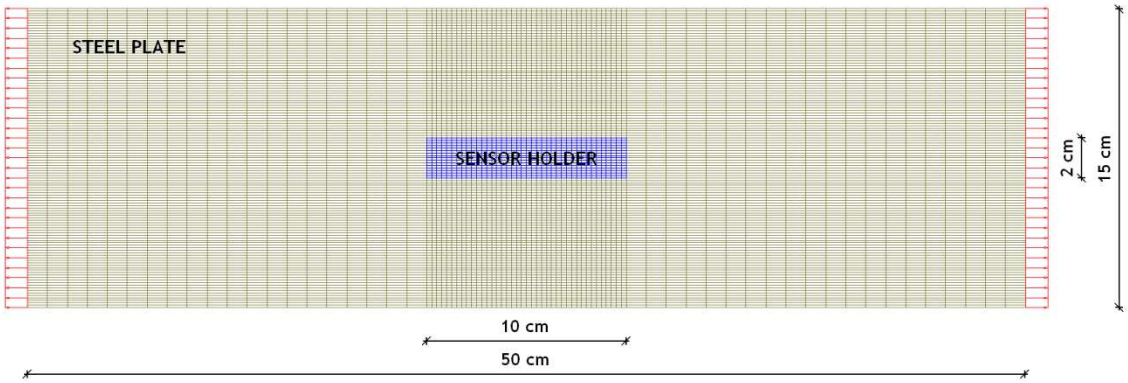

Figure 6.8 - Reference geometric data of the problem to be analyzed.

The steel plate and the CFRP laminate sensor holder were modeled with 4-noded rectangular plate elements, 1.25 mm wide. The finite elements of the sensor holder and nearby steel had a length of 2.50 mm whereas the remaining were 10 mm long. Two layers of volumetric finite elements link the plate and the laminate middle plans to the contact surfaces and a third layer of volumetric finite elements models the bonding epoxy adhesive placed between those, being its height equal to the interface thickness, conservatively taken as 0.2 mm.

The analyses were accomplished assuming linear elastic behavior for all materials. The deformability elastic parameters used in the model were obtained from experimental tests, and are as follows:

i. Steel: $E_s = 192.7$ GPa and $\nu_s = 0.25$;
ii. CFRP: $E_{CFRP} = 110$ GPa and $\nu_{CFRP} = 0.40$;
iii. Epoxy adhesive: $E_{ea} = 2.5$ GPa e $\nu_{ea} = 0.35$.

In these analyses the governing quantities considered for the readings deviation were the sensor holder length, and the width and thickness of the steel plate. The dimensions of the plate cross-sections adopted in the analyses were representative of the instrumented bars geometry of the bridge.

6.7.3. Analyses and results

When strain is transferred from the steel base to the CFRP sensor holder a minimum transfer length is required to reach a steady value, as it would be expected when two materials are perfectly bonded and one of them strains the other. This transfer length depends on the stiffness of the attached materials, as well as that of the adhesive, but also is largely influenced by the thickness of the interface. Therefore, the first set of numerical simulations was performed to determine how long the sensor should be to guarantee always a result deviation from the real value less than 1.5 %. For that purpose, the sensor length was varied between 3 cm and 10 cm, and the bar width was ranged from 2 cm to 15 cm.

The results are graphically shown in Figure 6.9(a), in which the deviation was taken as the ratio of the strain difference between the sensor and the steel over the applied steel strain, being the sensor strain the average value in the steady region. Two conclusions can be drawn from the data. The first is that as the bar width and sensor holder length increase the deviation diminishes, and the second is that only when the sensor length reaches 10 cm the deviation is equal or less than 1.5 % for bars wider than 7 cm. Consequently, the strain sensors applied on Luiz I Bridge have been manufactured with a length of 100 mm. The results obtained in this analysis were confirmed in a load test carried out at the laboratory, which is reported in section 6.8.1. It is worth noting that analogous conclusions would be obtained if the analyses were performed by varying the bar thickness instead of its width.

As the strain sensor holder is made of a material whose stiffness is of the same order of magnitude as that of the host material, some intrusion was to be expected, which could lead to large deviations between the measured and actual strains. In order to assess the intrusion level introduced by the strain sensor on the instrumented element, a parametric study was carried out, in which the geometric parameters at stake were the thickness and the width of the bar.

Figure 6.9(b) shows a maximum deviation on the gauged strain of about 10 %, which can be considered not acceptable. However, only when the bar is less than 5 cm wide and

10 mm thick the deviation becomes higher than 1.5 %. Since all elements to be instrumented on the bridge were wider and thicker than the previous limits, these results were classified as satisfactory. Furthermore, for the usual applications we can conclude that deviations are only relevant when very small bar cross-sections are to be monitored. It is also clear from the results that the most important geometric parameter is the steel bar thickness, since its increment decreases the deviation more significantly.

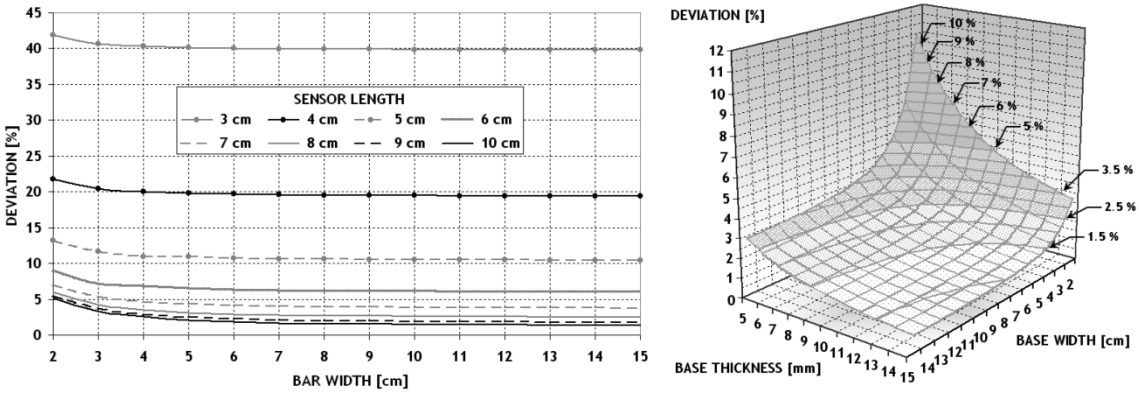

(a) (b)

Figure 6.9 - Results from the numerical analyses: (a) strain deviation *versus* sensor length and bar width; (b) strain deviation *versus* bar thickness and bar width.

6.8. Laboratory tests

6.8.1. Static behavior

An experiment with a simply supported "H" steel beam was performed to gauge the strain sensors response under static deformation. A pair of concentrated forces 50 cm apart was applied to the beam to carry out a symmetric four point bending test. The beam was incrementally loaded at a low constant rate up to the maximum value $F_{max} = 60$ kN, and then completely unloaded at an equal rate.

The strain sensors were installed on the lower and upper faces of the beam, between the two loading points. Transversely, all the strain sensors were placed over the beam's mid alignment as depicted in Figure 6.10. Four sensors were attached to the beam, two foil electric strain gages, termed as ESG1 and ESG2, and two fiber optic strain sensors, referred to as FOS1 and FOS2 (type I). As initially proposed by the manufacturer, these two fiber optic sensors only had 4 cm in length. The collected results are shown in Figure 6.10(a).

On both compressive and tensile fiber optic sensors the readings exhibited a deviation from the strains sensed by the foil gages, in average of 20 %, during the entire experiment. The test was repeated using 10 cm long fiber optic sensors replacing the previous ones, now termed as FOS3 and FOS4 (type II). This time, the readings between all sensors in the same face of the beam were almost coincident, never exceeding a difference of 1.5 % (see Figure 6.10(b)), which was also the estimate provided by the preliminary numerical study. The same test was performed with the sensors fully protected and no significant difference in the measurement was found. Consequently, this type of sensors was the one adopted for site installation. It is worth mentioning the fact that the maximum strain on both tests almost reached the yielding point, as the yielding stress and Young's modulus of the tested steel were respectively 235 MPa and 210 GPa.

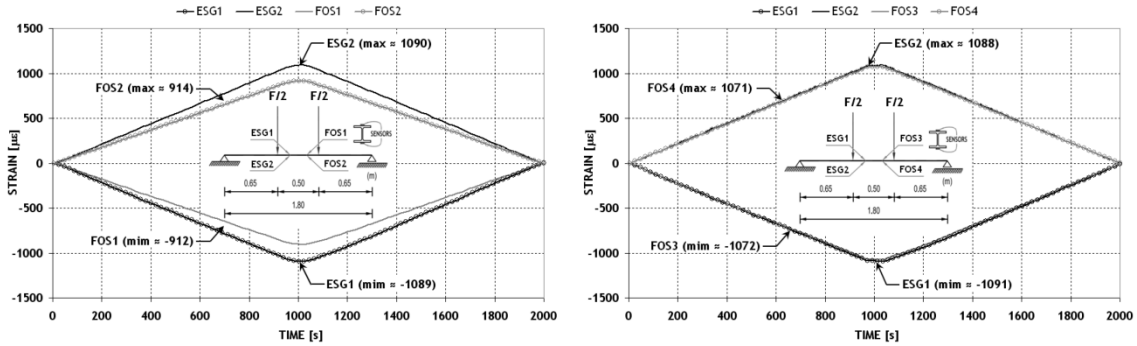

(a) (b)

Figure 6.10 - Static response evaluation of the fiber optic sensors: (a) FOS of type I; (b) FOS of type II.

6.8.2. Fatigue testing

Following the static tests, a tension-to-tension mechanical fatigue experiment was conducted on the instrumented beam, in order to characterize the sensor's response to cyclic loading. The maximum load applied was approximately 25 % of the yielding tensile load of the beam. The ratio between the minimum and maximum load was set as 0.1 and the loading frequency as 20 cycles per minute. The strain range generated on the gauged points was approximately 225 με, which was higher than the maximum strain amplitude expected in the monitored points of the bridge in its new operation stage. Figure 6.11(a) depicts the strain time series provided by the sensor FOS4 duly thermally compensated.

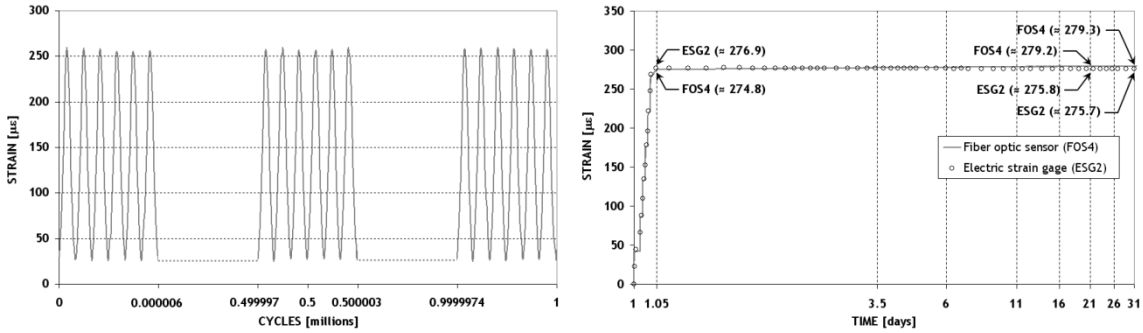

(a) (b)

Figure 6.11 - (a) Time series of the strain gauged by FOS4 during the cyclic load test; (b) results from the creep test.

As can be seen, after 1 million cycles no degradation occurred in the sensor's response. Therefore, it was concluded that the fiber optic strain sensor and its installation procedure were appropriate to be adopted in the monitoring project.

6.8.3. Creep evaluation

An experiment was carried out to appraise the performance of the fiber optic sensor and epoxy adhesive under long-term stresses. The test was conducted on the same beam previously presented using an identical loading setup. The load was applied by steps up to 15 kN, which was held for 30 days. The maximum strain produced by the loading on the beam's flanges at the constant bending region was about 275 με. This level of strain corresponds to the maximum permanent deformation that is expected for the sensors at the bridge after their installation. Figure 6.11(b) plots the results provided by the sensors attached to the tensile flange duly thermally compensated, adopting a logarithmic time axis. After the loading was completed, the strain captured by the fiber optic sensor slightly increased throughout the experiment, reaching at the end a value 1.6 % higher than at the beginning. Given that the readings collected by the foil strain gage remain almost constant, the increment of the strain detected by the fiber optic sensor can only be attributed to some moisture sensitivity of the sensor holder and/or of the adhesive, which are not to be expected when the protection is implemented. Nevertheless, the readings have stabilized after 20 days and its effect can be regarded as insignificant.

6.8.4. Assessment of temperature effects

To appraise the performance of the fiber optic strain sensors under thermal variations, as well as the efficiency of their protection, two experiments were conducted. The first test

was performed by applying 10 daily cycles of temperature to a steel specimen extracted from Luiz I Bridge, in which temperature varied from 0 ºC to 55 ºC. The second test consisted on one single temperature cycle ranging between 30 ºC and 60 ºC. Both tests were carried out on a climatic chamber equipped with a temperature sensor. The tested specimen was 685 mm long, 70 mm wide and 7 mm thick, on which a fiber optic strain sensor and a resistive thermometer were applied. Both sensors were shielded with the protection system described in section 6.6.1, and thus temperature in the steel in the surroundings of the sensor could be captured.

To fully understand the collected strain data it is necessary to have in mind the following: strain readings presented in Figure 6.12 were directly translated from wavelength shifts without considering the thermal effect as expressed by (6.2). Therefore, they do not represent the actual strain experienced by the steel, since they also hold the thermal response of the grating. The first graph exhibits the steel temperature and the experimental strain collected in the first test. As it can be seen there is an excellent correlation between those two quantities and results prove the repeatability of the sensors behavior. Moreover, the theoretical strain computed from the steel temperature matches the experimental strain. This theoretical strain was calculated using (6.2), taking the mechanical strain, $\Delta\lambda_\varepsilon$, and pressure, Δp, as zero and dividing the obtained wavelength shift $\Delta\lambda_B$ by $(P_\varepsilon \cdot \lambda_B)$, i.e. assuming that the wavelength shift is due to stress induced strain and not to temperature. The optical constants were supplied by the manufacturer and the thermal expansion coefficient of the steel was taken as 10^{-5}ºC^{-1}.

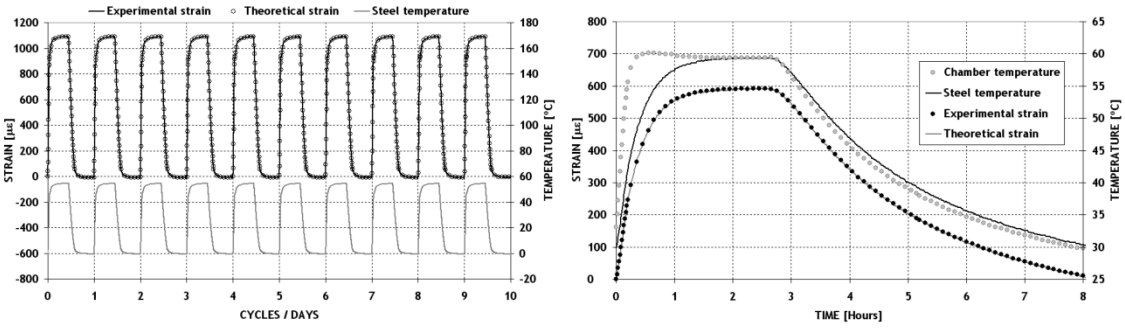

(a) (b)

Figure 6.12 - (a) Experimental and theoretical strains *versus* steel temperature for 12 cycles; (b) results from the one cycle temperature test.

The efficiency of the thermal shielding provided by the protection of the sensor can be appraised by looking at Figure 6.12(b). Temperature in the chamber increases rapidly at the beginning of the experiment whereas the steel temperature has a more smooth increase. Both temperatures reach the same value after 2 hours and have a similar

descending trajectory. Once again, the theoretical strains determined from the steel temperature as previously described overlap the experimental strains. Therefore, if the temperature in the shielded steel is gauged, thermal compensation can be accurately accomplished for the readings collected by the strain sensor so that stress induced strains can be obtained.

6.8.5. Evaluation of humidity effects

Given that the strain sensors are made of composite material prone to adsorb moisture from the air, which in turn may strain the grating by swelling, an experiment was conducted on the same specimen tested under temperature cycles to assess the effect of moisture on the readings provided by the strain sensors. Ten humidity cycles were applied by varying the relative humidity between 35 % and 85 % at constant temperature. Data collected by the strain sensor during the tests are plotted in Figure 6.13. A fair correspondence between the relative humidity and the strain measurements can be observed, as well as the repeatability of the results throughout the test. More important is the fact that the maximum increase of the strains was always below 4 με, which can be regarded as an excellent result. Therefore, it was concluded that the developed protection had the ability to control the adverse effects of moisture over the strain sensor.

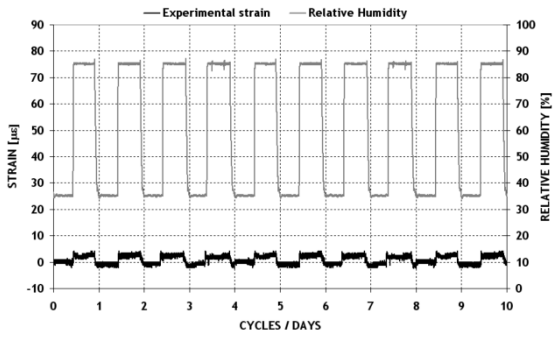

Figure 6.13 - Evolution of the readings acquired by the strain sensor during the relative humidity cycles.

6.9. Data collection system

6.9.1. Data Acquisition Sub-System (DASS)

The DASS holds a Si425-200 swept laser interrogator marketed by Micron Optics, Inc., a LT3000 1 x 15 fiber optic switch for single mode fibers supplied by Lightech FiberOptics, Inc., a desktop computer (PC) and a modem. These equipments are located at the LOS.

The Si425-200 is a robust, high-power, low-noise laser source, with one optical channel to be interrogated, capable of scanning FBGs with Bragg wavelengths within the operating range of 1520-1570 nm. The optical sensing interrogator uses an Ethernet port to network to the desktop computer for data analysis using on-board controls and LabView™ remote utility. For each scanned optical branch it can display the relative power of each sensor, exhibit the wavelength time series of any sensor on real-time, simultaneously present the readings of all sensors in a tabular form, and evaluate the signal frequency content for each sensor through a fast Fourier transform (FFT).

The adopted optical switch consists of a controller and optical modules of good repeatability, high isolation, small insertion loss and low back reflection. It enables the selection of a channel among 15 and is equipped with a LCD display and a keypad for manual control, both located on the front panel. The communication between the optical switch computer and the desktop is accomplished through a RS232 interface.

The maximum scanning frequencies are 50 Hz when only one optical channel is read and less than 2 Hz per optical channel when the signals of all the 15 optical channels are continuously acquired. The raw data, in wavelength format, is wireless send to a server that integrates the Data Storage/Processing Sub-System (DSPSS), located at the Faculty of Engineering of the University of Porto (FEUP).

Having in mind the targeted objectives for this monitoring project, which were previously presented herein (see section 6.5.1), the acquisition system should have the ability of providing data concerning the monitoring of bridge's response caused by live loads, mainly when the Metro vehicles are crossing the upper deck. Given that these vehicles travel over the bridge with an average speed around 7 m/s, the 2 Hz scanning rate provided by the set Si425-switch for continuous measurement of all sensors can be considered as sufficient. Nevertheless, dynamic observations can be performed if the optical branches are monitored one at a time, since the corresponding scanning frequency reaches 50 Hz.

The monitoring program has 3 different modules, which are:

i. Permanent monitoring of the optical branch that integrates the sensors placed on span 11 (see Figure 6.3), with an acquisition rate of 10 Hz;
ii. Continuous monitoring of all sensors with readings taken at every 5 minutes;
iii. Periodic monitoring of each optical branch with a sampling frequency of 5 Hz at pre-set 5-minute time windows.

The first module acquires data to be available on quasi real-time at a website portal designed for the bridge owner. The second module collects the measurements that are used for long-term assessment of the structure behavior, whereas the third module intends to collect readings during the Metro light train crossings so that long-term effects of live loads can be appraised.

6.9.2. Data Storage/Processing Sub-System (DSPSS)

One server located at FEUP, about 10 km from Luiz I Bridge, processes and manages the collected data. The raw readings acquired by the DASS according to the second and third monitoring modules are stored in weekly and monthly files, respectively, and then transferred to the DSPSS server through wireless connection.

The DSPSS is responsible for converting the raw data files to strain, temperature and displacement data. Statistical information is computed from the translated files, such as minimum, maximum and average values of the quantity at stake.

In order to retrieve the stress induced strains from the complete strain records, thermal compensation is made by using one of the 10 temperature records that is more suitable for each strain sensor. Therefore, it is possible to assess the long-term effects of live and environmental loads on the bridge's global behavior.

The strain, temperature and displacement readings from all 136 sensors are provided to the bridge owner through a website portal, specially developed for this monitoring project. It has the ability to generate regular observation reports and to send alerts by e-mail to the officials whenever the readings exceed the surveillance or the alert thresholds.

6.10. Monitoring results

In this section some results concerning the initial observation period of the bridge's performance, acquired by the monitoring system previously described, are presented. The strain data were collected by a sensor installed in the downstream lower chord of the upper deck in a section positioned at the middle of span 2, whereas the ambient temperature was measured by a temperature sensor located in the vicinity. The region of the bridge under analysis is identified by a rectangular dashed box in Figure 6.3, and the cross-section of the instrumented bar with the sensors is depicted in the inset of Figure 6.14(a).

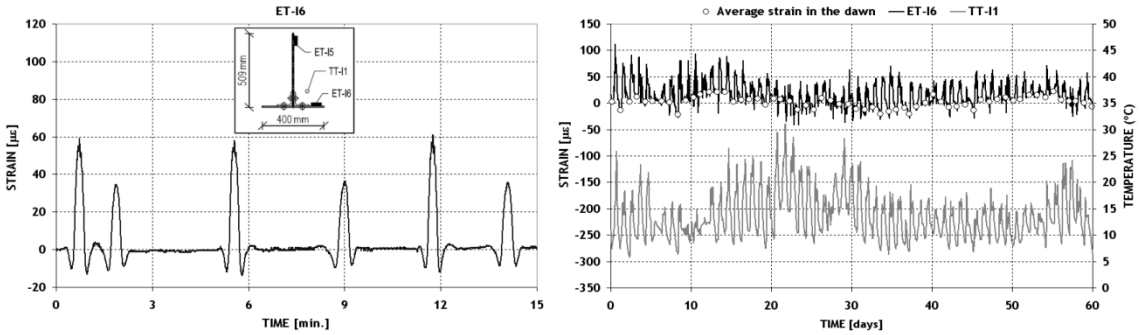

(a) (b)

Figure 6.14 - (a) 15-minutes strain record acquired by sensor ET-I6; (b) Results of sensors ET-I6 and TT-I1 during the first two months of observation.

The first plot of Figure 6.14 presents a typical strain record for a 15-minutes window, acquired under normal traffic conditions at an approximately constant temperature with a scanning rate of 5 Hz, which is suited for capturing the strain variations of the bridge caused by the slow crossings of the metro vehicles (speed lower than 25 km/h), since the dynamic effects become negligible. Each of the six positive peaks of the response has two negative lobes, the positive peak corresponds to the maximum effect generated by the metro vehicle when it crosses span 2 and the negative lobes are the result of its passage on the neighboring spans. Although these vehicles are constituted by 2 units that comprise 8 bogies with 2 axles, the deformation of the bar is mainly governed by the global effect of the metro travelling over the upper deck as result of the bending moment, being the contribution of the rotations at the bar ends small or even negligible. Additionally, a careful inspection of this plot allows the division of the positive peaks into 2 groups, one holding the peaks with maximum values close to 60 με, in correspondence with the crossings heading south that take place in the track closest to the girder where the bar is located, and the other group including the peaks with maximum strains around 35 με produced by the vehicles travelling in the opposite direction.

Figure 6.14(b) shows the results acquired by the strain sensor ET-I6 and the temperature sensor TT-I1 during the first two months of monitoring with a sampling frequency of 24 readings per day. It is perfectly clear the existence of daily cycles in both measured quantities. The strain data shown in the plot was obtained from the raw wavelength shift of the optical signal by subtracting the thermal component that affects directly the strain sensor response, assuming the temperature measured by TT-I1 as the one acting on the strain sensor. This assumption is acceptable for the night periods, and when the temperature is stabilized or varies slowly, but it can deviate considerably during the daytime periods due to solar radiation. Consequently, the 2-month strain time series displays daily peaks at the hottest instants. During this two months period, no trend has been detected in the strain measurements which could be ascribed to the creep of the strain sensor and/or of the bonding adhesive.

6.11. Summary and conclusions

In this chapter a fiber optic based monitoring system installed in the Luiz I Bridge was presented. The gentleness of some operations undertaken during its rehabilitation, the appraisal of the strengthening solutions performance and its significance as part of the world heritage, made the structural monitoring of its behavior during the new service stage mandatory. The monitoring system was designed to allow a direct comparison of the results collected in the load test conducted after the completion of the construction works with the measurements taken before the bridge rehabilitation to support its design.

The fiber optic sensing technology of the monitoring system relies on FBG sensors for measuring the joints and bearing supports displacements, the temperature of the steel and air, as well as the relevant strains in elements of the arch, upper deck, piers and suspension ties. More than 130 sensors were deployed on the bridge.

The fiber optic network has a tree configuration with a main optical cable branching into each of the optical fibers leads serially connecting a maximum of 10 sensors. Its design provided a high level of interchangeability of the gratings position in the light path of each optical branch, in order to maximize the number of sensors capable of being interrogated if any fiber breakage takes place. The WDM technique was adopted to identify and interrogate the sensors in each fiber lead, whereas the SDM method was implemented through an optical switch to distinguish sensors from different optical branches.

To grant suitable longevity to the monitoring system, proper methodologies and materials were adopted to accomplish the installation and protection of its several components, namely the sensors, optical cable, fibers, connectors and splice enclosures. The implemented solutions had also to take into account the steel properties and the visual impact on the structure as part of the world's heritage.

Given that strain sensors were specifically designed for the project, numerical analyses were carried out to optimize the CFRP holder dimensions and evaluate the readings deviation. Furthermore, since these sensors are fragile elements prone to failure during their installation or by deficient shielding, a complete experimental characterization of the sensors behavior and assessment of the protection efficiency were carried out. Instantaneous and time-dependant response of the sensors, as well as of the adhesives, was evaluated through static tests, whereas their fatigue performance was characterized by a cyclic loading experiment. All the results met the requirements set for the project. The suitability of the protection implemented for the sensors was tested under temperature and humidity cycles. Thermal compensation of the strain readings could be effectively accomplished and no significant influence of the moisture was detected in the tests.

The DASS integrating a swept laser interrogator and an optical switch allows the collection of raw data from all sensors with a scanning frequency of 2 Hz, suitable to assess the structure's response due to the metro slow crossings along the upper deck. Dynamic readings can be accomplished at a sampling rate of 50 Hz, for a single optical branch, by changing the acquisition program from the continuous monitoring module. The DSPSS translates the raw data of weekly and monthly files acquired by DASS into the physical quantities to be measured, as well as computes relevant statistical information from them. In the translating process thermal compensation is made so that long-term effects of loads on the structure are assessed. The monitoring data is made available to the officials through a website, which has also the ability to send safety alerts and produce automatic reports.

At last, it is worth noting the fact that at the completion of its installation and during the first year of service the monitoring system has efficiently performed the tasks for which it was designed, and no problems have occurred that could impede the regular interrogation of all sensors.

Chapter 7

Static and safety analyses of the Luiz I Bridge

7.1. Synopsis

The rehabilitation projects of old steel bridges are characterized by unique features that stand out from other areas of activity in the field of structural engineering. On one hand, these projects call for the participation of highly skilled and trained technicians with a sound knowledge on old materials and construction techniques, characteristic deterioration mechanisms and suitable inspection and diagnostic methods. On the other hand, very often the information concerning the bridge construction or any intervention carried out during its life is limited, or even lost. Additionally, and perhaps most important, the intervention in an old structure whose state of stress is not perfectly known, as well as its response to external loadings, may lead to severe problems during the rehabilitation works, and even result on counterproductive changes in the structural performance.

Structural identification emerges as a valuable process, through which, experimental data is collected in the field or at the laboratory aiming at the development of reliable numerical models for predicting the structural behavior. Subsequently, these models can be used to evaluate more accurately the bridge safety before, during and after the execution of the rehabilitation works. Furthermore, the appraisal and validation of strengthening solutions implemented in these projects is only made possible by adopting suitable strategies of structural identification.

In this chapter the experimental and numerical assessment of a centenary steel arch bridge is presented. The structure has been recently subjected to a rehabilitation and

strengthening process aiming at its adaptation to a new loading environment. The field tests conducted before and after the construction works are described, as well as the underlying guidelines in their conception and execution. The numerical models created to replicate the bridge response in its different conditions are detailed. The most significant changes produced in the structural behavior are outlined and discussed, as well as its particular aspects. Major findings regarding the effectiveness and/or efficiency of the strengthening applied to some critical elements are highlighted and duly analyzed, which constitute valuable information for future rehabilitation projects. Additionally, based on the updated numerical model for the new service conditions, a safety assessment of the bridge is performed according to the ultimate limit state regarding normal stresses, and the maximum live load safely carried by the upper deck is estimated.

7.2. Introduction

Structural identification stands as an integrated methodology for the condition and structural safety assessment of old bridges. It comprehends two main groups of techniques, commonly designated as experimental and analytical arts, the first devoted to nondestructive and destructive field testing and the second to the development, calibration and/or update of numerical models. Both supply the necessary data to assist the decision-making process concerning the posting, repair, rehabilitation, retrofit, strengthening, upgrade and decommissioning of old steel bridges (Aktan *et al.*, 1996).

Field tests are usually carried out before any action is undertaken on the bridges in order to appraise its actual behavior, namely to determine the real distribution of the internal forces among the structural components, as well as to accurately estimate the load-carrying capacity, which is often found to be clearly larger than that predicted from preliminary analyses (Saraf and Nowak, 1998). At the same time, the experimental assessment after the completion of the construction works plays an equally crucial role, since it constitutes the only reliable method to evaluate the effectiveness and/or efficiency of the implemented strategy, and, when is the case, to decide the corrective measures to be implemented (Allen and Rens, 2004).

With regard to the modeling of old steel bridges, the physical completeness constitutes a major issue in the selection of the approach to adopt. In order to reach the established targets it has always to balance the complexity required for its development with the

quality of the expected results. Furthermore, it must take into consideration the monitored quantities and the location of the instrumented points and sections.

Some examples of rehabilitation and strengthening projects implemented on old metallic bridges are reported in technical literature. One of the most famous rehabilitation works was performed on the Brooklyn Bridge (Figure 7.1(a)), the oldest of New York City's East River bridges, opened to traffic in 1883 (Serzan, 1995). The work was completed in 1991, and essentially comprised the replacement of wire rope, solid rod suspenders, cable posts, stays and main cable wire wrapping, the adjustment of suspenders and the cleaning and repainting of the entire main bridge superstructure. In this project the critical aspects were the selection of the best suited rehabilitation strategy and the definition of the construction works to execute.

Nascé (1993) has presented the restoration study of an iron truss arch bridge built in 1889 over the Adda River, named as Paderno Bridge, whose trussed box girder supported over the arch carries both a road and a railway (Figure 7.1(b)). The main problems were related to its state of preservation and significant deficiencies in result of shortcomings of the original project. Several criteria were adopted for the restoration project, which led to the standardization of the residual bearing capacity of the elements at a level acceptable for service purposes. Firstly, given the bridge had been classified as a monument to be preserved, the appearance of the structure could not be altered through extensive strengthening, replacement of a large amount of its components or substitution of damaged rivets by bolts. Secondly, the restoration works would have to be compatible with short service interruptions, and should take into account the small budget available.

(a) (b)

Figure 7.1 - Steel and iron bridges that underwent rehabilitation works (I): (a) Brooklyn Bridge in New York City, USA (Serzan, 1995); (b) Paderno Bridge in Italy (Nascé, 1993).

De Voy and Williams (2007) reported the strengthening of a cast iron arched bridge supporting a non-structural concrete deck resting on iron beams (Figure 7.2(a)). The structure located in Coalport, United Kingdom, was originally constructed in 1800 with a

timber deck, carrying a single traffic lane only. Given that restrictions to the traffic were frequently violated in what concerns the type of vehicle, maximum load and number of vehicles on the deck, the bridge owners decided to strengthen it. The implemented scheme resulted in a discreet solution that permitted to increase the load capacity and to remove the one vehicle at a time restriction. It comprised two main interventions. Firstly, the replacement of the non-structural deck with a lightweight structural reinforced concrete slab of similar depth, designed to span between the vertical supports so that flexural loading on the beams could be removed. Secondly, the strengthening of the arch ribs by bonding thick steel plates.

Another recent rehabilitation project implemented on a 19th century iron continuous truss bridge was designed by Gonçalves *et al.* (2008) (Figure 7.2(b)). The bridge is constituted by a concrete slab supported on a grid of stringers and crossbeams carried by the girders lower chords, which is a very common structural scheme for many contemporary structures still in operation. The main problems that led to the intervention can be summarized as being: excessive deflection of the spans; deformation of the diagonals out of the girders plane; severe corrosion at several locations widespread throughout the bridge; structural damage of various girders elements; inoperative expansion joints and bearings. The operations were performed on the structure so that safety, serviceability and fatigue limit states could meet the present standards without jeopardizing the heritage and the environment.

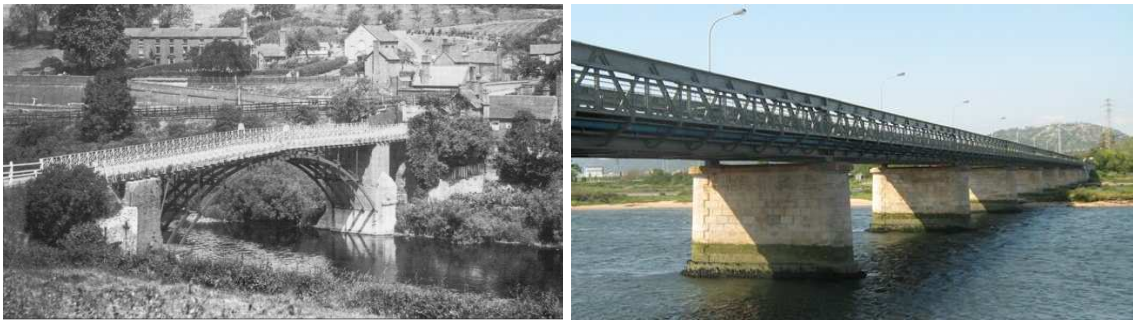

(a) (b)

Figure 7.2 - Steel and iron bridges that underwent rehabilitation works (II): (a) Coalport Bridge in United Kingdom (De Voy and Williams, 2007); (b) Fão Bridge in Portugal (Gonçalves *et al.*, 2008).

The structural identification as a whole, or only for some of its components, has been applied to assess the load-carrying capacity and the condition of several old steel bridges, and subsequently assist the rehabilitation, strengthening and/or upgrade designs whenever necessary.

Boothby and Craig (1997) have conducted a field test on a historic truss bridge in the Chester County, Pennsylvania, with the purpose of obtaining an accurate load rating of the structure (Figure 7.3(a)). Bonded foil resistance strain gages were applied to the steel structure, as well as LVDTs for measuring the deflection. A double-axle dump truck, crawling at a pre-set speed along different paths, turned possible to record the influence lines for the monitored quantities. The results made clear that costly repairs were completely unnecessary and enabled to point out the weak points of the structure.

Three deteriorated simply supported steel girder bridges, built between 1926 and 1931 in Michigan, were subjected to proof load tests by Saraf and Nowak (1998). The main objectives of the experimental campaign were to determine if the structures could safely carry the maximum allowable legal truck traffic load without any restriction and to develop a procedure for proof load testing in old bridges. Two military tanks were used to gradually increase the mid-span moment up to a predetermined proof level, while strain and deflection data were collected.

Farhey *et al.* (2000) have carried out a structural deterioration assessment of a steel truss bridge (Figure 7.3(b)), constructed in 1915, based on a methodology that integrated the microstructural analysis and diagnostic field testing with conventional procedures (measurement of strains and deflections under static or quasi-static loadings). The study stood as a demonstration of the use of emerging and conventional condition-assessment techniques for formulating effective and feasible rehabilitation.

(a) (b)

Figure 7.3 - Tested bridges (I): (a) Chester County Bridge 196, Pennsylvania, USA (Boothby and Craig, 1997); (b) Tindall Bridge in Freemont, Ohio, USA (Farhey *et al.*, 2000).

Spyrakos *et al.* (2004) have presented an experimental and analytical study for the condition assessment and strengthening design of a two-span railway steel truss bridge, constructed around 1890, and still operating. After the validation of a numerical model based on field testing data, the analysis and design calculations for the new types of trains

specified by the bridge owner showed that the main truss system could carry the new loads. Strengthening was only required for the transverse secondary beams.

The analysis of another century railway steel truss bridge, completed in 1896, was accomplished by Ermopoulos and Spyrakos (2006). In situ measurements of deflections and strains were taken for static positions of a six-axle engine truck, which helped to validate a numerical model employed to evaluate the bridge load-carrying capacity. The critical members were identified and strengthening schemes were proposed.

DelGrego *et al.* (2008) have conducted a research to experimentally appraise the structural behavior and influence of aging on a railroad steel truss bridge (Figure 7.4(a)), built in 1905 and located in Connecticut. The study was carried out to evaluate the structural behavior and live load distribution throughout the bridge based on an extensive strain monitoring program. Data was collected under service conditions for different trains over three-week observation period and led to relevant findings regarding: i) actual live load distribution; ii) load sharing between multiple eyebars in individual truss diagonals; iii) distribution of shear through indeterminate panels; iv) relevant out-of-plane bending caused by the rotations at the crossbeams ends; and v) need of using field monitoring to better understand the behavior of older bridges before any design plans for renovation are considered.

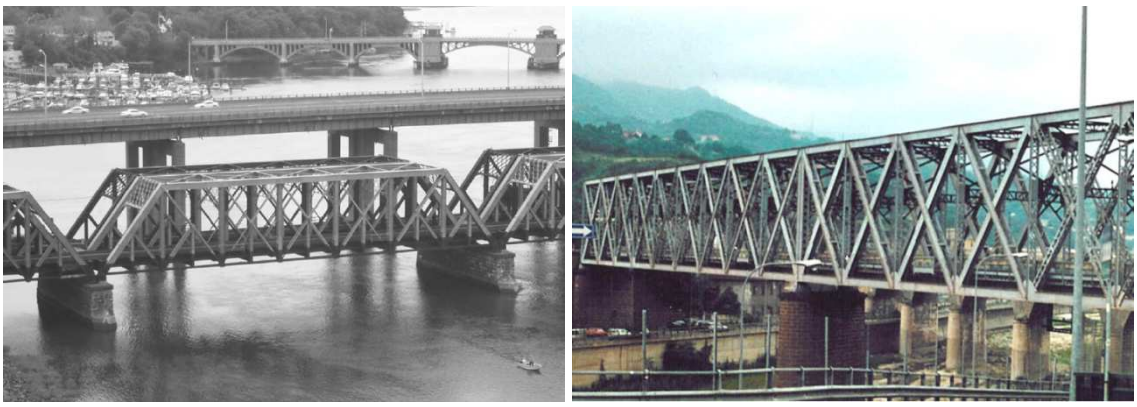

(a) (b)

Figure 7.4 - Tested bridges (II): (a) Railroad truss bridge in Connecticut, USA (DelGrego *et al.*, 2008); (b) Campasso Bridge, Italy (Brencich and Gambarotta, 2009).

Brencich and Gambarotta (2009) have presented the assessment, reclassification and rehabilitation procedures of a highly skewed steel truss railway bridge opened to traffic in 1915 (Figure 7.4(b)). The principal aims of the study were to investigate the feasibility of increasing the crossing loads permitted by the owner and to assess the effects of corrosion in the structure's behavior as well as in its safety levels. The structure's material was

chemically and mechanically characterized through in situ and laboratory tests. Load tests were performed by slow crossing sets of carriages over the bridge to assess its behavior. The detailed analysis and assessment of the structure have successfully limited the retrofitting works required by the reclassification, and concluded that corrosion induced defects did not play a relevant role on the global response of the bridge.

In this chapter the experimental and numerical assessment of the structural behavior of a centenary steel arch double-deck bridge, the Luiz I Bridge, is presented. The structure was recently rehabilitated and strengthened in order to allow the integration of its upper deck in the infrastructure of a light metro network. The main objectives that guided the development of this study were:

i. To collect data from the real structural response in order to validate and/or update the numerical models developed to simulate the bridge behavior in its different conditions;
ii. To support the rehabilitation project regarding the study of alternative solutions and procedures, and ultimately to enable the selection of the best strategy to meet the complexity of the technical, economic and aesthetic issues at stake;
iii. To analyze the changes occurred in the structural behavior due to the rehabilitation and strengthening process undertaken;
iv. To appraise the suitability and performance of the strengthening schemes executed in key elements;
v. To test and validate the fiber optic based monitoring system installed during the construction works, which was designed to measure the bridge response in its new mission;
vi. To set a baseline of the structural behavior for the new service period, so that any changes produced in the short and medium-term can be identified.

In light of the above, the field tests carried out before and after the rehabilitation are reported, focusing on the testing strategies, loading procedures and monitored parameters. The modeling approaches adopted for this study, either to capture the global behavior of the bridge or the local response of the structural elements, are detailed, and the adequacy of the implemented models appraised. In the end, the safety assessment of the bridge for its new rehabilitated condition is performed and the live load-carrying capacity of the upper deck estimated.

7.3. Luiz I Bridge

7.3.1. Historic background

The bridge was designed by the Belgium engineer Théophile Seyrig, a former partner of Gustave Eiffel in previous projects, after an international competition for a double-decked crossing over the Douro river to connect the cities of Porto and Vila Nova de Gaia (see Figure 7.5). Its construction was awarded to the *Société Anonyme de Constructions et des Ateliers de Willebroeck*, and took place between December 1881 and May 1886 (Azeredo and Azeredo, 2002; Seyrig, 1884).

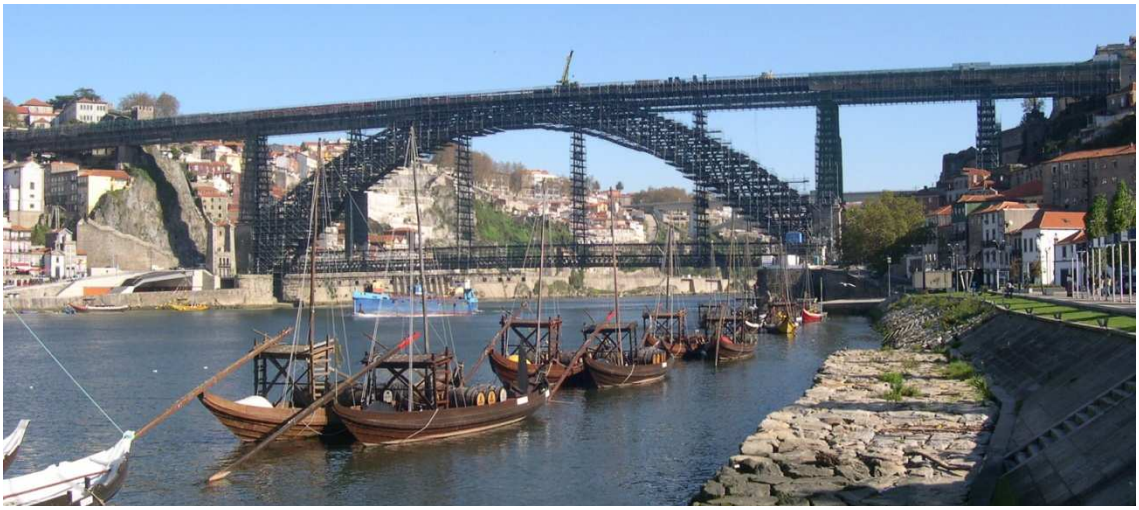

Figure 7.5 – View of Luiz I Bridge during the rehabilitation works.

Before its public opening, proof load tests were conducted on the bridge to check for any unexpected and unsafe behavior. By 1905 the first tram line for the crossing of electric trolley cars was installed on the upper deck, which was duplicated 26 years later when construction works were performed to repair deteriorated parts of the structure and to apply a bituminous layer over the wooden pavement. In 1954 the pavements of both decks were replaced in order to reduce the permanent load. Five years later the trams were substituted by trolleybuses (road vehicles) with the purpose of stopping the electrochemical corrosion induced in the metallic piers. In the early 1990s the traffic of vehicles powered by electricity supplied from overhead lines on the upper deck was ceased and the public transportation ensured with buses propelled by diesel engines. By 1996 the bridge decisively contributed for the world heritage site award from UNESC to the historic center of Porto, and the technical study addressing the viability of using the upper deck for the passage of metro trains is also presented (Coelho *et al.*, 1996). The rehabilitation and strengthening design of the bridge is completed in late 2003, and the

corresponding construction works were initiated in the following year and lasted till the end of 2005.

7.3.2. Deficiencies and inadequacies before the rehabilitation

A large number of elements exhibited evidences of corrosion, mostly localized, even though for some components it was classified as severe and thus requiring a prompt repair. The most deteriorated areas were located in the arch crown, mainly due to the droppings of pigeons and seagulls, and also in the northern spans of the upper deck as a consequence of being more sheltered and surrounded by a moister environment. On the contrary, the condition of the piers and suspension ties was found to be fairly good.

Some plates of the arch bars suffered from buckling problems causing an increase of the stresses in the remaining material of the cross-sections. Moreover, a great number of arch elements under compression did not have the necessary buckling strength, a problem originated by the insufficient knowledge of this phenomenon at the time of the bridge design. Although no signs of fatigue crack propagation had been found in the bridge, the characteristics of the original steel and the new loading conditions made critical the fatigue failure, which ultimately led to the strengthening of the upper deck.

The main evidences of deficiencies and inadequacies on the bridge are shown in Figures 7.6 and 7.7 and listed below:

i. Generalized detachment of the steel coating together with the appearance of corrosion;
ii. Occasional loss of rivets as a result of the corrosion growth;
iii. Existence of large amount of birds droppings in the arch crown;
iv. Poor design of the arch joints promoting the accumulation of dirt and the retention of rain water;
v. Water infiltration and presence of humidity between overlapped plates causing pockets of corrosion and rivets failure;
vi. Buckling of diagonal plates of the box-type bars and of single slender flange plates of the lower chords in the arch;
vii. Significant loss of cross-sectional material in the cantilevers, crossbeams and stringers under the upper deck pavement due to corrosion;
viii. Deterioration coupled with severe damages of the roller bearings at the upper deck abutments restraining the longitudinal displacements;

ix. Serious deficiencies in the steel corbels supporting the expansion joints at the ends of the upper deck as a result of poor design and extreme loading.

(a) (b) (c)

(d) (e) (f)

(g) (h) (i)

Figure 7.6 - Anomalies and deficiencies (I): (a) degradation of the steel coating and rust below the pavement of the upper deck; (b) rupture of a rivet connecting components of an arch diagonal; (c) local buckling of a "X" plate in an arch diagonal; (d) buckling of the lower chord flange at the arch crown (GRID, 2001); (e) droppings of birds over the lower bracing of the upper deck at the arch; (f) poor detail of a typical arch joint; (g) deteriorated roller bearing at the north abutment of the upper deck; (h) pockets of corrosion in the arch support; (i) widespread rust and dust in the upstream roller bearing at the south abutment of the lower deck.

(a) (b) (c)

Figure 7.7 - Anomalies and deficiencies (II): (a) cracks and corrosion in the steel corbel at the north abutment of the upper deck (GRID, 2001); (b) pockets of corrosion between overlapped riveted plates pertaining to the flange of the upper chord at the arch crown (GRID, 2001); (c) accumulation of garbage between the girder and the arch vertical at the north abutment of the lower deck.

7.3.3. Rehabilitation and strengthening works

In order to eliminate the problems previously described and to endow the bridge with the necessary load-carrying capacity to withstand the new loadings, the rehabilitation and strengthening plan established the following works:

i. Complete replacement of the existing floor system of the upper deck (crossbeams, stringers and light-weight concrete pavement) by a new steel grid capable of bearing the loads applied by the metro trains, road emergence vehicles and pedestrians (see Figure 7.8(a) and (b));
ii. Repair of the corroded or damaged elements in the arch and upper deck, particularly gusset plates, "X" plates and angles of the composed elements, and rivets (see Figure 7.8(c));
iii. Generalized strengthening of diagonals in the upper deck girders, suspension ties, side plans of the arch, and in the bracing system of the piers (see Figure 7.8(d) and Figure 7.9(b));
iv. Strengthening of the verticals of the upper deck girders, "legs" of the suspension ties, and of some verticals of the arch (see Figure 7.9(a));
v. Replacement of transverse bracing diagonals in the arch (vertical plans) and in the upper deck (vertical and horizontal plans) (see Figure 7.9(d));
vi. Replacement of the I-beams that constitute the upper deck girders in spans 6 and 7 due to insufficient strength and to enable the direct support of the railway sleepers (see Figure 7.9(e));

vii. Cleaning and lubrication of all original roller bearings and replacement of the supports at the upper deck abutments by disk bearings (see Figure 7.9(f));

viii. Replacement of the expansion joints of the upper deck to make possible an adequate installation of the rails and corresponding expansion devices;

ix. Removal of the old coating through hydroblasting and subsequent 3-layer epoxy painting (see Figure 7.9(g)).

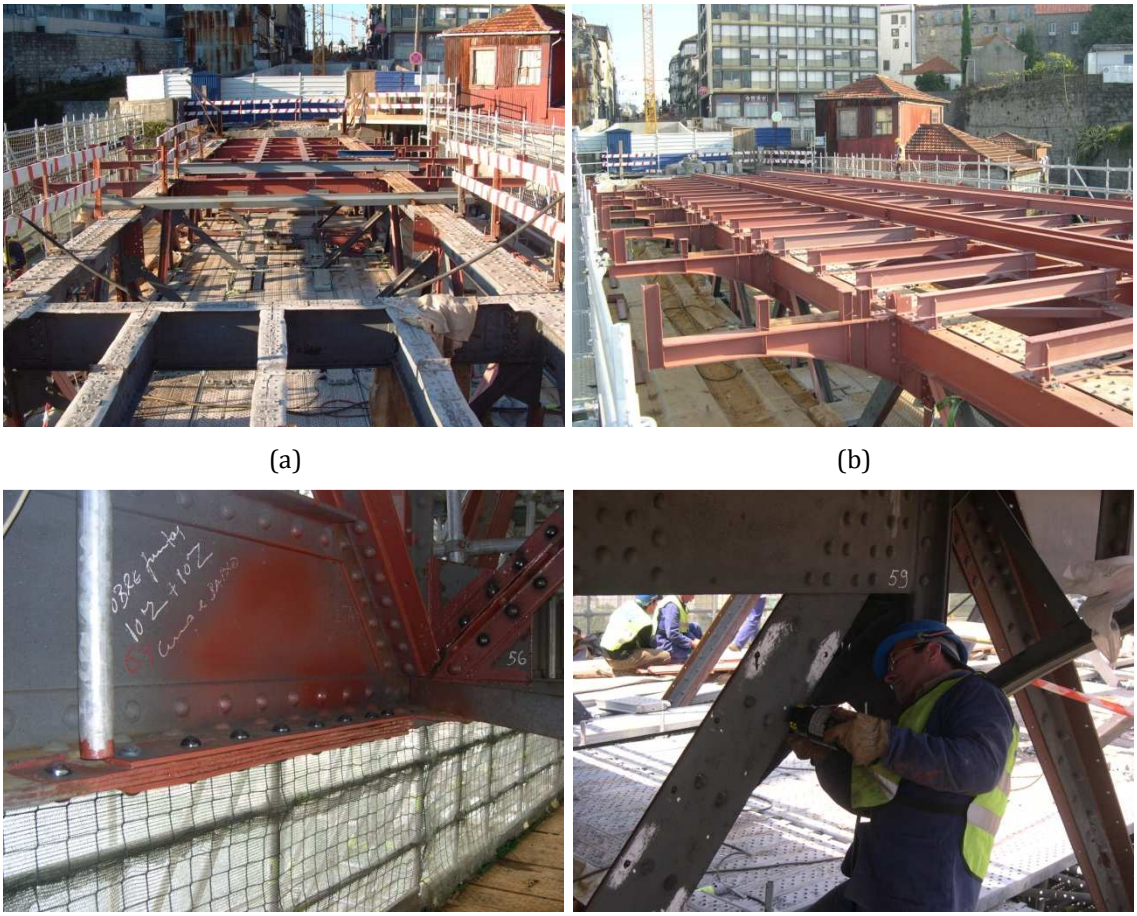

(a) (b)

(c) (d)

Figure 7.8 - Rehabilitation and strengthening of the bridge (I): (a) removal of the old light-weight concrete pavement and supporting grid (cantilevers, crossbeams and stringers); (b) installation of the new floor system; (c) repair of a damaged lower chord flange; (d) drilling of an upper deck diagonal flange to attach the strengthening.

(a) (b) (c)

(d) (e)

(f) (g)

Figure 7.9 - Rehabilitation and strengthening of the bridge (II): (a) strengthening applied to the legs and diagonals of the piers over the arch; (b) arch diagonal after the strengthening and painting; (c) top joint of the upper deck girder after the strengthening (diagonal and vertical) and the erection of the new cantilever; (d) new transverse vertical bracing of the arch; (e) replacement of the main I-girders at the arch crown; (f) cleaning and lubrication of an original roller bearing of the upper deck; (g) hydroblasting of the steel surface.

7.4. Field testing

7.4.1. Objectives

Targeting the main objective of the bridge rehabilitation project, which consisted in making possible the safe crossing of metro vehicles on the upper deck, the first field test, henceforth named as Test 1, was conducted both to study the mechanics of the bridge behavior and to evaluate the best method of analysis for its reliable simulation, particularly regarding the upper deck and the arch. On the other hand, this test sought to provide an improved insight of the strain/stress distribution among the structural elements when the bridge is subjected to external loadings similar to the service conditions. Additionally, the results collected during Test 1 allowed the evaluation of the composite action level between the concrete pavement and the floor system steel grid of the upper deck, and, in turn, to quantify its contribution to the bridge stiffness.

In this way, the measurements taken from the first test assisted the development of numerical models suitable for the study of different rehabilitation and strengthening alternatives. Furthermore, these models enabled the safety assessment of critical structural elements during the intervention, either due to the local transient change of the structural system at the upper deck or to the increase of the permanent load caused by the installation of the scaffolding and part of the construction yard on the bridge.

After the completion of the intervention a second test was carried out, from now on identified as Test 2, with the aim of collecting data to permit an experimental comparison of the bridge response between the two conditions. Therefore, a careful location of the instrumented cross-sections and points and a suitable replication of the loading scenarios were followed. In this way, the changes in the structural behavior would become perfectly perceptible, namely in what concerns the stiffness modification and the magnitude of the strain/stress generated by the same loading level. Consequently, the appraisal of the effectiveness and/or efficiency of the strengthening adopted in the most stressed bridge components became straightforward.

Complementarily, the motivation for conducting the second test was twofold. Firstly, given the installation of a novel fiber optic based monitoring system to monitor the structural behavior under the new operating conditions, the validation of the readings acquired by the sensors under controlled loadings became mandatory. Secondly, the long-term monitoring of the bridge with the purpose of detecting any changes in its structural

properties called for a thorough characterization of the rehabilitated bridge condition to serve as baseline.

7.4.2. Loading procedures

Taking into consideration the objectives of the tests previously outlined, the loadings applied during both tests were kept below the legal maximum service loads. Therefore, the structure was expected to have an elastic behavior, which was completely confirmed by the inexistence of significant residual readings for the monitored quantities after the bridge unloading. In order to enable an easy extraction of the results representative of the bridge response and to reduce data post-processing errors, both tests were conducted during the night to minimize the effect of the temperature variations in the gages stability and in the structural behavior.

Taking into account the fact that before the rehabilitation both decks served as urban road crossings, in Test 1 dump trucks were used to load the bridge only on its upper deck while traffic was closed at the lower one. With regard to Test 2, the monitoring plan integrating the project design had established the use of metro vehicles to replicate the new service actions on the upper deck, and the simultaneous loading of the lower deck with dump trucks to maximize the arch response (GRIDb), 2003). Yet, after a careful analysis of the geometry and the loads associated to the empty metro train, it was concluded that the level of loading applied to the upper deck would be less that that provided by dump trucks in similar loading conditions, both in terms of total and distributed load, as it can be depicted in Figure 7.10 (GRID, 2005). Therefore, and given the fact that the renewed upper deck had been designed to allow the crossing of emergency road vehicles, the use of metro units in the second field test was discarded. Furthermore, it was given privilege to the acquisition of experimental influence lines through the non-simultaneous slow crossing of dump trucks over both decks (a pair at the upper deck and a single unit at the lower deck), rather than loading both decks at the same time with different vehicles. The experimental comparison of the structural behavior, before and after the intervention, also made the utilization of identical vehicles in both field tests inevitable.

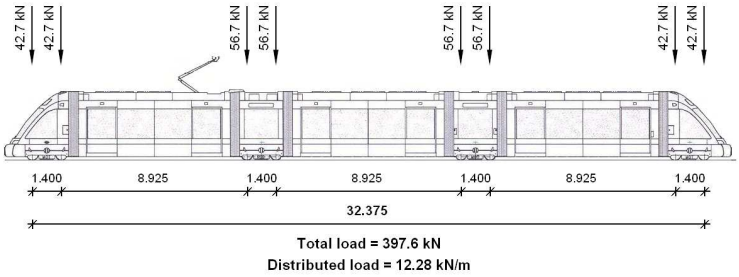

(a)

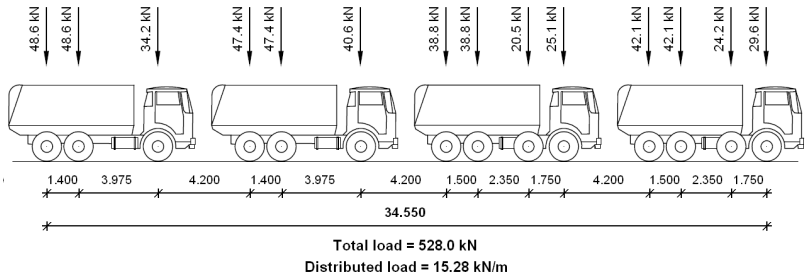

(b)

Figure 7.10 - Vehicles and loads: (a) metro vehicle without passengers; (b) typical line of dump trucks during Test 2.

The vehicles used to load the bridge on both tests were unloaded three and four-axle single-unit dump trucks, with an average gross weight of 128.8 kN in Test 1 and 131.5 kN in Test 2. The distance between the rear tandem axles ranged from 1.35 m to 1.50 m for all vehicles, whereas in the four-axle trucks the front tandem axles were 1.70 m to 1.80 m apart. The distance between the two end axles of the trucks fell within the range of 4.50 - 6.00 m.

In both field tests, keeping always the entire bridge closed to the traffic, two types of loading scenarios were performed, static and quasi-static. Static load cases aimed at maximizing the bridge response for the monitored parameters by performing a small number of static positions of the vehicles. The quasi-static tests were executed to evaluate the regularity of the structural behavior under moving loads, by providing for instance deformed shapes of the upper deck from the displacement measurements. Additionally, these tests also enabled to perceive the level of significance of the load position in the bridge response.

For the static loading scenarios, sets of dump trucks were lined up in single or double formations, positioned at pre-defined locations over the bridge. The lower deck was always loaded by a single line of vehicles, either immobilized at the cross-section center or at the downstream lane. In the upper deck the transversely centered loadings were

conducted with two lines of vehicles and the eccentric loadings applied by placing a single line at the downstream side. Figure 7.11 shows the position of the vehicles in the cross-section of both decks during the static loading scenarios. As regards the quasi-static testing, two side-by-side test trucks traversed the upper deck in one direction with a crawling speed below 5 km/h, whereas in the lower deck the test was conducted using a single unit transversely centered.

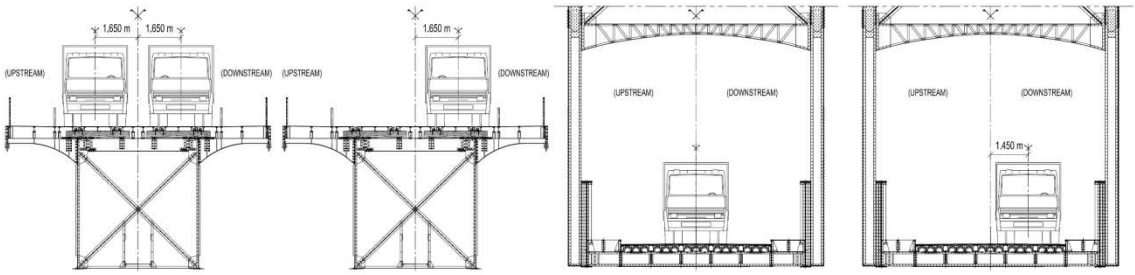

(a) (b) (c) (d)

Figure 7.11 - Transverse positioning of the vehicles in the static tests: (a) load cases 1 to 7; (b) load cases 8 to 11; (c) load cases 12 to 15; (d) load cases 16 to 19.

In Test 1 only the upper deck was loaded. A set of 10 trucks, distributed along two lines (Figure 7.11(a)), was sequentially positioned along the bridge upper deck to accomplish the first five load cases (LC 1 to LC 5), distributing the load over an approximately length of 44.20 m. The load center was consecutively located over pier M1, arch crown, pier P4 and at the middle of spans 12 and 11, respectively. The following two load cases (LC 6 and LC 7) only required two lines of four vehicles, covering a loading length close to 34.55 m, centered in spans 3 and 2 of the same deck, respectively. Then, the eccentric load cases (Figure 7.11(b)) were carried out by replicating three of the first 5 load cases with a single 5-truck line immobilized in the downstream side (LC 8, LC 9 and LC 10). The schematic positioning of the loading lines on the bridge during the static tests is depicted in Figure 7.12. After that, two slow crossings by a pair of vehicles took place over the upper deck, one at a time and in each direction.

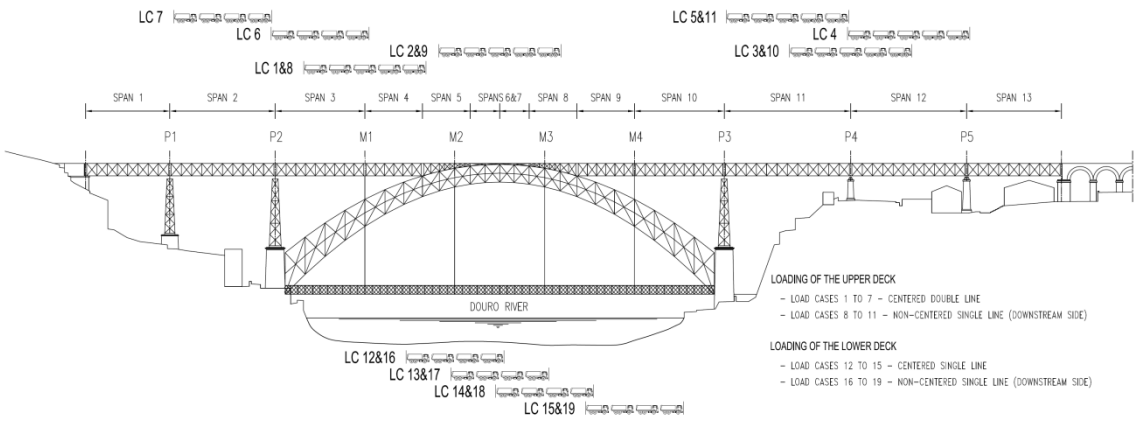

Figure 7.12 - Elevation of the vehicles positioning in the static tests.

With respect to Test 2, the loading procedure on the upper deck was almost identical to the first test, yet complemented by a non-centered 5-truck loading line (Figure 7.11(b)) over span 11 (LC 11). In addition, four static load cases were conducted on the lower deck by a 4-truck single line aligned with the deck centerline (Figure 7.11(c)), whose load center was successively positioned over the suspension tie M2, middle of the central span, and suspension ties M3 and M4 (LC 12 to LC 15). The four eccentric load cases (LC 16 to LC 19) replicated the previous ones by offsetting the vehicles to the downstream lane (Figure 7.11(d)). Additionally, two non-simultaneous slow crossings were carried out at the lower deck with a single truck travelling in each direction.

A 5-key identification code is provided for each loading event, which holds the data about the test, load case, loading scenario, path and loaded deck, with the purpose of enabling the interpretation and analysis of the results in the next sections. Table 7.1 summarizes the information for the labeling of the loading events.

Table 7.1 – Identification codes for loading events.

Code entry	*Description*	*Configuration*
1	Test	1 or 2
2	Load case	1 2 3 4 5 6 7 8 9 10 11[a] 12[a] 13[a] 14[a] 15[a] 16[a] 17[a] 18[a] 19[a] 20 21 22[a] 23[a]
3	Loading scenario	S Q
4	Path	C D C D C
5	Loaded deck	U L U L

Code entry 3 - Static (S), Quasi-static (Q);

Code entry 4 - Centerline (C), Downstream (D);

Code entry 5 - Upper deck (U), Lower deck (L);

[a] Load cases only carried out in Test 2.

The initial number identifies the test (1 or 2), whereas the following number(s) specify the load case (1 to 23). The third entry, either S (static) or Q (quasi-static), allows the recognition of the loading scenario, whereas the fourth indicates the load path as C (centerline) or D (downstream). The fifth entry in the code points to the loaded deck, with the lower and upper decks being identified by the letter L and U, respectively. As an example, 211SDU is the code for the eleventh load case in Test 2, conducted as a static load in the downstream path on the upper deck.

7.4.3. Instrumentation and data collection

In Test 1, conducted before the rehabilitation, three parameters were measured:

i. Strains in the steel surface of 12 bars cross-sections;
ii. Vertical displacements at the arch crown and at the mid-span of the spans 2, 3, 11 and 12;
iii. Ambient temperature.

Regarding Test 2, carried out just after the completion of the construction works and before the reopening of the bridge upper deck to the traffic, the instrumentation consisted in the structural health monitoring system presented in Chapter 6, complemented with sensors for measuring the displacements of the upper deck. Therefore, 47 additional cross-sections of bridge components were instrumented with strain gages, thus reaching a total number of 59 gauged cross-sections. Figures 7.13 and 7.14 show the location of the bridge cross-sections from where strain measurements were taken, as well as the transverse positioning of the strain gages.

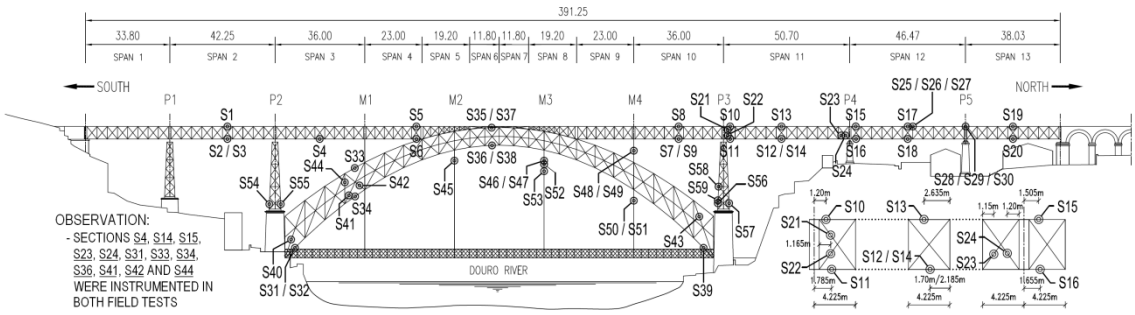

Figure 7.13 - Location and identification of the bridge cross-sections equipped with strain gages.

Furthermore, for this second test, vertical displacements were also measured at the middle of spans 1, 4, 10 and 13, and temperature was collected both from the ambient and the steel surface at 10 different points of the bridge. Horizontal displacements of the upper deck ends at both abutments were also monitored, as well as the relative horizontal displacement between the upper deck and the top of pier P4. The location of the sensors for measuring the displacements is depicted in Figure 7.15. Table 7.2 presents the type and the number of sensors used to measure the parameters in the field tests, as well as their location on the bridge.

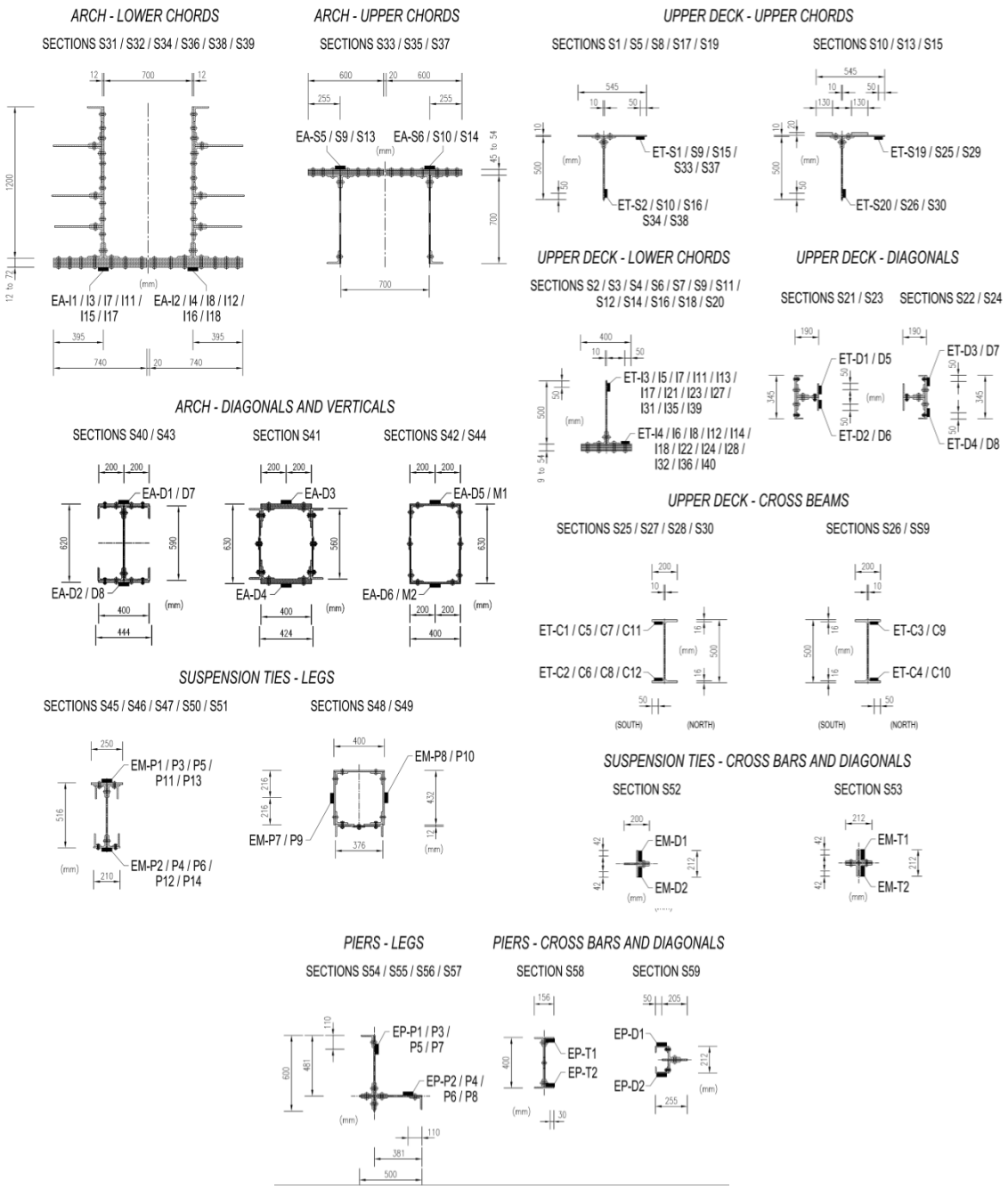

Figure 7.14 - Location of the strain gages at bars cross-sections.

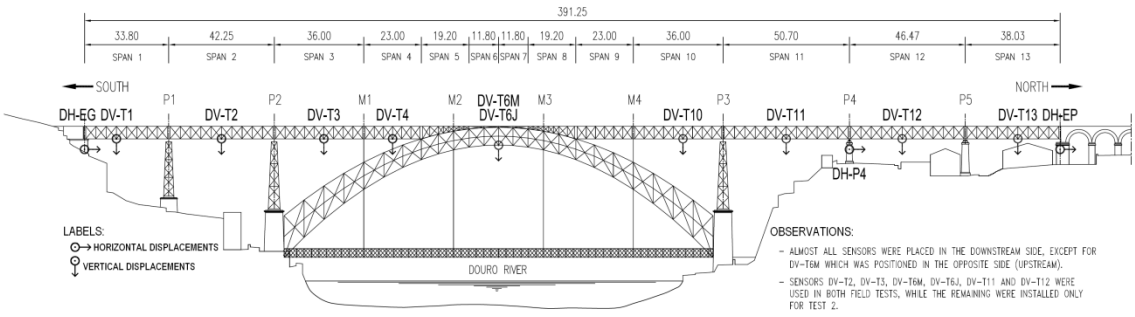

Figure 7.15 - Location of the displacement sensors on the bridge.

Table 7.2 – Instrumentation in the field tests.

Test	*Parameter*		*Location*	*Sensors (No.)*
1	Strains	*A*	Chords, diagonals and verticals	Foil strain gages[a] (8+4+2)
		UD	Chords and diagonals	Foil strain gages[a] (6+4)
	Vertical displacements	*A*	Crown	Liquid leveling system[a] (2)
		UD	Middle of the 2nd, 3rd, 11th and 12th spans (lower chords)	Liquid leveling system[a] (4)
	Ambient temperature	*UD*	Pier P4	RTDs[a] (1)
2	Strains	*A*	Chords, diagonals and verticals	Composite strain sensor[b] (18+8+2)
		UD	Chords, diagonals and crossbeams	Composite strain sensor[b] (40+8+12)
		P	Legs, diagonals and cross bars	Composite strain sensor[b] (12+2+2)
		ST	Legs, diagonals and cross bars	Composite strain sensor[b] (10+2+2)
	Vertical displacements	*A*	Crown	Liquid leveling system[a] (2)
		UD	Middle of the 1st, 2nd, 3rd, 4th, 10th, 11th, 12th and 13th spans (lower chords)	Liquid leveling system[a] (8)
	Horizontal displacements	*UD*	Sliding supports at the deck ends and roller bearings at pier P4	LVDTs[a] (2+1)
	Steel & Ambient Temperature	*A*	Lower and upper chords	Temperature sensor[b] (2[c]/2[d]+1[c]/1[d])
		UD	Lower chords	Temperature sensor[b] (2[c]/2[d])

Labels: A – Arch, UD – Upper deck, P – Piers, ST – Suspension ties; [a] electric; [b] fiber optic; [c] in the steel; [d] of the ambient.

It is noteworthy that, in both tests and for each instrumented bar cross-section, a pair of strain gages was attached, suitably placed about the symmetry axes, if any, so that bending contributions could be canceled or at least detected. Also, taking advantage of the transverse symmetry of the bridge, the monitored points and sections were mostly located in the downstream side, and only at some specific locations the instrumentation was replicated in the opposite side. More importantly, in order to achieve the direct comparison of the bridge response for similar loading conditions, before and after the intervention, the bars cross-sections monitored in Test 1 were also duly instrumented in Test 2. Yet, the positioning of the gages for some sections couldn't be kept from one test to the other, namely with regard to the upper deck bars. For a better interpretation of the results presented in the following sections, namely the comparison of strains in the cross-sections monitored during both tests, Figure 7.16 shows the position of the strain gages, as well as their labels.

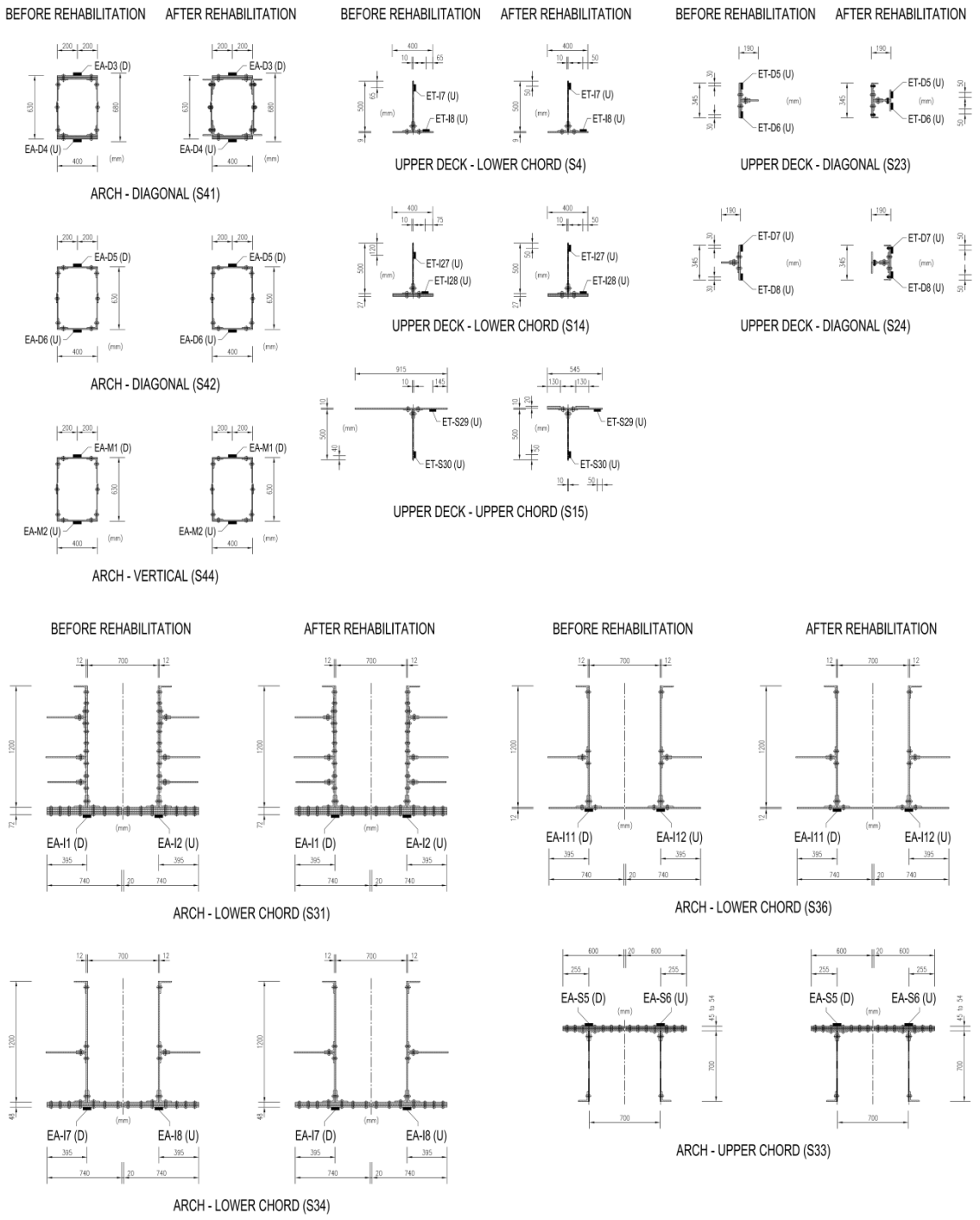

Figure 7.16 - Location of the strain gages at bars cross-sections monitored in both tests.

During both tests the field data was simultaneously collected from all sensors through the utilization of automatic and programmable acquisition systems and recording equipments. In Test 1, two data loggers *DT500* from *dataTaker®* were adopted, housed inside observations stations located in the technical path of the upper deck at piers M1 and P4. The maximum sampling rate achieved in this test was one reading at each 10 seconds. As regards the Test 2, two different systems were used, depending on the nature of the sensors. For the fiber optic sensors the signals acquisition was performed through the

combined action of a *Si425-200* swept laser interrogator, supplied by *Micron Optics, Inc.* and a fiber optic switch, model *LT3000*, manufactured by *LIGHTech Fiberoptics, Inc.*, both located at the COS of the structural health monitoring system (see Chapter 6). The maximum scanning frequency set for the test was 0.2 Hz. In what concerns the electric sensors, the interrogation was accomplished by a system identical to that implemented in the first test, yet with a maximum acquisition rate of 0.25 Hz.

7.5. Finite Element Modeling

For the purpose of this study, two complete 3D finite element (FE) linear elastic models have been developed, one to simulate the bridge condition before the rehabilitation and strengthening works, and the other to simulate the bridge behavior during its new service phase, henceforth referred to as Models A and B, respectively. Figure 7.17 shows a general view of Model B.

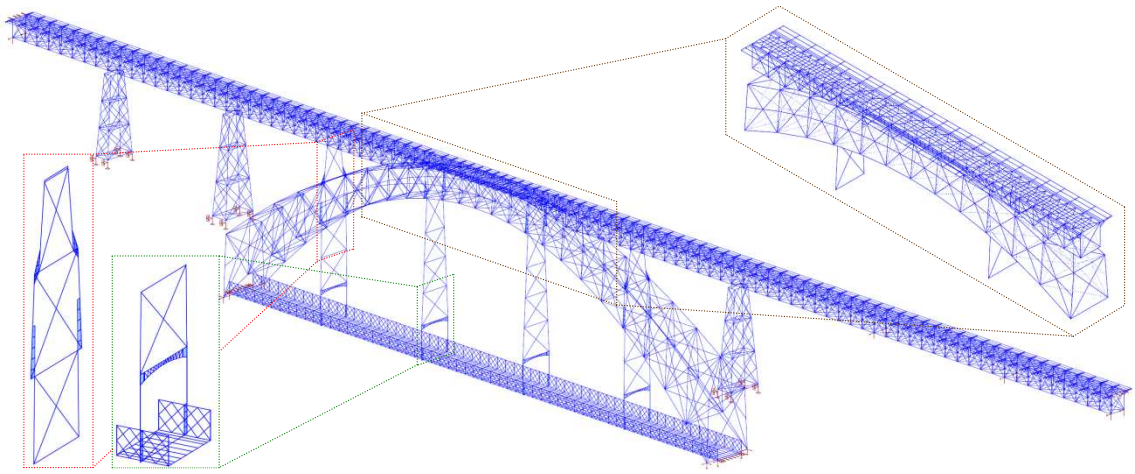

Figure 7.17 – FE model of Luiz I Bridge (Model B).

7.5.1. Finite elements

The models were created on the basis of two-node 3D frame elements, which have three translational degrees of freedom (DOFs) and three rotational DOFs at each node. Consequently, these elements account for one axial force, two shear forces, one torsion moment and two bending moments, in correspondence with the DOFs. Their deformation holds contributions from the shear forces. In some cases, the four-node shell elements have also been adopted in the modeling process, in order to simultaneously simulate the slab and plate actions of a thin 2D structural element.

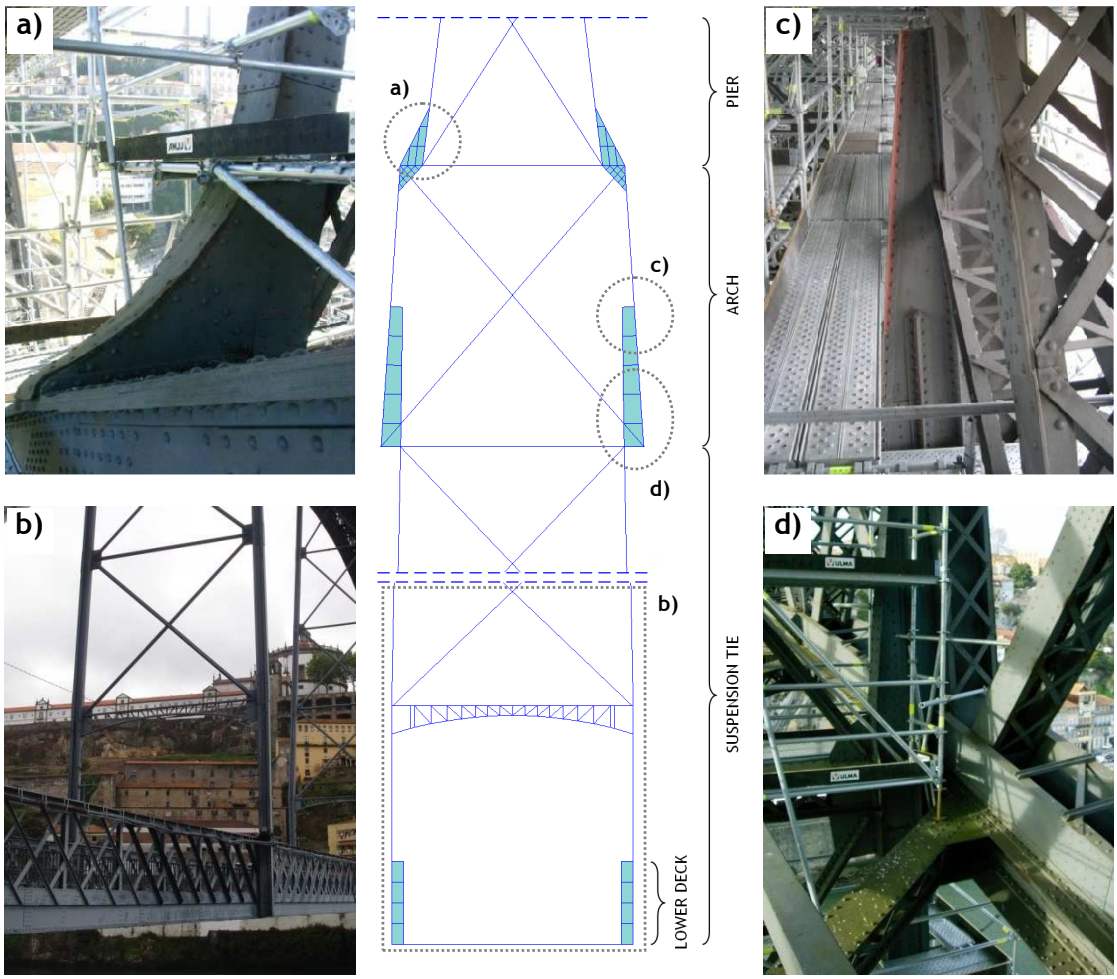

Figure 7.18 - Modeling of the bridge in the alignments M1 and M4: (a) detail of the footing of pier M4; (b) support provided by the suspension tie M4 to the lower deck; (c) connection of the suspension tie M4 to the arch vertical; (d) detail of the arch joint where the suspension tie M1 connects to the arch vertical.

Two different situations required this alternative or complementary approach. The first was related with the connection between some important elements of the structure wherein an improvement in replicating the force transmission mechanisms was needed. This is the case of the connections of the suspension ties to the arch (upper level) and to the lower deck (lower level), and of the footings of piers M1 and M4 over the arch. Figure 7.18 depicts a transverse view of the model in the alignment of the suspension ties M1 and M4.

The second situation was compelled by the significance that shear stresses have for the upper deck I-girders response at the two spans over the arch crown. On one hand the span to height ratio is low (6.4) and on the other the rail loads are directly applied along these elements. For these girders the web was modeled by means of shell elements and the flanges simulated with frame elements. A detail of the upper deck modeling at the arch

crown is shown in Figure 7.19. The statistics of Model B are as follows: 55080 DOFs, 16880 frame FEs and 1670 shell FEs.

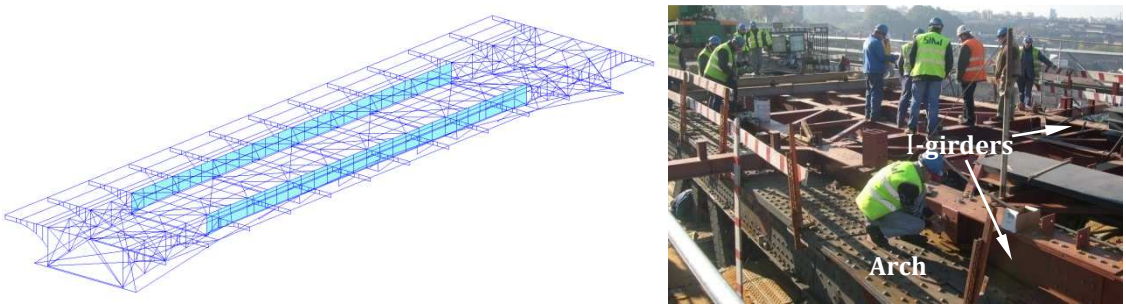

(a) (b)

Figure 7.19 - Modeling of the upper deck at the arch crown: (a) I-girders simulated by shell (web) and frame (flanges) elements; (b) installation of the new upper deck steel structure during the rehabilitation.

7.5.2. Geometry, material and cross-section properties

The geometry of the bridge and cross-section properties of the elements were defined on the basis of the documents produced by the in-depth survey and inspection of the structure, carried out after the viability study and before the rehabilitation and strengthening works (GRID, 2001). Particular attention was paid to the determination of section properties of latticed members, namely the moments of inertia and torsional constant. Therefore, for the diagonals, verticals and bracings of the arch suitable reduction factors were computed according to the procedure proposed by Duan *et al.* (2000) in order to consider the actual section integrity. For an accurate characterization of the original steel, specimens were then taken from several parts of the bridge (arch, piers and upper deck) and mechanical tests made, which included fatigue, tensile strength and impact (Coelho *et al.*, 1996).

Creating a 3D FE model of any structure always requires the adoption of reference lines and axes to support its geometrical representation. However, the discretization of some parts of the structure into several elements leads to a non accurate relative positioning of their gravity center, which in turn may decisively influence the data analysis. In order to eliminate this source of error the structural axes of all elements were adequately moved from the reference geometric axes of the model, an operation herein termed as offsetting. In practical terms, and taking a simply supported beam as an example, if the structural axis is translated from the midline connecting the two supports (geometric axis) any

longitudinal force applied at the supports level produces bending in the beam as a result of the load eccentricity.

Aiming at properly capturing the stiffness contribution provided by the light-weight concrete pavement on both decks (Model A) or only on the lower deck (Model B), the stringers, crossbeams and chords supporting it were modeled as steel-concrete composite bars. The mechanical properties were computed from equivalent elements made of a single material (weighed properties). Figure 7.20 shows the cross-sections of the decks in both models.

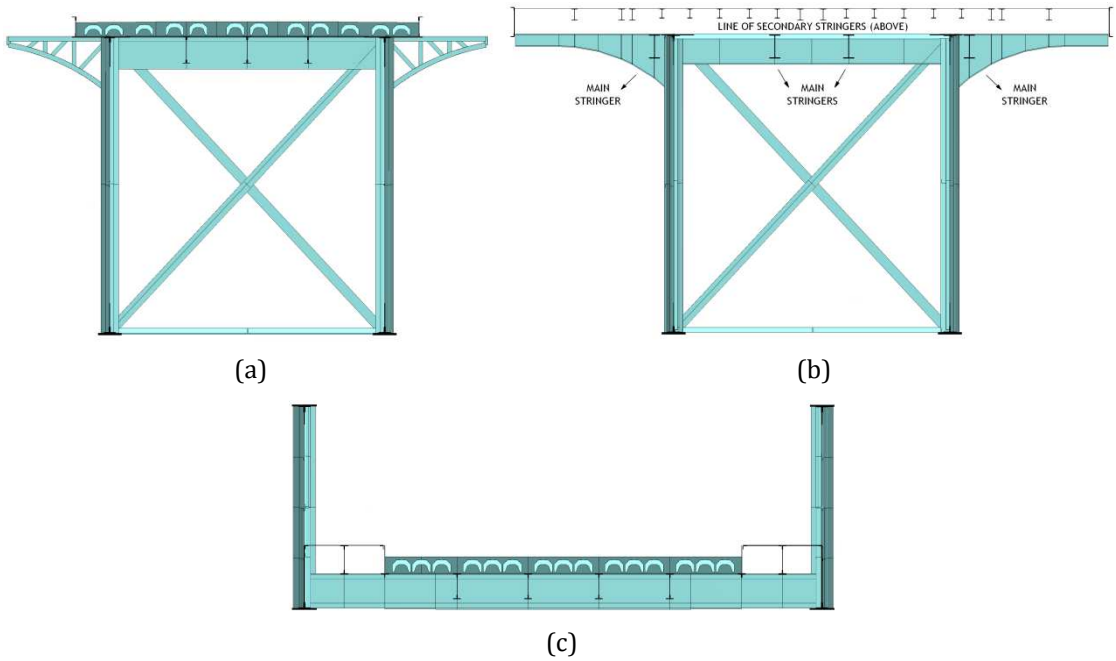

Figure 7.20 - Modeling of the decks cross-sections with the bars shown as extruded profiles: (a) upper deck before the rehabilitation; (b) upper deck after the rehabilitation; (c) lower deck.

Regarding the modeling of the strengthened elements of the bridge in the post-rehabilitation condition, a similar difficulty emerges as the original and new-added steels do not present the same elastic parameters. Therefore, following a similar procedure the mechanical properties were computed from equivalent elements made of a single material. The Young's moduli (E) and Poisson's ratios (ν) of the materials adopted in the models are as follows:

i. Original steel, $E_{os} = 192.7$ GPa and $\nu_{os} = 0.25$;
ii. New-added steel, $E_{ns} = 210$ GPa and $\nu_{ns} = 0.30$;
iii. Original concrete, $E_{oc} = 32$ GPa and $\nu_{oc} = 0.166$.

Furthermore, with respect to the new steel grid on the upper deck that carries the loads from pedestrians and emergence road vehicles, although it is considered to be a secondary

structural component, its stiffness was taken into account by including the corresponding stringers as longitudinal bars positioned at the upper level of the deck (see Figure 7.20(b)).

7.5.3. Boundary conditions

The supports of both decks at the abutments only prevent vertical and transverse displacements. Taking into account the high stiffness of the masonry piers P4 and P5 (see Figure 7.12) and the characteristics of the steel bearings that transfer the loads from the upper deck, the lower nodes of the girders in the supports alignments have the transverse and vertical movements completely restricted. The connection between the upper deck and the metallic piers founded in the river banks is made by apparatus similar to those of the masonry piers. Therefore, the devices were modeled by defining separately coincident nodes in the bottom chords of the upper deck girders and in the top of small rigid vertical bars fixed to the top of the piers. Using master-slave coupling for the transverse rotations and for the vertical and transverse displacements of the coincident nodes the expansion hinge effect is properly simulated. In what concerns the bearing conditions of the arch, these were replicated by pinned supports.

7.5.4. Variant and refined models

Taking advantage of the FE modeling to simulate the bridge behavior for different conditions, a set of numerical simulations was conducted with the purpose of assessing the impact of several structural variables on the bridge performance. The parameters addressed in this sensitivity study were:

i. Stiffness of the light-weight concrete pavements;
ii. Stiffness of the cladding plates of the new upper deck floor system that carries pedestrian loads and emergency road vehicles;
iii. Stiffness of the secondary stringers pertaining to the new upper deck floor system.

Table 7.3 lists the variant models developed for this sensitivity analysis and presents a short description of them.

Table 7.3 – Description of the models used in the results analysis.

Condition	*Model*	*Description*
Pre-rehabilitation	A	Base model (stiffness contribution from the light-weight concrete pavements is included)
	A1	Model generated from Model A for which the chords, stringers and crossbeams of both decks only hold the steel section (stiffness contribution from the light-weight concrete pavements is disregarded)
Post-rehabilitation	B	stiffness of the cladding plates covering the new upper deck floor system is disregarded)
	B1	Model generated from Model B by including the stiffness of the cladding plates covering the new upper deck floor system
	B2	Model generated from Model B by not taking into account the stiffness of the secondary stringers integrating the new upper deck floor system
	C1	Sub-model of the 1st panel of span 11 (downstream upper deck girder)
	C2	Sub-model of the 6th panel of span 11 (downstream upper deck girder)
	C3	Sub-model of the 12th panel of span 11 (downstream upper deck girder)
	C4	Sub-model of the 1st panel of span 12 (downstream upper deck girder)

In the course of the analysis performed to the results of the field tests, particularly the upper deck strains collected in Test 2, the improvement of the modeling was needed. As shown in the following section, a large discrepancy between critical experimental data and the predictions supplied by the reference global model was found, which called for a new modeling strategy. This new approach consisted in the combined use of the 3D global model of the bridge and sub-models of the upper deck girders panels. These sub-models were constructed by modeling the plates and angles integrating the built-up bars through panels of shell finite elements, duly connected by stiff bars at the matching nodes. Table 7.3 includes a short description of the four sub-models developed for this study. The sub-model created to simulate the behavior of the 1st panel of span 11 of the downstream upper deck girder is depicted in Figure 7.21.

This type of multi-level modeling has been successfully implemented for the stress analysis at the joints of steel truss bridges (Kiss and Dunai, 1998). For this study the procedure adopted to numerically estimate the strains for the targeted panels was as follows:

i. In the sub-model unitary displacements and rotations are sequentially imposed on the four vertices of the panel and on the upper chord mid-span node, six per each one, in correspondence to the degrees of freedom of the counterpart nodes in the 3D global model;
ii. Construction of an influence matrix correlating each of the unitary displacements or rotations to the strains to be predicted;

iii. Final calculation of the numerical results by multiplying the influence matrix by a vector holding the displacements and rotations at the corresponding nodes of the 3D global model, computed for the loading scenario under consideration.

This type of modeling proved to be a useful tool for a refined analysis as it was capable of properly capture the load path, secondary bending induced by the warping torsion, interaction of structural elements, geometrical stress concentrations and other effects neglected by traditional strategies.

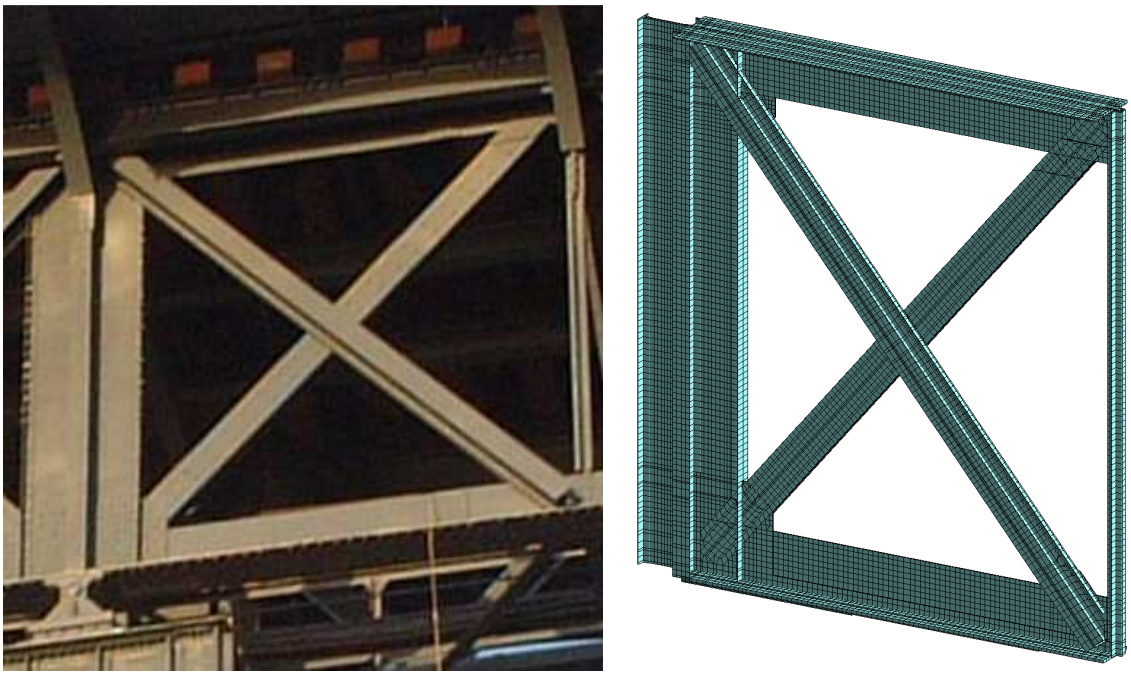

(a) (b)

Figure 7.21 - Modeling of the 1st panel of span 11 of the downstream upper deck girder: (a) picture of a typical girder panel; (b) finite elements mesh.

7.6. Analysis of the results

7.6.1. Static load cases

7.6.1.1. Displacements

Tables 7.4 and 7.5 list the maximum values recorded for the vertical displacements of the upper deck girders and of the arch crown in Tests 1 and 2, respectively, as well as the numerical estimates calculated from the corresponding models for the same load cases.

Table 7.4 – Vertical displacements measured and calculated for the static loading scenarios conducted in Test 1.

Test code	*Gage*	δ_1 *(mm)*	$\delta_{FEM}^{[1]}$ *(mm)*	$\delta_{FEM}^{[2]}$ *(mm)*	$\Delta^{[1]}$ *(%)*	$\Delta^{[2]}$ *(%)*
17SCU	DV-T2	8.69	8.86	10.54	1.93	21.27
16SCU	DV-T3	7.77	8.18	9.19	5.23	18.22
12SCU	DV-T6J	5.81	5.89	6.14	1.39	5.74
12SCU	DV-T6M	5.76	5.89	6.14	2.29	6.68
15SCU	DV-T11	11.31	11.23	14.48	-0.69	28.05
14SCU	DV-T12	7.88	7.62	10.04	-3.29	27.41

δ_1 – Displacements measured in Test 1; $\delta_{FEM}^{[i]}$ – Displacements calculated from the FE model [i]; $\Delta^{[i]} = \delta_{FEM}^{[i]}/\delta_1 - 1$; Total load applied in Test 1: 1034 kN (8 trucks), 1288 kN (10 trucks); [1] – Model A, [2] – Model A1; Positive values correspond to downward displacements.

Table 7.5 – Vertical displacements measured and calculated for the static loading scenarios conducted in Test 2.

Test code	*Gage*	δ_2 *(mm)*	$\delta_{FEM}^{[1]}$ *(mm)*	$\delta_{FEM}^{[2]}$ *(mm)*	$\delta_{FEM}^{[3]}$ *(mm)*	$\Delta^{[1]}$ *(%)*	$\Delta^{[2]}$ *(%)*	$\Delta^{[3]}$ *(%)*
27SCU	DV-T1	-1.31	-1.30	-1.11	-1.64	-0.78	-15.40	25.30
27SCU	DV-T2	10.38	10.25	9.72	11.19	-1.29	-6.33	7.81
26SCU	DV-T3	9.07	9.09	8.77	9.65	0.20	-3.36	6.41
21SCU	DV-T4	8.85	9.35	9.22	9.53	5.70	4.18	7.73
22SCU	DV-T6J	5.74	5.96	5.87	6.07	3.79	2.25	5.74
22SCU	DV-T6M	5.79	5.91	5.83	6.02	2.14	0.63	4.05
25SCU	DV-T10	-2.24	-2.21	-1.91	-2.73	-1.15	-14.6	21.83
25SCU	DV-T11	13.44	13.14	12.32	14.56	-2.27	-8.36	8.36
24SCU	DV-T12	9.62	9.40	8.75	10.59	-2.33	-9.08	10.04
24SCU	DV-T13	-1.80	-2.22	-1.94	-2.73	23.27	7.60	51.55

δ_2 – Displacements measured in Test 2; $\delta_{FEM}^{[i]}$ – Displacements calculated from the FE model [i]; $\Delta^{[i]} = \delta_{FEM}^{[i]}/\delta_2 - 1$; Total load applied in Test 2: 1057 kN (8 trucks), 1315 kN (10 trucks); [1] – Model B, [2] – Model B1, [3] – Model B2; Positive values correspond to downward displacements.

For both tests the correlation between the experimental data and the numerical results supplied by the base models is excellent, presenting an average difference lower than 2.5 %. Only for sensor DV-T13 a large difference can be pointed out, yet it is associated to a small upward deformation of the upper deck in span 13 caused by the loading of a neighboring span (span 12). The results presented in these tables allow to draw important inferences regarding the influence of the floor systems on the global response of the upper deck before and after the rehabilitation. The results predicted by Model A1 reveal a significant impact of the light-weight concrete pavement on the upper deck deformation

before the rehabilitation, with a contribution to its stiffness around 25 %. On the contrary, the influence of this pavement on the arch crown displacements is minimum, since these are mainly controlled by the arch stiffness.

As regards the numerical results estimated by Models B1 and B2, two conclusions can be made. Firstly, when the membrane action of the steel cladding plates of the new floor system is considered (see Figure 7.22), the estimated vertical displacements are about 5 % lower than those measured. This effect is even more prominent in the upward deformation of the spans. Secondly, if the secondary stringers that constitute the new floor system are disregarded the estimates are 10 % higher than the observed vertical displacements. In this way, disregarding the plates stiffness in the reference Model B, in opposition to the inclusion of the secondary stringers, stand as the right options in developing the numerical model to accurately characterize the bridge response after the rehabilitation. Finally, it is worth mentioning that any of the variant models estimate displacements of the arch crown very close to the field measurements, therefore proving the low influence of the analyzed structural parameters on the arch deformability.

(a) (b) (c)

Figure 7.22 - Floor system of the upper deck after the bridge rehabilitation: (a) sleepers and secondary crossbeams resting on the main stringers, which carry metro and pedestrian loads, respectively; (b) execution of a bolted connection at the joint of a secondary stringer; (c) placement and attachment of the steel cladding plates over the secondary stringers.

Table 7.6 – Horizontal displacements measured and calculated for the static loading scenarios conducted in Test 2.

Test code	*Gage*	δ_2 *(mm)*	$\delta_{FEM}^{[1]}$ *(mm)*	$\delta_{FEM}^{[2]}$ *(mm)*	$\delta_{FEM}^{[3]}$ *(mm)*	$\Delta^{[1]}$ *(%)*	$\Delta^{[2]}$ *(%)*	$\Delta^{[3]}$ *(%)*
21SCU	DH-EG	2.91	4.62	4.49	4.83	58.84	54.24	66.07
	DH-P4	3.05	4.66	4.53	4.84	52.80	48.68	58.84
	DH-EP	2.96	4.62	4.50	4.81	56.23	51.97	62.49

δ_2 – Displacements measured in Test 2; $\delta_{FEM}^{[i]}$ – Displacements calculated from the FE model [i]; $\Delta^{[i]} = \delta_{FEM}^{[i]}/\delta_2 - 1$; Total load applied in Test 2: 1057 kN (8 trucks), 1315 kN (10 trucks); [1] – Model B, [2] – Model B1, [3] – Model B2; Positive values correspond to displacements in the north direction.

Table 7.6 compares the maximum horizontal displacements measured in Test 2 with the numerical values calculated from Model B and its variants. The results concern the anti-symmetric loading of the arch, whose deformation impels a horizontal translation of the upper deck as if it was a rigid body. For that reason, the magnitude of the displacements at the several monitored points is very close. This behavior is clearly illustrated in Figure 7.23.

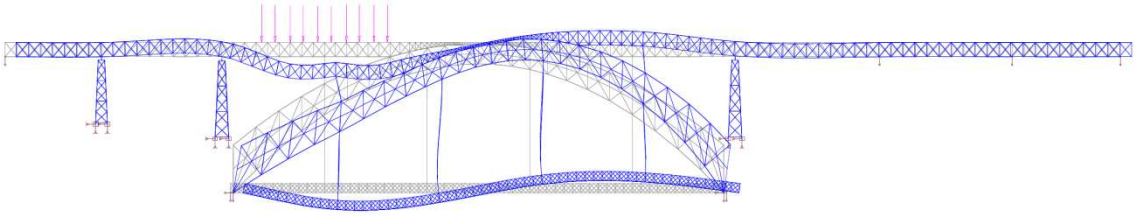

Figure 7.23 – Deformed mesh of Model B for the 2nd static load case (test code 21SCU).

However, the most relevant fact is the large difference between the numerical estimates and the field data, which is in average around 55 % for either model. As likely cause for these results a non-linearity of contact may be indicated, which might occur between the end verticals of the arch (at its supports) and the masonry bases where piers P2 and P3 are based on (see Figure 7.24).

(a) (b) (c)

Figure 7.24 - North end of the arch: (a) downstream view at the support level; (b) view of the joint at the top cross-bar of the end vertical frame; (c) detailed view of the joint at the top.

If the contact between the steel structure and the masonry is fully made the structural system of the bridge is significantly changed because the arch is no longer hinged supported and becomes fixed at the ends. This causes a substantial increase of the arch stiffness for horizontal displacements, namely those that are generated by anti-symmetric loadings. Note that, the gap between the steel structure and the masonry is partially filled

at the lower level, namely by large infrastructure cables. Furthermore, there are several evidences of contact at the upper level of the joint as the stone of the masonry is split at several locations.

This hypothesis for interpreting the horizontal displacements measured at the upper deck supports is strengthened by the results collected during the quasi-static loading events carried out in Test 2. Nevertheless, the only way that would have assuredly clarified this suggestion would have been the instrumentation of the arch upper chords at the supports. If the contact was made, the upper chords would have been necessarily loaded and the corresponding deformation captured by the strain sensors.

Table 7.7 – Strains measured and calculated for the static loading scenarios conducted in Test 1.

Element	*Section*	*Test code*	*Gage*	ε_1 ($\mu\varepsilon$)	$\varepsilon_{FEM}^{[1]}$ ($\mu\varepsilon$)	$\varepsilon_{FEM}^{[2]}$ ($\mu\varepsilon$)	$\Delta^{[1]}$ (%)	$\Delta^{[2]}$ (%)
ALC	S34	12SCU	EA-I7	-20.12	-20.67	-21.29	2.75	5.80
			EA-I8	-21.05	-20.73	-21.34	-1.51	1.40
	S36		EA-I11	19.42	20.69	20.14	6.56	3.70
			EA-I12	21.05	21.31	20.78	1.25	-1.27
AUC	S33	11SCU	EA-S5	-33.62	-36.63	-37.75	8.95	12.29
			EA-S6	-36.81	-38.10	-39.21	3.50	6.51
AD	S41		EA-D3	-32.63	-30.22	-30.95	-7.38	-5.16
			EA-D4	-34.03	-30.77	-31.52	-9.59	-7.38
	S42		EA-D5	43.42	42.92	44.06	-1.14	1.47
			EA-D6	28.95	45.75	47.34	58.02	63.52
UDLC	S4	16SCU	ET-I7	85.53	93.55	90.42	9.37	5.72
			ET-I8	124.74	117.98	118.76	-5.42	-4.79
	S14	15SCU	ET-I27	119.71	128.97	123.72	7.73	3.35
			ET-I28	140.49	132.01	133.20	-6.03	-5.19
UDUC	S15		ET-S29	11.46	11.59	23.94	1.13	108.93
			ET-S30	-7.29	-10.44	14.28	43.23	-295.8
UDD	S23		ET-D5	102.27	95.70	100.58	-6.42	-1.65
			ET-D6	76.14	74.08	79.22	-2.70	4.05
	S24		ET-D7	-105.75	-105.37	-99.95	-0.36	-5.48
			ET-D8	-113.79	-109.45	-106.22	-3.81	-6.65

ε_1 – Strains measured in Test 1; $\varepsilon_{FEM}^{[i]}$ – Strains calculated from the FE model [i]; $\Delta^{[i]} = \varepsilon_{FEM}^{[i]}/\varepsilon_1 - 1$; Total load applied in Test 1: 1034 kN (8 trucks), 1288 kN (10 trucks); [1] – Model A, [2] – Model A1; Acronyms: ALC – Arch lower chord, AUC – Arch upper chord, AD – Arch diagonal, UDLC – Upper deck lower chord, UDUC – Upper deck upper chord, UDD – Upper deck diagonal.

7.6.1.2. Strains

Arch and upper deck (Test 1)

The maximum steel strains measured in Test 1 and the corresponding predictions supplied by the numerical Models A and A1 are listed in Table 7.7. In general, the strains experienced by the arch elements are considerably lower than those of the upper deck bars. On the other hand, the difference between the readings acquired by the pair of strain gages applied to the arch elements is generally small in opposition to the instrumented cross-sections at the upper deck, mainly those pertaining to the chords. The numerical results estimated by the reference model (Model A) correlate very well with the field data, being the average difference lower than 5 %. However, for some sensors the readings diverge significantly, namely sensors EA-D6 and ET-S30.

In the first case, the instrumented diagonal connects to the arch lower chord at a critical joint, whose mechanical behavior is more demanding. This joint is depicted in Figure 7.18(d), and is located in the alignment where the suspension tie M1 connects to the arch with a large eccentricity of the bars axes. In spite of the detailed modeling of the bridge in this region, the global model (Model A) is not able to suitably reproduce the local deformation of latticed elements under significant bending and torsion.

In the second case, the monitored section is located at the upper chord of the upper deck, over which the old light-weight concrete pavement rested on before the bridge rehabilitation. In fact, the lower level of the measured strains proves the composite action between the steel elements and the concrete slab, which hampers the characterization of the state of strain in the steel. Even though, the estimates provided by Model A1, which ignores the stiffness contribution from the concrete pavement, confirm the composite action in that the strains of section S15 largely increase.

Another important observation that stands out from the data is the fact that the predicted values of Model A1 are very similar to those estimated by the reference model. With respect to the arch strains, this result was expected since, on one hand, the modifications produced in Model A1 haven't included the properties of the arch elements. On the other hand, the arch response depends only on the load transmitted by the upper deck through piers M1, M4 and the arch crown, which remains unchanged in Model A1 given that the relative stiffness between the upper deck spans has experienced no significant changes.

As regards the upper deck, particularly for the lower chords, in light of the increase of the vertical displacements from Model A to Model A1 (see Table 7.4), it would be expected a

significant raise in the strains. Yet, this magnification of the steel deformation is not verified. The vertical deformation of the upper deck is controlled by its bending stiffness, which is mainly result of the axial stiffness of the longitudinal elements that constitute the cross-section. The decrease of the upper deck bending stiffness in Model A1 is a consequence of the higher deformability of the cross-section at the upper level, caused by the exclusion of the concrete pavement that holds a significant axial stiffness.

With respect to the strains, the bending moment acting in the upper deck is carried by a couple of longitudinal forces, one at the level of the upper chords and the other at the level of the lower chords, whose magnitude is similar. As neglecting the concrete pavement at the upper level, the relative stiffness of the spans in Model A1 is kept almost unaltered, and for the same loadings the bending produced in the upper deck is approximately the same. In addition, the center of the compression forces only experiences a small downward displacement, and consequently the arm of the couple only shortens slightly. Therefore, similar tension and compression forces are generated in the elements, which for bars with unchanged mechanical properties inevitably cause an equal deformation of the material. This is the case of the strains estimated for the upper deck lower chords. On the other hand, as a consequence of the contribution of the concrete pavement for the stiffness of the upper elements, the strains in the upper chords of the upper deck in Model A are significantly lower.

Arch and piers (Test 2)

Table 7.8 presents the maximum strains, both measured and calculated, in the arch and piers for the static load cases in Test 2. Once more, similarly to the results of Test 1, the readings from the pairs of strain gages attached to the arch show little differences between themselves. Yet again section S42 is an exception.

The piers legs also reveal an almost uniform strain distribution. In addition, in the case of pier P2 (sections S54 and S55) the deformation of both monitored legs is very similar. However, for pier P3 (sections S56 and S57) a significant difference is found. Taking into account the characteristics of the bearings that support the upper deck at the top of the piers (roller bearings) and bearing in mind that these devices were subjected to a careful cleaning and lubrication of its components (see Figure 7.25), it was expected that loads transferred from the upper deck would have only vertical component, and therefore would be equally distributed among the four legs. However, the experimental results suggest that in the case of pier P3 some bending has taken place, which may have been

caused by a horizontal component of the load transferred from the upper deck due to the existence of some friction or deficient performance of the bearings.

Table 7.8 – Strains measured and calculated for the static loading scenarios conducted in Test 2 (arch and piers).

Element	*Section*	*Test code*	*Gage*	ε_2 ($\mu\varepsilon$)	$\varepsilon_{FEM}^{[1]}$ ($\mu\varepsilon$)	$\varepsilon_{FEM}^{[2]}$ ($\mu\varepsilon$)	$\varepsilon_{FEM}^{[2]}$ ($\mu\varepsilon$)	$\Delta^{[1]}$ (%)	$\Delta^{[2]}$ (%)	$\Delta^{[3]}$ (%)
ALC	S34	22SCU	EA-I7	-21.86	-21.84	-21.61	-22.16	-0.09	-1.15	1.38
			EA-I8	-22.40	-21.80	-21.54	-22.13	-2.66	-3.82	-1.22
	S39		EA-I17	-13.93	-15.58	-15.64	-15.65	11.82	12.25	12.37
			EA-I18	-13.66	-15.59	-15.55	-15.67	14.11	13.87	14.68
AUC	S33		EA-S5	-31.15	-35.40	-34.97	-36.01	13.65	12.27	15.61
			EA-S6	-34.43	-39.95	-39.50	-40.62	16.02	14.72	17.99
AD	S40	21SCU	EA-D1	-21.31	-21.23	-19.88	-21.64	-0.36	-6.72	1.53
			EA-D2	-19.13	-21.36	-20.19	-21.77	11.68	5.52	13.81
	S41		EA-D3	-29.51	-27.88	-27.60	-28.29	-5.53	-6.46	-4.13
			EA-D4	-26.23	-24.50	-24.29	-24.86	-6.59	-7.40	-5.22
	S42		EA-D5	43.17	53.29	52.70	54.18	23.43	22.08	25.50
			EA-D6	26.78	31.69	31.33	32.21	18.34	17.00	20.27
PL	S54	26SCU	EP-P1	-33.33	-30.23	-30.32	-30.10	-9.30	-9.02	-9.71
			EP-P2	-30.87	-30.32	-30.41	-30.19	-1.78	-1.49	-2.21
	S55		EP-P3	-32.24	-29.70	-29.83	-29.47	-7.87	-7.48	-8.58
			EP-P4	-31.15	-29.78	-29.91	-29.54	-4.41	-4.00	-5.16
	S56	25SCU	EP-P5	-42.08	-34.96	-34.63	-35.38	-16.93	-17.71	-15.92
			EP-P6	-37.98	-35.01	-34.68	-35.43	-7.82	-8.69	-6.72
	S57		EP-P7	-31.42	-35.53	-35.17	-36.08	13.07	11.92	14.85
			EP-P8	-30.05	-35.59	-35.22	-36.15	18.43	17.21	20.30

ε_2 – Strains measured in Test 2; $\varepsilon_{FEM}^{[i]}$ – Strains calculated from the FE model [i]; $\Delta^{[i]} = \varepsilon_{FEM}^{[i]}/\varepsilon_2 - 1$; Total load applied in Test 2: 1057 kN (8 trucks), 1315 kN (10 trucks); [1] – Model B, [2] – Model B1, [3] – Model B2; Acronyms: ALC – Arch lower chord, AUC – Arch upper chord, AD – Arch diagonal, PL – Pier leg.

The numerical estimates of the piers strains deviate from the field data almost 10 %, in average, whereas for arch strains that value reaches 8 %, a value slightly higher than that obtained in the analysis of the results of Test 1. Furthermore, variant Models B1 and B2 provide results similar to the estimates of the reference model. Thus, it is shown that generalized modifications in the upper deck stiffness do not produce significant changes in the deformation of the arch and piers.

(a) (b)

Figure 7.25 - Load transfer from the upper deck to piers P1, P2 and P3: (a) side view of the top of pier P2 after the rehabilitation process; (b) view of the upstream bearing located at the top of pier P1 (picture taken from the technical path of the upper deck).

Upper deck (Test 2)

Strains of the upper deck, either measured or numerically estimated for the static load cases conducted in Test 2, are listed in Table 7.9. Two relevant features stand out from the chords results. Firstly, almost all chords sections reveal large gradients for the experimental strains, which are generally much higher than those predicted by the numerical analysis. Secondly, the correlation between the field data and the numerical estimates is significantly better for the flanges than for the webs, being the average deviation of 12 % and 62 %, respectively, for the lower chords, and of 22 % and 53 % for the upper chords.

With respect to the strains measured in the diagonals, the results may be distinguished depending on the location of the gages in the cross-section. For the diagonals instrumented in the flange of the original T section (sections S22 and S24), the gauged strains compare well with the numerical estimates, even though for section S22 field data shows some bending. As regards the diagonals equipped with gages applied to the strengthening angles (sections S21 and S23), the discrepancy between the readings and the values predicted from the Model B is very large, and for section S23 the sign is even switched. The causes that explain this behavior of the diagonals will be properly addressed in the analysis of the results obtained from the quasi-static loadings (section 7.6.2).

Table 7.9 – Strains measured and calculated for the static loading scenarios conducted in Test 2 (upper deck).

Element (region)	*Section*	*Test code*	*Gage*	ε_1 ($\mu\varepsilon$)	$\varepsilon_{FEM}^{[1]}$ ($\mu\varepsilon$)	$\varepsilon_{FEM}^{[2]}$ ($\mu\varepsilon$)	$\varepsilon_{FEM}^{[3]}$ ($\mu\varepsilon$)	$\Delta^{[1]}$ (%)	$\Delta^{[2]}$ (%)	$\Delta^{[3]}$ (%)
UDLC (support)	S11	25SCU	ET-I21	12.98	-2.08	-0.83	-3.81	-116.02	-106.42	-129.35
			ET-I22	-39.62	-50.90	-48.42	-54.56	28.46	22.22	37.70
	S16		ET-I31	-69.67	-40.89	-40.51	-41.04	-41.31	-41.86	-41.09
			ET-I32	-61.48	-58.41	-57.71	-59.31	-5.00	-6.12	-3.52
UDLC (mid-span)	S4	26SCU	ET-I7	64.21	98.51	98.05	99.12	53.42	52.70	54.36
			ET-I8	116.12	125.58	123.86	128.48	8.14	6.66	10.64
	S12	25SCU	ET-I23	88.8	136.60	135.52	138.17	53.82	52.61	55.60
			ET-I24	142.08	135.38	133.03	139.07	-4.72	-6.37	-2.12
	S14		ET-I27	89.48	129.49	128.45	131.22	44.72	43.55	46.65
			ET-I28	161.2	139.16	136.72	143.34	-13.67	-15.18	-11.08
UDUC (support)	S10		ET-S19	39.62	30.32	31.22	30.65	-23.48	-21.20	-22.63
			ET-S20	4.10	9.22	7.67	11.75	124.96	87.04	186.58
	S15		ET-S29	54.64	63.65	54.77	79.75	16.48	0.24	45.95
			ET-S30	32.79	43.18	36.95	54.08	31.68	12.69	64.94
UDUC (mid-span)	S13		ET-S25	-91.53	-68.81	-54.88	-93.48	-24.83	-40.05	2.13
			ET-S26	-39.62	-38.83	-26.37	-60.90	-2.00	-33.44	53.71
UDD	S21		ET-D1	4.10	54.62	53.14	56.89	1232.2	1196.0	1287.5
			ET-D2	5.46	53.47	52.16	55.32	879.28	855.37	913.27
	S22		ET-D3	-78.55	-71.99	-71.05	-73.27	-8.35	-9.55	-6.72
			ET-D4	-91.53	-74.89	-73.77	-76.51	-18.18	-19.40	-16.41
	S23		ET-D5	-10.93	2.77	2.58	3.32	-125.36	-123.58	-130.42
			ET-D6	-23.91	-5.70	-5.82	-5.21	-76.17	-75.68	-78.21
	S24		ET-D7	-90.16	-84.97	-84.86	-85.14	-5.76	-5.88	-5.57
			ET-D8	-92.90	-85.86	-85.52	-86.48	-7.58	-7.94	-6.91
UDC	S25	24SCU	ET-C1	-13.66	-21.47	-22.69	-22.40	57.19	66.07	63.97
			ET-C2	40.98	43.02	39.16	47.61	4.99	-4.43	16.18
	S26		ET-C3	-71.04	-70.98	-67.95	-76.24	-0.09	-4.35	7.32
			ET-C4	38.25	104.50	104.46	103.03	173.20	173.09	169.36
	S27		ET-C5	-17.76	-19.58	-20.97	-22.09	10.25	18.09	24.38
			ET-C6	34.84	42.33	38.63	47.16	21.49	10.89	35.36

ε_2 – Strains measured in Test 2; $\varepsilon_{FEM}^{[i]}$ – Strains calculated from the FE model [i]; $\Delta^{[i]} = \varepsilon_{FEM}^{[i]}/\varepsilon_2 - 1$; Total load applied in Test 2: 1057 kN (8 trucks), 1315 kN (10 trucks); [1] – Model B, [2] – Model B1, [3] – Model B2; Acronyms: UDLC – Upper deck lower chord, UDUC – Upper deck upper chord, UDD – Upper deck diagonal, UDC – Upper deck crossbeams.

As regards the crossbeam at the middle of span 12, the measured strains compare satisfactorily or well with the estimates provided by Model B, except for sensor ET-C4 to which the measurement has produced a result 63 % lower than that supplied by the

numerical analysis. Finally, for the lower chords, diagonals and crossbeams the estimates from the variant Models B1 and B2 are very close to the values calculated by the reference Model B, pointing to a residual influence of the secondary stringers and cladding plates on their deformation. However, the stiffness contributions from these elements have a significant impact on the upper chords strains, which is a direct consequence of their participation in the upper deck bending stiffness.

7.6.1.3. Torsion of the upper deck and arch

One of the most relevant aspects in the structural behavior of bridges holding two or more tracks (railway) or traffic lanes (roadway) is their deformability under the action of eccentric loadings. Moreover, the transverse distribution of the loads among the components of the floor system, namely stringers, and the participation of each load-carrying girders to support the forces and bending moments induced in the deck, are also crucial issues to be assessed regarding the performance of the deck. In this context, the deformability of the upper deck was experimentally evaluated in both tests through static loading lines transversely displaced towards the downstream side. These load cases replicated the same longitudinal positioning of some centered static ones conducted with two loading lines (LC 8 to LC 11). Figures 7.11 and 7.12 depict respectively the transverse and longitudinal location of the test trucks on the bridge.

Table 7.10 – Vertical displacements measured for comparable centered and non-centered static loading scenarios.

		Centered loading		*Non-centered loading*		
Location	*Sensor*	*Test code*	δ_c *(mm)*	*Test code*	δ_{nc} *(mm)*	Δ *(%)*
Span 3	DV-T3	11SCU/21SCU	6.10[a]/6.56[b]	18SDU/28SDU	6.98[a]/8.19[b]	14.50[a]/24.77[b]
Span 4	DV-T4	21SCU	6.73[b]	28SDU	7.87[b]	16.94[b]
Span 11	DV-T11	25SCU	10.22[b]	211SDU	12.67[b]	23.96[b]
Arch crown	DV-T6J	12SCU/22SCU	4.42[a]/4.36[b]	19SDU/29SDU	4.96[a]/4.90[b]	12.21[a]/12.17[b]
	DV-T6M		4.38[a]/4.40[b]		3.85[a]/3.88[b]	-12.17[a]/-11.79[b]

δ_c – Displacements under centered loading per 1000 kN of applied load; δ_{nc} – Displacements under non-centered loading per 1000 kN of applied load; $\Delta = \delta_{nc}/\delta_c - 1$; Total load applied in Test 1: 642 kN (5 trucks), 1288 kN (10 trucks); Total load applied in Test 2: 647 kN (5 trucks), 1315 kN (10 trucks); [a] Results for Test 1; [b] Results for Test 2; Positive values correspond to downward displacements.

Table 7.10 presents the vertical displacements measured in both tests for centered and non-centered loadings. Each line concerns load cases in which the load center in the bridge elevation is located at the same position. In order to allow an accurate comparison of the results the values listed in the table were normalized for a standard applied load of

1000 kN. Before the rehabilitation, the downstream girder deflection at span 3 under an eccentric loading was 14.5 % higher than that of a centered one, whereas after the rehabilitation it reached 24.8 %. Therefore, the replacement of the old light-weight concrete pavement by a new steel grid has decreased the torsion stiffness of the upper deck about 10 %. Nevertheless, the new torsional deformability of the upper deck can be regarded as satisfactory. The vertical displacements measured in span 11 also prove that the increase of the downstream girder caused by the eccentric loading was 24 % after the rehabilitation.

Although readings taken from span 4 are presented in the table they cannot be included in this analysis. Span 4 is completely supported by the arch, and therefore its deformation holds an important fraction from the settlements of its supports (rigid body movement), which precludes its use in the assessment of the upper deck torsion deformability.

With respect to the arch crown, for both tests the increase of the downstream vertical displacement induced by the eccentric loading was 12 %, which was the same magnitude of the reduction experienced in the upstream side. The collection of identical results lies on the fact that displacements at the arch crown are mainly controlled by the arch stiffness, and for this substructure the rehabilitation works had little impact in altering its behavior.

Table 7.11 – Strains measured for comparable centered and non-centered static loading scenarios in Test 2.

			Centered loading		*Non-centered loading*		
Location	*Section*	*Sensors*	*Test code*	ε_c ($\mu\varepsilon$)	*Test code*	ε_{nc} ($\mu\varepsilon$)	Δ (%)
Span 11	S14[a]	ET-I27	25SCU	68.04	211SDU	82.31	20.97
		ET-I28		122.57		142.45	16.22
	S12[b]	ET-I23		67.52		61.20	-9.35
		ET-I24		108.03		96.02	-11.11

ε_c – Strains under centered loading per 1000 kN of applied load; ε_{nc} – Strains under non-centered loading per 1000 kN of applied load; $\Delta = \varepsilon_{nc}/\varepsilon_c - 1$; Total load applied in Test 2: 647 kN (5 trucks), 1315 kN (10 trucks); [a] Downstream lower chord; [b] Upstream lower chord.

As regards the load distribution between the main girders of the upper deck under the action of eccentric loadings, Table 7.11 shows the strains measured in both downstream and upstream lower chords at the middle of span 11 for Test 2. The span under analysis holds the conditions for an accurate evaluation since it was both symmetrically and eccentrically loaded (LC 5 and LC 11, respectively) and both lower chords are instrumented with strain gages.

The field data indicate an average increase of 18.6 % in the strains of the downstream girder, to which a decrease of only 10.2 % in the deformation of the upstream girder is associated. By comparing these results with the vertical displacements measured in the same span (see Table 7.10), the variation of the steel strains in the lower chords is considerably lower, which points to a higher deformation of the longitudinal elements located at the upper level of the deck cross-section. In fact, the average increase of the strains measured in the downstream upper chord at the middle of span 11 (section S13) was higher than 26 %.

7.6.1.4. Experimental evaluation of the bridge rehabilitation

One of the main goals of conducting both tests was to obtain field data that enabled a direct and clear assessment of the changes produced in the bridge behavior as a consequence of the construction works. Table 7.12 lists the vertical displacements measured before and after the bridge rehabilitation for the same static load cases at the same points of the structure. For the sake of comparability, the values are normalized for a reference load of 1000 kN.

Table 7.12 – Vertical displacements measured for comparable static loading scenarios.

	Before the rehabilitation		*After the rehabilitation*		
Sensor	*Test code*	δ_1 *(mm)*	*Test code*	δ_2 *(mm)*	Δ *(%)*
DV-T2	17SCU	8.40	27SCU	9.82	16.81
DV-T3	16SCU	7.51	26SCU	8.58	14.15
DV-T6J	12SCU	4.51	22SCU	4.36	-3.22
DV-T6M	12SCU	4.47	22SCU	4.40	-1.53
DV-T11	15SCU	8.78	25SCU	10.22	16.41
DV-T12	14SCU	6.12	24SCU	7.31	19.59

δ_1 – Displacements in Test 1 per 1000 kN of applied load; δ_2 – Displacements in Test 2 per 1000 kN of applied load; $\Delta = \delta_2/\delta_1 - 1$; Total load applied in Test 1: 1034 kN (8 trucks), 1288 kN (10 trucks); Total load applied in Test 2: 1057 kN (8 trucks), 1315 kN (10 trucks); Positive values correspond to downward displacements.

The average increase of the deflection experienced by the upper deck was of 16.7 %, which indicates a reduction of the upper deck bending stiffness of the same magnitude, as a result of the replacement of the old light-weight concrete pavement by a new steel grid for carrying the loads from the pedestrians and emergency road vehicles. Note that, in the analysis of the vertical displacements measured for the static load cases in both tests (Tables 7.4 and 7.5), the numerical simulations supplied by the variant models had already proved the influence of the old concrete pavement in controlling the bending

deformation of the upper deck before the rehabilitation. Moreover, the results allowed to infer that the new steel grid, namely the secondary stringers, had a much lower contribution to the bending stiffness of the upper deck. As regards the vertical displacements measured at the arch crown, the normalized values were very similar, and therefore confirmed once more the small impact of the rehabilitation in the structural behavior of the arch.

Table 7.13 – Strains measured for comparable static loading scenarios.

			Before the rehabilitation		*After the rehabilitation*		
Element	*Section*	*Sensor*	*Test code*	ε_1 ($\mu\varepsilon$)	*Test code*	ε_2 ($\mu\varepsilon$)	Δ (%)
ALC	S31	EA-I1 (D)	12SCU	-10.88	22SCU	-9.62	-11.62
		EA-I2 (U)		-10.68		-9.95	-6.81
	S34	EA-I7 (D)		-15.62		-16.62	6.43
		EA-I8 (U)		-16.34		-17.03	4.24
AUC	S33	EA-S5 (D)	11SCU	-26.10	21SCU	-23.69	-9.24
		EA-S6 (U)		-28.57		-26.18	-8.38
AD	S41	EA-D3 (D)		-25.33		-22.44	-11.41
		EA-D4 (U)		-26.41		-19.94	-24.50
	S42	EA-D5 (D)		33.70		32.82	-2.61
		EA-D6 (U)		22.47		20.36	-9.39
AV	S44	EA-M1 (D)		-7.35		-2.70	-63.28
		EA-M2 (U)		-11.03		-7.89	-28.45
UDLC	S4	ET-I7 (U)	16SCU	82.71	26SCU	60.72	-26.58
		ET-I8 (U)		120.63		109.81	-8.97
	S14	ET-I27 (U)	15SCU	92.92	25SCU	68.04	-26.78
		ET-I28 (U)		109.05		122.57	12.40
UDUC	S15	ET-S29 (U)		8.90		41.55	367.05
		ET-S30 (U)		-5.66		24.93	540.60
UDD	S23	ET-D5 (U)		79.38		-8.31	-110.47
		ET-D6 (U)		59.10		-18.18	-130.76
	S24	ET-D7 (U)		-82.08		-68.55	-16.48
		ET-D8 (U)		-88.33		-70.64	-20.03

ε_1 – Strains in Test 1 per 1000 kN of applied load; ε_2 – Strains in Test 2 per 1000 kN of applied load; $\Delta=\varepsilon_2/\varepsilon_1-1$; Total load applied in Test 1: 1034 kN (8 trucks), 1288 kN (10 trucks); Total load applied in Test 2: 1057 kN (8 trucks), 1315 kN (10 trucks); Acronyms: ALC – Arch lower chord, AUC – Arch upper chord, AD – Arch diagonal, AV – Arch vertical, UDLC – Upper deck lower chord, UDUC – Upper deck upper chord, UDD – Upper deck diagonal; U – Upstream side of the cross-section, D – Downstream side of the cross-section.

The comparison of the maximum strains measured before and after the rehabilitation of the bars sections instrumented in both tests is made in Table 7.13. The following observations can be made from the collected data:

- In average, the strains in the arch lower chords have not varied significantly, and the difference between the readings of both tests falls within the measurement error;

- In spite of have not been strengthened, the instrumented arch upper chord (section S33), located in the 4th downstream panel from the south support, experienced a slight decrease of the deformation in Test 2;

- The deformation of the tension diagonal (section S42) was slightly reduced after the rehabilitation, whereas the strains measured after the rehabilitation for the compression diagonal (section S41) decreased much more, which is directly related to the strengthening of the bar;

- Although no strengthening to the instrumented vertical has been applied (section S44) the deformation of this arch element was largely reduced. Taking into account the relatively low level of the measured strains in both tests, is very likely that the construction works performed on the arch have changed the load path towards the strengthened diagonals, and therefore also altered the load transferred for the verticals;

- The readings collected in the upper deck lower chords point to an average decrease of 12 % in Test 2. However, this is a misleading observation as it will be demonstrated in the results analysis of the quasi-static loadings. As already stated in section 7.6.1.2, for the same loading conditions of the upper deck in both tests the bending moments generated in it are almost the same since the relative stiffness of the spans remains approximately equal. Taking into consideration that the bending moment of the upper deck is carried by a couple, whose center of the compression forces experiences only a small change as a result of the replacement of the concrete pavement by a secondary steel grid, and that the lower chords were not strengthened, the strains measured in these elements should be virtually identical. Yet, this is not the case for two reasons. On one hand, for elements not loaded directly, the exact positioning of the test vehicles over the deck is very relevant since it influences the so-called secondary moments, which in turn impact on the strain fields. On the other hand, the monitored sections of the bars were not exactly located in

the same position and the location of the web gages in the cross-section is also slightly different.

- The deformation of the upper chord of the upper deck has significantly enlarged after the bridge rehabilitation, which is in conformity with the replacement of the previous stiff concrete pavement by a less stiff steel grid;
- The upper deck diagonal subjected to compressive axial forces (S24) experienced a large decrease of the deformation, whereas for the monitored tension diagonal (S23) the measured strains were of a magnitude much smaller, and even of compressive nature. Both diagonals were equally strengthened, and therefore this result appears as baffling. However, it is imperative to bear in mind that the strain gages were not attached at the same positions in both cross-sections. For section S24 the sensors were applied to the flange of the old T section, whereas for section S23 they were glued to the strengthening angles of the web free end (see Figure 7.16). This fact points to a transverse distribution of the strains highly variable in the diagonals. A complete interpretation of their behavior is presented in the following section.

7.6.2. Quasi-static loadings

As previously mentioned in section 7.4, two slow crossings of a pair of test vehicles, side by side, took place on the upper deck in both tests. In Test 2 the lower deck was also loaded twice by a single truck travelling at a crawling speed. The results collected from both loadings, either on the upper or lower deck, revealed no meaningful differences in the monitored quantities, which proved the repeatability of the bridge response. Consequently, data presented in this section are always related to the first loading event. These tests supplied the response of the structure for a moving load different from a unitary concentrated force. Yet, for the sake of simplicity, the plots obtained from the tests will henceforth be designated as experimental influence lines, and the corresponding curves estimated by the models as numerical influence lines.

7.6.2.1. Test 1

Strains

Figure 7.26 shows the experimental influence lines collected in Test 1 by the strain sensors installed in the upper deck. With the purpose of assisting the interpretation of the

test results and to assess the ability of Model A to replicate the bridge behavior, the numerical estimate for each sensor are overlapped in the graphs (Model A), as well as the estimate of the strain induced by the axial force in the instrumented section (Model A - axial), henceforth referred to as axial strain.

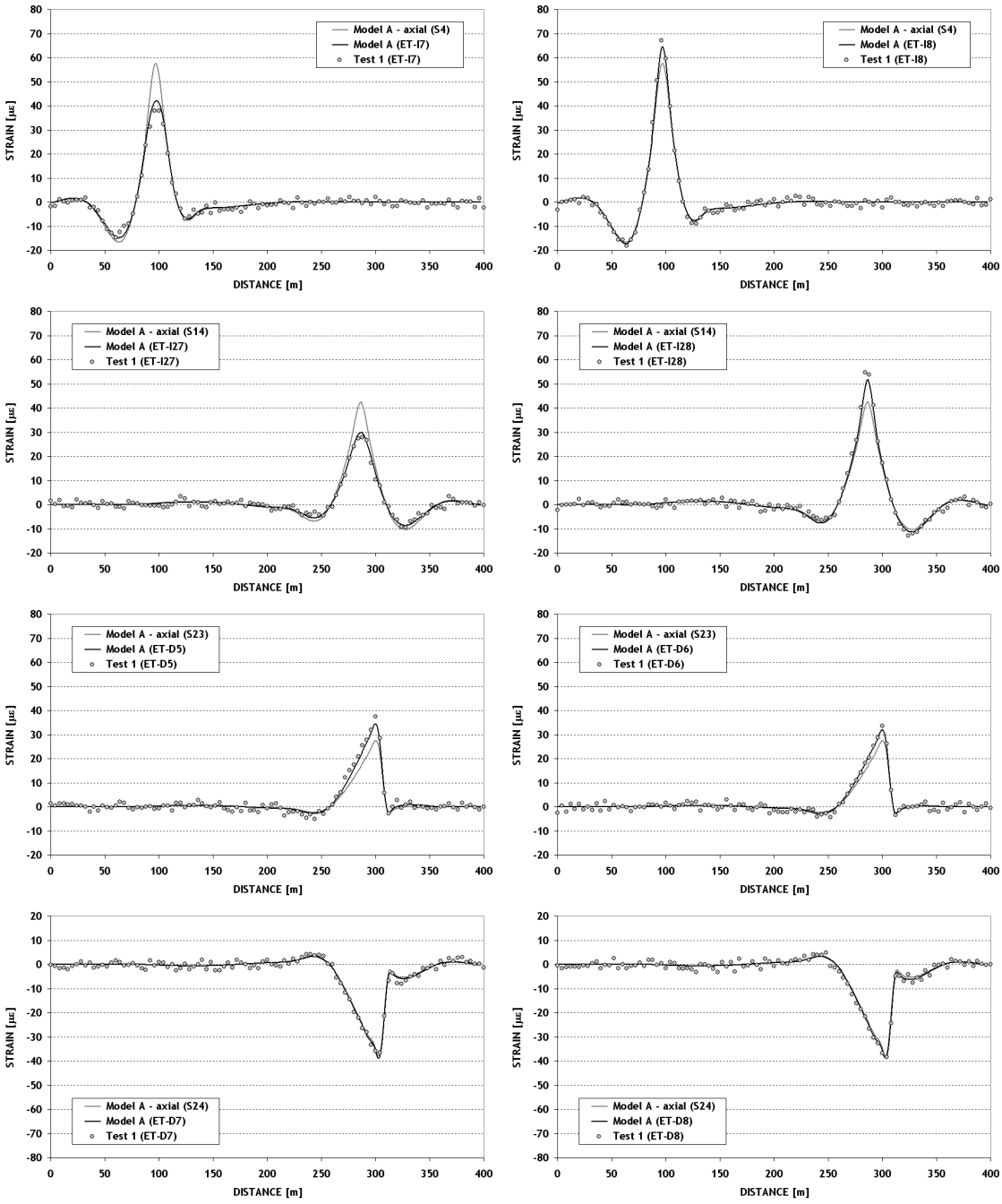

Figure 7.26 - Influence lines for the steel strains in the upper deck (Test 1).

In general, a good correlation between the experimental results and the predictions supplied by the numerical analysis is found. Furthermore, strains collected by the sensors attached to the lower chords significantly diverge from the axial strains of the members, revealing the existence of large strain gradients which are replicated by the 3D frame

model. The results also show that the axial force acting on these elements is mainly carried by the flange which is the stiffest component of the cross-section.

With respect to the strain readings acquired in the diagonals flanges, the gradient is much smaller (S23) or even null (S24). Taking into account the location of the sensors in the cross-sections (see Figure 7.16) and the fact that the equilibrium of the members forces at the girders joints is made through the flanges of the T sections, it would be expected that deformation of section S24 was higher than the axial strain, similarly to the results obtained for section S23. However, the transverse bending of section S23 is significantly higher than that of section S24, as a consequence of a much larger rotation of the lower joint of the tension diagonal than that of the compression diagonal, where the downstream bearing of pier P4 is located (see Figure 7.13). This is caused by the fact that in the lower joint of the tension diagonal the diagonals are positioned on opposite sides of the girder middle plane, whereas at the support both diagonals are on the same side. Moreover, the torsion stiffness of the girder vertical over the support is much higher than that of the vertical in the tension diagonal.

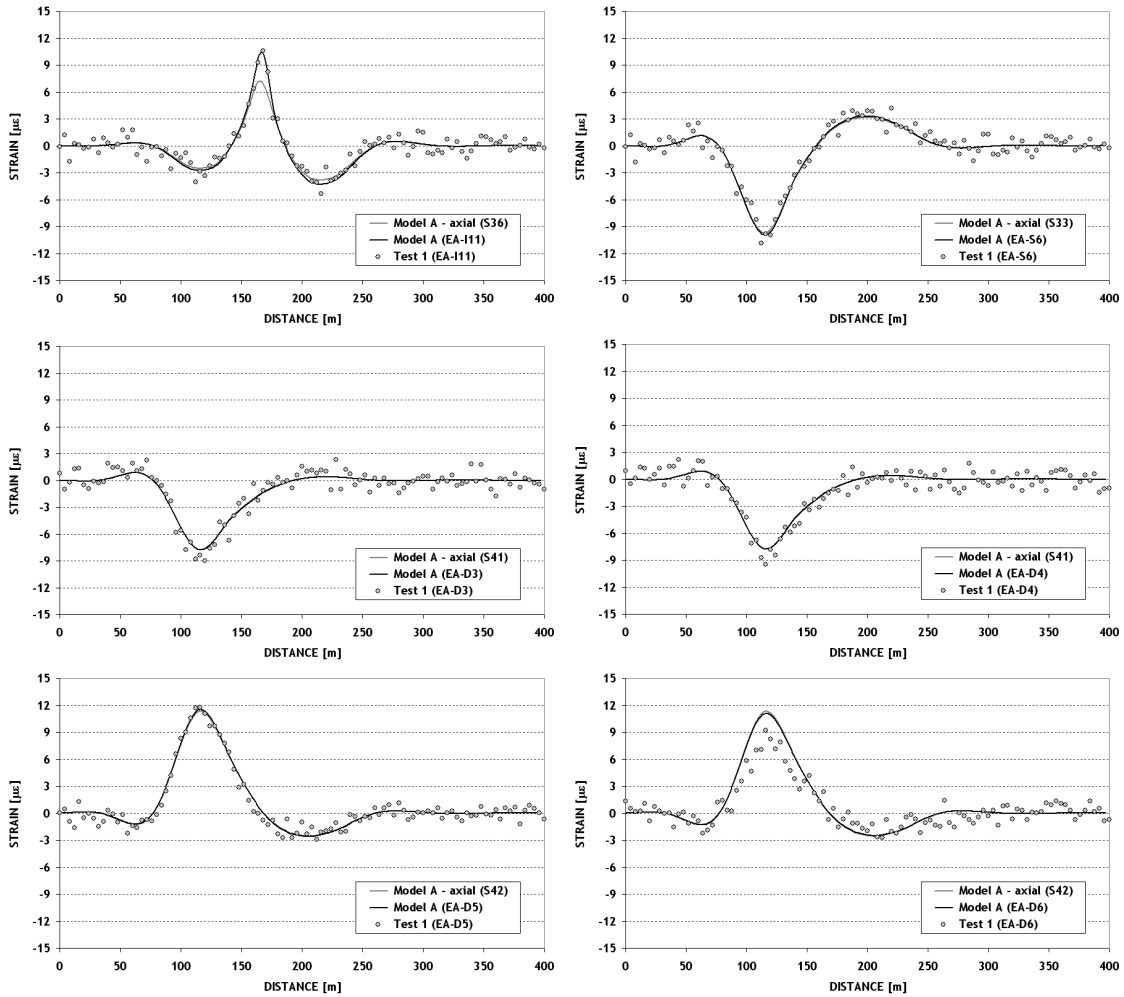

Figure 7.27 - Influence lines for the steel strains in the arch (Test 1).

Influence lines acquired by the strain gages attached to arch elements are depicted in Figure 7.27. The results show a fair correlation with the numerical estimates for almost sensors, except for sensor EA-D6 at section S42. Similarly to the results collected from the static loadings, these field data indicate once more a prominent strain gradient for this section which is not accurately reproduced by the reference model. Another relevant aspect worth to mention is the small or null bending component in the remaining sections.

The differences between the numerical and experimental results tend to be smaller in the quasi-static loadings when compared with the readings collected during the static load cases, particularly for sensors whose measurements deviate the most, e.g. EA-D6. Therefore, it can be concluded that a thorough characterization of the vehicles positioning in the static tests may play an important role in the accurate simulation of the bridge response from the numerical analysis, namely for parameters of local nature such as the steel strains.

Displacements

The slow crossings of the test trucks carried out in Test 1 produced results of poor quality for the vertical displacements, and therefore their presentation and discussion was precluded. The main reason for this setback was related to the high sensitivity of the liquid leveling system to the vibrations induced by the trucks and magnified by the rigid concrete pavement. For Test 2, suitable measures were adopted in order to mitigate the instability of the readings acquired by this measuring system.

7.6.2.2. Test 2

Displacements

Figure 7.28 presents the continuous record of the displacement transducers that measured the longitudinal movements of the monitored supports during the slow crossings on the upper deck. For an assessment of the bridge response the influence lines provided by the reference Model B are also shown.

An inspection to all graphs allows to conclude that the maximum displacements measured by all transducers are much lower than the numerical estimates. Moreover, the shapes of the curves diverge significantly, mainly between piers P2 and P3, when the arch is loaded. In this region, the direction of displacement is caused by the antisymmetric deformation of the arch, which is a consequence of the position of the vehicles with respect to the arch crown. Compelled by its movement, the upper deck is displaced in the longitudinal

direction as a rigid body, and consequently the longitudinal displacements at the observed supports are very similar during the period in which the arch is loaded.

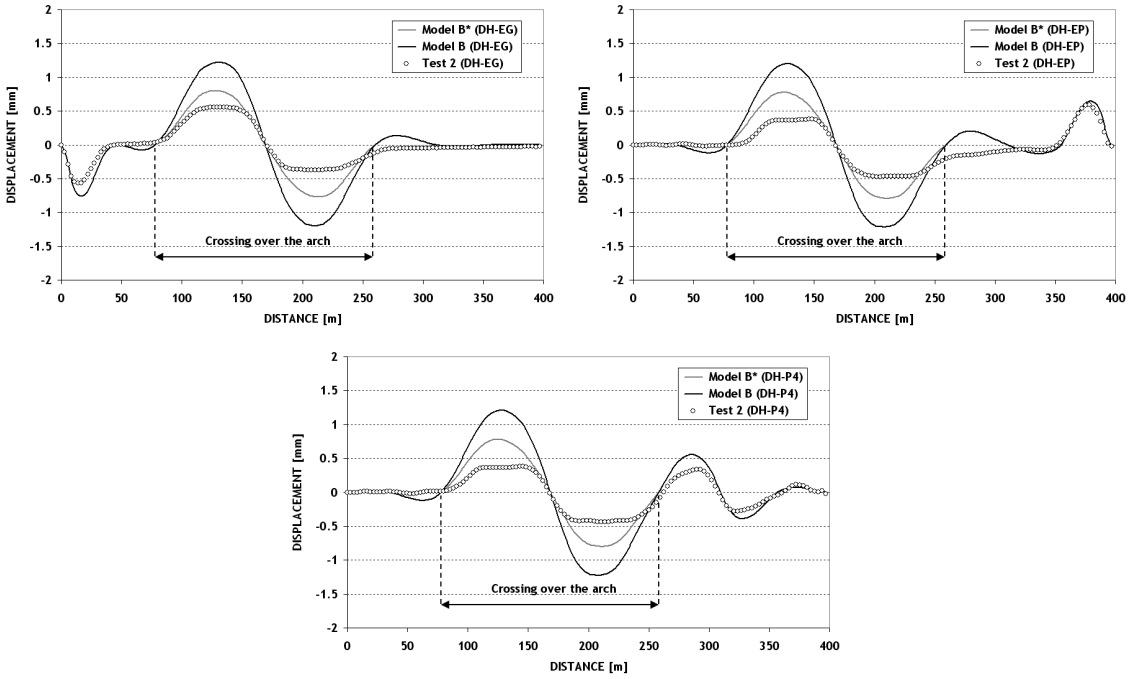

Figure 7.28 - Influence lines for the bearings displacements at the upper deck (Test 2 – displacements towards the north direction are positive).

For any graph a higher stiffness in the bridge response and a clear flattening of the curves in the regions of maximum displacement are perceptible. This behavior may be explained in light of the existence of a nonlinear contact between the arch and the walls of the masonry bases on which piers P2 and P3 rest, occurring alternately depending on the vehicles position. In order to evaluate this hypothesis, the charts of Figure 7.28 also depict the plots produced by the numerical analysis when the non-linear contact is simulated at the top nodes over the arch supports, labeled as "Model B*". In a simplified form, the nonlinear contact was replicated by rigid longitudinal supports that only generate reaction forces when the nodes move towards the river banks. Figure 7.29 shows the deformed mesh of the model for the vehicles position that maximizes the longitudinal displacement of the upper deck. The location of the nonlinear supports is identified by the arrows. At the left support the node moves towards the river, and consequently no reaction takes place, whereas in the opposite side the displacement is blocked. Even though the results exhibit a clear improvement, the new plots clearly do not fit the experimental results in the regions of maximum displacement. The remaining difference may be caused by additional restrictions in the expansion joints at the upper deck ends. Nevertheless, these possible restrictions are not sufficient to prevent the proper deformation of the deck under thermal action (Costa *et al.*, 2008b).

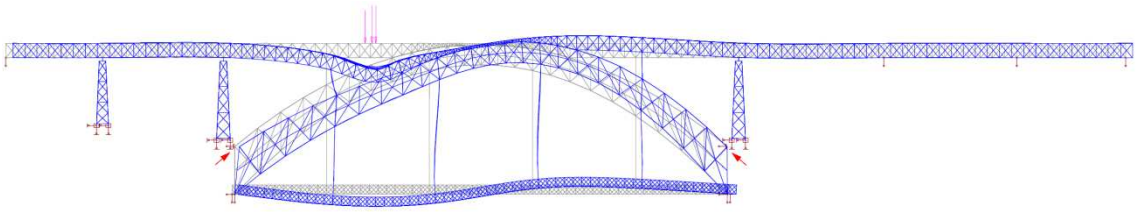

Figure 7.29 – Deformed mesh of Model B* for the maximum longitudinal displacement of the upper deck induced by the slow crossing.

Figures 7.30 and 7.31 depict the experimental influence lines for the vertical displacements and the numerical counterparts. The correspondence between the results for the downward displacements is very good. However, for the upper deck spans supported by the arch, the measured upward displacements deviate from the predictions supplied by the reference Model B. This difference is maximum for the readings acquired by the sensor DV-T4. The impact of a nonlinear behavior of the arch joints at the supports was also evaluated, and the variant numerical estimates are presented for sensors DV-T3, DV-T4 and DV-T10, referred to as "Model B*". The new plots compare very well with the field data, and therefore the existence of contact between the end vertical frames of the arch and the masonry walls of the piers bases can be regarded as very plausible (see Figure 7.24).

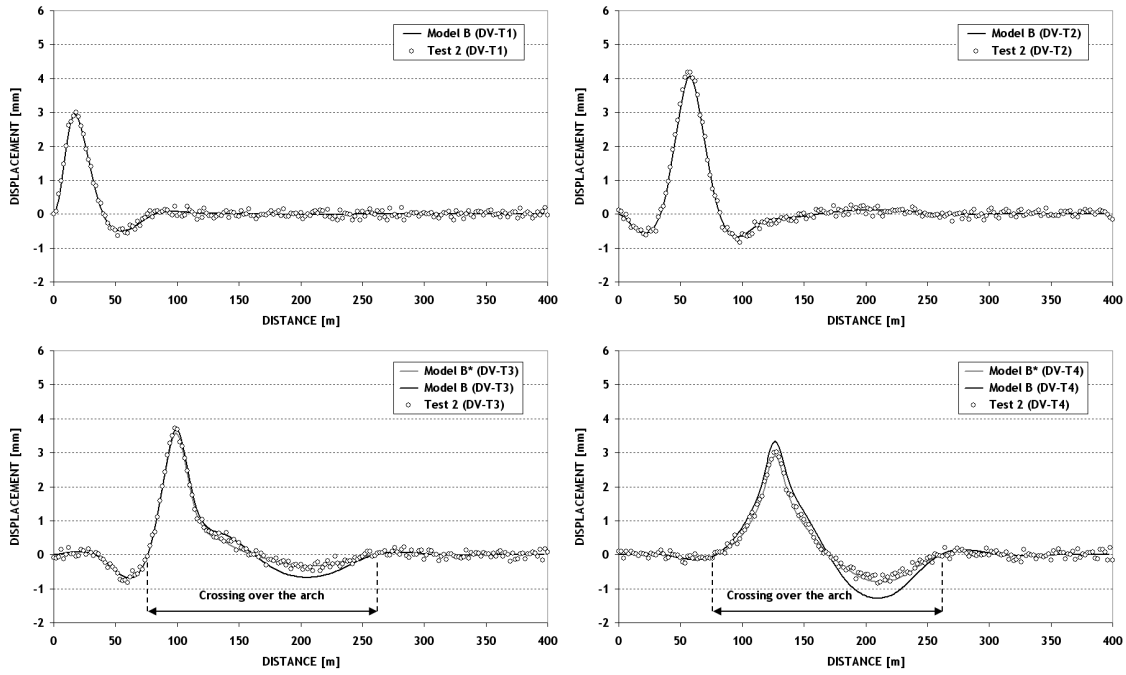

Figure 7.30 - Influence lines for the vertical displacements of the upper deck and arch (Test 2 - downward displacements are positive) (I).

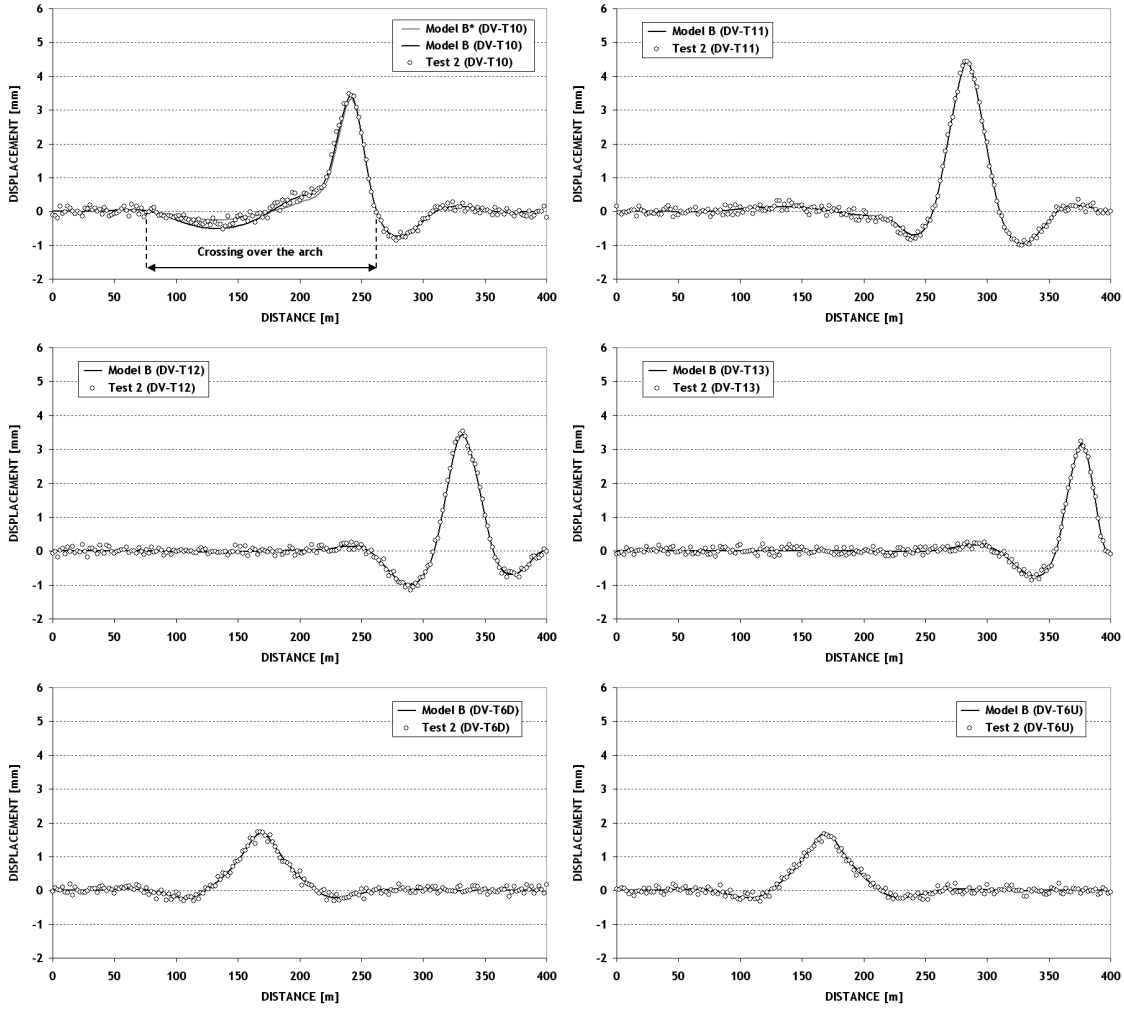

Figure 7.31 - Influence lines for the vertical displacements of the upper deck and arch (Test 2 - downward displacements are positive) (II).

Strains of the upper deck lower chords

Figure 7.32 shows the strains measured in representative sections of the lower chords of the upper deck. In the graphs three types of numerical estimates are also plotted, described as follows:

i. Strain generated in the monitored section by the axial force provided by the reference Model B (axial strain);
ii. Strain at the sensor position induced by the axial force and bending moments estimated by the reference Model B;
iii. Strain predicted by the sub-model that replicates the upper deck girder panel where the instrumented section is located, for which the input actions are the displacements and rotations calculated with the reference Model B.

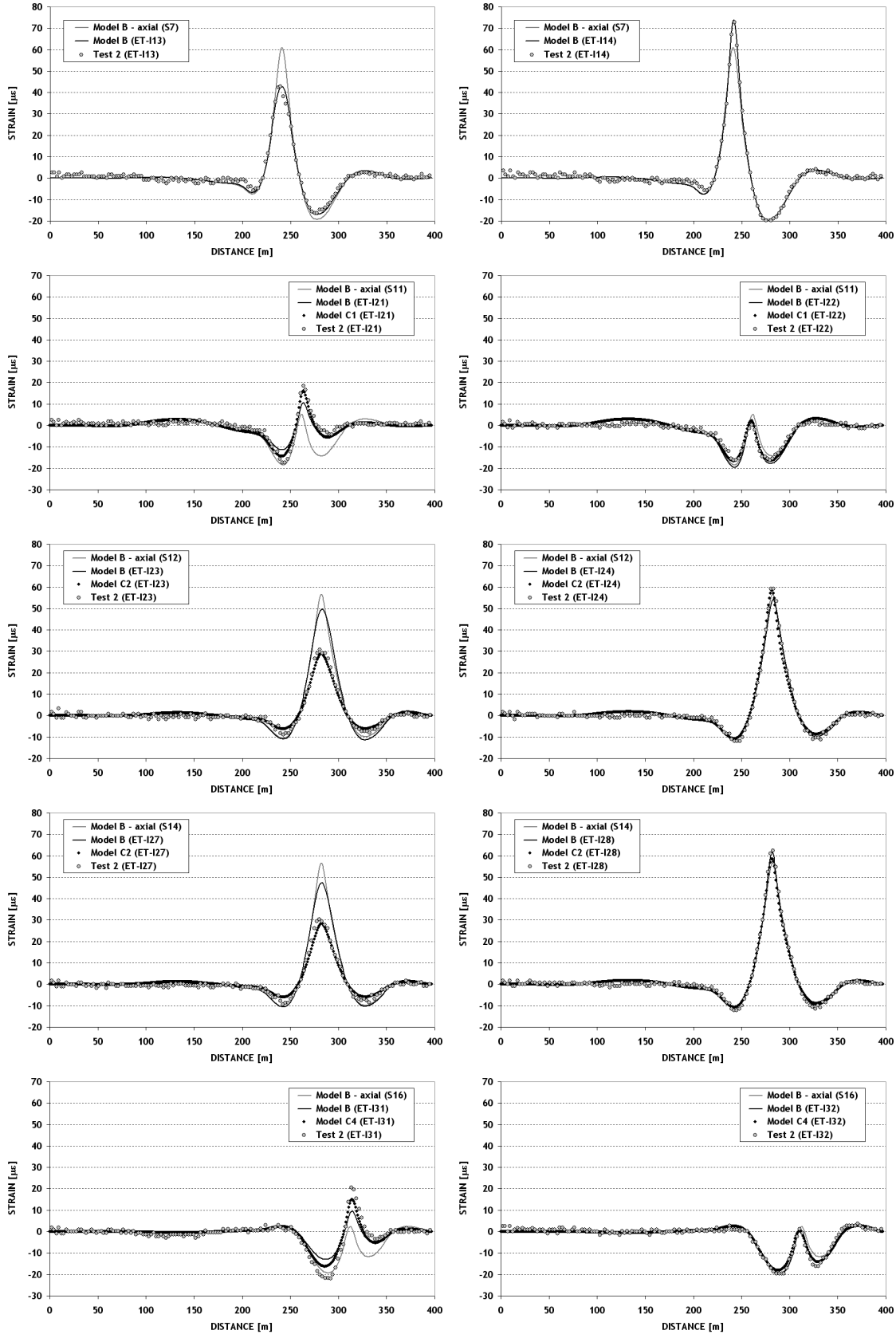

Figure 7.32 - Influence lines for the steel strains in the lower chords of the upper deck (Test 2).

First, the strains measured at the sections flanges are very close to the axial strain, whereas the strains gauged in the webs highly deviate. Moreover, for the webs some experimental lines are either substantially lower, as is the case of mid-span sections (S7, S12 and S14), or clearly higher, as is the case of the support sections (S11 and S16). This fact shows unequivocally that the axial force is mainly carried by the flanges, hence positioning the load center close to these stiff components. In addition, these data also confirm the observations pointed out from the results collected in Test 1.

Second, the strains calculated from the bars forces (axial and bending) estimated by Model B fit better with the test results. The improvement is more clear for the webs. Nevertheless, for the sensors attached to the webs the discrepancy between the experimental data and the numerical predictions is large, except for sensor ET-I13 in section S7. Model B is only able to partially replicate the strain gradient in the sections through the bending moments. The simulation of the actual state of strain is clearly enhanced when the bending tends to be uniform throughout the element.

A third major observation is that the numerical predictions provided by the sub-models compare better with the experimental lines, particularly for the webs strains. Figures 7.33 and 7.34 are presented in order to support the interpretation of the results. Figure 7.33 shows the deformed shape of the upper deck girder panel where sections S13 and S14 are located, estimated by Model B for the static load case 5 (test code 25SCU), as well as the corresponding diagram of the in-plane bending moments. Figure 7.34 depicts the deformed shape calculated by sub-model for the same panel (Sub-model C2) and the corresponding map of normal stress in the longitudinal direction of the elements.

Although the results presented in both figures are associated to a static load case, the behavior of the panel is similar when the upper deck is loaded by a moving load. In spite of the rotations and displacements at the five key nodes of both models are equal, by comparing the figures large differences in the deformed shapes stand out, particularly at the lower level. In both models, four key nodes are located at the intersection points of the verticals axes with the diagonals axes, which takes place at the chords flanges, whereas the fifth node is located at the upper chord mid-span over the axis defined by the upper key nodes.

While in Model B the bending of the chords is mainly controlled by the nodes rotation, in sub-model C2 it is caused by the eccentricity of the axial force since the normal stresses are concentrated in the flange. Although in Model B the bars axes are properly positioned in space by using the offsetting operation (displacement of the bar axis from the nodes

through rigid links), the modeling is not able to properly replicate the load path. It is worth mentioning that the key nodes of Sub-model C2, to which the displacements and rotations are imposed, are located at the intersection of a rigid T whose dimensions comprise the angles connecting the web and the flange plates.

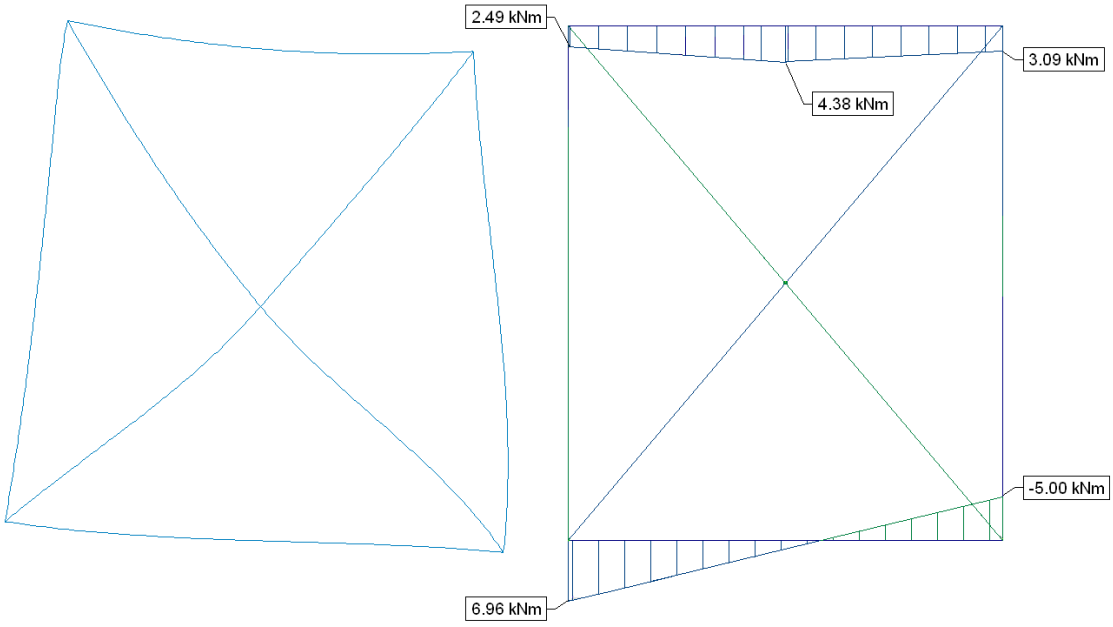

(a) (b)

Figure 7.33 - Results provided by the reference Model B for the 6th panel of the downstream upper deck girder in span 11 for the static load case 5 (test code 25SCU): (a) deformed shape; (b) in-plane bending moments of the chords.

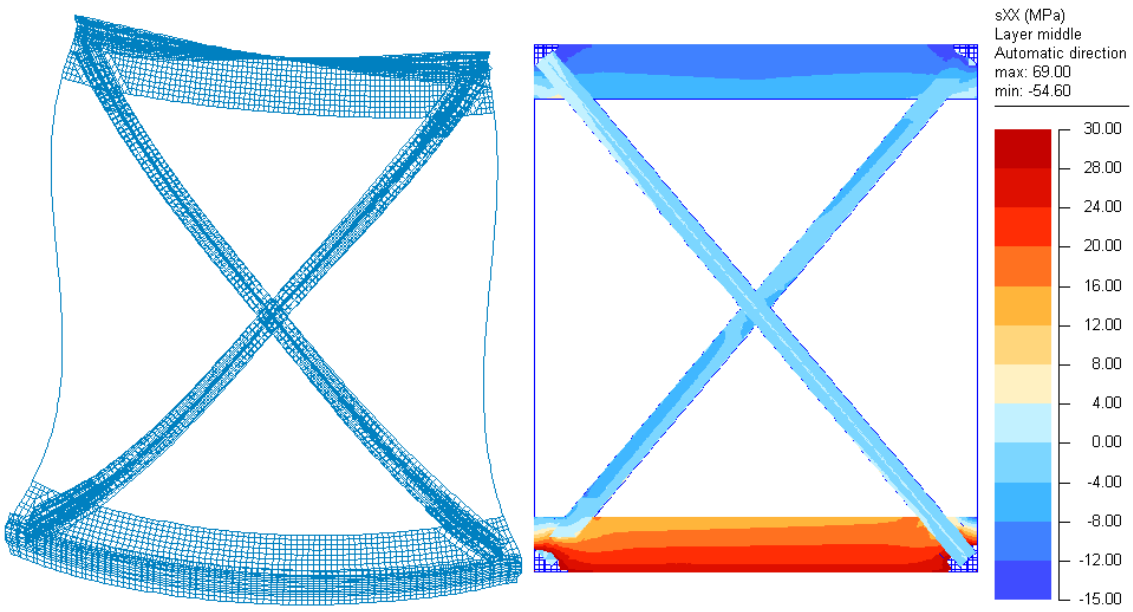

(a) (b)

Figure 7.34 - Results provided by the Sub-model C2 for the static load case 5 (test code 25SCU): (a) deformed shape; (b) longitudinal normal stresses.

Strains of the upper deck upper chords

The experimental and numerical results obtained for representative sections of the upper chords of the upper deck are presented in Figure 7.35. In general, the conclusions drawn for the lower chords strains are also valid for these elements, being the most relevant the fact that numerical estimates provided by the sub-models have a better correlation with the field data than the predicted values of Model B.

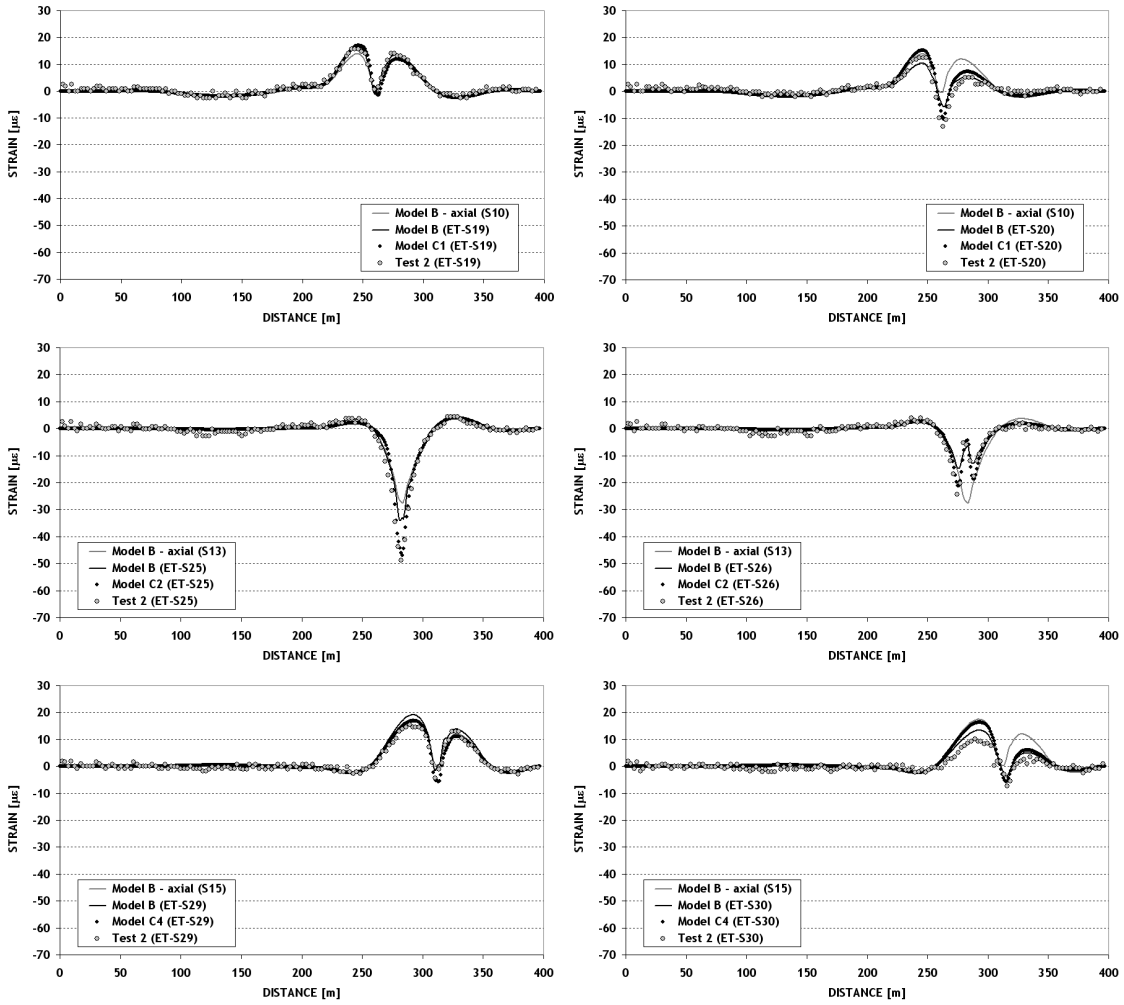

Figure 7.35 - Influence lines for the steel strains in the upper chords of the upper deck (Test 2).

The deformation of the flanges matches the axial strain estimated by Model B for sections located in panels close to the supports (sections S10 and S15). However, for the section in the mid-span panel the results deviate significantly (section S13). With respect to the deformation of the webs, the experimental strains are considerably different from the estimates provided by Model B. In particular, the plots are completely different in the regions of the highest magnitude for section S13. For this section, it is clearly perceptible that the section deformation holds two main components.

The first is caused by the axial force acting in the element as a result of the upper deck bending, and therefore it translates a global behavior. The second is produced by the upper chord bending that takes place when the loads are applied within the panel, which can be regarded as a local behavior and was not initially foreseen. This bending of the upper chord increases the compressive deformation of the flange and decreases the deformation in the web, and may even induce tensile strains as recorded during the tests for sections S1 and S8, located at the middle of spans 2 and 10, respectively, whose influence lines are presented in Figure 7.36.

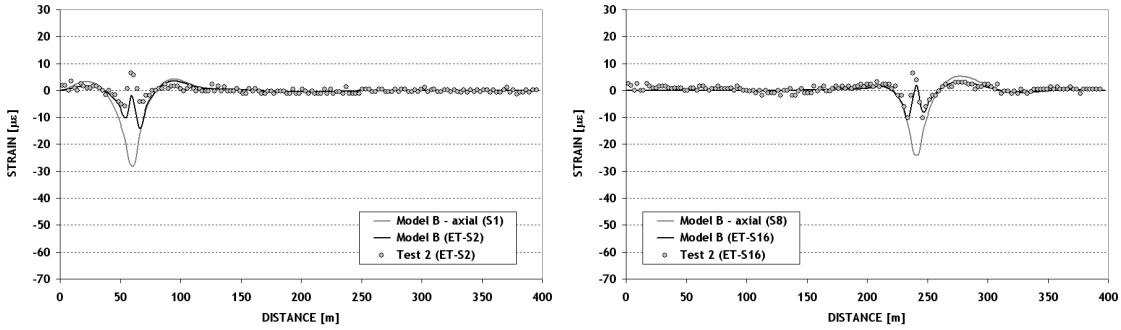

Figure 7.36 - Influence lines for the flange strains in sections S1 and S8 (Test 2).

Figure 7.37 shows the structural elements located at the level of the upper chords and their connections with the purpose of preventing their instability by bending. The main stringers are connected to the upper chords at the middle of the panel through angles (inner stringers) and gusset plates (outer stringers). However, when loads are applied to the stringers some part of the load is transferred to the upper chords through the bracing system causing bending in those elements. This behavior is enhanced by the stiffness of the connection as the proximity of the stringers to the upper chords increases. For the monitored sections the upper chord bending exhibited a higher impact in the mid-span panel than in the support panels as a consequence of the following reasons:

i. At the supports the vertical is very stiff in the plane of the girder;
ii. The free length of the upper chords is smaller in the panels near the supports; and
iii. The instrumented sections in the support panels are close to the stiff verticals (see Figure 7.13).

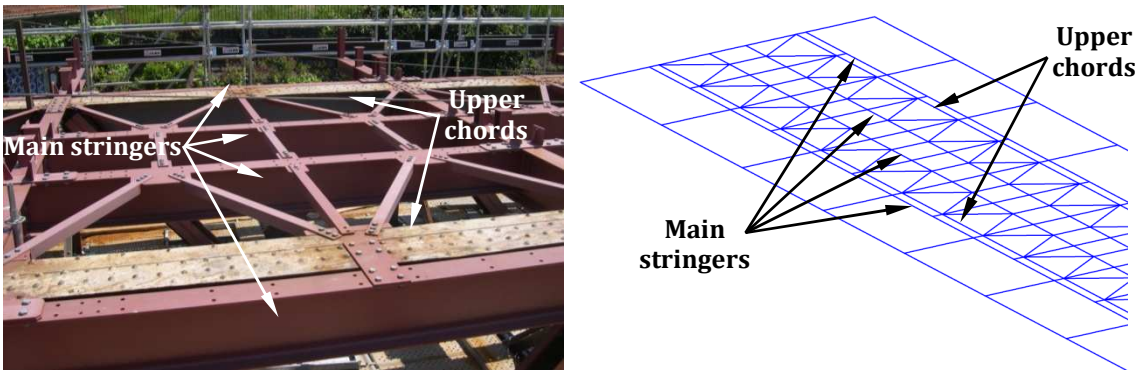

(a) (b)

Figure 7.37 - Structural system at the upper level of the upper deck: (a) view of the upper deck before the installation of the new floor system; (b) partial view of Model B for the same region.

Strains of the upper deck diagonals

The strains measured and estimated for the instrumented sections of the upper deck diagonals are depicted in Figure 7.38. For this analysis two sets of cross-sections are selected, one in which the strain gages are attached to the flanges of the original T section (sections S22 and S24), and the other in which the cross-sections were instrumented in the strengthening angles applied to the web free end (sections S21 and S23).

For the first pair the axial force is compressive, and consequently the strains are negative. The readings present a magnitude very similar to the numerical axial strain (Model B – axial), which in turn is close to the numerical estimates at the sensors position (Model B). Therefore, results show a small strain gradient in the alignment of the gages. Furthermore, the values predicted by the sub-models fit perfectly the field data whereas the estimates from Model B deviate in the region of maximum response.

For the second pair of diagonals the obtained results are deeply different. The elements are subjected to tensile axial force so it would be expected to observe positive strains. However, the sign of the readings is negative and their magnitude significant. Moreover, values are very similar for both sensors, showing an apparent uniform distribution of the strains in the cross-section of both diagonals. Note that, the strains measured during the slow crossings confirmed the data collected in the static loadings. Several hypotheses were raised, such as bad execution of the strengthening, inability of this type of strengthening to reduce the stresses/strains, or even a counterproductive effect of the strengthening.

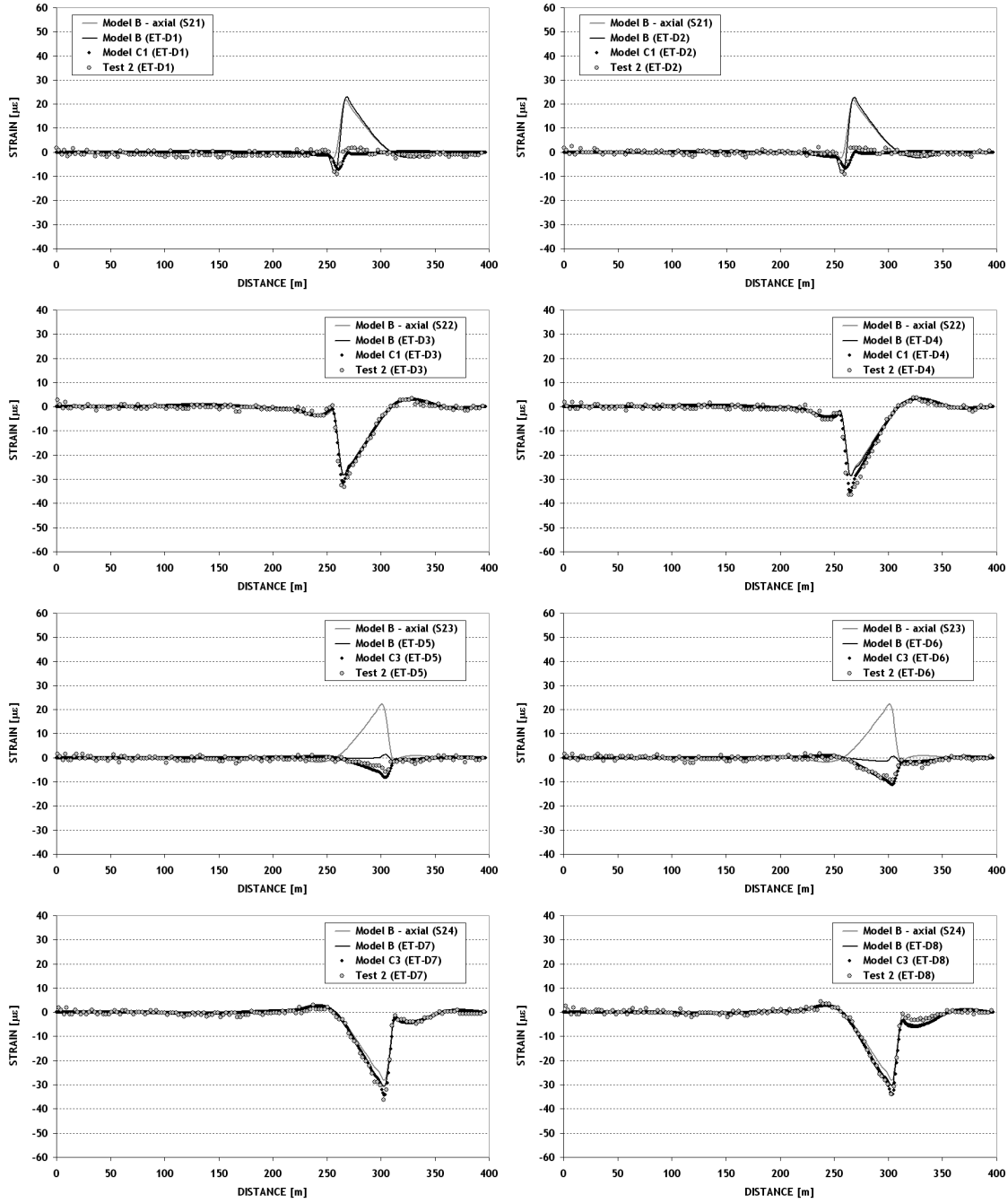

Figure 7.38 - Influence lines for the steel strains in the diagonals of the upper deck (Test 2).

Numerical estimates from Model B indicate that sensors should have captured readings close to the axial strain (section S21) or almost zero (section S23). On the contrary, sub-models supply numerical solutions very close to the measured values. In order to disclose the causes for these results, Figures 7.39 and 7.41 depict 3D views of the normal stresses distribution in the 1st and 12th panels of span 11, respectively, for the static load case 5 (test code 25SCU), with insets showing detailed views at the joints. Figures 7.40 and 7.42 present the elevation of the same panels with the maps of normal stresses for the chords webs, strengthening angles of the diagonals and cover/gusset plates of the joints, as well

as the plan view of the normal stresses distribution throughout the two diagonals. In any of these figures the normal stresses are acting in the longitudinal direction of the elements.

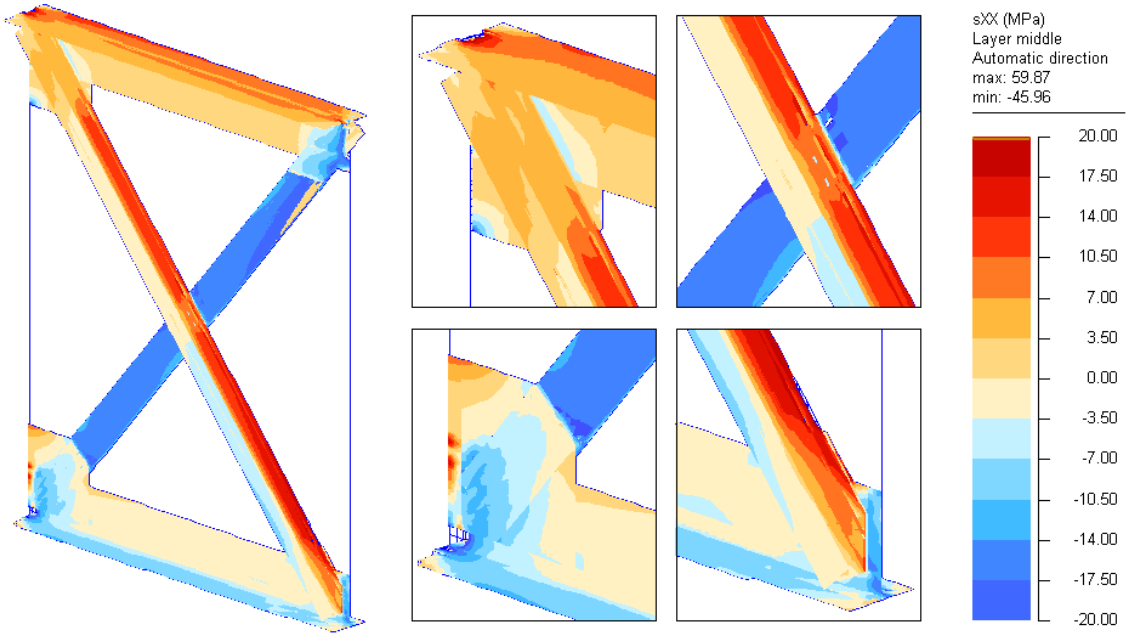

Figure 7.39 – 3D view of the distribution of the normal stresses provided by the Sub-model C1 for the 1st panel of the downstream girder of the upper deck in span 11 during the static load case 5 (test code 25SCU).

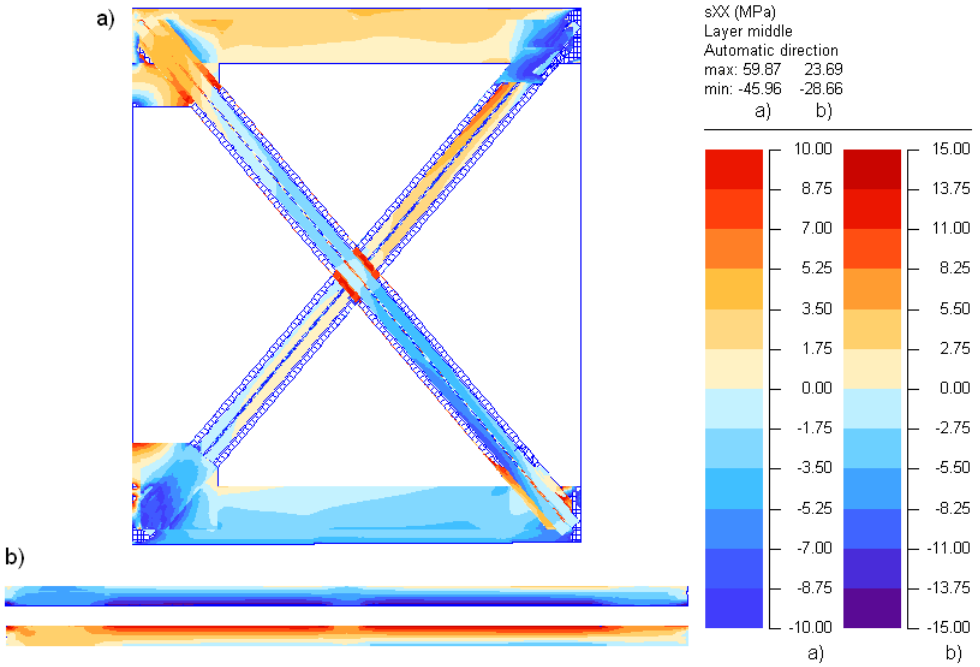

Figure 7.40 - Normal stresses provided by the Sub-model C1 for the 1st panel of the downstream girder of the upper deck in span 11 during the static load case 5 (test code 25SCU): (a) elevation; (b) projected view of the diagonals.

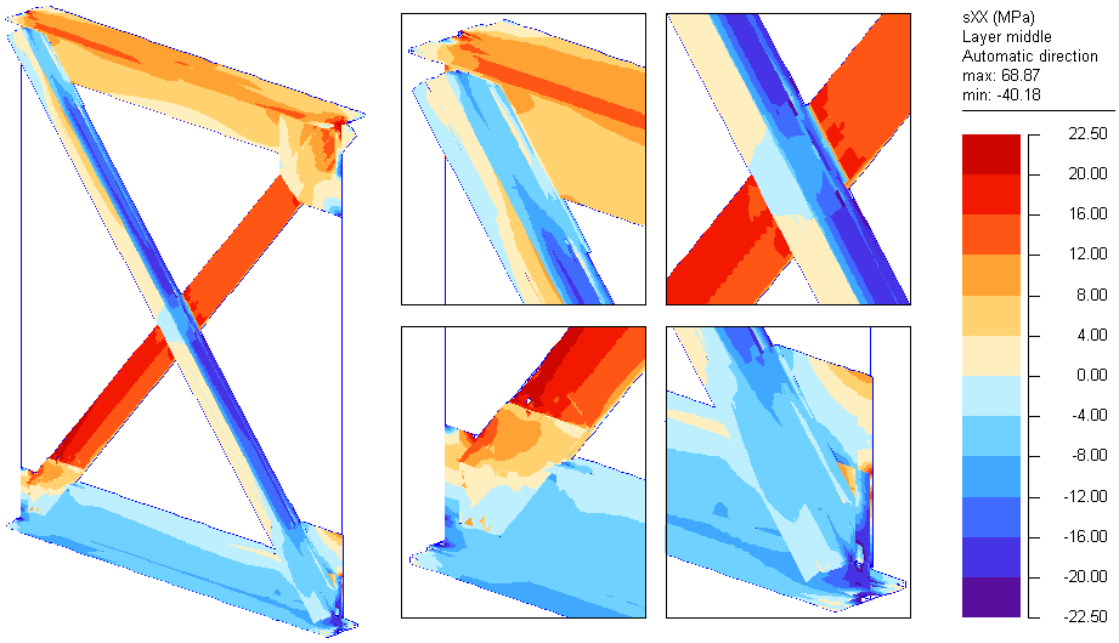

Figure 7.41 - 3D view of the distribution of the normal stresses provided by the Sub-model C3 for the 12th panel of the downstream girder of the upper deck in span 11 during the static load case 5 (test code 25SCU).

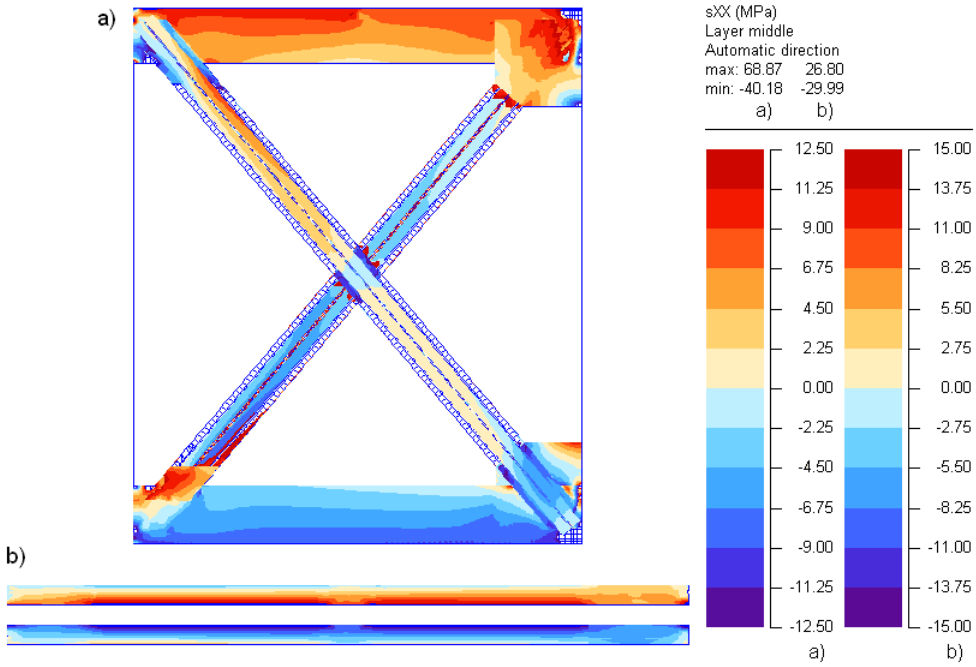

Figure 7.42 - Normal stresses provided by the Sub-model C3 for the 12th panel of the downstream girder of the upper deck in span 11 during the static load case 5 (test code 25SCU): (a) elevation; (b) projected view of the diagonals.

These numerical results clearly show that the load in the diagonals is mainly transmitted throughout the flange of the original T cross-section, and only a small part is carried by the web in a region close to the flange. Moreover, the strengthening angles of the web reveal a

level of stress much lower, and in some regions even of opposite sign. In this way, the existence of a huge transverse strain gradient caused by the load eccentricity in the diagonals is disclosed. This eccentricity is a direct consequence of the equilibrium of forces at the joints that has to take place in the plane of the chords webs, given that the connection between the chords and the diagonals is established through the T-flange (see Figure 7.51). This fact is proven by the stress flow at the diagonals ends.

In order to experimentally validate these findings, the diagonal comprising section S23 was instrumented with four additional electric strain gages in a near section. Two sensors were placed in the same relative position as the fiber optic sensors ET-D5 and ET-D6, referred to as SG3 and SG4, respectively, and the other two sensors were applied to the flange of the original T section, identified as SG1 and SG2. The instrumentation of the monitored diagonal is depicted in Figure 7.43.

(a) (b)

Figure 7.43 - Instrumentation of the tension diagonal holding section S23: (a) attachment of the electric strain gages to the strengthening angles of the section's web; (b) detailed view of the diagonal equipped with the fiber optic sensors (ET-D5 and ET-D6) and the electric strain gages (SG3 and SG4).

Figure 7.44 shows the continuous record of the strains collected by the four electric sensors and the two fiber optic sensors during a passage of a train of two vehicles in the downstream track. The electric and fiber optic sensors located in the same position measured the same compressive deformation in the strengthening angles, whereas the strain gages in the flange captured positive strains of much higher magnitude.

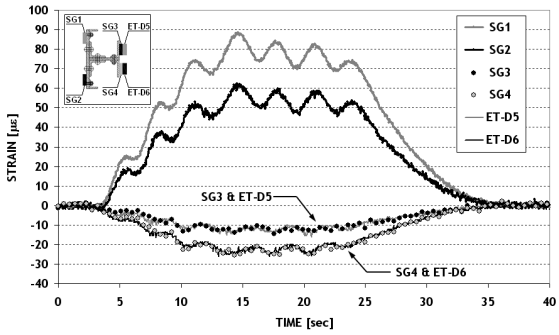

Figure 7.44 - Strain records collected by the sensors during the crossing of a train with two vehicles in the new service period.

In addition to the high transverse bending the diagonal also exhibits a significant in-plane bending. This bending impacts differently on the pairs of sensors located in the flange and in the strengthening angles, showing a higher influence on the angles, i.e. the deviation of the readings collected by sensors ET-D5(SG3) and ET-D6(SG4) from their average value is much higher than that of the strains acquired by sensors SG1 and SG2. This is due to the increase of bending in the angles generated by the warping torsion of the diagonal. These results clearly indicate that the safety evaluation of the diagonals must be mandatorily performed by taking into account the load eccentricity of the bars.

Strains of the upper deck crossbeams

The strains measured by the sensors applied to the crossbeam in the middle of span 12 during the quasi-static loadings are presented in Figure 7.45, in which the numerical plots supplied by Model B are overlapped to enable the analysis of the results. The response very localized of the crossbeam and the low acquisition frequency of the readings has resulted in a density of measurements less adequate to accurately capture the strain peaks. Nevertheless, the results collected from both slow crossings produced maximum values very similar for each sensor, with an error tendentially larger for the most sensitive sensors (ET-C3 and ET-C4).

The influence lines estimated by Model B compare well with the readings collected by the strain gages installed at the end sections (S25 and S27). However, for the mid-span section of the crossbeam (S26) strains diverge enormously. Figure 7.46(a) shows the exact location of the strain gages in the upper deck cross-section. These results are qualitatively very different from the measurements taken during the static loadings, since they reveal a clear improvement of the correlation at the support sections and at the lower flange of the mid-span section. However, the deformation measured in the upper flange of the mid-span section is much higher than the numerical estimate, in opposition to the data collected in

the most severe static load case (see Table 7.9). The general improvement of the correspondence between the field data and the numerical estimates in the quasi-static tests is easily explained by the importance of the vehicles positioning when loading structural elements whose response is very localized.

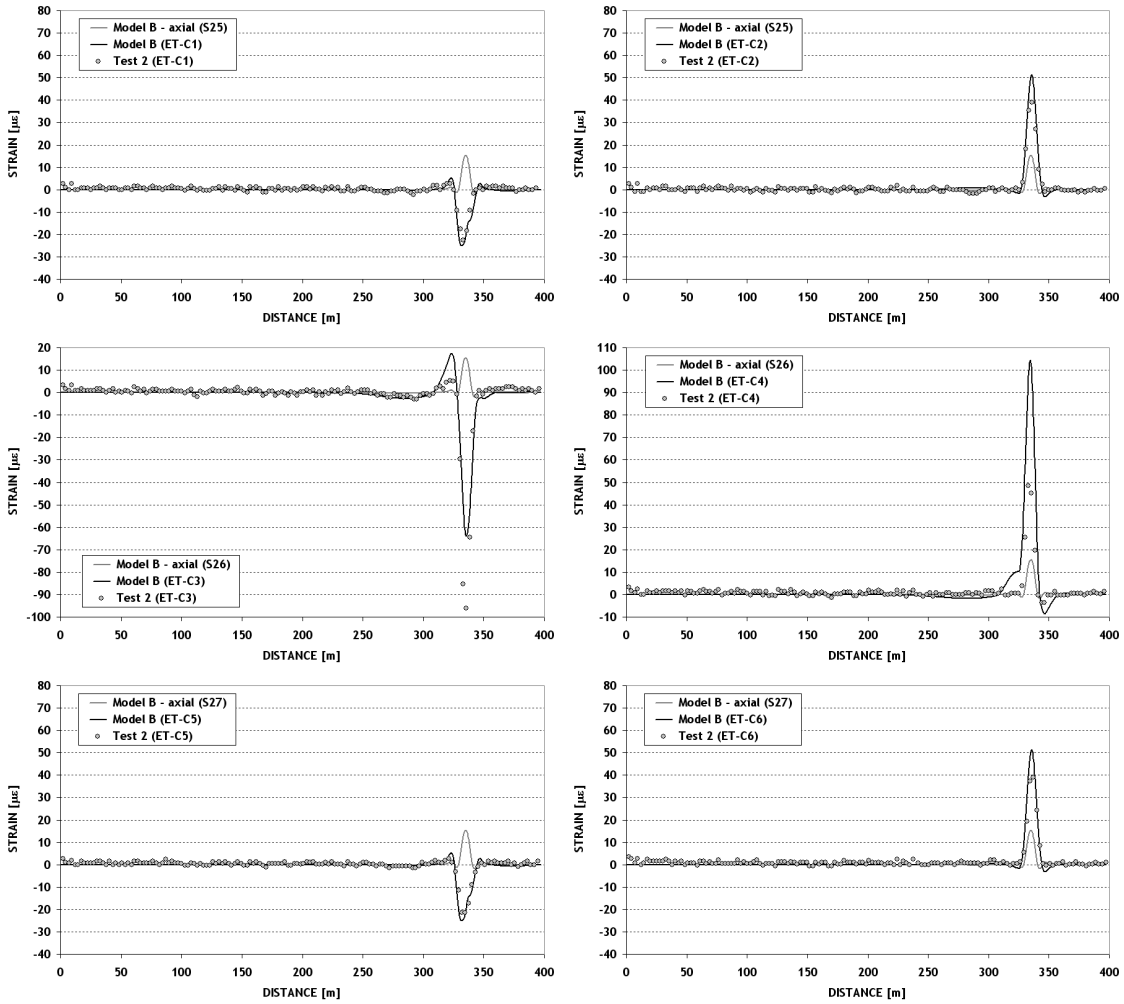

Figure 7.45 - Influence lines for the steel strains in the upper deck crossbeam located in the middle of span 12 (Test 2).

One major aspect that stands out from the experimental results is the difficulty in interpreting the strains measured in the mid-span section. The compression of the upper flange is nearly twice the tension of the lower flange, a difference that cannot be attributed to the existence of a high compressive axial force since the corresponding deformation is small and positive (see Figure 7.45). Figure 7.46(b) shows the axial force and bending moment diagrams of the crossbeam estimated by Model B for the static load case 4 (24SCU). The relative proportion of the numerical strains at the sensors positions for this load case is very similar to that of the peak strains numerically estimated for the slow crossings.

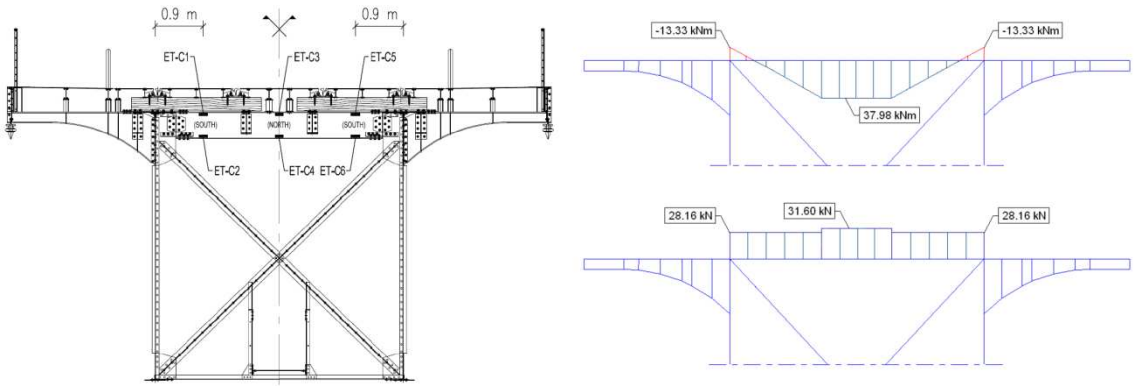

(a) (b)

Figure 7.46 - Upper deck crossbeam at the middle of span 12: (a) location of the strain sensors; (b) bending moment (top) and axial force (bottom) diagrams estimated from Model B for the static load case 4 (test code 24SCU).

Given the baffling nature of the results obtained for section S26 from the field test, a comparison with the readings collected by the sensors under the new service conditions, two years after the reopening of the upper deck, is carried out. To this end, the combined properties of the upper deck cross-section symmetry and sensors positioning were used to extract the relevant data from the non-centered crossings of the trains. In this way, the monitoring results could be compared with the measurements taken during Test 2 for centered loadings. Moreover, in order to reduce the measurement errors 20 crossings were considered, 10 in each direction. Table 7.14 lists the strain peaks normalized with reference to the strain in sensor ET-C4 for the results from the quasi-static loading scenarios of Test 2, for the corresponding numerical estimates, and for the monitoring data collected two years after the bridge rehabilitation.

Table 7.14 – Normalized maximum strains for the mid-span crossbeam of span 12.

		Sensors					
Description	Test code	ET-C1	ET-C2	ET-C3	ET-C4	ET-C5	ET-C6
Test 2 results	220QCU	-0.46	0.80	-1.98	1.00	-0.44	0.80
	221QCU	-0.39	0.73	-2.06	1.00	-0.44	0.74
Numerical estimates	220QCU & 221QCU	-0.26	0.49	-0.61	1.00	-0.24	0.48
Monitoring results	In service	-0.24	0.40	-0.88	1.00	-0.28	0.47

Observations: values are normalized with reference to the strain in sensor ET-C4; the monitoring results were collected two years after the bridge rehabilitation.

Although in the new service conditions sensor ET-C3 measures compressive strains higher than the numerical estimates, for the remaining sensors the results are very similar. On the contrary, in spite of the fact that both slow crossings have produced similar

measurements, the test data clearly deviate from the monitoring results. In light of this information it can be concluded that the behavior of the crossbeam has experienced significant changes in the first two service years, and that the monitored service response of the crossbeam can be properly simulated by the reference Model B.

A likely reason for the behavior identified in the field test may be associated to the steel cladding plates and secondary stringers of the new upper deck floor system (see Figure 7.22). When the field test was carried out all steel elements pertaining to the floor system were properly assembled through bolted connections. However, two years of service later a generalized loosening of the bolts connecting the plates to the secondary stringers had been identified, and a large number of bolts were even missing or broken. This fact may have significantly altered the load path in the transverse direction of the upper deck, leading to a structural behavior similar to that of the numerical model.

Strains of the arch and piers

In general, strains measured in the arch and piers elements fairly agree with the numerical influence lines, as can be seen in Figures 7.47 and 7.48. These plots present characteristic results of the measurements taken from the monitored cross-sections. For almost all elements experimental data revealed the existence of negligible strain gradients, which was also confirmed by the numerical analysis through the comparison of the axial strains with the estimates provided by Model B. However, once more, in section S42 the sensors recorded strain peaks significantly different in magnitude. At last, it is worth mentioning that sensors in sections S56 and S57, located at the feet of the pier P3 legs, measured similar maximum strains, in contrast with the results that had been collected in the static loadings. Therefore, the existence of significant friction in the upper deck bearings over pier P3, or their malfunction, could not be confirmed.

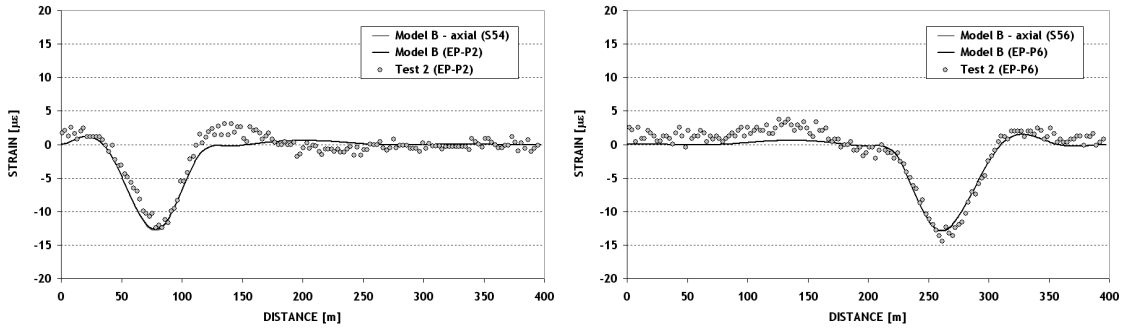

Figure 7.47 - Influence lines for the steel strains in arch and piers elements (Test 2) (I).

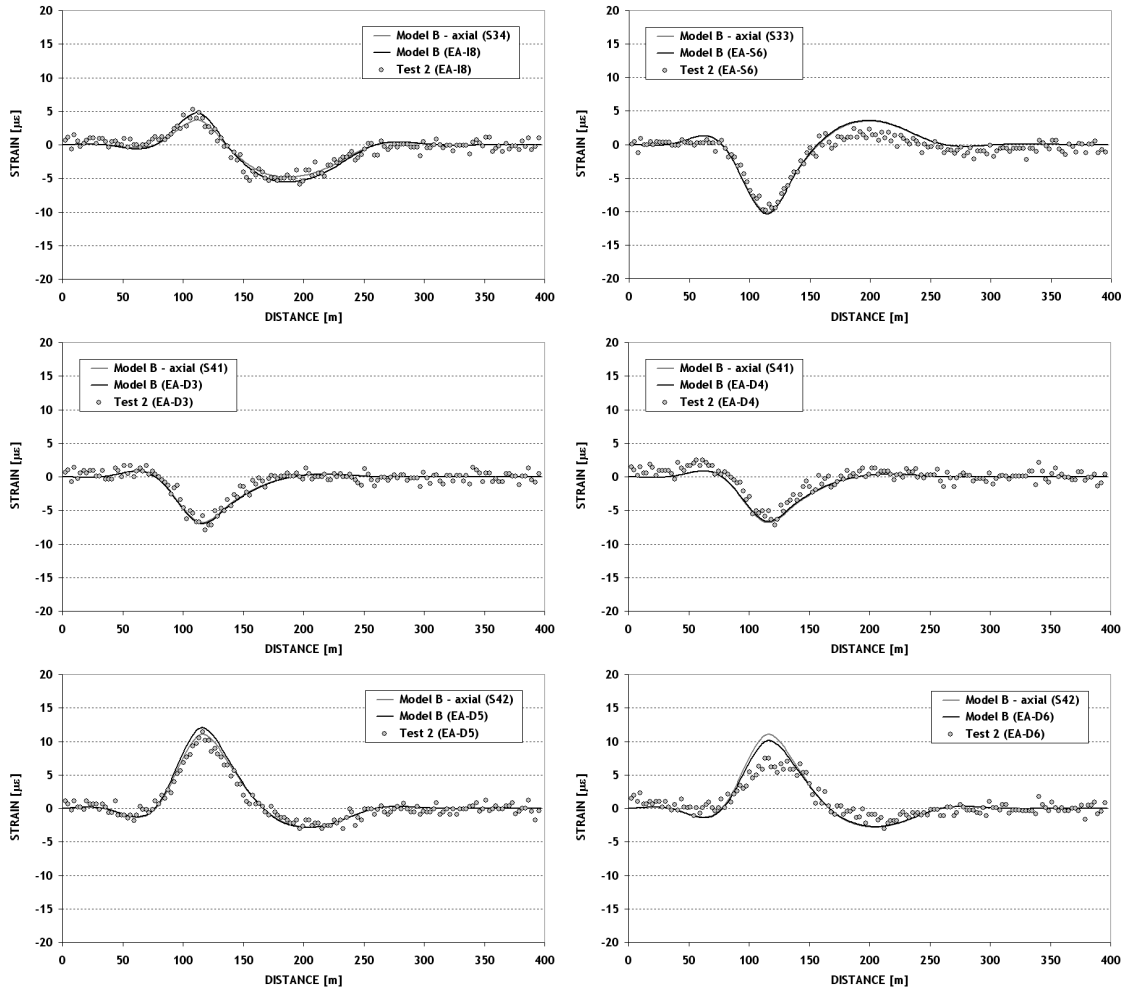

Figure 7.48 - Influence lines for the steel strains in arch and piers elements (Test 2) (II).

7.6.2.3. Experimental evaluation of the bridge rehabilitation

In order to enable the experimental comparison of the influence lines recorded during the slow crossings carried out in both field tests, Figures 7.49 and 7.50 depict the equivalent strains for the crossing of a pair of vehicles with a total gross weight of 100 kN, in cross-sections of the arch and upper deck elements, respectively.

The strains in the arch chords (EA-I8 and EA-S6) reveal that the level of maximum deformation was kept almost unaltered, pointing to an average reduction lower than 3.7 %, hence validating the data extracted from the static loadings (see section 7.6.1.4). With respect to the monitored arch diagonals, both elements experienced a decrease of the deformation, in average of about 19.1 % and 19.7 % for sections S41 and S42, respectively. While for the first diagonal the reduction is in line with the estimation provided by the static testing, the data for the second diagonal show a much larger decrease of the deformation. If in the first case the result is a consequence of the applied strengthening, the outcome for the second diagonal can only be explained by a variation in

the load path inside the statically indeterminate arch produced by the rehabilitation works.

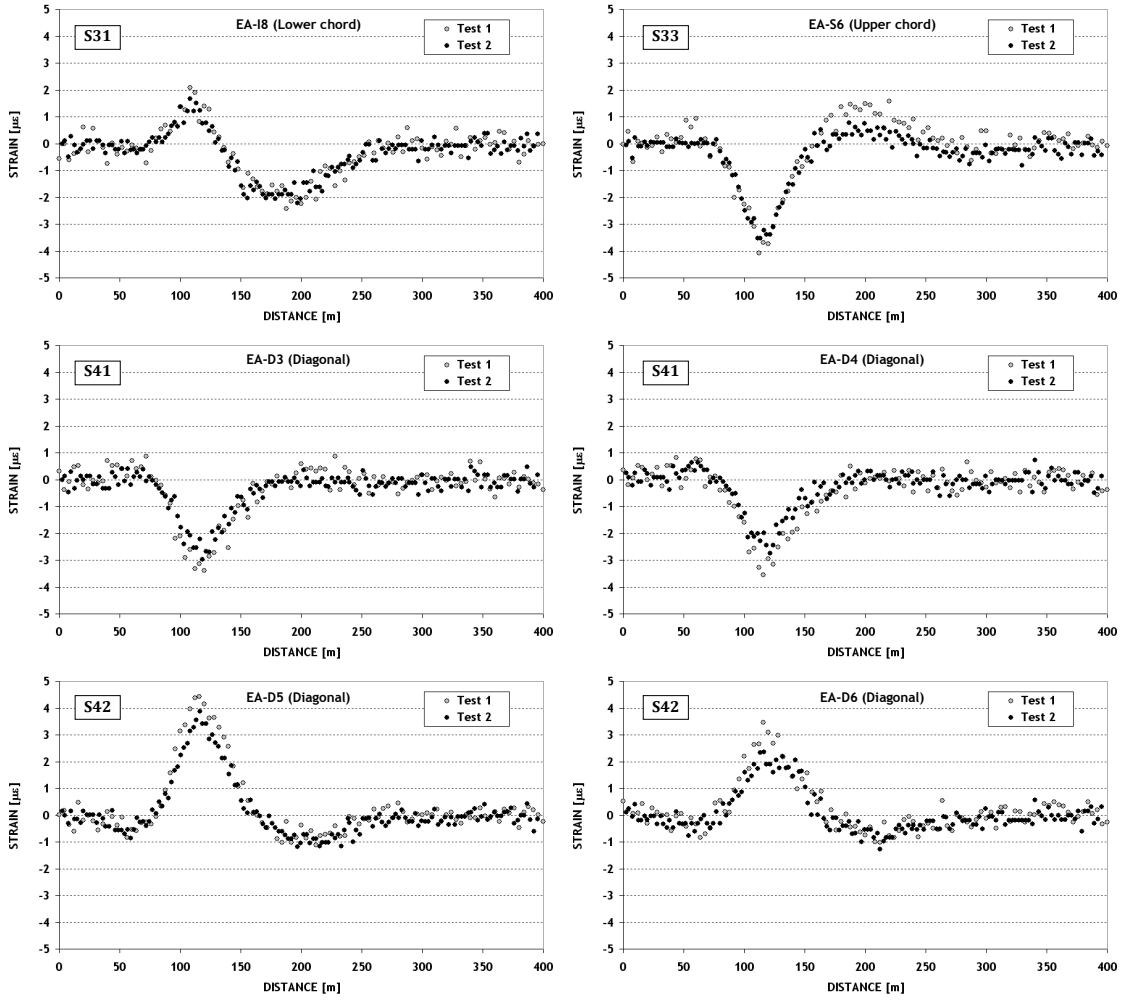

Figure 7.49 - Experimental influence lines of the steel strains in arch elements before and after the bridge rehabilitation.

The experimental influence lines of the lower chords of the upper deck show a decrease of the maximum deformation in the webs higher than 30 %, concomitantly with a small decrease or a slight increase of the deformation in the flanges. These results indicate an increase of the strain gradients in the bars, but also point to a level of acting force very similar in both tests since the most part of the load is carried by the flange.

With respect to the upper deck diagonals, for section S23 the comparison cannot be made, since it was instrumented with gages in different positions. As it was previously pointed out the diagonals hold an important component of transverse bending deformation that prevents the direct comparison of the measurements taken from this section. From the strains collected in section S24 an average reduction of the deformation close to 17 % can be inferred, a value slightly lower than that estimated by the static loadings. Although the

main strengthening of the diagonals was performed by attaching two angles of large cross-sectional area to the web free end of the original T cross-section, two other small angles (with half cross-sectional area) were applied to the flange, one in each end, and duly connected to the chords webs through riveting as depicted in Figure 7.51. Therefore, taking into account the findings previously presented for the main strengthening angles, the two angles attached to the flange of the T cross-section were responsible for the reduction of its level of deformation.

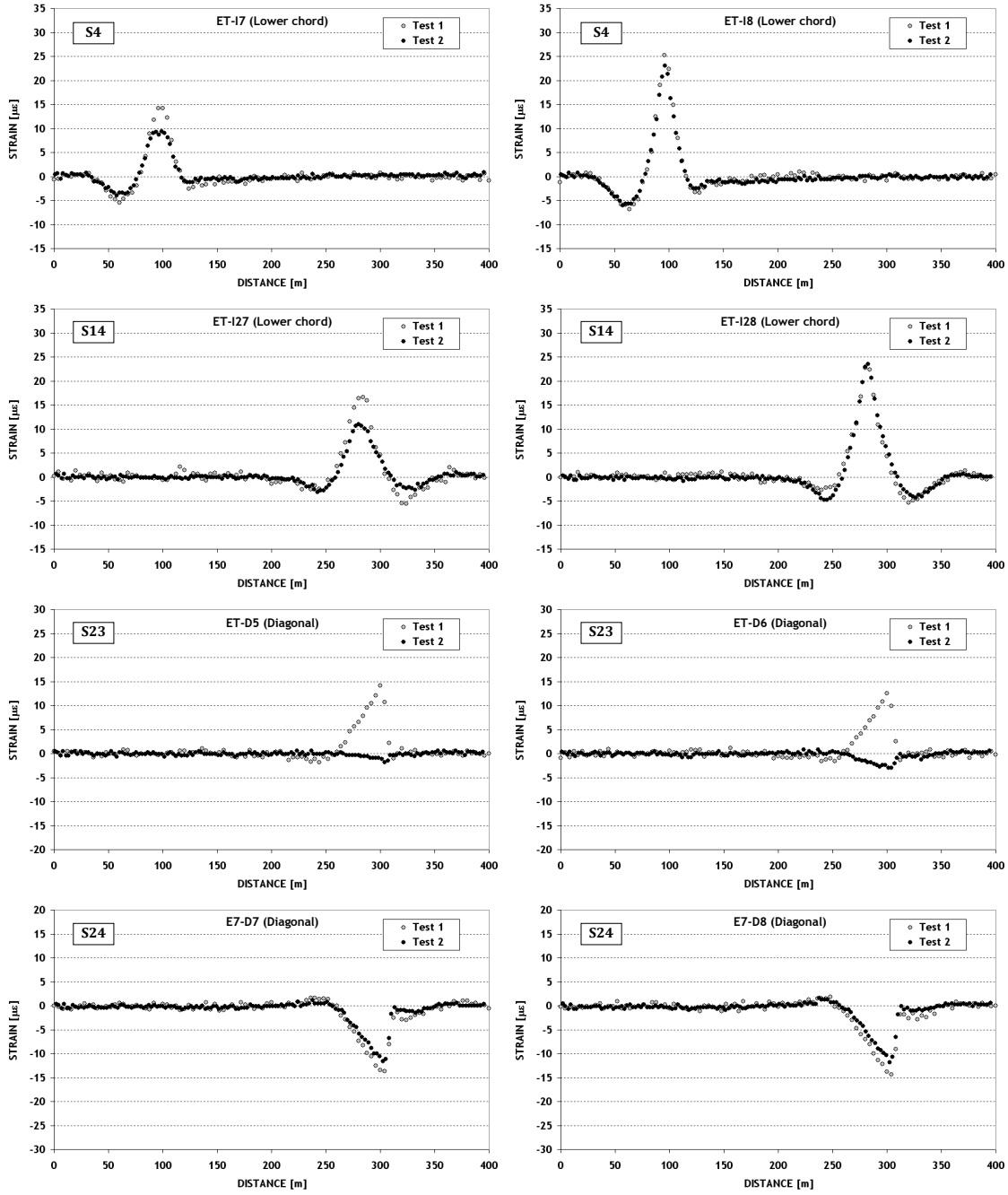

Figure 7.50 - Experimental influence lines of the steel strains in upper deck elements before and after the bridge rehabilitation.

(a) (b)

Figure 7.51 - Strengthening of an upper deck diagonal: (a) detailed view of an upper joint over a girder support; (b) detailed view of a lower joint.

7.7. Safety assessment of the bridge

7.7.1. Introduction

Test 2, conducted after the completion of the rehabilitation works and before the reopening of the upper deck to the traffic, has enabled the collection of field data from the actual response of the structure, and therefore made possible a suitable update of the numerical model developed to simulate the bridge behavior for the new service conditions. Hence, given that this enhanced model is more reliable than that of the rehabilitation design, its use to obtain accurate estimates of the safety parameters stands out as a pertinent and useful task. Furthermore, it may allow the identification of unexpected critical aspects, as well as to devise and implement the appropriate measures for their correction or prevention.

7.7.2. Ultimate limit states

The assessment of the ultimate limit states was performed only with the internal forces and moments of the bars that generate normal stresses in the material. Therefore, shear forces and torsion were not taken into account in this analysis. The design values of the forces and moments induced by the several actions were calculated by the following expression

$$E_d = m\acute{a}x\begin{cases}\gamma_g \cdot G_{dl} + \gamma_w \cdot Q_w + \gamma_{q,1} \cdot \psi_0 \cdot Q_{ll} + \gamma_{q,2} \cdot \psi_0 \cdot Q_{SV} \\ \gamma_g \cdot G_{dl} + \gamma_w \cdot \psi_0 \cdot Q_w + \gamma_{q,1} \cdot Q_{ll} + \gamma_{q,2} \cdot Q_{SV}\end{cases} \quad 7.1$$

where G_{dl} is the characteristic force or moment generated by the permanent loads, Q_w is the characteristic force or moment caused by the wind, Q_{SV} is the characteristic force or moment due to the design train in the upper deck, and Q_{ll} is the characteristic force or moment induced by the remaining variable actions, which comprise road traffic loads at the lower deck and pedestrian loads on both decks. The combination factors, ψ_0, and the partial safety factors γ_w, $\gamma_{q,1}$ and $\gamma_{q,2}$, for the wind, variable and train actions, respectively, were adopted according to the Portuguese national code (RSAEEP, 1983), whereas the safety factor for the permanent actions, γ_g, was considered as established by the Eurocode 0 (EN1990-prAnnexA2, 2003). The values are listed in Table 7.15.

Table 7.15 – Values for combination factors and partial safety factors.

Loads	ψ_0	γ_g	γ_w	$\gamma_{q,1}$	$\gamma_{q,2}$
Self-weight	---	1.35	---	---	---
Remaining dead loads	---	1.35	---	---	---
Road live load at the lower deck	0.6	---	---	1.5	---
Pedestrian live load at the lower deck	0.6	---	---	1.5	---
Rail live load at the upper deck	0.8	---	---	---	1.5
Pedestrian live load at the upper deck	0.8	---	---	1.5	---
Wind	0.4	---	1.5	---	---

The characteristic forces and moments ascribed to permanent loads were evaluated by assuming the bridge fully loaded at once in its final structural scheme. This option was taken due to two main reasons:

i. Lack of detailed information related to the original construction process;
ii. Extreme difficulty in assessing the forces redistribution among the structural elements, as a result of the interventions carried out in the bridge during its life, namely the last one that enabled the integration of the upper deck into the metro network.

For this study the pedestrian and road traffic actions at the lower deck were assumed with the values and arrangements established by Portuguese national code (RSAEEP, 1983) for class I bridges, whereas the pedestrian loads at the upper deck correspond to the actions prescribed by the same code for rail bridges. The quantification of the characteristic wind loads followed the procedure adopted in the viability study, which consisted in estimating the reference values through the Portuguese national code (RSAEEP, 1983) factored by a

suitable reduction coefficient for long structures, stipulated by the guidelines of the Belgium Institute for the Standardization (IBN) (Coelho *et al.*, 1996). With respect to the design train the axle loads were considered as extreme (see Table 7.16), with the geometry depicted in Figure 7.52. In order to induce the maximum bridge response either single or double trains, with one or two vehicles, were considered.

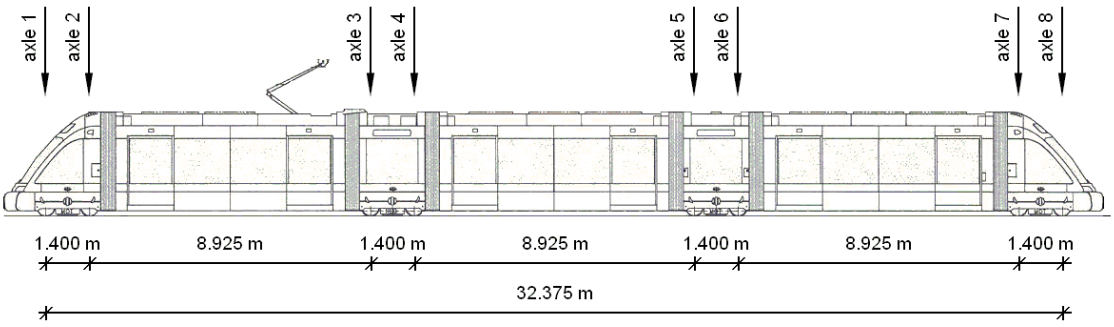

Figure 7.52 - Standard vehicle of the train considered in the safety assessment.

Table 7.16 – Axle loads for the metro vehicle under different service conditions (kN).

Axle	*Self-weight*	*Light load*	*Normal load*	*Heavy load*	*Extreme load*
1	42.7	48.8	52.5	56.1	60.0
2	42.7	48.8	52.5	56.1	60.0
3	56.7	72.8	83.2	93.6	110.0
4	56.7	72.8	83.2	93.6	110.0
5	56.7	72.8	83.2	93.6	110.0
6	56.7	72.8	83.2	93.6	110.0
7	42.7	48.8	52.5	56.1	60.0
8	42.7	48.8	52.5	56.1	60.0
Total	397.5	486.4	542.5	598.6	680.0

The resistance capacity of the structural members was calculated according to the specifications in Eurocode 3 (EN1993-1-1, 2005) for two different scenarios. Firstly, for members in which the axial forces are predominant the bending resistance was determined assuming the non-existence of any instability. With respect to the resistance to axial forces, buckling was considered for elements under centered compressive loading. Secondly, for members subjected to large bending moments and small axial forces, the resistance capacity to bending was calculated taking into account the lateral-torsional buckling and the resistance capacity to axial load not affected by any instability phenomenon.

The design resistance values for non-strengthened members were estimated on the basis of the yield strength, σ_{rd}, experimentally determined from samples extracted from the bridge during the execution of the viability study (Coelho *et al.*, 1996). For elements entirely made of modern steel the yield strength was defined from the material specifications according to Eurocode 3 (EN1993-1-1, 2005). As regards the strengthened elements the resistance capacity was estimated as the maximum carrying force or moment for which either the original or modern steel reached the yielding point. The design resistance of all members was performed by considering the properties of the gross cross-section and an elastic distribution of stresses across the cross-section (Class 3 sections).

The safety factors for the structural elements were calculated through the following expression

$$S.F. = \frac{N_{Ed}}{N_{Rd}} + \frac{M_{y,Ed}}{M_{y,Rd}} + \frac{M_{z,Ed}}{M_{z,Rd}} \qquad 7.2$$

where N_{Ed}, $M_{y,Ed}$ and $M_{z,Ed}$ are the design values of the axial force, bending moment about the strong axis and bending moment about the weak axis, respectively, and N_{Rd}, $M_{y,Rd}$ and $M_{z,Rd}$ are the corresponding design resistances. A safe condition of an element is translated by a safety factor lower than 1.

Two scenarios were studied in the safety analysis. In the first, only the prevailing axial force or bending moment was taken into account, a procedure that had been also adopted both in the viability study and in the rehabilitation project. In the second scenario, both the axial force and bending moments were considered in the estimation of the safety factor.

Particular attention was given to the upper deck diagonals. In light of the results obtained from the field tests, these elements are subjected to a high transverse bending induced by the eccentricity of the axial load. Therefore, the safety of the diagonals was also assessed taking into account this fact, and the safety factor became the ratio between the design axial force acting in the bar, P, and the maximum eccentric load that can be carried by the bar under non-linear geometric behavior, P_{max}, as schematically described by Figure 7.53 and mathematically translated by Equations 7.3 and 7.4. The ultimate load P_{max} is obtained when the stress at the extreme fibers reaches the yield strength of the material, a condition that is translated by Equation 7.5.

$$\delta = e \cdot \left[sec\left(\frac{\pi}{2} \cdot \sqrt{\frac{P}{P_E}} \right) - 1 \right] \qquad 7.3$$

$$M_{max} = P \cdot (\delta + e) \tag{7.4}$$

$$f_y = P_{max} \cdot \left[\frac{1}{A} + \frac{e \cdot c}{I} \cdot sec\left(\frac{\pi}{2} \cdot \sqrt{\frac{P_{max}}{P_E}} \right) \right] \tag{7.5}$$

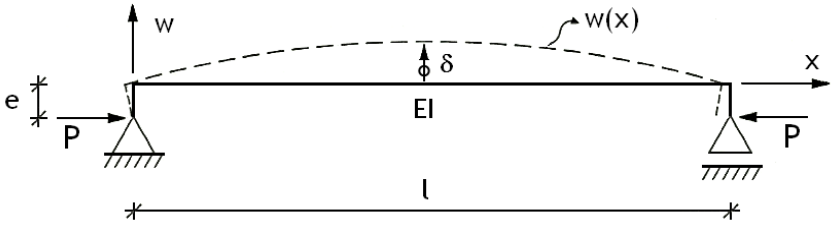

Figure 7.53 - Non-linear geometric behavior of a bar subjected to an eccentric compressive load P.

In Equations 7.3 to 7.5, δ is the camber of the bar, e is the eccentricity of the load, P_E is the Euler critical load, M_{max} is the bending moment at mid-span, A and I are the cross-sectional area and inertia, c is the distance perpendicular to the bending axis from the most stressed fiber to the center of gravity of the cross-section, and f_y is the yield strength of the material.

Table 7.17 – Safety factors for the ultimate limit states with respect to normal stresses.

	Element	*S. F. (1)*	*S. F. (2)*		*Element*	*S. F. (1)*	*S. F. (2)*
Arch	Upper chords	0.50	0.75	Lower deck	Upper chords	0.70	1.10
	Lower chords	0.41	0.56		Lower chords	0.39	1.59
	Diagonals	0.73	1.27		Diagonals	0.53	1.55
	Verticals	0.35	0.72		Verticals	0.14	1.29
	Cross bars	0.86	3.72		Crossbeams	1.14	1.37
	Bracing	0.97	1.31		Crossbeams (S. ties)	2.24	2.76
Piers	Legs	0.68	1.17		Stringers	0.45	0.47
	Diagonals	0.07	0.43	Upper deck	Upper chords	0.36	0.61
	Cross bars	0.77	0.94		Lower chords	0.72	1.12
Suspension ties	Legs	0.59	1.34		Diagonals	0.83/1.35[a]	1.06
	Diagonals	0.31	0.64		Verticals	0.31	1.05
	Cross bars	0.26	1.01		Crossbeams	0.33	0.75
	Cross bars (arch)	0.43	0.81		Stringers	0.32	0.35

S.F. (1) – Computed using only the mandatory internal axial force or bending moment; S.F. (2) – Computed taking into account the axial force and the bending moments; [a] Computed based on the non-linear geometric behavior of a column under eccentric axial load.

Table 7.17 lists the safety factors calculated for the several structural elements of the bridge. In general, for the substructures targeted in the rehabilitation project (arch, piers, suspension ties and upper deck) the safety is verified by a large amount when only the prevailing axial force or bending is considered. However, for some cross-bars and sway bracing elements of the arch the safety margin is significantly lower. Among the arch cross-bars the critical elements are those that support the upper deck, whereas the extreme forces generated in the sway system are caused by the wind loading, a result that had also been found in the viability study.

With respect to the upper deck diagonals, despite of the high value of the parameter, safety is clearly assured if the load is taken as centered. However, when realistically the eccentricity is considered, the safety factor becomes much higher than one, which causes deep concern. It is worth mentioning that after the bridge rehabilitation the average increase of the diagonals cross-sectional area was almost 1.65 times, which was translated into an average increase of the Euler critical load (P_E) of about 3.6 times, and corresponds to an increase of the load capacity (P_{max}) close to 80 %. Nevertheless, although one of the main construction works have been the strengthening of the upper deck diagonals, the level of safety for many of these elements is inadequate.

As regards the lower deck, one has to bear in mind that neither the viability study nor the rehabilitation project, in a first stage, included this substructure of the bridge. Only during the intervention it was decided to perform basic cleaning operations to the deck, as well as to apply a new coating to the steel surface. Nonetheless, this safety study led to the conclusion that a judicious strengthening of the crossbeams near the suspension ties is capable to ensure a safety level in accordance with the modern standards. On the other hand, this safety evaluation was based on the assumption that the resistance capacity of a member would be exhausted when the most stressed fiber would reached the yielding point, thus neglecting any plastic reserve of resistance. Furthermore, the local failure of a crossbeam does not necessary lead to a local or global collapse of the lower deck, since its structural scheme allows some level of forces redistribution (change in the load path).

In the second scenario of the safety evaluation, for which both axial force and bending moments are considered, the obtained results are very different, since for the majority of the most stressed elements of each type the safety cannot be verified, and for many of them by a large amount. This may be caused by the fact that Equation 7.2 holds a linear combination of the three partial safety ratios, equally contributing to the global parameter, which may constitute a very conservative assumption in some cases.

Last but not least, it is important to highlight that for both decks the most critical chords are the elements located at the level opposite to that of the floor system, i.e. the lower chords in the upper deck and upper chords in the lower deck. This points to a significant role played by the floor system in the elastic distribution of the bending induced forces among the elements of the deck cross-section. In addition, particular attention should be paid to these critical chords in the future if any modification to the present service conditions of the bridge is intended, e.g. replacement of the metro trains.

7.7.3. Load rating

Taking into account the characteristics of the traffic in the upper deck for the new service conditions, namely the crossing of vehicles with well-known geometry and axle loads within well-defined bounds, load rating stands as the suitable analysis for the identification of the most sensitive elements to an increase of the traffic loads, that is, the elements that may restrict the passage of heavier vehicles in the future. In fact, an element may have a relatively low safety factor and yet present a low rating factor close to one, as well as the opposite. Therefore, the information provided by the load rating complements the safety evaluation as performed in the previous section.

For this study the adopted standard load model corresponds to a train of one or two vehicles, depicted in Figure 7.52, for an extreme load configuration described in Table 7.16. Rating factors were calculated for each structural element based on the following expression

$$R.F. = min \begin{cases} \left(\sigma_{rd} - \gamma_g \cdot \sigma_{dl} - \gamma_w \cdot \sigma_w - \gamma_{q,1} \cdot \psi_0 \cdot \sigma_{ll}\right) / \left(\gamma_{q,2} \cdot \psi_0 \cdot \sigma_{SV}\right) \\ \left(\sigma_{rd} - \gamma_g \cdot \sigma_{dl} - \gamma_w \cdot \psi_0 \cdot \sigma_w - \gamma_{q,1} \cdot \sigma_{ll}\right) / \left(\gamma_{q,2} \cdot \sigma_{SV}\right) \end{cases} \qquad 7.6$$

where σ_{rd} is the steel strength, σ_{dl} is the stress generated by the permanent load, σ_w is the stress caused by the wind, σ_{SV} is the stress due to the standard train, σ_{ll} is the stress induced by the remaining variable actions. For the elements in which a compressive axial force prevails the steel strength was assumed as the ratio between the design buckling resistance and the cross-sectional area, whereas for members mainly subjected to bending the steel strength was assumed as the stress generated in the steel by the bending moment that causes lateral-torsional buckling.

Rating factors estimated for the critical elements of each type are listed in Table 7.18. For the scenario that considers only the prevailing force or bending moment, the cross-bars on which the upper deck is supported are once more the arch members with the lowest

rating factor. However, the obtained result indicates a significant capacity reserve to carry additional load (more than 50 %). With respect to the piers, the most sensitive members are the transverse bars of the horizontal bracing, and yet the increase of the upper deck traffic loads appears not to be a problem in the future.

Table 7.18 – Rating factors.

	Element	*R. F. (1)*	*R. F. (2)*		*Element*	*R. F. (1)*	*R. F. (2)*
Arch	Upper chords	5.42	2.29	Piers P1 to P3	Legs	3.25	0.86
	Lower chords	5.80	4.74		Diagonals	36.77	4.39
	Diagonals	2.97	-2.66		Cross bars	1.67	1.20
	Verticals	12.95	2.74	Upper deck	Upper chords	5.23	2.92
	Cross bars	1.52	-53.56		Lower chords	1.79	-0.32
	Bracing	6.37	-1.58		Diagonals	1.47/0.47[a]	0.84
Piers M1 and M4	Legs	5.14	-26.23		Verticals	5.69	-2.65
	Diagonals	10.17	3.24		Crossbeams	2.93	1.41
	Cross bars	49.37	5.85		Stringers	3.42	3.17
	Cross bars (arch)	5.70	1.87		Bracing	2.69	-1.21

R.F. (1) – Computed using only the mandatory internal axial force or bending moment; R.F. (2) – Computed taking into account the axial force and the bending moments; [a] Computed for an ultimate compressive strength estimated from the non-linear geometric behavior of a column under eccentric axial load.

As regards the upper deck, the critical members are once more the diagonals. When the load is considered as aligned with the bar axis the load capacity is satisfactory, pointing to an apparent large reserve. However, when the analysis is performed taking into account the actual load path identified in the field tests (eccentric load), the rating factor is drastically reduced for a large number of bars, with some bars presenting values lower than 0.5, which at first sight might seem as unsafe. In light of the results estimated for both safety and rating factors it is extremely important to highlight the following.

During the inspections conducted for the viability study and rehabilitation project, as well as during the construction works, no evidences of any distress in the diagonals were found that could be ascribed to instability problems. More importantly, for the pre-rehabilitation condition the compression diagonals had a much lower buckling resistance and carried higher permanent loads due to the self-weight of the old deck concrete pavement. Therefore, it is possible to conclude that the bridge either was never subjected to the level of loading stipulated by the codes or it has alternative load paths, namely through the tension diagonals, which are mobilized even for low levels of loading.

Another important aspect that stands out from the rating factors of the upper deck elements is the higher sensitivity of the lower chords to an increase of the traffic loads, for which the lowest rating factor is less than 35 % of that of the critical upper chord. This finding confirms the conclusion that had been drawn in the previous section.

Finally, some relevant observations can be inferred from the scenario for which both the axial force and bending moments are considered. The calculated rating factors show negative values for many elements, and even with extreme magnitudes, which might suggest that no live load could be applied to the upper deck. However, these extremely severe factors are not plausible. In fact, the criterion adopted to estimate the rating factors implies a linear elastic behavior of the material up to the maximum load capacity is reached, that is, no reserve of plastic resistance is used. Although might be admissible for a large number of bars, it is not accurate for the members strengthened with angles and plates of modern steel, as is the case of the piers legs supported by the arch.

7.7.4. Fatigue limit state

The fatigue strength of the original steel adopted in this analysis was evaluated through laboratory tests on specimens sampled from the bridge during the viability study (Coelho *et al.*, 1996). The results revealed that the best fitting fatigue curve was that of category D of the AASHTO specifications (AASHTO, 1992), stipulated for elements with riveted connections, which is very similar to the curve of the detail category 71 in Eurocode 3 – Part 1-9 (EN1993-1-9, 2005). The reference value adopted for the fatigue strength was $\Delta\sigma_R = 70$ MPa at 2 million cycles, as proposed by the recommendations of UIC for iron elements of the 19th century (UIC778-2, 1986). The fatigue limit for constant amplitude stress ranges was considered as $\Delta\sigma_D = 52$ MPa at 5 million cycles, and the cut-off limit was taken as $\Delta\sigma_L = 29$ MPa at 100 million cycles.

For the new elements the strength characteristics of the steel for the fatigue analysis were $\Delta\sigma_C = 160$ MPa, $\Delta\sigma_D = 118$ MPa and $\Delta\sigma_L = 65$ MPa, in correspondence to the fatigue strength curve of the detail category 160 established by Eurocode 3 – Part 1-9 (EN1993-1-9, 2005). In the viability study an estimation of the damage accumulation induced by the heavy traffic on the bridge up to its rehabilitation was made for the most stressed element. In practical terms, this result was translated into a consumption of about 11 % of the fatigue life.

The characterization of the traffic considered in this fatigue assessment is described in Table 7.19. The axle loads of the train vehicles are listed in Table 7.16 and the loads geometry is depicted in Figure 7.52. The method adopted in this analysis is based on the Palmgren-Miner rule of cumulative damage provided by Eurocode 3 – Part 1-9 (EN1993-1-9, 2005) for the fatigue life calculation of components under variable loading. According to this rule, when the cumulative damage D of Equation 7.7 is lower than 1 the fatigue safety is assured for the period under consideration. However, taking into account the information obtained in the viability study, the limit for the damage induced in the original steel by the future traffic was considered as 0.89.

$$D = \sum_{i=1}^{n} \frac{n_i}{N_i} \qquad 7.7$$

n_i is the number of cycles associated with the stress range $\gamma_{Ff} \cdot \Delta\sigma_i$ for band i in the factored spectrum, and N_i is the number of cycles obtained from the factored fatigue strength curve ($\Delta\sigma_C/\gamma_{Mf}$) for a stress range of $\gamma_{Ff} \cdot \Delta\sigma_i$, whereas γ_{Ff} and γ_{Mf} are the partial safety factors for the equivalent constant amplitude stress range and for the fatigue strength, respectively.

Table 7.19 – Average composition of the traffic for a standard year.

Description	*Single crossings*[a]	*Double crossings*[b]
Train with 2 heavily loaded vehicles	15265	1675
Train with 2 normally loaded vehicles	22115	2455
Train with 2 lightly loaded vehicles	4600	525
Train with 1 normally loaded vehicle	3085	160
Train with 1 lightly loaded vehicle	2405	105
Total	47470	4920

[a] Single train crossings per each direction; [b] Two trains crossing the upper deck in opposite directions.

Stress range spectra for the application of the cumulative damage method were obtained by rainflow cycle counting from the stress curves generated in the structural elements by the crossing of the trains. To this end, influence lines calculated from Model B were properly factored in order to account for the dynamic response of the structure. The corresponding dynamic amplification factors were calculated according to the specification of Annex C in Eurocode 1 – Part 1-2 (EN1991-2, 2003), and the values obtained for the analyzed structural elements of the upper deck are listed in Table 7.20. In this calculation the maximum speed considered for the trains crossing was 15 m/s and the

natural frequencies of interest were taken from the ambient vibration test conducted after the bridge rehabilitation (Chapter 8).

Table 7.20 – Dynamic amplification factors.

Structural element	$1 + \varphi$
Main girders of spans 1 to 4	1.107
Main girders of spans 5 to 8	1.267
Main girders of spans 9 to 13	1.085
Crossbeams	1.308
Stringers	1.188

In order to meet a likely increase of the traffic in the future, this study considered four different annual average growth rates (1 %, 1.5 %, 2 % and 2.5 %) for three different periods of service time (50, 75 and 100 years). Furthermore, similarly to the procedure previously adopted for the estimation of the safety and rating factors, for the chords and diagonals two scenarios were appraised, one in which the stresses are caused only by the axial force and the other that considers bending contributions as well. The results of the fatigue assessment are summarized in Table 7.21.

Table 7.21 – Fatigue damage accumulation indices for the upper deck.

Period		*50 years*				*75 years*				*100 years*			
AAGR of the traffic		*1%*	*1.5%*	*2.0%*	*2.5%*	*1%*	*1.5%*	*2.0%*	*2.5%*	*1%*	*1.5%*	*2.0%*	*2.5%*
Upper chords	a)	0.00	0.00	0.00	0.00	0.01	0.01	0.01	0.01	0.01	0.01	0.02	0.02
	b)	0.41	0.47	0.54	0.62	0.71	0.87	1.09	1.37	1.09	1.46	1.99	2.76
Lower chords	a)	0.05	0.06	0.07	0.08	0.09	0.11	0.14	0.18	0.14	0.19	0.26	0.36
	b)	0.19	0.22	0.25	0.29	0.33	0.40	0.50	0.63	0.50	0.67	0.92	1.28
Diagonals	a)	0.00	0.00	0.00	0.00	0.00	0.00	0.00	0.01	0.00	0.01	0.01	0.01
	b)	0.05	0.06	0.06	0.07	0.09	0.11	0.13	0.16	0.13	0.18	0.24	0.33
Crossbeams	c)	1.05	1.20	1.37	1.58	1.80	2.22	2.77	3.49	2.77	3.71	5.07	7.02
Stringers	c)	0.13	0.15	0.17	0.20	0.22	0.28	0.35	0.44	0.35	0.46	0.63	0.88

AAGR – Annual average growth rate; a) Computed using only the mandatory internal axial force; b) Computed taking into account the axial force and the bending moments; c) Computed using only the bending moment about the strong axis.

A careful inspection of the results leads to the conclusion that the elements predominantly subjected to axial loads (chords and diagonals) present a fatigue life of at least 100 years when the assessment is performed only with the stresses caused by the axial force. If the bending stresses are also considered the diagonals continue to reveal an excellent fatigue resistance. With respect to the chords, only after 75 to 100 years is expected the

appearance of any fatigue related problems. As expected, the crossbeams were found to be the critical elements, for which the study indicates a safe fatigue life of at least 50 years. However, it is worth mentioning that the dynamic amplification factors used in this analysis were estimated by considering a traveling speed for the trains of 54 km/h (15 m/s), which is a relatively high value for the present traffic conditions. Therefore, it is most likely that fatigue related problems may not occur for longer periods of time. In what concerns the stringers, the estimates point to a high fatigue strength.

7.8. Summary and conclusions

This chapter presents a comprehensive study of a centenary double-deck steel arch bridge that underwent a deep rehabilitation and strengthening process in order to enable the integration of its upper deck in a light metro network. To this end, field tests were conducted before and after the construction works, which comprised static and quasi-static loading scenarios, accomplished by using several dump trucks. The experimental assessment of the bridge behavior under the applied loadings was made by monitoring the vertical displacements of the upper deck spans and of the arch crown, the horizontal displacements at the bearings of the upper deck girders, as well as the steel strains in sections of key members of the suspension ties, piers, arch and upper deck.

The main objectives to attain through the collection of the field data were:

i. To develop reliable numerical models able to accurately simulate the bridge behavior before, during and after the intervention;
ii. To assist the rehabilitation and strengthening design in the selection of schemes to implement;
iii. To allow an experimental comparison of the bridge response between the pre and post-rehabilitation conditions in order to appraise the changes in the structural behavior;
iv. To evaluate the efficiency and/or effectiveness of the strengthening adopted in the most stressed members;
v. To test the novel fiber optic based monitoring system installed in the bridge to capture its response during the new service conditions;
vi. To establish a baseline condition of the bridge behavior from which any future variations in the structural properties could be detected.

In this study, the numerical analyses were conducted based on two different strategies for the modeling. In the first, the global behavior of the bridge was simulated by 3D FE models created on the basis of two-node frame elements, judiciously complemented with four-node shell elements to improve the simulation of the connection between substructures. Additionally, steel strains of the bridge elements were estimated from the internal forces (axial force and bending moments). In the second strategy, the deformation of key elements of the upper deck was numerically estimated through the combined use of the 3D global model of the bridge and of the 3D shell based sub-models of the corresponding girders panels, taking the displacements and rotations calculated by the global model as input data to the refined models.

Conclusions drawn from the experimental and numerical results can be summarized as follows:

- The old light-weight concrete pavement decisively impacted the global bending deformation of the upper deck, whereas the secondary stringers that integrate the new floor system have a smaller contribution to its present stiffness, leading to an average increase of the deformation of about 17 % ;
- The replacement of the upper deck floor system significantly increased the strains of the upper chords, although no relevant influence on the deformation of the remaining elements of the bridge was observed. Nevertheless, strain gradients in the upper deck lower chords experienced a considerable increase as a result of a smaller deformation of the webs;
- The torsion stiffness of the upper deck decreased about 10 % after the bridge rehabilitation, and the strains difference between the girders lower chords under eccentric loading for the new bridge condition led to a value close to 30 %;
- In general, the strengthening of the bridge elements has enabled a significant decrease of their deformation, namely arch and upper deck diagonals. Furthermore, for some non-strengthened arch elements the steel strains were also reduced, which was likely induced by changes in the forces distribution (load path) within the statically indeterminate structure;
- In almost all monitored arch and piers elements the experimental strains revealed a small bending component, whereas the upper deck elements, namely chords and diagonals were subjected to high strain gradients;

- The global models developed to simulate the bridge behavior before and after the rehabilitation were able to accurately replicate the vertical displacements of the structure. Strains estimated from the numerical internal forces compare well with the test data of the elements subjected to small bending, namely the arch and piers, and of the flanges pertaining to the upper deck elements, specifically the chords and diagonals. On the contrary, the strains predicted for the upper deck chords webs and diagonals strengthening angles are of lower or poor quality;

- The sub-models of the upper deck girders panels supplied superior numerical estimates for the elements strains. For both diagonals and chords the load path, warping torsion, elements connections and stress concentrations were properly simulated;

- The numerical results clearly pointed out an eccentric loading of the upper deck diagonals, which could be experimentally verified by monitoring the response of one diagonal during the crossing of a metro train in the new service phase;

- The constraints to the longitudinal displacements of the upper deck, identified from the field data collected after the bridge rehabilitation, could only be partially interpreted through the numerical analysis by simulating a contact non-linearity at the arch ends. The remaining difference, in magnitude and/or shape, is most likely caused by additional restrictions to the movement at the upper deck ends, generated by the friction in the expansion joints;

- Static and quasi-static tests provided complementary results. While in the first case the maximum response was appraised within safe limits, in quasi-static testing the regularity of the bridge behavior was assessed. The numerical analyses accurately estimated the displacements induced by static loadings, yet often failed to supply fair results for the steel strains, since these quantities are of local nature and largely depend on the exact vehicles positioning and on the members connections. On the contrary, the correlation between the strain data and the numerical estimates improved for the quasi-static crossings, in spite of the lower loading level;

- The strain data collected from the upper deck crossbeam highlighted the importance of establishing a well characterized baseline condition through

field testing, so that the identification of changes in the structural behavior during the service phase is made possible;

The safety of the bridge and the load-carrying capacity of its members under the new service conditions were also appraised. To this end, two scenarios of analysis were considered, one in which only the predominant internal force was taken into account, and the other where all the internal forces were adopted. The assessment made has led to the following conclusions:

- The elements pertaining to the substructures targeted in the rehabilitation present a suitable safety level and high rating factors for the first scenario. However, for a large number of elements the results drastically change when the second scenario is considered. Nevertheless, the analyses were conservatively performed by not taking into account any reserve of plastic resistance, i.e. assuming that failure takes place when the most stressed fibers reach the limit of elasticity;

- Although the rehabilitation project did not included the lower deck in the strengthening evaluation (given that its use was kept unchanged), the safety of its elements can be regarded as adequate, except for the crossbeams near the suspension ties. However, their failure does not inevitably imply a local or global collapse, and their strengthening in order to meet the present standards is small and localized. Therefore, the corresponding construction works can be easily executed during future maintenance operations;

- In light of the strains collected from the upper deck diagonals during the field tests, a clear identification of their load path was accomplished. The eccentricity of the load was perfectly characterized as consequence of the connections at the girders joints. Therefore, for members under compression the safety assessment was also performed assuming a non-linear geometric behavior. For this scenario, the analyses revealed unsuitable safety and rating factors, which, however, should not be regarded as distressing values. In fact, the strengthening of the diagonals led to an average increase of their load capacity of almost 65 % and the permanent loads were reduced as a result of the floor system replacement. Therefore, the safety level was largely incremented with respect to the pre-rehabilitation condition, during which no evidences of distress caused by buckling were identified;

- For both bridge decks the girders chords located at the level of the floor systems present a much higher safety level and load-carrying capacity than their counterparts, i.e. lower chords in the upper deck and upper chords in the lower deck. For these elements particular attention should be paid if any changes occur to the service conditions in the future;

- Regarding fatigue analysis, all elements of the upper deck have a suitable resistance for at least 50 years, being the crossbeams the most sensitive elements as a result of their higher stress ranges and larger number of loading cycles.

Chapter 8

Modal analysis of the Luiz I Bridge

8.1. Synopsis

Dynamic testing for characterizing the behavior of bridges immediately after their construction is nowadays a common procedure, and even compulsory for the most significant structures. However, the collection of field dynamic data to support the rehabilitation, strengthening or upgrade designs of old steel bridges has not had the impact that would be expected, due to the small number of such engineering projects and also as a consequence of the shortage of case studies for which the added value is unquestionable. In this context, the report of successful examples is essential for the development of a consolidated knowledge in this field among the civil engineering community so that the optimization of future projects becomes feasible.

In this chapter the modal analysis of a centenary steel arch bridge recently rehabilitated and strengthened is reported. The ambient vibration test conducted after the construction works is described and the experimental results are compared with the field dynamic data collected during the previous condition. Structural identification is completed by means of 3D finite element models that replicate both service phases, before and after rehabilitation, being subsequently used to simulate different scenarios by changing specific structural parameters. The results analysis brought to light important findings concerning the changes produced in the bridge dynamic behavior and the variables controlling it.

8.2. Introduction

Although the current infrastructure maintenance and management systems, such as those related to bridges, continue to use the periodic visual inspections as the main source of information, among the technical and scientific communities the view that this approach cannot effectively meet the growing demands of modern societies is consensual. In fact if, on the one hand, the full operational potential of the structures cannot be explored by conservative decision-making processes based on scarce and non measurable information, on the other hand, the financial resources available for repair, rehabilitation, strengthening, upgrading or replacement are increasingly limited. Furthermore, often problems not perceived by visual inspection can only be disclosed through procedures that include the measurement of key parameters. Consequently, the use of nondestructive testing tools is emerging as a valuable solution to assist the condition assessment of existing structures, both in terms of its load-carrying capacity and serviceability (DeWolf *et al.*, 2002). Moreover, data obtained through these means are essential for the quantification of parameters and identification of mechanisms that are to be integrated in the numerical models that support reliable and objective structural evaluation (Farhey, 2005).

In this context, model calibration based on experimental measurement emerges as a key task, for which the selection of the model space and of the strategy for the numerical modeling and physical completeness are the kernel problems. The indices adopted for correlating the experimental and the numerical analyses must account for several factors, among which are the numerical robustness, ability to rationally smear and linearize unavoidable nonlinearity and nonstationarity, and insensitivity to typical variance and bias errors (Aktan *et al.*, 1998).

While some researchers have pointed out the intrinsic difficulties in performing vibration testing in large bridges, such as nonstationary excitation (Catbas *et al.*, 2007), high levels of damping, nonlinear boundary or continuity conditions and nonideal connections/interfaces between structural members and components (Farhey, 2005), is unquestionable that dynamic testing stands as an innovative way of great potential in the structural identification of bridges for condition assessment (Aktan *et al.*, 1997; DeWolf *et al.*, 2002). It becomes imperative when assessing the seismic vulnerability of a structure and corresponding retrofit design (Cheung *et al.*, 2007), and can play a decisive role in the rehabilitation of centenary steel bridges, both in supporting the project design and in validating their performance for the new structural condition. Bearing in mind that system

identification targets the development of mathematical models to characterize the input-output behavior of an unknown system supported on experimental data, field-calibrated models by means of dynamic tests have proven to be highly reliable in simulating the global response (Aktan *et al.*, 1998).

Several examples of dynamic tests performed in old steel bridges have been reported in technical literature, of which the most significant cases regarding repair, rehabilitation, upgrade or strengthening projects are herein shortly presented.

Ren *et al.* (2004b) have studied the dynamic properties of a steel-girder tied arch bridge by modal analysis and ambient vibration testing. Field data was collected for the construction of reliable 3D finite element models, which in turn were used to evaluate the concrete deck influence on the overall dynamic behavior of the structure. Ultimately, the study aimed at assisting the seismic evaluation of the bridge and its likely retrofit.

The dynamic properties of the Brooklyn Bridge have recently been investigated by Ye *et al.* (2005). Modal testing was accomplished by ambient vibration monitoring and forced vibration tests. The experimental mode shapes and natural frequencies compared well with the numerical results obtained by a detailed 3D finite element model, which will assist the seismic evaluation of the structure according to current standards and help to establish the rehabilitation and maintenance plans.

(a) (b)

Figure 8.1 – Tested bridges (I): (a) I-24 Tennessee River Bridge, Kentucky, USA (Ren *et al.*, 2004b); (b) Brooklyn Bridge, USA (Ye *et al.*, 2005).

Ermopoulos and Spyrakos (2006) were responsible for carrying out a systematic study of a 19th century railway bridge, still in service, which included dynamic field measurements. A 3D finite element model was developed by the researchers and its validity was checked by comparing the results from numerical calculations with those from the field measurements. The correspondence for the first 3 eigen-periods was found to be

appropriate. The validated model was then employed to assess the suitability of the bridge to carry the loads specified by current codes, and if necessary to devise a suitable strengthening scheme.

Spyrakos *et al.* (2004) have tested a two-span historic railway steel truss bridge, part of the southern railway network of Greece. The lowest 3 natural frequencies for vertical mode shapes were extracted from the test data and compared against the values estimated by a 3D finite element model. After its calibration the model was used to appraise the load-carrying capacity of the bridge to withstand heavier train loads, as well as the seismic and wind actions stipulated by present design codes.

Harik *et al.* (1997) have carried out dynamic testing on a double-deck cantilever through-truss bridge to support a study for the assessment of its structural integrity under the action of seismic loads. The mode shapes and the associated natural frequencies of the structure were extracted from experimental data recorded during a four-hour ambient vibration test. These modal properties were subsequently used to calibrate a 3D finite element model which was then utilized for seismic response analysis enabling the identification of critical elements.

(a) (b)

Figure 8.2 – Tested bridges (II): (a) Brent-Spence Bridge, USA (Harik *et al.*, 1997); (b) Toutle River Bridge, Washington, USA (Roeder *et al.*, 2000).

A steel tied-arch bridge was analyzed by Roeder *et al.* (2000). The Toutle River Bridge suffered from significant dynamic response and cracking, being representative of a set of similar bridges in the State of Washington, as well as of their main deficiencies. The experimental study encompassed the measurement of the free vibration response of the structure after the passage of trucks. The collected strains and accelerations have enabled the identification of natural periods of vibration and mode shapes, which in turn were compared with the predictions from finite element analysis. The validated 3D model was

used to estimate the dynamic response due to truck loading responsible for fatigue damage.

Gonçalves *et al.* (2008) have also reported the execution of dynamic tests before and after the rehabilitation of a through truss steel bridge built in the late 19th century. In a first stage the experimental results served to assist the design by calibrating the numerical model. After the completion of the works the field data was used to assess the effectiveness of the strengthening schemes.

The safety of the Roebling Bridge, over the Ohio River, was assessed by Ren *et al.* (2004a) based on current standards. The dynamic properties of this historic suspension bridge were experimentally determined through an ambient field test under natural excitation. The procedure adopted for the model updating relied on matching the vibrating frequencies and mode shapes estimated by the numerical analysis with the corresponding field measured values. Ultimately, the actual structural condition and different deterioration and loading scenarios were to be numerically simulated in order to appraise the need to strengthen the structure.

Zaki and Abu-Hamd (2007) have presented the use of dynamic testing techniques to evaluate the modal properties of a 90 years old steel railway bridge crossing the River Nile in Egypt. The dynamic testing enabled to evaluate the evolution of the modal parameters of each span at different stages of the repair plan, which was carried out without interrupting the traffic. The results have proved the effectiveness of the rehabilitation strategy and helped to understand the influence of the progress stage of the works.

(a) (b)

Figure 8.3 – Tested bridges (III): (a) Roebling Suspension Bridge, USA (Ren *et al.*, 2004a); (b) Qanater steel railway bridge, Egypt (Zaki and Abu-Hamd, 2007).

Caglayan *et al.* (2011) were engaged in a project for the dynamic and seismic assessment of a railway bridge located in a seismic region of Turkey. A baseline 3D numerical model

was developed to simulate the bridge response by adopting several presumed stiffness parameters. The optimization procedure consisted in minimizing the difference between numerical and experimental data by changing the uncertain quantities. Ultimately, the calibrated model was used to rate the load-carrying capacity of the bridge and to appraise the structural behavior under seismic loadings. It was concluded that damaged lower cross bracings needed to be replaced and additional supports had to be installed.

In this chapter a study regarding the modal identification of the Luiz I Bridge, which has undergone a rehabilitation and strengthening process in order to enable its use for the passage of new light metro vehicles, is presented. In section 8.3, the scope of this study is established and the main objectives to be achieved are identified. Then, the experimental program adopted in the ambient vibration test performed for the new service conditions is described, as well as the data processing implemented for the extraction of the modal parameters, always with reference to the previous test conducted to support the viability study of the project. In section 8.5, the new 3D finite element models developed to simulate the dynamic response of the bridge, before and after the construction works, are reported and the adopted modeling strategy is detailed. From the direct comparison of the field results and by correlating these with the numerical estimates, major conclusions could be drawn regarding the evolution of the level of vibration, modal parameters and stiffness of the bridge. The reliability and accuracy of the pre-rehabilitation condition model is also appraised by comparing its predicted values with the numerical data supplied by the model created for the viability study. At the end, the main structural variables that control the modal parameters are disclosed through a sensitivity analysis.

8.3. Scope and objectives

The rehabilitation and strengthening of the bridge was carried out following an assent given by a viability study performed to analyze the structural effects that would result from using the upper deck to support a new light metro double line (Coelho *et al.*, 1996).

In addition to the safety evaluation of the bridge for different ultimate limit states regarding the static response, in this study the dynamic analysis was also conducted through a complete modal identification of the structure, based on the execution of an ambient vibration test and on the development of 2D and 3D finite element models. Subsequently, these validated models were used to predict the seismic response of the bridge and to quantify its performance under the passage of the metro trains taking into

account the dynamic interaction between the structure and the vehicles (Calçada *et al.*, 2002). The data produced by this viability study played a decisive role in the rehabilitation design by enabling the optimization of the strengthening schemes to be implemented.

After the completion of the construction works a second ambient vibration test was executed for the purpose of identifying the changes produced in the dynamic properties of the bridge for the new service conditions. Additionally, given the depth of the intervention undertaken on the upper deck it was also targeted the evaluation of its stiffness variation, both in the transverse and vertical directions. Furthermore, the calibration and/or update of a new numerical model based on additional and improved information than that available for the viability study would enable its use in replicating the bridge response for the new dynamic loadings, and consequently its integration within a structural health monitoring system to perceive any alterations produced over the time.

In summary, the main objectives of the work presented in this chapter are as follows:

i. Execution of a new complete ambient vibration test of the bridge for its new service condition aiming at the experimental identification of its modal parameters;
ii. Development of new 3D numerical models of the bridge to simulate the pre and post-rehabilitation behaviors, on the basis of updated geometric, mechanical, boundary and kinematic data collected during the construction works;
iii. Validation and/or calibration of the developed models based on the data taken during both tests;
iv. Evaluation of the changes occurred in the bridge, particularly in the upper deck, both in terms of modal parameters and bending stiffness;
v. Development of a sensitivity analysis through numerical simulations generated by the validated models with the purpose of finding the parameters with more influence on the dynamic behavior of the bridge.

8.4. Ambient vibration testing

The ambient vibration tests conducted before and after the rehabilitation and strengthening of the bridge sought to evaluate its vibration response under normal operation, mostly induced by the wind and traffic, (both roadway and railway), and to identify the modal parameters for both conditions. The first test, henceforth termed as Test 1, was performed to support the viability study and, subsequently, also the

rehabilitation design. With respect to the second test, hereafter referred to as Test 2, the dynamic measurements served to detect the changes produced in the structural behavior as a result of the construction works, and to establish a sound baseline for the dynamic characteristics of the bridge in the new service phase in order to enable its structural health monitoring. Taking into account that the description of Test 1 has already been done in an earlier article (Calçada *et al.*, 2002), in this section the focus is placed on the experimental procedure, data processing and modal identification implemented in Test 2. Yet, for the sake of clarity, all differences between the two tests are pointed out.

8.4.1. Testing program

For recording the bridge vibrations a total of 28 measurement sections were defined, 19 in the upper deck and 9 in the lower deck, located as depicted in Figure 8.4. However, in Test 1 the accelerations of the lower deck were only collected at the joints in correspondence with the suspension ties and during Test 2 no measurements were taken at section 19. All sections of the upper deck were instrumented with two seismographs, one positioned at each side of the deck on the sidewalks limits, upstream and downstream. On the lower deck a single device was used to record the upstream accelerations, even though for Test 2 the vibration response has also been occasionally acquired from the downstream side to unveil eventual torsion modes.

For the entire duration of the tests two reference stations were set on the upper deck at section 15, and for Test 2 an additional reference was introduced at section 23 (upstream). While two recorders were permanently kept at the upper deck reference stations, the third reference recorder was only used during the ambient vibration test of the lower deck. The remaining recorders acted as moving sensors, being consecutively placed at the other sections. In all measuring points the accelerations were measured along three orthogonal directions oriented according to the natural reference axes of the bridge (longitudinal, vertical and transverse).

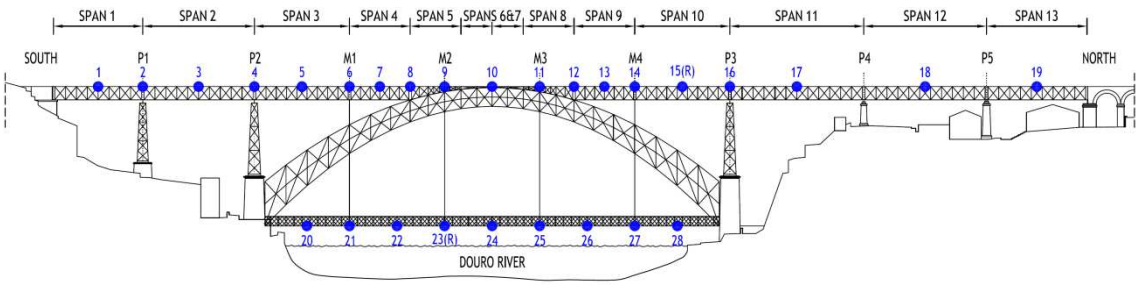

Figure 8.4 - Layout of the measurement sections.

All the 4 measuring devices are essentially constituted by one tri-axial force balance accelerometer, an analogue to digital (A/D) converter, a battery that enables a 1-day test autonomy, and a memory card for recording the acquired data. Figure 8.5 shows a picture of one seismograph duly stationed during Test 2. In Test 1 the resolution of the converters was 16 bits and for Test 2 it was enhanced to 18 bits. Furthermore, in the second test the seismographs were upgraded with GPS sensors to continuously update the time of the internal clocks, and consequently synchronization between units was improved.

Since such units are autonomous and the definition of the acquisition timetable was previously performed by connecting each measuring unit to a laptop, the need of using long electrical cables was overcome, which permitted a faster execution of the tests. Acceleration time series were collected during setups of 6 and 16 minutes, with sampling frequencies of 50 and 100 Hz in the first and second tests, respectively. In spite of these values being imposed by the filters of the acquisition equipments, the frequency content of interest for this bridge, below 10 Hz, was perfectly captured.

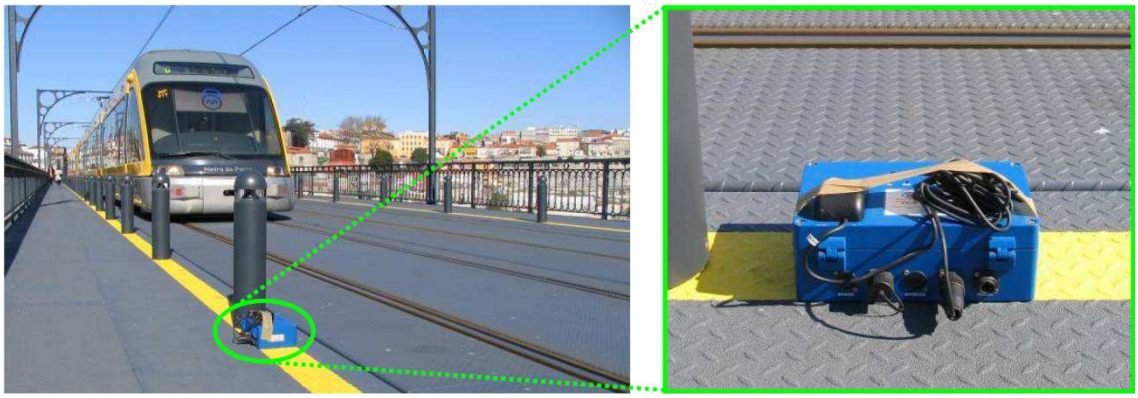

(a) (b)

Figure 8.5 - Experimental setup: (a) position of the measuring apparatus on the upper deck (sidewalk limit); (b) detail of the seismograph.

8.4.2. Data processing and modal identification

In order to accurately capture the modal parameters of the bridge, particularly those associated to vibration modes of different types with very close natural frequencies, the collected signals of each section were pre-combined to obtain enhanced time series for analysis. The new vibration signals were the half-sum of vertical, half-difference of vertical, and half-sum of transverse accelerations (upstream-downstream), which enabled an improved modal extraction of vertical bending, torsional and transverse bending modes, respectively.

The identification of the resonant frequencies of the bridge for both tests was accomplished in the frequency domain using the Peak-Picking method (PP) (Felber, 1993), which is one of the simplest techniques available for data processing of the vibration response of structures subjected to natural excitation. However, for Test 2 more sophisticated identification algorithms were used to confirm the estimates supplied by the first analysis, namely the PolyMax method adapted for ambient vibration tests (Peeters and Van der Auweraer, 2005) and the Covariance driven Stochastic Subspace Identification method (SSI-COV) based on correlations calculated from the acquired times series and on the fitting of a stochastic state space model (Peeters and De Roeck, 1999). Notwithstanding the better results obtained with these techniques, for the sake of comparison of experimental estimates from both tests only the parameters identified with the PP method are herein presented. Details regarding the results provided by the other two methods can be found elsewhere (Cunha *et al.*, 2006).

In light of the above, normalized power spectral density functions (NPSD) were estimated from the acceleration time series of each measuring section (longitudinal and 3 pre-combined signals), as well as the coherence functions associated to the simultaneous measurements at the several sections. Subsequently, in order to highlight the natural frequencies, the average normalized power spectra (ANPSD) were computed taking into account all the NPSDs of the same type. While in Test 1 the 6 min records were divided into 8 segments without overlapping, in Test 2 the 16 min time series were divided into time segments of 4096 reading points (40.96 s) with an overlap of 50 %, which led to a frequency resolution of approximately 0.02 Hz for all spectra. Figure 8.6 presents the ANPSDs of vertical and transverse accelerations obtained for both tests in the range 0-5 Hz, in which the spectra of Test 2 are separated by decks.

A careful inspection of the peaks appearing in these spectra permitted to identify the natural frequencies of the bridge. Furthermore, the plots also disclose the following:

i. Natural frequencies associated to vertical bending modes are clearly captured by the spectra obtained from the readings of both decks, thus revealing a global nature;
ii. Natural frequencies associated to transverse bending modes are just local, since only the movement of one of the decks is mobilized. The exception is the frequency of 0.952 Hz, whose mode shape mobilizes the deformation of both decks (see Figure 8.6(b)).

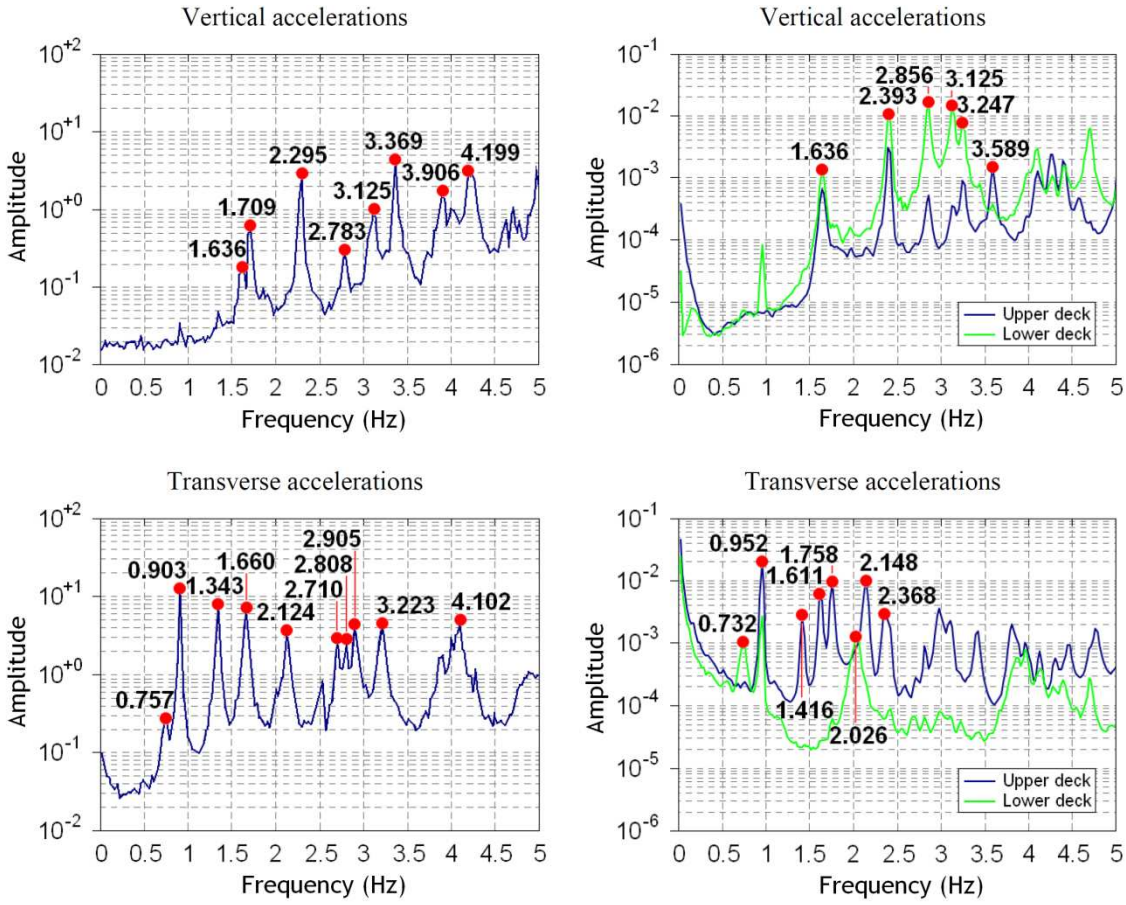

(a) (b)

Figure 8.6 - ANPSDs estimated for the bridge during both ambient vibration tests: (a) before the rehabilitation; (b) after the rehabilitation.

The identification of the mode shapes within the range of 0-5 Hz was performed on the basis of the transfer functions relating the ambient response at each section with the one collected at the reference sections, duly validated by the corresponding coherence functions. The ratios between the values of these transfer functions related to each natural frequency in a linear scale enabled the estimation of the modal coordinates, whose corresponding sign was evaluated by checking the phase evolution. In section 8.6 the experimental estimates and corresponding numerical counterparts are presented and discussed.

8.5. Finite Element Modeling

Only the specific aspects of the dynamic analysis are herein presented since the details related to other modeling issues, namely, the adopted finite elements, geometry, material and section properties, were reported in Chapter 7.

8.5.1. Boundary conditions

A key issue of the FE modeling of this bridge lies on the restrictions of the longitudinal displacements of the decks. In the lower deck, the constraints are essentially caused by the steel expansion joints at both ends (see Figure 8.7(a)). Three reasons decisively contribute for this fact:

i. The expansion joint itself does not permit a complete free movement, which is intended for favorably control the behavior of the pendulum system constituted by the lower deck and the suspension ties;
ii. At the girders ends the lower chords flanges are laterally leaned against thick steel plates attached to the abutment masonry (see Figure 8.7(c));
iii. The gaps that would allow some expansion movement are filled with compacted material, and during the rehabilitation process no actions were taken to execute any cleaning (see Figure 8.7(b)).

(a) (b) (c)

Figure 8.7 - North abutment of the lower deck: (a) general view; (b) expansion joint of the deck; (c) contact between the lower chords flanges and a thick steel plate attached to the masonry.

Regarding the upper deck, the restraints have different causes depending on the phase of analysis. Before the rehabilitation the extreme degradation of the steel bearings at the abutments, including damage of some of their components, as well as the lack of maintenance of the remaining apparatus over the piers, strongly prevented the intended performance of the structure. This major inadequacy was experimentally confirmed before the beginning of the rehabilitation by measuring the expansion displacements induced by the daily cyclic thermal action. At the time it was possible to estimate that the longitudinal translation of the upper deck rigidity center from the arch crown towards the north abutment was about 30 m (Costa *et al.*, 2004b). It is also noteworthy that in this

phase the expansion joints located at the upper level were not restraining the movements as they were of metallic cantilevered teeth type and were in good condition.

After the rehabilitation the constraints are likely caused by two factors:

i. At the upper level of the expansion joints significant forces are mobilized. Indeed, steel plates covering the gap are attached to the steel structure and leaned against steel plates fixed to the masonry of the abutment. In Figure 8.8(b) signs of rust in the large contact surfaces of theses plates are depicted;
ii. Although expansion devices are applied to the rails in the vicinity of the abutments, out of the upper deck, to prevent the appearance of thermal induced forces (see Figure 8.8(c)), friction is also generated due to the very structure of the apparatus, even though it is of smaller magnitude.

(a) (b) (c)

Figure 8.8 - South abutment of the upper deck in the new service phase: (a) general view; (b) cover plates of the expansion joint; (c) expansion device of a rail.

It is also important to bear in mind that the inadequate original bearings at the abutments were replaced and the remaining upper deck supports were cleaned and lubricated, and therefore the constraints induced by these were minimized. In light of the above, the stiffness coefficients of the springs adopted in the reference FE models to simulate the restrictions to the longitudinal displacements of both decks are listed in Table 8.1. These coefficients were estimated through a calibration procedure performed on the basis of an iterative trail-and-error process, in which the vibrating frequencies and mode shapes estimated by the numerical analysis were matched to the corresponding experimental values.

Table 8.1 – Characteristics of the longitudinal springs adopted in the reference models.

		Model A				*Model B*	
Location		*Type (No.)*	*Stiffness constant*	*Location*		*Type (No.)*	*Stiffness constant*
Upper deck	North abutment (lower level)	Nodal (2)	195,000 kN/m	Upper deck	North abutment (upper level)	Nodal (4)	295,000 kN/m
	South abutment (lower level)	Nodal (2)	195,000 kN/m		South abutment (upper level)	Nodal (4)	295,000 kN/m
	Piers P1 to P5 (lower level)	Nodal (2)	55,000 kN/m		Piers P1 to P5	---	---
Lower deck	North abutment (lower level)	Linear (1)	320,000 kN/m^2	Lower deck	North abutment (lower level)	Linear (1)	320,000 kN/m^2
	South abutment (lower level)	Linear (1)	320,000 kN/m^2		South abutment (lower level)	Linear (1)	320,000 kN/m^2

Model A – Model representative of the pre-rehabilitation condition;

Model B – Model representative of the post-rehabilitation condition;

Linear spring is distributed along the width of the lower deck.

8.5.2. Mass

For the modal analysis of the models the mass matrices were calculated assuming whole the mass concentrated in the nodes. The translational movements along the three reference orthogonal directions were defined as the only dynamic DOFs. The mass of the structural elements was considered through the mass densities of the cross-section properties of the frame and shell elements. Special attention was paid to the mass of the light-weight concrete pavements to prevent its overestimation. For that, the material density of the steel-concrete composite crossbeams only included the fraction corresponding to the steel, in opposition to the longitudinal elements over which the pavement rested (stringers and chords).

All permanent non-structural loads were properly converted into concentrated mass applied in the nodes. The sources of this additional mass are the technical walkway between the girders of the upper deck, pipes and cables of infrastructures crossing the decks, frames supporting the overhead power lines, rails, sleepers, sidewalks, decorative elements, bolts and rivets, stiffeners, and “X” , gusset and cover plates.

Table 8.2 – Description of the models used in the sensitivity analysis.

Condition	*Model*	*Description*
Pre-rehabilitation	A	Base model
	A1	The longitudinal springs at the supports of both decks are removed
	A2	The longitudinal springs at the supports of the upper deck are removed
	A3	The longitudinal springs at the supports of the lower deck are removed
	A4	The longitudinal springs at the abutments supports of both decks are made rigid
	A5	The longitudinal springs at the abutments supports of the upper deck are made rigid
	A6	The longitudinal springs at the supports of the lower deck are made rigid
	A7	The pinned supports of the arch are replaced by fixed ones
	A8	The crossbeams and stringers of both decks hold the steel section only
	A9	The offsets applied to the bars are eliminated
Post-rehabilitation	B	Base model
	B1	The longitudinal springs at the ends of both decks are removed
	B2	The longitudinal springs at the ends of the upper deck are removed
	B3	The longitudinal springs at the ends of the lower deck are removed
	B4	The longitudinal springs at the ends of both decks are made rigid
	B5	The longitudinal springs at the ends of the upper deck are made rigid
	B6	The longitudinal springs at the ends of the lower deck are made rigid
	B7	The pinned supports of the arch are replaced by fixed ones
	B8	The secondary stringers of the upper deck floor system are not considered
	B9	The primary stringers of the upper deck are removed
	B10	The crossbeams and stringers of the lower deck hold the steel section only
	B11	The crossbeams at the upper deck are made rigid*
	B12	The offsets applied to the bars are eliminated

* This condition indirectly simulates the membrane stiffness of the cladding plates in the new floor system.

8.5.3. Variant models

Taking advantage of the FE modeling, and subsequent numerical analyses for the estimation of the modal parameters, a set of numerical simulations was conducted with the purpose of assessing the impact of several structural variables on the accurate modal identification of the bridge. The quantities included in this sensitivity study were:

i. Level of restriction to the longitudinal displacements of the decks;
ii. Supporting conditions of the arch;
iii. Stiffness of the light-weight concrete pavements;

iv. Stiffness of the supporting stringers of the new steel grid (main stringers) (see Figure 7.20(b));
v. Stiffness of the stringers pertaining to the floor system of the rehabilitated upper deck (secondary stringers) (see Figure 7.20(b));
vi. Transverse bending stiffness of the upper deck crossbeams for the new bridge condition;
vii. Positioning of the bars structural axes.

The description of the variant models used in the sensitivity analysis is presented in Table 8.2, where Models A and B simulate the bridge behavior before and after the rehabilitation, respectively, for the reference conditions previously described.

8.6. Analysis of results

8.6.1. Vibration levels

Figure 8.9 presents the vertical and transverse acceleration time series acquired at the measuring sections 15 and 17 in Test 2, which include the maximum values measured during the whole testing period. The peak value of the vertical acceleration slightly exceeded 0.20 g, what constitutes a considerable rise compared to the maximum reading recorded in Test 1 (0.12 g) (Cunha and Calçada, 1999).

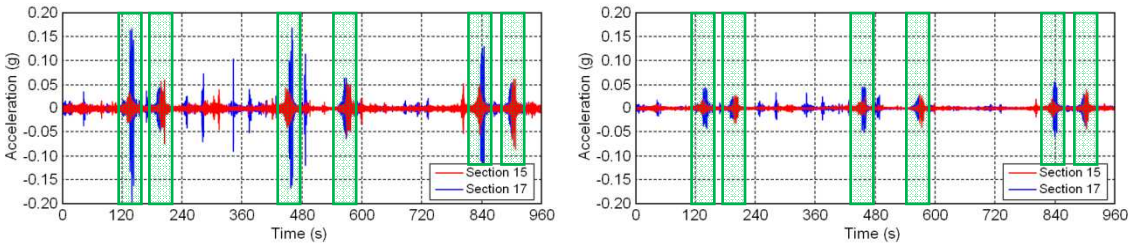

Figure 8.9 - Acceleration time series collected at sections 15 and 17 during Test 2 (16 minutes): (a) vertical vibrations; (b) transverse vibrations.

However, this increase of the vertical vibration level does not imply a decay of the structural behavior as the main dynamic loads are quite different, since before the upper deck served the road traffic and now is crossed by rail vehicles. Moreover, it depends on the acquisition frequency adopted in the tests, which was much higher for Test 2. On the other hand, although the new maximum vertical acceleration is a value relatively high in

terms of pedestrian comfort, its relevance is mitigated by the fact that it includes significant high frequency contributions. Similarly to the vibration response observed before the rehabilitation process, also the transverse accelerations in Test 2 are considerably lower than the verticals, in a proportion of 1:4, approximately.

Furthermore, a careful inspection of Figure 8.9(a), which includes time series simultaneously recorded at different measuring sections, enables the identification of the metro trains passage. Taking into account that vehicles crossing the upper deck in the new service phase are of the same type, double crossings are rare, and that the first measuring section traversed by a vehicle is the one whose accelerations are first recorded, 6 passages of the metro can be identified, three in each direction.

Table 8.3 – Experimental natural frequencies.

Mode number	*Mode type*	*Before rehabilitation[1] (Hz)*	*After rehabilitation[2] (Hz)*	*Δ (%)*
1st	1st T	0.757	0.732	-3.30
2nd	2nd T	0.903	0.952	5.43
3rd	3rd T	1.343	1.416	5.44
4th	4th T	1.660	1.611	-2.95
5th	1st V–L	1.636	1.636	0.00
6th	5th T	2.124	1.758	-17.23
10th	2nd V	2.295	2.393	4.27
13th	5th V	3.125	3.247	3.90
14th	6th V	3.369	3.589	6.53

Vibration modes are numbered according to the order of the identified modes after the rehabilitation; T – Transverse mode; V – Vertical mode; L – Longitudinal mode; $\Delta = [2] / [1] - 1$.

8.6.2. Natural frequencies

In this section an analysis of the natural frequencies identified in both tests within the range of 0-3.6 Hz is performed. A combined inspection of the power spectra presented in Figure 8.6 and of the experimental natural frequencies listed in Table 8.3 leads to the following comments:

i. Although 15 natural frequencies were obtained in Test 1 the quality of the field data only allowed to reliably identify 9 vibration modes;
ii. For each of the 14 natural frequencies identified in Test 2 it was possible to identify the corresponding mode shape;

iii. The first vertical bending mode identified in Test 1 is associated to two natural frequencies in the corresponding ANPSD (1.636 Hz and 1.709 Hz), which suggests a likely nonstationary behavior of the structure caused by the support conditions (this specific mode shape holds a large translation component of the upper deck as it will be described in the following section).

Comparing the natural frequencies extracted from both tests for the same vibration modes small differences are found, not reaching 6.6 %, except for the 6th mode in which the reduction exceeded 17 %. Nevertheless, a slight increase of these parameters appears to be the tendency. A switch of the relative position of the 4th and 5th modes is also detected, potentiated by the close proximity of the values.

One peculiar aspect that is highlighted from the identification of the natural frequencies is the fact that the value of the 1st vertical bending mode (5th mode) remained unaltered, in spite of the significant operations performed on the upper deck. From a structural point of view, this fact is a fortunate coincidence, since it was not specifically planned by the rehabilitation design. In addition, given the close proximity of the natural frequencies and the frequency resolution achieved for both tests (of about 0.02 Hz) the estimated values may fall within the same measuring interval. On the other hand, if field data were processed using alternative identification methods some difference could be found (Cunha *et al.*, 2006).

Table 8.4 shows the natural frequencies calculated from the numerical Models A and B, as well as the percentage variation from the field estimates. It is noteworthy that for the analysis of the results representative of the phase before the rehabilitation two sets of numerical values are used, one regarding the numerical simulations performed within this work and the other containing the values predicted within the viability study (Calçada *et al.*, 2002).

In general, as regards to numerical frequencies supplied by the models of this work the correlation with the experimental values can be classified as very good, being the average of the absolute deviations of 1.35 % and 1.99 %, respectively for the pre and post-rehabilitation phases. Consequently, the adopted modeling strategy proved to be extremely feasible in accurately replicating the natural frequencies of the bridge. Furthermore, the numerical model that simulates the dynamic behavior of the bridge before the rehabilitation shows a clear improvement with respect to the one developed for the viability study, pointing for an accuracy increase of 4 times.

Table 8.4 – Summary of natural frequencies of the bridge.

		Before rehabilitation			*After rehabilitation*		
Mode number	*Mode type*	*Identified (Hz)*	*Numerical[3]/[3*] (Hz)*	*Δ (%)*	*Identified (Hz)*	*Numerical[4] (Hz)*	*Δ (%)*
1st	1st T	0.757	0.759/0.821	0.26/8.45	0.732	0.738	0.82
2nd	2nd T	0.903	0.908/0.945	0.55/4.65	0.952	0.925	-2.84
3rd	3rd T	1.343	1.400/1.455	4.24/8.34	1.416	1.399	-1.20
4th	4th T	1.660	1.657/1.528	-0.18/-7.95	1.611	1.650	2.42
5th	1st V–L	1.636	1.636/1.561	0.00/4.58	1.636	1.662	1.59
6th	5th T	2.124	2.016/1.870	-5.08/-11.96	1.758	1.737	-1.19
7th	6th T	---	2.042/---	---	2.026	2.015	-0.54
8th	7th T	---	2.626/---	---	2.148	2.131	-0.79
9th	8th T	---	3.227/---	---	2.368	2.404	1.52
10th	2nd V	2.295	2.274/2.328	-0.92/1.44	2.393	2.365	-1.17
11th	3rd V	---	2.806/---	---	2.856	2.801	-1.93
12th	4th V	---	2.949/---	---	3.125	2.998	-4.06
13th	5th V	3.125	3.126/3.080	0.03/-1.44	3.247	3.198	-1.51
14th	6th V	3.369	3.399/3.469	0.89/2.97	3.589	3.362	-6.32

Vibration modes are numbered according to the order of the identified modes after the rehabilitation; T – Transverse mode; V – Vertical mode; L – Longitudinal mode; [3] – Model A; [3*] – Model developed for the viability study; [4] – Model B; Δ = Numerical / Identified - 1.

Another aspect of interest in the numerical results is the changes in the ordering of the vibration modes. The close proximity of the natural frequencies of the 9th and 10th modes (8th transverse and 2nd vertical bending modes) after the rehabilitation made their numerical calculation more difficult, resulting in the inversion of the modes. More importantly, the ordering of the vibration modes from the 8th to the 12th position is completely altered between Models A and B.

8.6.3. Mode shapes

Mode shapes provided by the numerical Models A and B are shown in Figures 8.10 and 8.11, represented in the left- and right-hand sides, respectively. The deformed shape of the bridge is defined by the upper chords of the upper deck and by the lower chords of the lower deck. Even though transverse bending modes engage torsion deformation of the upper deck in some extent, their configuration is represented in the figure by plan views whereas the vertical bending modes are presented in elevation. Simultaneously, the modal coordinates extracted from both tests are plotted over the numerical mode shapes in order to enable an easy and immediate evaluation of the results.

The analysis of the correlation between identified and calculated parameters is accomplished by graphical comparison and by means of the Modal Assurance Criterion (MAC) (Allemang, 2003), with the corresponding parameter estimated through equation 5.1.

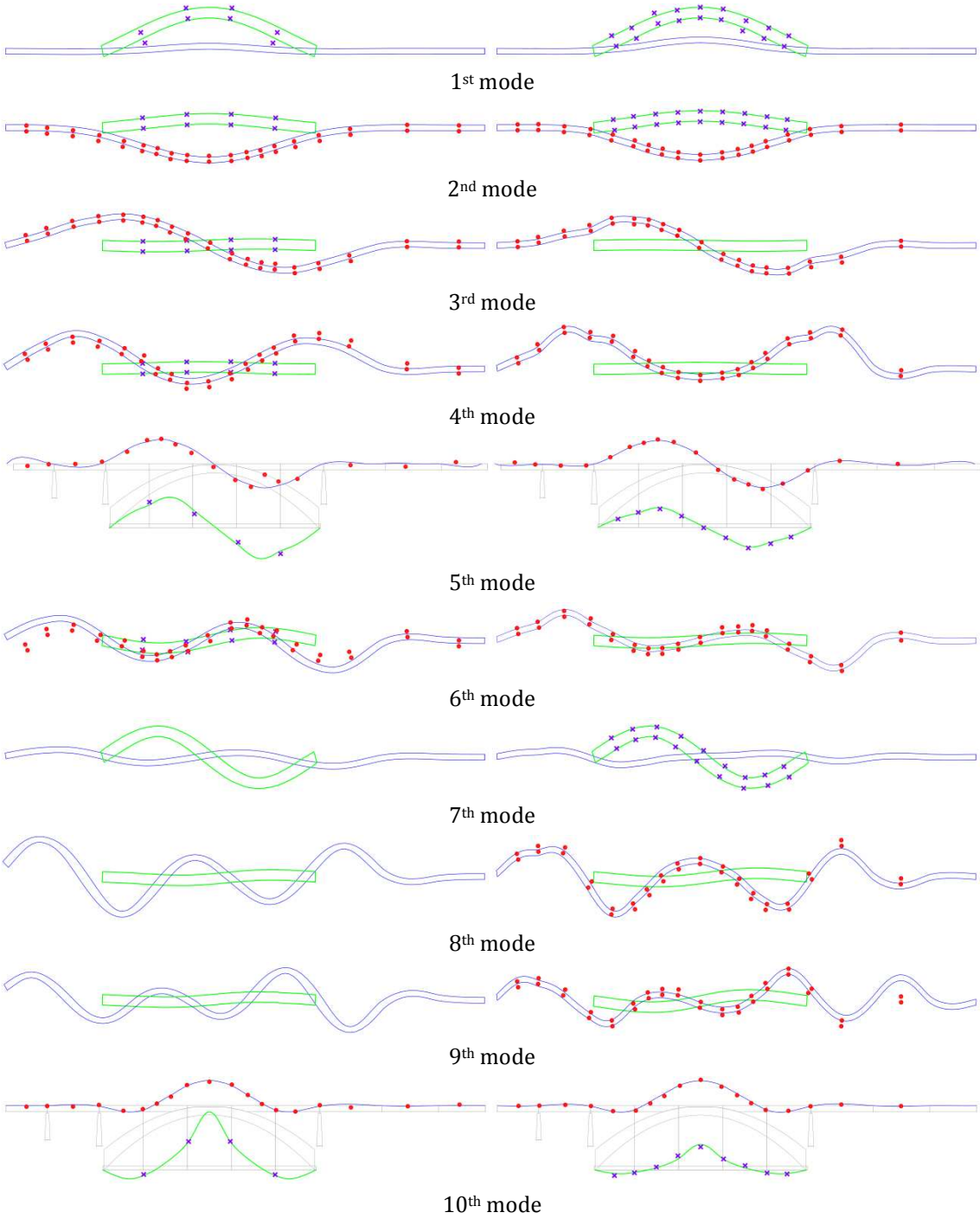

Figure 8.10 - Identified mode shapes before (left) and after (right) the rehabilitation (I).

Experimental coordinates: ● upper deck, ✖ lower deck.

Elevation and plan view: ——— upper deck, ——— lower deck.

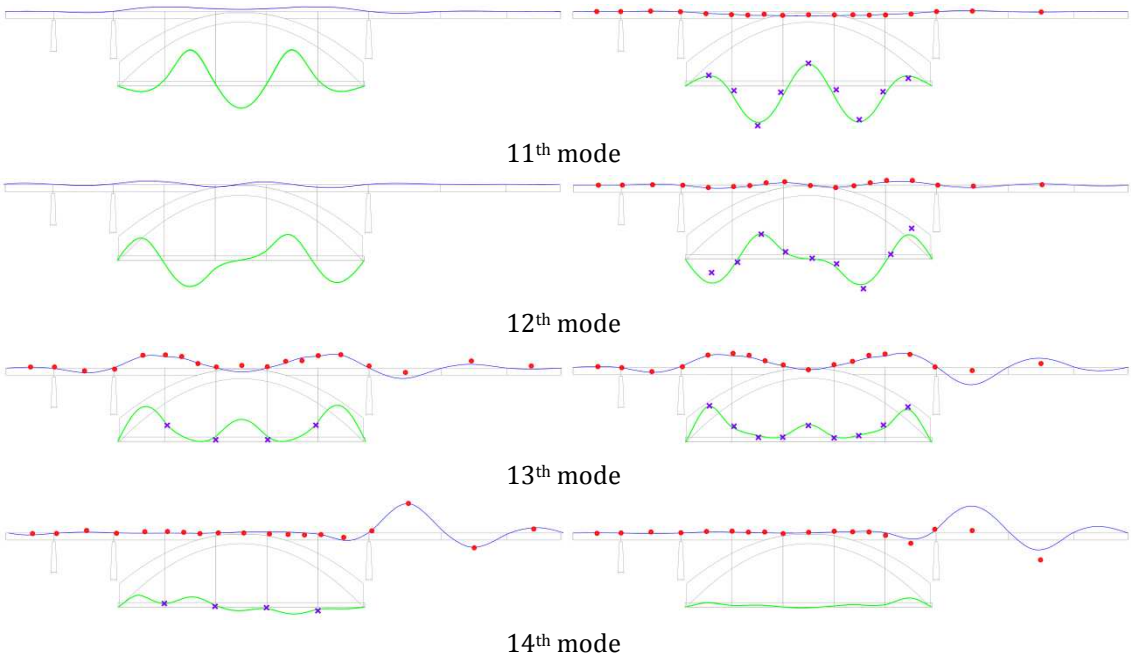

Figure 8.11 - Identified mode shapes before (left) and after (right) the rehabilitation (II).
Experimental coordinates: ● upper deck, ✖ lower deck.
Elevation and plan view: ——— upper deck, ——— lower deck.

In general, the experimental modal components compare well with the mode shapes estimated by the models, exhibiting a slightly better match for the post-rehabilitation condition, particularly with respect to transverse modes. Yet, it should be pointed out that for some vibration modes the similarity level is poor as a consequence of the lower quality of the field test data. These are the cases of the 5th transverse bending mode (6th mode) before the rehabilitation and of the 6th vertical bending mode (14th mode) in the new condition.

The changes produced in the structure response regarding its stiffness can also be inferred by a careful examination of the mode shapes. The transverse bending modes after the rehabilitation reveal a less smooth deformed shape of the upper deck near the steel piers. Since the strengthening of these structural elements was very limited this fact suggests a clear decrease of the transverse bending stiffness of the upper deck, which will be properly analyzed in section 8.6.4.

The MAC values comparing the numerical and experimental vibration modes for the pre- and post-rehabilitation conditions, labeled as MAC(1) and MAC(2), respectively, are shown in the chart of Figure 8.12(a). The calculation of these indicators was made on the basis of the modal displacements obtained at the measuring sections for each direction of interest, transverse or vertical. Additionally, the values estimated with the model developed for the viability study are also presented, termed as MAC(0).

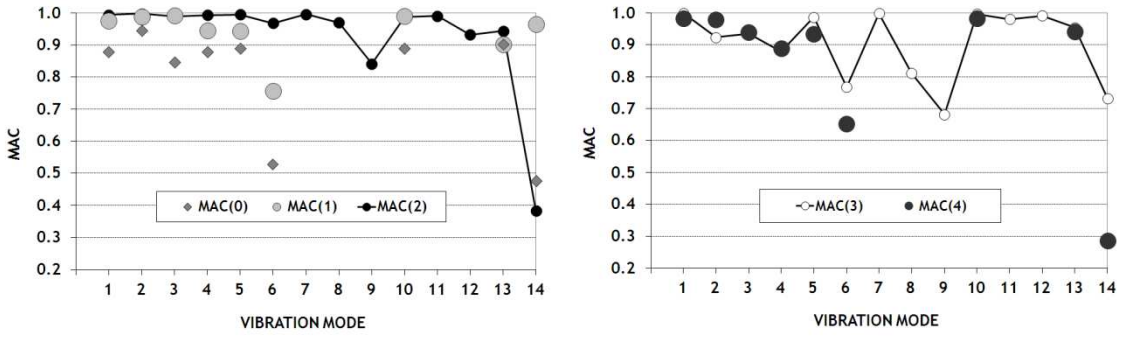

(a) (b)

Figure 8.12 - MAC estimates: (a) MAC(0) – identified and calculated mode shapes before the rehabilitation (viability study model), MAC(1) – identified and calculated mode shapes before the rehabilitation (Model A), MAC(2) – identified and calculated mode shapes after the rehabilitation (Model B); (b) MAC(3) – numerical mode shapes before and after the rehabilitation (Models A and B), MAC(4) – experimental mode shapes before and after the rehabilitation.

As it can be seen, indicators MAC(1) and MAC(2) are for almost vibration modes higher than 0.90. The values of the 6th and 14th modes regarding Test 1 and 2, respectively, confirm once more the lower quality of the corresponding experimental data. When excluding these two modes, the average value of MAC(1) is 0.96 and of MAC(2) is 0.98. However, as it would be expected, a trend of degradation of these indicators as the mode order increases is perceptible, which is explained by the fact that the deformed shapes are successively more winding and therefore require a larger number of points to be captured. The clear improvement of the results calculated from Model A compared to the values from the model of the viability study is also evidenced. Therefore, in view of the above, the reliability of the numerical models developed in this work for the accurately replication of the bridge modal parameters is once again highlighted.

The changes produced in the mode shapes as a result of the rehabilitation process are objectively appraised through the calculation of two other MAC indicators, one correlating the modal parameters estimated by Models A and B, labeled as MAC(3), and the other comparing the experimental modes identified in both tests, named as MAC(4). The values are plotted in the chart of Figure 8.12(b). With respect to the first indicator, the values associated with the first vibration modes, both transverse and vertical, remain above 0.90. However, for the higher order modes, particularly the transverse, the values decrease, which is consequence of the less smooth deformed shape of the upper deck after the rehabilitation. This evidence is further confirmed by the results of MAC(4), and apparently more pronouncedly. Still, one has to bear in mind that the experimental mode worse identified is exactly the last, which may lead to biased conclusions.

8.6.4. Stiffness variation

The change of the natural frequencies of a structure, in particular of a bridge, is an issue of extreme value since the structural performance may significantly vary, and often negatively, depending on the characteristics of the dynamic loading. Yet, the stiffness of the bridge, as a whole and its relative distribution among the structural components, decisively controls the static response. Therefore, if data collected from dynamic testing could be used to estimate the stiffness change from a reference state, as is the case of the pre-rehabilitation condition, the information would be extremely useful. Moreover, some advantages of the ambient vibration testing compared to the static load tests, such as non-disruption of the traffic and fastness of execution, may compel the selection of the first, particularly in the context of in-service monitoring.

Table 8.5 – Distribution of the mass in the bridge.

Substructures	*Before rehabilitation[5] (t)*	*After rehabilitation[6] (t)*	*Δ (%)*
Upper deck	2265.7	1848.0	-18.44
Lower deck	938.5	938.5	0.00
Piers	128.7	137.6	6.88
Suspension ties	69.5	89.3	28.46
Arch	1255.8	1309.2	4.25
Total	4658.3	4322.6	-7.21

$\Delta = [6] / [5] - 1.$

The evaluation of the stiffness variation based on modal data requires a judicious selection of the vibration modes, but also an accurate quantification of the mobilized mass. The expression for the modal calculation of this parameter between two structural conditions is given by equation 5.2.

The input data for using this equation are given in Tables 8.3, 8.5 and 8.6. Table 8.3 summarizes the natural frequencies of the vibration modes identified in both tests and their percentage deviation, Table 8.5 lists the mass distribution in the bridge and its proportional variation, and Table 8.6 gives the modal masses for each direction of interest estimated from the numerical analyses.

Table 8.6 – Modal mass variation estimated from the numerical analyses.

		Before rehabilitation[7]			*After rehabilitation[8]*			*Δ (%)*		
Mode number	*Mode type*	*L** *(t)*	*T** *(t)*	*V** *(t)*	*L** *(t)*	*T** *(t)*	*V** *(t)*	*L**	*T**	*V**
1st	1st T	1.7	457.0	1.5	1.5	535.3	1.5	-10.40	17.13	-1.62
2nd	2nd T	1.8	896.2	4.7	2.2	953.8	6.3	19.60	6.43	35.00
3rd	3rd T	2.6	809.4	9.1	5.5	823.0	7.8	112.73	1.68	-13.37
4th	4th T	2.7	574.7	5.7	1.1	461.0	9.9	-57.93	-19.79	73.63
5th	1st V–L	771.5	0.3	1042.3	1232.1	0.4	1025.8	59.70	16.75	-1.59
6th	5th T	7.2	992.7	5.0	0.8	409.7	7.7	-88.58	-58.73	53.13
7th	6th T	7.7	732.6	6.4	3.9	531.2	6.7	-49.30	-27.49	4.36
8th	7th T	9.6	736.8	9.6	3.8	470.9	11.3	-60.31	-36.08	17.91
9th	8th T	12.1	843.9	14.1	148.9	498.5	21.8	1129.40	-40.93	54.69
10th	2nd V	26.4	0.6	258.4	37.2	0.7	244.1	40.91	19.06	-5.52
11th	3rd V	1729.4	5.5	266.5	5.3	6.4	268.1	-99.69	15.09	0.59
12th	4th V	34.7	21.2	369.1	27.2	30.0	396.4	-21.39	41.19	7.39
13th	5th V	45.3	45.5	369.6	42.7	67.3	394.1	-5.69	47.98	6.62
14th	6th V	21.8	83.1	199.1	6.6	71.7	144.0	-69.55	-13.68	-27.70

Vibration modes are numbered according to the order of the identified modes after the rehabilitation; T – Transverse mode; V – Vertical mode; L – Longitudinal mode; L* – Longitudinal direction; T* – Transverse direction; V* – Vertical direction; $\Delta = [8] / [7] - 1$.

In order to appraise the variation of the vertical bending stiffness experienced by the upper deck, the vertical vibration mode to be selected must have a configuration for which the deformation shape of the remaining elements is minimal. The most suitable candidate is therefore the 6th vertical vibration mode (14th mode) where the deformation is almost restricted to the four north spans (see Figure 8.11). From Table 8.5 the mass of the upper deck was reduced by more than 18 %, to which corresponds a ΔM value of 0.816, whereas the increase of the natural frequency shown in Table 8.3 was about 6.5 % ($\Delta f = 1.065$). These data point to a stiffness reduction of 7.4 %, i.e. a ΔK of 0.926. Yet, if the vertical modal mass variation from the numerical analysis is used ($\Delta M = 0.723$) the new estimate for the stiffness decrease is 18 % ($\Delta K = 0.820$), which is very close to the value inferred from the static load tests carried out on the bridge (Costa *et al.*, 2008b).

With regard to the change of the transverse bending stiffness of the upper deck, the task is made more difficult due to the fact that in all transverse modes the arch and piers are deformed. The selection of the candidate vibration mode met the following criteria:

i. Non-existence of rotation at the arch crown;
ii. Minimization of the transverse deformation of the arch and metallic piers;

iii. Existence of at least one upper deck span whose deformation has inflection points and small transverse displacements at the supports.

The most suited vibration mode is the 7th transverse (8th mode) and the best fitting span the 11th (see Figures 8.4 and 8.10). Since this mode shape was not identified in Test 1, the data used for the analysis is supplied by the numerical analysis. Nevertheless, the validity of the conclusions is ensured by the reliability of the models developed for this work. Taking the ratio of the natural frequencies listed in Table 8.4 as $\Delta f = 0.812$ (2.131/2.626) and the ratio of the corresponding modal mass for the transverse direction as $\Delta M = 0.639$ (1-36.08/100), the estimate obtained for the reduction of the transverse bending stiffness of the upper deck is about 58 % ($\Delta K = 0.421$). A static analysis of span 11, considered as a single simply supported bridge, points to a close value of stiffness decrease ($\Delta K = 0.456$) when a uniform transverse load is applied, thus proving the adequacy of the adopted procedure.

8.7. Sensitivity analysis

As mentioned earlier, the FE modeling enabled the analysis of the contribution of several structural parameters for the accurate definition of the modal parameters of the bridge. The natural frequencies calculated from the base Models A and B, and the corresponding deviations in the estimates produced by different simulation scenarios are given in Tables 8.7 and 8.8, respectively. The description of each variant model was made in Section 8.5.3, and the variables under analysis were the:

i. Restriction level of the decks longitudinal displacements;
ii. Supporting conditions of the arch;
iii. Effect of the light-weight concrete pavements;
iv. Influence of the new steel floor system;
v. Contribution of the upper deck main stringers in the new bridge condition;
vi. Impact of offsetting the bars structural axes from the reference geometric axes;
vii. Transverse bending stiffness of the upper deck at the upper level.

Table 8.7 – Variation of the natural frequencies from the sensitivity analysis for the pre-rehabilitation condition of the bridge.

		Model									
Mode number	*Mode type*	*A*	*A1*	*A2*	*A3*	*A4*	*A5*	*A6*	*A7*	*A8*	*A9*
		(Hz)	*Δ (%)*								
1st	T	0.759	-20.7	0.0	-20.7	16.7	0.0	16.7	0.0	-28.2	7.8
2nd	T	0.908	-0.2	0.0	-0.2	3.1	0.1	3.1	0.2	-5.1	0.8
3rd	T	1.400	-0.2	-0.2	0.0	0.7	0.7	0.0	0.0	-12.7	0.3
4th	T	1.657	-0.8	-0.8	-0.1	1.9	1.9	0.0	0.1	-19.1	0.3
5th	V – L	1.636	-37.5	-37.6	0.0	15.5	15.5	0.0	1.3	-9.0	1.1
6th	T	2.016	-0.2	-0.5	0.4	2.9	3.1	0.3	0.0	-20.4	0.8
7th	T	2.042	-10.0	-0.1	-10.0	11.4	-0.5	11.4	0.0	-47.4	5.9
8th	T	2.626	-0.8	-0.7	0.0	1.8	1.8	0.0	0.1	-17.7	0.7
9th	T	3.227	-0.4	-0.3	0.0	1.1	1.0	0.0	0.1	-29.9	0.5
10th	V	2.274	-0.1	0.0	0.0	0.0	0.0	0.0	0.7	-4.8	2.8
11th	V	2.806	0.0	0.0	0.0	0.0	0.0	0.0	0.0	-9.0	10.0
12th	V	2.949	-1.6	-1.8	0.5	0.4	0.4	0.0	0.2	-8.3	15.1
13th	V	3.126	-1.2	-0.1	-1.2	0.4	0.2	0.3	0.2	-7.0	14.5
14th	V	3.399	-0.6	-0.6	0.0	8.3	8.3	0.0	0.0	-18.0	2.1

Vibration modes are numbered according to the order of the identified modes after the rehabilitation; T – Transverse mode; V – Vertical mode; L – Longitudinal mode; $\Delta = [Ai] / [A] - 1$.

The collected results lead to the following comments.

- *Models A1 to A6 and B1 to B6:* constraints on the longitudinal displacements of the decks ends only influence a limited number of vibration modes, the two transverse where the deformed shape of the lower deck is predominant (local modes) and the first vertical to which is associated a significant component of longitudinal movement on the upper deck (see Figure 8.10 and Table 8.6);

- *Models A2 to A3, A5 to A6, B2 to B3 and B5 to B6:* there is no cross effect of the support conditions at both decks ends for the vibration modes influenced by them, e.g. restrictions to the longitudinal displacements of the upper deck do not generate changes in the natural frequencies of the vibration modes associated with the movement of the lower deck;

Table 8.8 – Variation of the natural frequencies from the sensitivity analysis for the post-rehabilitation condition of the bridge.

		Model											
Mode number	*Mode type*	*B*	*B1*	*B2*	*B3*	*B4*	*B5*	*B6*	*B7*	*B8*	*B9*	*B10*	*B11*	*B12*
		(Hz)	*Δ (%)*											
1st	T	0.738	-19.8	0.0	-19.8	14.9	0.0	13.8	0.3	-0.1	-0.3	-26.0	0.3	6.9
2nd	T	0.925	-1.1	0.0	-1.1	4.6	0.0	3.7	0.2	-0.5	-1.1	-2.3	0.9	1.7
3rd	T	1.399	-0.1	0.0	-0.1	0.1	0.0	0.0	0.0	-1.5	-1.5	0.0	2.9	0.6
4th	T	1.650	-0.2	-0.2	0.0	0.2	0.2	0.0	0.1	-3.8	-2.9	-0.5	7.6	1.6
5th	V – L	1.662	-36.5	-36.5	0.0	3.4	3.4	0.0	1.2	-5.0	-6.6	-0.2	0.1	1.6
6th	T	1.737	-0.5	-0.2	-0.3	0.3	0.3	0.1	0.0	-4.4	-3.5	0.1	10.9	1.8
7th	T	2.015	-8.9	0.0	-8.9	10.6	0.0	9.5	0.0	-0.5	-0.2	-45.5	1.4	6.2
8th	T	2.131	-0.2	-0.2	0.0	0.1	0.2	-0.1	0.1	-5.2	-4.8	-0.1	14.7	2.4
9th	T	2.404	-0.4	-0.2	-0.2	0.9	0.2	0.6	0.1	-6.0	-4.5	-0.2	9.7	2.3
10th	V	2.365	-0.2	-0.1	-0.1	0.0	0.0	0.0	0.6	-0.5	-0.5	-2.3	0.0	3.4
11th	V	2.801	-0.4	-0.1	-0.2	0.1	0.0	0.1	0.0	0.0	0.0	-5.1	0.0	14.0
12th	V	2.998	-4.3	-4.3	0.6	0.1	0.1	0.1	0.2	-0.1	-0.1	-5.3	0.0	17.3
13th	V	3.198	-0.9	-0.1	-0.9	0.2	0.0	0.2	0.2	-1.3	0.1	-4.5	0.1	13.1
14th	V	3.362	-0.1	0.0	-0.1	0.0	0.0	0.0	0.0	-3.0	0.1	-1.1	0.9	2.4

Vibration modes are numbered according to the order of the identified modes after the rehabilitation; T – Transverse mode; V – Vertical mode; L – Longitudinal mode; $\Delta = [Bi] / [B] - 1$.

- *Models A and B:* bearing in mind the identified natural frequencies and the excellent correlation with the numerical estimates provided by the reference numerical models, there is no doubt that the real supporting conditions of the decks, before and after the rehabilitation of the bridge, correspond neither to free or blocked movement, but on the contrary they are representative of an intermediate state;

- *Models B and B5:* Yet, elastic springs applied at the ends of the upper deck to simulate the post-rehabilitation condition have an impact very close to the blocking of the displacements;

- *Models A and A8:* when the stiffness of the light-weight concrete pavements is not taken into account a general softening in Model A occurs. The influence on the transverse modes associated to large deformation of the lower deck is very strong, but the impact on the remaining transverse modes is also very significant. The natural frequencies of the vertical vibration modes undergo a

smaller decrease, 2.5 times less, except for the last vertical mode for which the impact is much higher.

- *Models B and B8:* the secondary stringers in the new floor system have a minor influence, although increasingly, on the global transverse modes, and also affects the first vertical mode which holds a large longitudinal movement of the upper deck;

- *Models B and B9:* the stiffness contribution of the main stringers of the new steel grid is also similar, although slightly inferior for the transverse modes and higher in the first vertical mode;

- *Models B and B10:* for the new condition of the bridge, simulated by Model B, the influence of the concrete pavement stiffness of the lower deck is substantially smaller, yet influencing in the same extent the transverse local modes of this deck and only slightly the vertical vibration modes;

- *Models B and B11:* the membrane stiffness of the cladding plates in the new floor system, simulated by crossbeams rigid to transverse bending, has some influence on the transverse modes, yet when accounted for it leads to higher deviations of the numerical frequencies over the identified values;

- *Models A/B and A9/B12:* the non-offsetting of the bars structural axes leads to the general stiffening of both models, with some significance in the transverse modes and decisively impacting the vertical modes associated to predominant deformed shapes of the lower deck.

It is worth highlighting that the non-cross and localized influence of the decks supporting conditions, at their ends, on the bridge natural frequencies has enabled the calibration and/or update of the elastic coefficients of the longitudinal springs listed in Table 8.1, on the basis of a small number of vibration modes (1st, 5th and 7th modes) by matching the numerical frequencies with the field measured values.

8.8. Summary and conclusions

This chapter has presented a study regarding the modal identification of a centenary double-deck steel arch bridge, which underwent rehabilitation and strengthening works in order to integrate its upper deck into the light metro infrastructure network of Porto.

Two ambient vibrations tests were conducted to collect data from the pre and post-rehabilitation conditions. Data from the first test were used to assist the viability study of the project, and subsequently also its design, whereas the measurements from the second test, herein detailed, helped to identify the changes produced in the behavior of the bridge for the new service conditions, and also provided a sound baseline for structural health monitoring. The design and execution of the second test was comprehensively reported, which included testing procedures, instrumentation and signal acquisition, and differences from the first test were pointed out. Additionally, the data processing and modal extraction techniques implemented for the structural identification were also presented. Three-dimensional finite element models were constructed to support the modal analysis, and in turn experimental data served to validate and/or update the numerical models. Two new base models have simulated the pre and post-rehabilitation conditions of the bridge, and variant models were generated for a sensitivity analysis aimed at evaluating the influence of several structural parameters on the dynamic properties.

The results of this study led to the following conclusions:

i. Measured natural frequencies for the same vibration modes have experienced small changes, presenting a slight tendency to increase after the bridge rehabilitation;
ii. With respect to the mode shapes the deformed configuration of the upper deck became less smooth near the steel piers for the transverse vibration modes, particularly as the order increases;
iii. The modal parameters identified from both tests corresponded very well with the estimates supplied by the numerical models developed for this study;
iv. The new model that replicates the pre-rehabilitation condition of the bridge has provided estimates of improved quality in relation to those that had been calculated in the viability study;
v. The vertical bending stiffness of the upper deck was reduced by 18 %, whereas the transverse one reached a decrease of 58 %, values very close to the static estimates, either experimental or numerical;
vi. Constraints on the longitudinal displacements of both decks decisively contribute to control the natural frequencies of some vibration modes;
vii. The light-weight concrete pavements of the decks clearly stiffen the bridge and the new floor system and steel grid of the upper deck have comparatively a smaller impact in the natural frequencies;

viii. The accurate relative positioning of the bars structural axes in the models is crucial in controlling the natural frequencies of the vibration modes for which the lower deck deformation is predominant (local modes).

Chapter 9

Conclusions and future research

9.1. General remarks

The present PhD research project was focused on the use of structural identification oriented towards the rehabilitation assessment of old steel bridges, by addressing the monitoring and numerical modeling aspects.

Electric resistance versus fiber optic strain sensors

Within a research project aimed at developing and applying procedures for the evaluation of the structural integrity of steel railway bridges, in **Chapter 2** two parallel monitoring systems installed in a railway bridge (Trezói Bridge) were presented. One system was based on electric strain gages and the other on fiber optic strain sensors.

The electric monitoring system was designed and installed on the bridge to supply the experimental data for the research project, while the fiber optic monitoring system was applied aiming at two main objectives. Firstly, to evaluate the reliability of the former and to check its efficiency, and secondly to provide some redundancy of the measurements at critical locations.

In addition, rails cross-sections in the vicinity of the bridge abutments were instrumented with strain gages in order to characterize the actual passing traffic. The measurements enabled the collection of data regarding the vehicles characteristics, including the number of axles and their spacing, as well as the velocity spectra, moving directions and traffic density.

The electric strain sensors consisted of foil strain gages pre-glued to rectangular epoxy bases acting as sensor holders. These surface mountable sensors did not require any soldering operations at the field, thus allowing a quick and flexible installation without jeopardizing the reliability of the measurements. The fiber optic strain sensors had the fiber optic grating protected and back supported on a polyimide base. As the bare fiber with the grating is not fixed to the polyimide base, it allows its direct and free gluing onto the surface to be gauged.

The structural response of the bridge due to the railway traffic was monitored in two different observation campaigns. The first one was carried out just after the sensors have been installed with the vehicles speed restrained for safety reasons. In the second observation campaign data was acquired to enable the characterization of the bridge behavior under normal operation conditions.

The main conclusions regarding the evaluation of the strain monitoring systems were: i) static components of the signals acquired by both systems, fiber optic and electric based, during the monitoring campaigns were in excellent agreement; ii) however electrical signals were not able to capture the dynamic component with a frequency content higher than 5 Hz as a consequence of a malfunction in the acquisition system which was later identified through laboratory tests; iii) still, the adopted installation procedure was suitable; iv) in spite of some interferences in the electrical signals during the field measurements have been found, both types of sensors have alike capability for dynamic observation under normal conditions; and v) strains measured by the electric sensors presented enough quality for the estimation of the fatigue life in the bridge members.

The assessment of the bridge behavior and the traffic monitoring led to the following conclusions: i) girders chords presented a significant in-plane bending, a behavior very different from that of a pure truss system; ii) chords at the same girder cross-section exhibited different levels of deformation, being lower at the top where the floor system contributes to the bridge bending stiffness; iii) strains varied substantially along the upper chord in the girder panel at the support; iv) critical points for fatigue resistance were located at mid-span lower joints of the girders; and v) a simple experimental scheme was successfully used to characterize the crossing traffic.

Monitoring systems implementation

Following one of the main objectives of this thesis, **Chapters 3** and **6** presented the monitoring systems installed in two old steel bridges that underwent rehabilitation and

strengthening works, the Pinhão Bridge and the Luiz I Bridge, respectively. The gentleness of some of these operations, the evaluation of the strengthening schemes performance and the historic, cultural, and economic significance of these bridges made the structural monitoring of their behavior mandatory.

The first monitoring system consists in an electric sensors network whereas the second relies entirely on fiber optic sensors. Both were designed to be installed during the construction works so that it could be possible to use the general scaffolding system in order to access the structure elements. Three major requirements were considered for the installation of the monitoring systems: i) welding solutions for attaching strain sensors to the steel surface were not permitted due to the chemical properties of the host materials; ii) reliable data concerning the structures in-service behavior had to be assured for at least a decade; and iii) strain sensors attached to the bridges had to have a minimum impact in their aesthetics.

As after the completion of the works these systems served to collect data of the bridges response in their new condition under controlled loading scenarios (field tests), the location of the sensors took into account the cross-sections observed during the load tests carried out before the interventions to assist the upgrade design of the bridges. Therefore, straightforward appraisal of the changes produced in the structural behavior was possible. The parameters measured by these systems are: i) steel strains in cross-sections of bridge elements; ii) horizontal displacements at roller and sliding bearings of the decks; iii) crossbeam rotations; and iv) temperature at the steel surface and of the ambient.

Novel sensor holders were developed and new application procedures adopted in order to fulfill the monitoring objectives. Therefore, a complete experimental characterization of the sensors behavior was carried out. Short-term and time-dependent responses of the sensors, as well as of the adhesives, were evaluated through static tests, whereas their fatigue performance was characterized by cyclic loading experiments. All the results met the requirements set for both projects. Special protection measures were also devised to ensure an adequate durability of the sensors, as well as to guarantee metrological stability under ambient conditions. Laboratory experiments were conducted to evaluate the sensors response to temperature and humidity cycles. For both types of sensors a fair correspondence between the ambient parameters and the readings was verified. The developed protection system has enabled to create a proper thermal insulated environment capable of shielding the sensors from temperature peaks.

Concerning the development of the fiber optic strain sensors numerical analyses were carried out aiming at: i) the estimation of the minimum length of the CFRP holders able to ensure the measurement of the steel strain with an error within acceptable values; and ii) the evaluation of the deviation between the readings and the actual strain acting on the host material influenced by the dimensions of the instrumented element. The results led to the adoption of 10 cm long holders and permitted to verify their suitability for measuring the strains in the bridge components.

The electric monitoring system implemented in the Pinhão Bridge is constituted by a sensing network that spreads throughout the bridge from two observation stations using a tree structure, with a central set of main cables serially branching into secondary cables up to the sensors, grouped by measured parameters and by instrumented points or cross-sections. In the Luiz I Bridge the fiber optic network has a tree configuration with a main optical cable branching into each of the optical fiber leads serially connecting a maximum of 10 sensors. Its design provided a high level of interchangeability of the gratings position in the light path of each optical branch, in order to maximize the number of sensors capable of being interrogated if any fiber breakage takes place. The WDM multiplexing technique was adopted to identify and interrogate the sensors in each fiber lead, whereas the SDM method was implemented through an optical switch to distinguish sensors from different optical branches.

The DASSs allow the collection of raw data from all sensors with a sampling rate of 100 Hz for the Pinhão Bridge and of 2 Hz for the Luiz I Bridge. In spite of this relatively low scanning rate, the bridge response to the metro slow crossings along the upper deck is fairly accomplished. Still, dynamic readings for a single optical branch can be performed at a sampling rate of 50 Hz. The DSPSSs of both monitoring systems translate the continuous monitoring raw data acquired by the DASSs into the physical quantities to be measured, and compute relevant statistical information. In this processing procedure thermal compensation is made so that long-term effects of loads on the bridges are assessed.

Static analysis

The planning and execution of static and quasi-static field tests conducted in the Pinhão Bridge and the Luiz I Bridge were presented in **Chapters 4** and **7**, respectively. The collection of data aimed to accomplish the following main objectives: i) to characterize the global response of the bridges and to provide an improved insight of the strain/stress distribution among the structural elements; ii) to evaluate the level of composite action between the concrete pavement and the steel grid of the floor systems, quantifying their

contribution to the bridges stiffness; iii) to assist the development and validation of the FE models adopted in the analyses of different rehabilitation and strengthening alternatives at the design stage; iv) to assess the effectiveness and/or efficiency of the adopted strengthening solutions after the completion of the construction works; and v) to allow a direct comparison of the bridges performance, before and after the rehabilitation, and consequently to favor the conclusions drawing . Other objectives to attain by conducting the field tests before the reopening of the bridges were: i) to validate the readings acquired by the novel sensors that integrate the permanent monitoring systems under controlled loading conditions; ii) to provide a baseline condition to serve as a reference for the data collected by the structural monitoring systems in order to detect any deviation of the structures behavior over the time; and iii) to accurately calibrate the response measured by key sensors which could be used in the development of future bridge weigh-in-motion systems.

For both bridges, and in both field tests (before and after the rehabilitation), two types of loading scenarios were performed, static and quasi-static. The loading of the decks was made by dump trucks. Static load cases aimed at maximizing the bridges response for the monitored parameters by performing a set of static positions of the vehicles. The quasi-static tests were executed to verify the regularity of the structural behavior under moving loads and to check divergent or baffling results collected in the static loadings, namely the displacements of supports or the deformation of bridges elements. The loads were applied either transversely centered or eccentrically so that the lateral load distribution and torsion deformation of the decks could be appraised. In order to enable a clear perception of the changes in the structural behavior, namely in terms of stiffness and strain/stress variations, the field tests conducted after the bridges rehabilitation have replicated some of the loading scenarios applied in the first tests.

The instrumentation used in the field tests carried out before the bridges rehabilitation was specifically designed and installed for acquiring data during only their execution. It did not have the additional purpose of monitoring the structural response under service conditions. On the contrary, in the field tests conducted after the completion of the construction works the data collection was made through the installed structural health monitoring systems, duly supplemented by additional sensors. The measured parameters in the field tests were: i) steel strains; ii) vertical displacements of the decks; iii) longitudinal displacements at the supports; iv) rotations at the girders joints; and v) ambient and steel temperature.

Modal analysis

In **Chapters 5** and **8**, the ambient vibration tests carried out in the Pinhão Bridge and the Luiz I Bridge, respectively, were presented. The main objective of these dynamic tests was to complement and/or confirm the results obtained in the static field tests. Additionally, other goals to achieve were: i) to support the rehabilitation projects by enabling the bridges condition assessment through the experimental identification of their modal parameters; ii) to supply in-situ data for the validation and/or updating of the models to be used firstly in the evaluation of alternative strengthening strategies and then in the prediction of the bridges response for the new service stage (as part of a likely structural health monitoring system); iii) to identify the changes produced in the dynamic properties of the bridges as a result of the construction works; and iv) to appraise the effectiveness of the implemented strengthening in terms of stiffness variation.

For that purpose, both tests were conducted without significant restrictions to the traffic. Acceleration time series were collected at several sections of the spans in the longitudinal, transverse and vertical directions. Two devices were permanently stationed at the main reference sections, one at each side of the deck, and, when necessary, one at the secondary reference section (lower deck of Luiz I Bridge in Test 2), all located away from any node of the mode shapes to be identified (reference sensors). The remaining sensors were successively placed at the other measurement sections (moving sensors). Vibrations were recorded at both upstream and downstream limits, thus allowing the accurate identification of vertical, transverse and torsional mode shapes.

Tri-axial linear seismographs were used to collect the accelerations, with integrated A/D converters, large battery autonomy, data storage capacity, and external GPS sensor to enable an independent and synchronized operation. The trigger parameters for the data acquisition were previously programmed for each seismograph using a laptop. Therefore, the implemented experimental setup did not require the use of any communication cables and suppressed time-consuming operations in the dynamic tests.

For an accurate identification of different types of modes with very close natural frequencies the signals collected in each section were pre-combined to obtain enhanced time series. The data pre-processing produced new half-sum of vertical, half-difference of vertical and half-sum of transverse accelerations (upstream-downstream) for an improved modal extraction of vertical bending, torsional and transverse bending modes, respectively. NPSD functions were estimated from the acceleration time series of each measuring section, as well as the coherence functions associated to the simultaneous

measurements at the several sections. Subsequently, in order to highlight the natural frequencies, the ANPSDs were computed taking into account all the NPSDs of the same type, and their estimation was accomplished in the frequency domain using the Peak-Picking method. The identification of the mode shapes within the range of interest was performed on the basis of the transfer functions relating the ambient response at each section with the one collected at the reference sections, duly validated by the corresponding coherence functions. The signal change in the coordinates of each mode shape was simultaneously detected by tracking the phase of the transfer functions at the resonant frequencies.

Numerical modeling

For the purpose of an accurate numerical simulation of the bridges behavior, one of the main objectives targeted in this PhD research project, global 3D FE linear elastic models have been developed aiming at the replication of the pre and post-rehabilitation conditions. The models were created on the basis of a mixed modeling approach by using frame and shell finite elements with six DOFs per node.

In the case of the Pinhão Bridge, shell elements were used to replicate the in-plane and out-of-plane deformations of the deck slab. This type of finite elements was also adopted to simulate the webs of crossbeams and stringers, as well as all flat plates of the girders U-chords, whose strains had been measured in the static field tests. For these structural members only the flanges and connecting angles were modeled by frame elements. All the remaining members of the bridge were also simulated by frame elements. The continuity in the chords between panels differently modeled was assured by body constraints at the corresponding joints.

With respect to Luiz I Bridge, almost all members of the 3D global model were simulated through frame elements. Shell elements were only adopted to improve the connection between different substructures or to replicate the webs of the I-plate girders of the upper deck over the arch crown. However, shortcomings in its ability to supply good strain estimates for some key members of the upper deck has impelled the development of a new modeling strategy. The new approach consisted in the combined use of the 3D frame global model and sub-models of the upper deck girders panels. The latter were constructed by modeling their components through panels of shell finite elements rigidly connected at the matching nodes.

The accuracy of the global models was also ensured by: i) taking into account the material properties and the geometry of the structures and of their members reported in the

surveys conducted before the rehabilitations; ii) computing weighed cross-sectional properties for the frame elements that model strengthened and composite members; iii) applying suitable reduction factors to the cross-sectional properties of the latticed members in order to consider the actual section integrity; iv) keeping the symmetry properties of the structures; v) a proper space positioning of the frame elements (offsetting operation).

The modeling strategies implemented for both bridges proved to be adequate to fulfill the targeted goals. They have enabled to accurately capture the load path, secondary bending induced by warping torsion, interaction between structural members, geometrical stress concentrations and other effects neglected by traditional approaches.

Concerning the modal analysis, the mass of the structural elements was considered through the mass densities of the cross-section properties of the frame and shell elements. All permanent non-structural loads were properly converted into concentrated masses applied in the nodes. Special attention was paid to the members of the floor systems to prevent the overestimation of the mass. The combined evaluation of the preliminary numerical results with the field data compelled the development of new models (Pinhão Bridge) and the judicious update of some key parameters (Luiz I Bridge). For the rehabilitated condition of the Pinhão Bridge a global model was developed by assembling three models of a single span, connected through double hinged bars replicating the actions of the expansion joints and of the bolt-bars. With respect to the Luiz I Bridge, restrictions to the free longitudinal movement of the decks were simulated by springs whose coefficients were estimated through a calibration procedure on the basis of the experimental data.

Sensitivity analyses and safety assessment

Taking advantage of the models suitably updated and/or validated, the assessment of the impact of several structural parameters on the bridges behavior, both static and dynamic, was possible through numerical simulation of different scenarios in which key properties were varied. The variables addressed in these analyses were:

Both bridges: i) stiffness of the concrete pavements;
ii) stiffness of the (main) stringers of the decks steel grid.

Pinhão Bridge: i) bending stiffness of the crossbeams;
ii) transverse rotational stiffness of the girders joints.

Luiz I Bridge:
i) stiffness of the secondary stringers of the upper deck floor system;
ii) stiffness of the cladding plates of the upper deck floor system;
iii) transverse bending stiffness of the upper deck;
iv) level of restriction to longitudinal displacements of the decks;
v) supporting conditions of the arch;
vi) positioning of the bars structural axes.

The safety of the bridges and the load-carrying capacity of their members for the new service conditions were evaluated. Three main reasons made these analyses pertinent and useful. Firstly, the updated models are more reliable than those developed in the rehabilitation designs, and therefore can provide improved estimates of the safety parameters. Secondly, analyses carried out at the design stage of rehabilitation projects concerning old steel bridges often follow procedures that can result in costly or unsafe solutions. Thirdly, the assessment may allow the identification of unexpected critical aspects, and subsequently lead to the adoption of adequate corrective measures.

Ultimate limit states were assessed by taking into account only the internal forces that generate normal stresses in the material. In general, the actions adopted in the analyses were the same as those of the designs and the maximum structural effects computed according to the corresponding codes. The strength of the existing materials was taken from the tests of the viability studies. The resistance capacity of the structural members was evaluated according to the European standards for the design of steel structures. Safety factors were estimated by using either the normal stresses (Pinhão Bridge) or the members forces (Luiz I Bridge), depending on the criterion adopted at the design stage. Furthermore, in the safety analysis of the Luiz I Bridge two scenarios were studied. In the first one, only the prevailing axial force or bending moment was taken into account, as performed in the viability study and rehabilitation design, whereas in the second scenario all internal forces were considered. Given the experimental strains measured in the upper deck diagonals, the safety of these elements was also appraised by considering a non-linear geometric behavior under eccentric axial load.

The load rating of the bridges was accomplished for different reasons. As regards the Pinhão Bridge, after the rehabilitation the structure was restricted to vehicles weighing less than 30 ton, since this had been the maximum load considered in the design for one single vehicle, as specified for class II bridges in the Portuguese national code. Rating factors for the critical members of each type could unveil the adequacy of the bridge load posting limit. With respect to Luiz I Bridge, the new mission of its upper deck, as part of

the metro network infrastructure, may lead in the future to the crossing of trains heavier than the current ones. Therefore, the identification of the most sensitive elements to an increase of the traffic loads emerged as a useful analysis.

Concerning the fatigue analysis, different approaches were adopted to assess the bridges safety. For the Pinhão Bridge the limit state was verified by comparing the fatigue resistance at a constant stress range with the maximum stress variation estimated for each critical element from the numerical analysis carried out with the design traffic loads. The limiting stress range was evaluated in the viability study for a 30 years extension period of the bridge service life on the basis of heavy traffic data supplied by the bridge owner.

In what concerns the Luiz I Bridge, the fatigue assessment was performed only for the upper deck. It was based on the Palmgren-Miner rule of cumulative damage for the fatigue life calculation of components under variable loading, assuming a consumption of about 11 % of the fatigue life in the old steel as estimated by the viability study. The stress spectra for the application of the cumulative damage method were obtained by rainflow cycle counting from the numerical stress curves generated in critical members by the trains. The dynamic effects were accounted for by duly factoring the static influence lines. In addition, different scenarios were considered, regarding the traffic, time-span of analysis and internal forces.

9.2. Conclusions

From the field tests, numerical analyses and safety assessment the following conclusions could be drawn:

General

- The global behavior of the bridges was well simulated as a 3D frame system, either for static or dynamic analysis, even though semi-rigid connections for some joints might improve the accuracy of the modal estimates.
- The numerical estimates for global static quantities compared well with the experimental results, indicating a good ability of the models for predicting vertical displacements with errors below 5 %.

- However, for steel strains the results supplied by the global models were often of lower quality. Nevertheless, if suitable modeling strategies are adopted the numerical estimates can present a maximum deviation from the field data smaller than 10 % in the most stressed members.

- The modal parameters identified from the ambient vibration tests, both the natural frequencies and mode shapes, agreed very well with the estimates supplied by the global numerical models.

- A detailed analysis of the shifts produced in some natural frequencies has permitted to obtain excellent estimates of the stiffness variations of the bridges.

- The floor systems, both the steel grids and the concrete pavements, undoubtedly contribute for the global deformation of the bridges and impact on the forces induced in the main truss girders.

- Static and quasi-static tests provided complementary results. While in the first case the maximum response of the structures was appraised within safe limits, in quasi-static testing the regularity of the bridges behavior was assessed. The numerical analyses have accurately estimated the displacements induced by static loadings. However, often failed to supply fair results for steel strains, since these parameters are of local nature and largely depend on the exact positioning of the vehicles and on the members connections. On the contrary, quasi-static crossings have allowed to improve the correlation between the strain data and the numerical estimates, even for a lower loading level.

- For both bridges the girders chords not located at the level of the floor systems presented a much lower safety level and load-carrying capacity than their counterparts. Therefore, particular attention should be paid to these members if changes are made in the service conditions in the future.

Pinhão Bridge

- The strengthening may be considered effective in that the rehabilitation led to an increase of the global vertical stiffness of the spans close to 20 %, and to an average decrease of the strains in the elements higher than 40 %, although it has only reached 25 % in the lower chords.

- Field data confirmed a large reduction of the vibrations at the deck level after the rehabilitation under similar traffic conditions.
- The natural frequencies of the identified vibration modes either remained constant or greatly increased with the rehabilitation process, whereas the mode shapes did not indicate any significant variation between the pre and post-rehabilitation conditions.
- However, a global vertical bending mode was identified after the bridge rehabilitation, which was confirmed by the numerical analysis and ascribed to the blocking of the bolt-bars.
- While the stringers stiffness influences both the vertical and transverse modes, the slab mainly impacts on the latter and a significant variation of the crossbeams stiffness has little effect on the vibration frequencies.
- The ultimate limit state for normal stresses cannot be verified for the upper chords, and consequently these elements were identified as the weakest components of the structure. Nevertheless, all the remaining structural members present a large safety margin.
- The fatigue resistance was found to be satisfactory.
- The live load-carrying capacity of the bridge is very close to the current posted limit. However, it could be easily increased through a judicious strengthening of the upper chords.

Luiz I Bridge

- The secondary stringers that constitute the new floor system of the upper deck have a smaller contribution to its stiffness than the old light-weight concrete pavement. As a result, an average increase of the upper deck deflection of about 17 % was identified.
- The replacement of the upper deck floor system significantly increased the strains of the upper chords, although no relevant influence on the deformation of the remaining elements of the bridge was observed.
- The torsion stiffness of the upper deck decreased about 10 % after the bridge rehabilitation. The strains difference between the girders lower chords under eccentric loading for the new bridge condition led to a value close to 30 %.

- In general, the strengthening of the bridge elements has enabled a significant decrease of their deformation, namely in the arch and upper deck diagonals. Furthermore, for some non-strengthened arch elements the steel strains were also reduced, which was likely induced by changes in the forces distribution (load path) within the statically indeterminate structure.

- For almost all arch and piers elements the experimental strains revealed a small bending component, whereas the upper deck elements, namely chords and diagonals are subjected to high strain gradients.

- The strains estimated from the frame elements of the global models compare well with the test data for members subjected to small bending, namely the arch and piers, and for the flanges of the upper deck elements (chords and diagonals). On the contrary, the strains predicted for the webs of the upper deck chords and for the diagonals strengthening angles are of lower or poor quality.

- The sub-models of the upper deck girders panels supplied superior numerical estimates for the elements strains. For both diagonals and chords the load path, warping torsion, elements connections and stress concentrations were properly simulated.

- The numerical results clearly pointed out an eccentric loading of the upper deck diagonals, which could be experimentally verified by monitoring the response of one diagonal during the crossing of a metro train in the new operational phase.

- The constraints to the longitudinal displacements of the upper deck, identified during the static field test carried out after the bridge rehabilitation, could only be partially interpreted through the numerical analysis by simulating a contact non-linearity at the arch ends. The remaining difference, in magnitude and/or shape, may be caused by additional restrictions to the movement at the upper deck ends, generated by the friction in the expansion joints.

- The strain data collected from the upper deck crossbeam highlighted the importance of establishing a well characterized baseline condition through field testing. The monitoring results permitted to identify a change in the crossbeam behavior during the service phase.

- The measured natural frequencies for the same vibration modes have experienced small changes, presenting a slight tendency to increase after the bridge rehabilitation.

- With respect to the mode shapes, the deformed configuration of the upper deck became less smooth near the steel piers for the transverse vibration modes, particularly as the order increases.

- The modal estimates supplied by the new model that replicates the pre-rehabilitation condition present a superior quality to those of the model developed for the viability study.

- Based on the modal results, the vertical bending stiffness of the upper deck was reduced by 18 %, whereas the transverse one reached a decrease of 58 %, values very close to the static estimates, either experimental or numerical.

- The restrictions to the longitudinal displacements of both decks decisively contribute to control the natural frequencies of some vibration modes.

- The non-offsetting of the bars structural axes leads to the general stiffening of the global models, with some significance in the transverse modes. It also decisively influences the vertical modes associated to predominant deformed shapes of the lower deck.

- The members pertaining to the substructures targeted in the rehabilitation present a suitable safety level and high rating factors when only the mandatory internal axial force or bending moment is considered. However, for a large number of members the results drastically change when all internal forces are taken into account. Nevertheless, the analyses were conservatively performed by not taking into account any reserve of plastic resistance, i.e. assuming that failure takes place when the most stressed fibers reach the limit of elasticity.

- Although the rehabilitation project did not included the lower deck in the strengthening evaluation, the safety of its elements can be regarded as adequate, except for the crossbeams at the suspension ties. However, their failure does not inevitably imply a local or global collapse, and their strengthening in order to meet the present standards is small and localized. Therefore, the corresponding construction works can be easily executed during future interventions.

- In light of the strains collected from the upper deck diagonals during the field tests, a clear identification of their load path was accomplished. The eccentricity of the load in these elements is a direct consequence of their connections at the girders joints. Therefore, for members under compression the safety assessment was also performed assuming a non-linear geometric behavior. For this scenario, the analyses revealed unsuitable safety and rating factors, which, however, should not be regarded as distressing values. In fact, the strengthening of the diagonals led to an average increase of their load capacity of almost 65 % and the permanent loads were reduced as a result of the floor system replacement. Therefore, the safety level was largely incremented with respect to the pre-rehabilitation condition, during which no evidence of distress caused by buckling was identified.

- Regarding fatigue analysis, all elements of the upper deck have a suitable resistance for at least 50 years, being the crossbeams the most sensitive elements as a result of their higher stress ranges and larger number of loading cycles.

9.3. Prospects for future developments

The work conducted within this thesis sought to contribute for the monitoring and rehabilitation assessment of old steel bridges through the adoption of an adequate structural identification framework. However, new developments are required to address the expectations raised by the huge effort invested in the development and installation of permanent monitoring systems. Consequently, in this section some future research topics are listed in the following paragraphs.

- Development, implementation and validation of processing procedures to extract useful information from the data continuously acquired by the monitoring systems, so that structural identification may be accomplished on a regular basis without the need of conducting costly and restrictive field tests.

- Detailed analysis of the long-term monitoring results of the bridges in order to evaluate either the bridges performance under the cyclic environmental loadings, namely those temperature related, or the metrological stability of the novel sensors specifically developed for the monitoring systems.

- Execution of a complete study concerning the structural safety of the upper deck diagonals of the Luiz I Bridge. To this end, experimental assessment of the actual state of stress installed in the critical elements, advanced numerical analyses capable of accurately replicating the non-linear behavior of the deck and its components, as well as a sound knowledge on the loading history and construction/rehabilitation sequences, are required.

- Application of damage detection techniques based on the simulation of likely failure scenarios, supported on the models experimentally validated after the rehabilitation and on the results from the continuous monitoring.

- Exploration of model updating techniques to assess any continuing deterioration mechanisms acting on the monitored structures, either of local or global nature, which might provide valuable knowledge for the maintenance and management of old steel bridges.

- Implementation of B-WIM systems in both bridges by taking advantage of the installed strain instrumentation, particularly related with its location, as well as of the specificities of each structure. The restrictions to the traffic in the Pinhão Bridge (class II bridge) and the characteristics of the crossing vehicles at the upper deck of the Luiz I Bridge, make them excellent candidates to serve as examples of the usefulness of these techniques to acquire actual traffic data.

References

AASHTO (1992). *Guide specifications for fatigue evaluation of existing steel bridges*. Washington, D.C.: American Association of State Highway and Transportation Officials.

Aktan, Farhey, D., Helmicki, A., Brown, D., Hunt, V., Lee, K. and Levi (1997). *Structural Identification for Condition Assessment: Experimental Arts*. Journal of Structural Engineering **123**(12): pp. 1674-1684.

Aktan, A., Catbas, F., Grimmelsman, K. and Tsikos, C. (2000). *Issues in infrastructure health monitoring for management*. Journal of Engineering Mechanics **126**(7): pp. 711-724.

Aktan, A. E., Farhey, D. N., Brown, D. L., Dalal, V., Helmicki, A. J., Hunt, V. J. and Shelley, S. J. (1996). *Condition assessment for bridge management*. Journal of Infrastructure Systems **2**(3): pp. 108-117.

Aktan, E., Catbas, N., Turer, A. and Zhang, Z. (1998). *Structural Identification: Analytical aspects*. Journal of Structural Engineering **124**(7): pp. 817-829.

Al-Emrani, M., Åkesson, B. and Kliger, R. (2004). *Overlooked secondary effects in open-deck truss bridges*. Structural Engineering International **14**(4): pp. 307-312.

Alampalli, S. and Lund, R. (2006). *Estimating fatigue life of bridge components using measured strains*. Journal of Bridge Engineering **11**(6): pp. 725-736.

Allemang, R. (2003). *The modal assurance criterion - twenty years of use and abuse*. Journal of Sound and Vibration **37**(8): pp. 14-21.

Allen, B. J. and Rens, K. L. (2004). *Condition assessment of the eastbound 6th Avenue viaduct using strain gauges*. Journal of Performance of Constructed Facilities **18**(4): pp. 205-212.

Ansari, F. (2007). *Practical implementation of optical fiber sensors in civil structural health monitoring*. Journal of Intelligent Material Systems and Structures **18**(8): pp. 879-889.

AREMA (2011). *Manual for railway engineering*. Landover, M.D., USA: American Railway Engineering and Maintenance Association.

Astaneh-Asl, A. (2008). *Progressive collapse of steel truss bridges, the case of I-35W collapse* In: Proceedings of the 7th International Conference on Steel Bridges, pp. 185-194. Guimarães, Portugal.

Azeredo, M. and Azeredo, M. A. (2002). *Bridges of Oporto: a love story*. Porto (Portugal): FEUP.

Bancila, R. and Cristescu, C. (1998). *Rehabilitation of steel bridges in Romania*. Journal of Constructional Steel Research **46**(1-3): pp. 73-75.

Barbosa, C., Costa, N., Ferreira, L. A., Araújo, F. M., Varum, H., Costa, A., Fernandes, C. and Rodrigues, H. (2008). *Weldable fibre Bragg grating sensors for steel bridge monitoring*. Measurement Science and Technology **19**(12): pp. 1-10.

Barke, D. and Chiu, W. K. (2005). *Structural health monitoring in the railway industry: a review*. Structural Health Monitoring **4**(1): pp. 81-93.

Bendat, J. and Piersol, A. (1986). *Random Data: Analysis and measurements procedures*. 2nd ed. New York, USA: John Wiley & Sons.

Bergmeister, K. S., U. (2001). *Global monitoring concepts for bridges*. Structural Concrete **2**(1): pp. 29-39.

Betz, D. C., Staudigel, L., Trutzel, M. N. and Kehlenbach, M. (2003). *Structural monitoring using fiber-optic Bragg grating sensors*. Structural Health Monitoring **2**(2): pp. 145-152.

Biezma, M. V. and Schanack, F. (2007). *Collapse of steel bridges*. Journal of Performance of Constructed Facilities **21**(5): pp. 398-405.

Boothby, T. E. and Craig, R. J. (1997). *Experimental load rating study of a historic truss bridge*. Journal of Bridge Engineering **2**(1): pp. 18-26.

Borges, J. F., Marecos, J. and Ferraz, L. C. (1955). *On the evaluation of the safety of old metallic bridges* In: Proceedings of the Symposium sur l'Observation des Ouvrages. RILEM. Lisbon, Portugal.

Brencich, A. and Gambarotta, L. (2009). *Assessment procedure and rehabilitation of riveted railway girders: The Campasso Bridge*. Engineering Structures **31**(1): pp. 224-239.

Brownjohn, J. M. W. (2007). *Structural health monitoring of civil infrastructure*. Philosophical Transactions of the Royal Society A **365**(1851): pp. 589-622.

Caglayan, O., Ozakgul, K., Tezer, O. and Uzgider, E. (2011). *Evaluation of a steel railway bridge for dynamic and seismic loads*. Journal of Constructional Steel Research **67**(8): pp. 1198-1211.

Calçada, R., Cunha, A. and Delgado, R. (2002). *Dynamic analysis of metallic arch railway bridge*. Journal of Bridge Engineering **7**(4): pp. 214-222.

Casas, J. and Cruz, P. (2003). *Fiber optic sensors for bridge monitoring*. Journal of Bridge Engineering **8**(6): pp. 362-373.

Catbas, F. and Aktan, A. (2002). *Condition and damage assessment: Issues and some promising indices*. Journal of Structural Engineering **128**(8): pp. 1026-1036.

Catbas, F. N., Ciloglu, S. K., Hasancebi, O., Grimmelsman, K. and Aktan, A. E. (2007). *Limitations in structural identification of large constructed structures*. Journal of Structural Engineering **133**(8): pp. 1051-1066.

Catbas, F. N., Susoy, M. and Frangopol, D. M. (2008). *Structural health monitoring and reliability estimation: Long span truss bridge application with environmental monitoring data*. Engineering Structures **30**(9): pp. 2347-2359.

Chajes, M. J., Mertz, D. R. and Commander, B. (1997). *Experimental load rating of a posted bridge*. Journal of Bridge Engineering **2**(1): pp. 1-10.

Chakraborty, S. and DeWolf, J. T. (2006). *Development and implementation of a continuous strain monitoring system on a multi-girder composite steel bridge*. Journal of Bridge Engineering **11**(6): pp. 753-762.

Chan, T. H. T., Yu, L., Tam, H. Y., Ni, Y. Q., Liu, S. Y., Chung, W. H. and Cheng, L. K. (2006). *Fiber Bragg grating sensors for structural health monitoring of Tsing Ma bridge:*

Background and experimental observation. Engineering Structures **28**(5): pp. 648-659.

Cheung, M. M. S., Noruziaan, B. and Yang, C.-Y. (2007). *Health monitoring data in assessing critical behaviour of bridges*. Structure and Infrastructure Engineering **3**(4): pp. 325-342.

Coelho, A. G., Freitas, J. A. M., Azeredo, M., Costa, A., Cruz, J. S., Santos, N. E. and Lopes, D. B. (1996). *Viability study for the integration of Luiz I Bridge upper deck in the Light Porto Metro Network* (in Portuguese). Technical Report, Porto: Instituto da Construção / FEUP / Metro do Porto, S.A.

Connolly, C. (2006). *Fibre-optic-based sensors bring new capabilities to structural monitoring*. Sensor Review **26**(3): pp. 236-243.

Conte, J., He, X., Moaveni, B., Masri, S., Caffrey, J., Wahbeh, M., Tasbihgoo, F., Whang, D. and Elgamal, A. (2008). *Dynamic testing of Alfred Zampa Memorial Bridge*. Journal of Structural Engineering **134**(6): pp. 1006-1015.

Costa, B. J. A., Dimande, A., C., F. and Figueiras, J. A. (2008a). *Assessment of Pinhão Bridge behavior during the field tests carried out to support the strengthening and rehabilitation designs* In: Proceedings of the 7th International Conference on Steel Bridges (ICSB'08). On Conference CD. Guimarães, Portugal.

Costa, B. J. A., Félix, C. and Figueiras, J. (2004a). *Monitoring of Luiz I Bridge structural behavior – Instrumentation plan* (in Portuguese). Technical Report, Porto, Portugal: FEUP.

Costa, B. J. A., Félix, C. and Figueiras, J. (2005). *Monitoring of Luiz I Bridge upper deck during the installation of the railway. Weekly Summary Reports of Observation between February 2004 and January 2005* (in Portuguese). Technical Report, Porto, Portugal: FEUP.

Costa, B. J. A., Félix, C. and Figueiras, J. A. (2004b). *Complementary monitoring to the present condition of the Luiz I Bridge* (in Portuguese). Technical Report, Porto, Portugal: FEUP.

Costa, B. J. A., Félix, C. and Figueiras, J. A. (2008b). *Experimental and numerical assessment of the structural behavior of a centenary metallic bridge* In: Proceedings of the 7th

International Conference on Steel Bridges (ICSB'08). On Conference CD. Guimarães, Portugal.

Costa, B. J. A., Félix, C. and Figueiras, J. A. (2009). *Design and installation of an electric based monitoring system applied to a centenary metallic bridge* In: Proceedings of the IV ECCOMAS Thematic Conference on Smart Structures and Materials (SMART'09). On Conference CD. Á. Cunha and J. D. Rodrigues (Eds.), Porto, Portugal.

Costa, B. J. A., Figueiras, J. A. and Félix, C. (2006). *Design and installation of the optic based monitoring system applied to the Luiz I bridge* In: Proceedings of the 3rd International Conference on Bridge Maintenance, Safety and Management (IABMAS'06). On Conference CD. P. J. S. Cruz and D. M. Frangopol (Eds.), Porto, Portugal.

Cunha, A. and Caetano, E. (2006). *Experimental modal analysis of civil engineering structures*. Sound and Vibration **40**(6): pp. 12-20.

Cunha, A., Caetano, E. and Delgado, R. (2001). *Dynamic tests on large cable-stayed bridge*. Journal of Bridge Engineering **6**(1): pp. 54-62.

Cunha, A. and Calçada, R. (1999). *Ambient vibration test of Luiz I Bridge* (in Portuguese). In: Proceedings of the 2éme Rencontre en Génie Parasismique des Pays Méditerranées / 4º Encontro Nacional de Sismologia e Engenharia Sísmica (Sismica99). Faro, Portugal.

Cunha, A., Magalhães, F. and Caetano, E. (2006). *Output-only modal identification of Luiz I Bridge before and after rehabilitation* In: Proceedings of the International Conference on Noise and Vibration Engineering (ISMA2006), pp. 1165-1178. Leuven, Belgium.

De Voy, J. and Williams, J. M. (2007). *Strengthening Coalport Bridge*. Structural Engineering International **17**(2): pp. 178-183.

DelGrego, M. R., Culmo, M. P. and DeWolf, J. T. (2008). *Performance evaluation through field testing of century-old railroad truss bridge*. Journal of Bridge Engineering **13**(2): pp. 132-138.

Deng, L. and Cai, C. S. (2007). *Applications of fiber optic sensors in civil engineering*. Structural Engineering and Mechanics **25**(5): pp. 577-596

DeWolf, J. T., Lauzon, R. G. and Culmo, M. P. (2002). *Monitoring bridge performance*. Structural Health Monitoring **1**(2): pp. 129-138.

Dimande, A. O., Rodrigues, C. F., Costa, B. J. A. and Figueiras, J. A. (2008a). *In service monitoring of the Trezói bridge behavior* (in Portuguese). Technical Report, Porto, Portugal: FEUP.

Dimande, A. O., Rodrigues, C. F., Costa, B. J. A. and Figueiras, J. A. (2008b). *Monitoring of the Trezói bridge behavior under railway traffic loads* (in Portuguese). Technical Report, Porto, Portugal: FEUP.

Doyle, C., Staveley, C. and Henderson, P. (2007). *Structural health monitoring using optical fibre strain sensing systems* In: Proceedings of the 4th International Workshop on Structural Health Monitoring, pp. 944-951. F.-K. Chang (Ed.), Stanford, CA, USA.

Duan, L., Reno, M. and Lynch, J. (2000). *Section properties for latticed members of San Francisco – Oakland Bay Bridge*. Journal of Bridge Engineering **5**(2): pp. 156-164.

ECCS (2008). *Assessment of existing steel structures – recommendations for estimation of remaining fatigue life.* Luxembourg (Luxembourg): European Communities.

EN1990-prAnnexA2 (2003). *Eurocode 0: Basis of structural design - prAnnex A2: Application for bridges*. Brussels, Belgium: European Committee of Standardization.

EN1990 (2003). *Eurocode 0: Basis of structural design*. Brussels, Belgium: European Committee of Standardization.

EN1991-2 (2003). *Eurocode 1: Actions on structures - Part 2: Traffic loads on bridges*. Brussels, Belgium: European Committee for Standardization.

EN1993-1-1 (2005). *Design of steel structures. Part 1-1: General rules and rules for buildings*. Brussels, Belgium: European Committee of Standardization.

EN1993-1-9 (2005). *Design of steel structures. Part 1-9: Fatigue strength of steel structures*. Brussels, Belgium: European Committee of Standardization.

Enevoldsen, I., Pedersen, C., Axhag, F., Johansson, O. and Töyrä, B. (2002). *Assessment and measurement of the Forsmo Bridge, Sweden*. Structural Engineering International **12**(4): pp. 254-257.

Ermopoulos, J. C. and Spyrakos, C. C. (2006). *Validated analysis and strengthening of a 19th century railway bridge*. Engineering Structures **28**(5): pp. 783-792.

Farhey, D. N. (2005). *Bridge instrumentation and monitoring for structural diagnostics*. Structural Health Monitoring **4**(4): pp. 301-318.

Farhey, D. N., Naghavi, R., Levi, A., Thakur, A. M., Pickett, M. A., Nims, D. K. and Aktan, A. E. (2000). *Deterioration assessment and rehabilitation design of existing steel bridge*. Journal of Bridge Engineering **5**(1): pp. 39-48.

Farhey, D. N., Thakur, A. M., Buchanan, R. C., Aktan, A. E. and Jayaraman, N. (1997). *Structural deterioration assessment for steel bridges*. Journal of Bridge Engineering **2**(3): pp. 116-124.

Farrar, C. R. W., K. (2007). *An introduction to structural health monitoring*. Philosophical Transactions of the Royal Society A **365**(1851): pp. 303-315.

Felber, A. J. (1993). *Development of a hybrid bridge evaluation system*. PhD, University of British Columbia, Vancouver, Canada.

Felber, A. J. and Cantieni, R. (1996). *Introduction of a new ambient vibration testing system. Description of the system and seven bridges tests*. Technical Report, Dubendorf, Switzerland: EMPA.

FiberSensing (2009). *FS 6200 – Strain Sensors: High Performance FBG Strain Sensors*. Technical sheet.

FiberSensing (2010). *FS 6300 – Temperatures Sensors: High Performance FBG Temperature Sensors*. Technical sheet.

Figueiras, J., Félix, C. and Costa, B. A. (2005). *Testing and monitoring of a centenary arch bridge*. Structure & Infrastructure Engineering **1**(1): pp. 63-73.

Figueiredo, M., Jesus, A., Pereira, H., Ribeiro, A., Natal, R., Moreira, P., Castro, P. T. and Fernandes, A. A. (2004). *Structural integrity evaluation of the Pinhão bridge* (in Portuguese). Technical Report, Porto: DEMEGI / FEUP.

Frangopol, D. M., Strauss, A. and Kim, S. (2008). *Bridge reliability assessment based on monitoring*. Journal of Bridge Engineering **13**(3): pp. 258-270.

Fu, C., AlAyed, H., Amde, A. and Robert, J. (2007). *Field performance of the fiber-reinforced polymer deck of a truss bridge*. Journal of Performance of Constructed Facilities **21**(1): pp. 53-60.

Fu, Y. and DeWolf, J. (2001). *Monitoring and analysis of a bridge with partially restrained bearings*. Journal of Bridge Engineering **6**(1): pp. 23-29.

Fuhr, P. L., Huston, D. R., Nelson, M., Nelson, O., Hu, J., Mowat, E., Spammer, S. and Tamm, W. (1999). *Fiber optic sensing of a bridge in Waterbury, Vermont*. Journal of Intelligent Material Systems and Structures **10**(4): pp. 293-303.

Geissler, K. (2002). *Assessment of old steel bridges, Germany*. Structural Engineering International **12**(4): pp. 258-263.

Ghosh, U. and Ghoshal, A. (2002). *Experiences in rehabilitation of steel bridges*. Structural Engineering International **12**(4): pp. 269-272.

Glišić, B. and Inaudi, D. (2007). *Fiber optic methods for structural health monitoring*. West Sussex (England): John Wiley & Sons.

Glišić, B., Posenato, D. and Inaudi, D. (2007). *Integrity monitoring of old steel bridge using fiber optic distributed sensors based on Brillouin scattering* In: Proceedings of the Nondestructive Characterization for Composite Materials, Aerospace Engineering, Civil Infrastructure, and Homeland Security. On Conference CD. H. F. Wu, A. A. Diaz and P. J. Shull (Eds.), San Diego, CA, USA. SPIE, Vol. 6531.

Gonçalves, F., Amaral, V. and Barata, D. (2008). *Rehabilitation and structural strengthening of the Fão Bridge over the Cávado River in Portugal* In: Proceedings of the 7th International Conference on Steel Bridges (ICSB'08), pp. II435-II444. Guimarães, Portugal.

GRID (2001). *Geometry survey and inspection of Luiz I Bridge: Performed works and tests* (in Portuguese). Lisbon: GRID – Consultas, Estudos e Projectos de Engenharia Lda.

GRID (2005). *Load test specifications – Rehabilitation design of Luiz I Bridge* (in Portuguese). Lisbon: GRID – Consultas, Estudos e Projectos de Engenharia Lda.

GRIDa) (2003). *Railway deck installation on the Luiz I Bridge – Monitoring and observation plan* (in Portuguese). Lisbon: GRID – Consultas, Estudos e Projectos de Engenharia Lda.

GRIDb) (2003). *Installation of the railway in the Luiz I Bridge upper deck: monitoring and observation plan* (in Portuguese). Lisbon: GRID – Consultas, Estudos e Projectos de Engenharia Lda

GRIDc) (2003). *Descriptive memory, drawings, and technical specifications of the execution design* (in Portuguese). Lisbon: GRID – Consultas, Estudos e Projectos de Engenharia Lda.

Harik, Allen, D., Street, R., Guo, M., Graves, R., Harison, J. and Gawry (1997). *Free and ambient vibration of Brent-Spence Bridge*. Journal of Structural Engineering **123**(9): pp. 1262-1268.

Helmerich, R., Kuhn, B. and Nussbaumer, A. (2007). *Assessment of existing steel structures. A guideline for estimation of the remaining fatigue life*. Structure and Infrastructure Engineering **3**(3): pp. 245-255.

Hemphill, D. (2004). *Structural health monitoring system for the east 12th street bridge* In: Proceedings of the Transportation Scholars Conference (Iowa State University). On Conference CD. Ames, IA, USA.

Hill, K. O. and Meltz, G. (1997). *Fiber Bragg grating technology fundamentals and overview*. Journal of Lightwave Technology **15**(8): pp. 1263-1276.

Holzinger, H., Jeschko, A., Robra, J. and Ramberger, G. (2002). *Strengthening of an old arch truss bridge, Austria*. Structural Engineering International **12**(4): pp. 276-280.

Hong He, L. L. and Lin, Y. (2009). *Study on the spatial division multiplexing technique of Fiber Bragg Grating sensors* In: Proceedings of the Symposium on Photonics and Optoelectronics. On Conference CD. IEEE, Institute of Electrical and Electronics Engineers Wuhan, China.

Howell, D. A. and Shenton III, H. W. (2006). *System for in-service strain monitoring of ordinary bridges*. Journal of Bridge Engineering **11**(6): pp. 673-680.

Hsieh, K. H., Halling, M. W. and Barr, P. J. (2006). *Overview of vibrational structural health monitoring with representative case studies*. Journal of Bridge Engineering **11**(6): pp. 707-715.

Hu, W.-H., Cunha, A., Caetano, E., Magalhães, F. and Moutinho, C. (2009). *LabVIEW toolkits for output-only modal identification and long-term dynamic structural monitoring*. Structure and Infrastructure Engineering **6**(5): pp. 557-574.

Inaudi, D. and Del Grosso, A. (2008). *Fiber optic sensors for structural control* In: Proceedings of the 14th World Conference on Earthquake Engineering. On Conference CD. Beijing, China.

Kääriäinen, J. and Pulkkinen, P. (2002). *Rehabilitation of Tornionjoki steel truss bridge, Finland*. Structural Engineering International **12**(4): pp. 273-275.

Karoumi, R., Wiberg, J. and Liljencrantz, A. (2005). *Monitoring traffic loads and dynamic effects using an instrumented railway bridge*. Engineering Structures **27**(12): pp. 1813-1819.

Kashima, S., Yanaka, Y., Suzuki, S. and Mori, K. (2001). *Monitoring the Akashi Kaikyo Bridge: first experiences*. Structural Engineering International **11**(2): pp. 120-123.

Kersey, A. D., Davis, M. A., Patrick, H. J., LeBlanc, M., Koo, K. P., Askins, C. G., Putnam, M. A. and Friebele, E. J. (1997). *Fiber grating sensors*. Journal of Lightwave Technology **15**(8): pp. 1442-1463.

Kiss, K. and Dunai, L. (1998). *Advanced model for the stress analysis of steel truss bridges*. Journal of Constructional Steel Research **46**(1-3): pp. 76-78.

Kister, G., Winter, D., Gebremichael, Y. M., Leighton, J., Badcock, R. A., Tester, P. D., Krishnamurthy, S., Boyle, W. J. O., Grattan, K. T. V. and Fernando, G. F. (2007). *Methodology and integrity monitoring of foundation concrete piles using Bragg grating optical fibre sensors*. Engineering Structures **29**(9): pp. 2048-2055.

Ko, J. M. and Ni, Y. Q. (2005). *Technology developments in structural health monitoring of large-scale bridges*. Engineering Structures **27**(12): pp. 1715-1725.

Lee, D. G., Mitrovic, M., Friedman, A., Carman, G. P. and Richards, L. (2002). *Characterization of fiber optic sensors for structural health monitoring*. Journal of Composite Materials **36**(11): pp. 1349-1366.

Li, H.-N., Li, D.-S. and Song, G.-B. (2004). *Recent applications of fiber optic sensors to health monitoring in civil engineering*. Engineering Structures **26**(11): pp. 1647-1657.

Li, S. and Wu, Z. (2007). *Development of distributed long-gage fiber optic sensing system for structural health monitoring*. Structural Health Monitoring **6**(2): pp. 133-143.

Liang, Y., Tennant, A., Jia, H., Xiong, X. and Ansari, F. (2005). *Implementation of long gauge fiber optic sensor arrays in civil structures*. In: Sensing Issues in Civil Structural Health Monitoring, pp. 403-412. F. Ansari (Ed.), Netherlands: Springer, ISBN: 978-1-4020-3660-6.

Lopes, N. T., Ribeiro, D. and Reis, A. (2008). *Upgrading of the Luiz I Bridge in Porto: design for fatigue resistance under new traffic demands* In: Proceedings of the 7th International Conference on Steel Bridges (ICSB'08), pp. II469-II478. Guimarães, Portugal.

Lu, W. and Mäkeläinen, P. (2003). *Advanced steel structures – structural fire design, fatigue design*. Helsinki, Finland: Helsinki University of Technology, Laboratory of Steel Structures, ISBN: 951-22-6732-2.

Maalej, M. and Rizkalla, S. H. (2000). *Fibre optic sensing and intelligent processing of sensor data for structural health monitoring* In: Proceedings of the 14th International Conference on Optical Fiber Sensors, pp. 234-237. Venice, Italy. SPIE, Vol. 4185.

Magalhães, F., Caetano, E. and Cunha, A. (2007). *Challenges in the application of stochastic modal identification methods to a cable-stayed bridge*. Journal of Bridge Engineering **12**(6): pp. 746-754.

Magalhães, F. and Cunha, A. (2011). *Explaining operational modal analysis with data from an arch bridge*. Mechanical Systems and Signal Processing **25**(5): pp. 1431-1450.

Majumder, M., Gangopadhyay, T. K., Chakraborty, A. K., Dasgupta, K. and Bhattacharya, D. K. (2008). *Fibre Bragg gratings in structural health monitoring – Present status and applications*. Sensors and Actuators A: Physical **147**(1): pp. 150-164.

Marécos, J., Castanheta, M. and Trigo, J. T. (1969). *Field observations of Tagus River suspension bridge*. Journal of Structural Division **95**(4): pp. 555-583.

Marques, F., Cunha, A., Fernandes, A. A., Caetano, E. and Magalhães, F. (2009). *Evaluation of dynamic effects and fatigue assessment of a metallic railway bridge*. Structure and Infrastructure Engineering **6**(5): pp. 635-646.

Marques, F., Hu, W. H., Moutinho, C., Magalhães, F. and Cunha, A. (2011). *Evaluation of dynamic effects and fatigue assessment of a railway bridge supported by temporary*

monitoring In: Proceedings of the 8th International Conference on Structural Dynamics (EURODYN'11). On Conference CD. Leuven, Belgium.

Matta, F., Bastianini, F., Galati, N., Casadei, P. and Nanni, A. (2008). *Distributed strain measurement in steel bridge with fiber optic sensors: validation through diagnostic load test*. Journal of Performance of Constructed Facilities **22**(4): pp. 264-273.

Measures, R. M. (2001). *Structural Monitoring with Fibre Optic Technology*. San Diego, California (USA): Academic Press, ISBN: 0124874304.

Mehrani, E., Ayoub, A. and Ayoub, A. (2009). *Evaluation of fiber optic sensors for remote health monitoring of bridge structures*. Materials and Structures **42**(2): pp. 183-199.

Moyo, P., Brownjohn, J. M. W., Suresh, R. and Tjin, S. C. (2005). *Development of fiber Bragg grating sensors for monitoring civil infrastructure*. Engineering Structures **27**(12): pp. 1828-1834.

Mrad, N., Sparling, S. and Laliberte, J. (2000). *Strain monitoring and fatigue life of Bragg grating fiber optic sensors* In: Proceedings of the Smart Structures and Materials 1999: Sensory Phenomena and Measurement Instrumentation for Smart Structures and Materials, pp. 82-91. J. Richard O. Claus; William B. Spillman (Ed.), Bellingham, Wash. Newport Beach, CA, USA. SPIE, Vol. 3670.

Mufti, A. (2001). *Guidelines for structural health monitoring - design manual*. Winnipeg, Manitoba, Canada: ISIS Canada.

Nascé, V. (1993). *Restoration of a 100 year old iron bridge, Paderno*. Structural Engineering International **3**(1): pp. 37-38.

NI (2007). *CompactRIO™ and LabVIEW™ Development Fundamentals*. Course Manual.

O'Connell, H. M. and Dexter, R. J. (2001). *Response and analysis of steel trusses for fatigue truck loading*. Journal of Bridge Engineering **6**(6): pp. 628-638.

Olofsson, J. and Elfgren, L. (2008). *Sustainable bridges – Assessment for future traffic demands and longer lives*. Available from: http://www.sustainablebridges.net/ (Accessed in May 11th, 2012).

Olund, J. and DeWolf, J. (2007). *Passive structural health monitoring of Connecticut's Bridge infrastructure*. Journal of Infrastructure Systems **13**(4): pp. 330-339.

Othonos, A. (1997). *Fiber Bragg gratings*. Review of Scientific Instruments **68**(12): pp. 4309-4341.

Ou, J. and Li, H. (2005). *The state-of-the-art and practice of structural health monitoring for civil infrastructures in the mainland of China* In: Proceedings of the 2nd International Conference on Structural Health Monitoring and Intelligent Infrastructure, pp. 69-88. Shenzhen, China.

Pearson, C. and Delatte, N. (2006). *Collapse of the Quebec Bridge, 1907*. Journal of Performance of Constructed Facilities **20**(1): pp. 84-91.

Peeters, B. and De Roeck, G. (1999). *Reference-based Stochastic Subspace Identification for Output-only Modal Analysis*. Mechanical Systems and Signal Processing **13**(6): pp. 855-878.

Peeters, B. and Van der Auweraer, H. (2005). *PolyMAX: a revolution in operational modal analysis* In: Proceedings of the 1st International Operational Modal Analysis Conference (IOMAC). On Conference CD. Copenhagen, Denmark.

Petroski, H. (1995). *Case histories and the study of structural failures*. Structural Engineering International **5**(4): pp. 250-255.

Pinto, J. V. (2005). *Metallic Bridge of Pinhão - Inspection and execution of the rehabilitation study. Structural design - Descriptive document* (in Portuguese). Porto: GEG – Gabinete de Estruturas e Geotecnia.

Ren, W., Harik, I., Blandford, G., Lenett, M. and Baseheart, T. (2004a). *Roebling suspension bridge. II: Ambient testing and live-load response*. Journal of Bridge Engineering **9**(2): pp. 119-126.

Ren, W., Zhao, T. and Harik, I. (2004b). *Experimental and analytical modal analysis of steel arch bridge*. Journal of Structural Engineering **130**(7): pp. 1022-1031.

Rodrigues, C., Cavadas, F., Félix, C. and Figueiras, J. (2012). *FBG based strain monitoring in the rehabilitation of a centenary metallic bridge*. Engineering Structures **44**: pp. 281-290.

Roeder, C., MacRae, G., Crocker, P., Arima, K. and Wong, S. (2000). *Dynamic response and fatigue of steel tied-arch bridge*. Journal of Bridge Engineering **5**(1): pp. 14-21.

RSAEEP (1983). *Regulation for the safety and actions of buildings and bridges* (in Portuguese). Lisbon, Portugal: Dec.-Lei n.º 235/83.

Salawu, O. S. and Williams, C. (1995). *Review of full-scale dynamic testing of bridge structures*. Engineering Structures **17**(2): pp. 113-121.

Saraf, V. and Nowak, A. S. (1998). *Proof load testing of deteriorated steel girder bridges*. Journal of Bridge Engineering **3**(2): pp. 82-89.

Sartor, R. R., Culmo, M. P. and DeWolf, J. T. (1999). *Short-term strain monitoring of bridge structures*. Journal of Bridge Engineering **4**(3): pp. 157-164.

Serzan, K. P. (1995). *Rehabilitation of the Brooklyn Bridge*. Structural Engineering International **5**(4): pp. 244-246.

Seyrig, T. (1884). *Pont Dom Luiz I à Porto*. Paris, France: Librairie Centrales des Chemins de Fer.

Shama, A. A., Mander, J. B., Chen, S. S. and Aref, A. J. (2001). *Ambient vibration and seismic evaluation of a cantilever truss bridge*. Engineering Structures **23**(10): pp. 1281-1292.

Shehata, E. and Rizkalla, S. (1999). *Intelligent sensing for innovative bridges*. Journal of Intelligent Material Systems and Structures **10**(4): pp. 304-313.

Sousa, H., Costa, B. J. A., Henriques, A. and Figueiras, J. A. (2010). *MENSUSMONITOR – Algorithm implementation for detecting live load events and assessment of structural effects on bridges* In: Proceedings of the 5th International Conference on Bridge Maintenance, Safety and Management (IABMAS'10). On Conference CD. R. Sause and D. M. Frangopol (Eds.), Philadelphia, PA, USA.

Sousa, H., Félix, C., Bento, J. and Figueiras, J. (2011). *Design and implementation of a monitoring system applied to a long-span prestressed concrete bridge*. Structural Concrete **12**(2): pp. 82-93.

Spyrakos, C. C., Kemp, E. L. and Venkatareddy, R. (1999). *Validated analysis of Wheeling suspension bridge*. Journal of Bridge Engineering **4**(1): pp. 1-7.

Spyrakos, C. C., Raftoyiannis, I. G. and Ermopoulos, J. C. (2004). *Condition assessment and retrofit of a historic steel-truss railway bridge*. Journal of Constructional Steel Research **60**(8): pp. 1213-1225.

Tam, H. Y., Lee, T., Ho, S. L., Haber, T., Graver, T. and Méndez, A. (2007). *Utilization of fiber optic Bragg grating sensing systems for health monitoring in railway applications* In: Proceedings of the 6th International Workshop on Structural Health Monitoring, pp. 1824-1825. F.-K. Chang (Ed.), Stanford, CA, USA.

Tennyson, R. (2001). *Installation, use and repair of fiber optic sensors*. Winnipeg, Manitoba, Canada: ISIS Canada.

Tennyson, R. C., Mufti, A. A., Rizkalla, S., Tadros, G. and Benmokrane, B. (2001). *Structural health monitoring of innovative bridges in Canada with fiber optic sensors*. Smart Materials and Structures **10**(3): pp. 560-573.

Tobias, D. H., Foutch, D. A. and Choros, J. (1996). *Loading spectra for railway bridges under current operating conditions*. Journal of Bridge Engineering **1**(4): pp. 127-134.

Todd, M. D., Nichols, J. M., Trickey, S. T., Seaver, M., Nichols, C. J. and Virgin, L. N. (2007). *Bragg grating-based fibre optic sensors in structural health monitoring*. Philosophical Transactions of the Royal Society A **365**(1851): pp. 317-343.

Tsamasphyros, G. J., Koulalis, E. A., Kanderakis, G. N., Furnarakis, N. K. and Astreinidis, V. Z. (2006). *Structural health monitoring of a steel railway bridge using optical fibre Bragg grating sensors and numerical simulation* In: Proceedings of the 3rd European Workshop on Structural Health Monitoring, pp. 341-348. A. Guemes (Ed.), Granada, Spain.

UIC778-2 (1986). *Recommendations for determining the carrying capacity of existing metal structures*. Union Internacional des Chemins de Fer.

Wang, M. L., Heo, G. and Satpathi, D. (1997). *Dynamic characterization of a long span bridge: A finite element based approach*. Soil Dynamics and Earthquake Engineering **16**(7-8): pp. 503-512.

Wang, Y., Tjin, C. S., Moyo, P., Zheng, X. and Brownjohn, J. M. W. (2001). *Simultaneous monitoring of the amplitude and location of loading with fiber Bragg grating sensor arrays* In: Proceedings of the Health Monitoring and Management of Civil

Infrastructure Systems, pp. 451-458. S. B. Chase and A. E. Aktan (Eds.), Newport Beach, CA, USA. SPIE, Vol. 4337.

Wikispaces. (2011). *Engineering Disasters [online]*. Available from: http://engineeringdisasters.wikispaces.com/ (Accessed in October 8th, 2011).

Wong, K.-Y. (2007). *Design of a structural health monitoring system for long-span bridges*. Structure and Infrastructure Engineering **3**(2): pp. 169-185.

Ye, Q., Fanjiang, G.-N. and Yanev, B. (2005). *Investigation of the dynamic properties of the Brooklyn Bridge*. In: Sensing Issues in Civil Structural Health Monitoring, pp. 65-72. F. Ansari (Ed.), Netherlands: Springer, ISBN: 978-1-4020-3660-6.

Zaki, M. A. and Abu-Hamd, M. H. (2007). *Rehabilitation assessment of a steel railway bridge by dynamic field testing*. Structure and Infrastructure Engineering **3**(4): pp. 343-353.

Zhan-feng, G., Yan-liang, D., Bao-chen, S. and Xiu-mei, J. (2007). *Strain monitoring of railway bridges using optic fiber sensors*. Journal of Quality in Maintenance Engineering **13**(2): pp. 186-197.

Zhao, J. and DeWolf, J. T. (2002). *Dynamic monitoring of steel girder highway bridge*. Journal of Bridge Engineering **7**(6): pp. 350-356.

Zhou, Y. E. (2006). *Assessment of bridge remaining fatigue life through field strain measurement*. Journal of Bridge Engineering **11**(6): pp. 737-744.